

Stellingen

1. Van der Werf et al. (1995) betitelen het systeem waarin vast Ca-maleaat wordt omgezet in vast Ca-D-malaat als een twee-fasen systeem, terwijl dit een drie-fasen systeem is.

Van der Werf MJ, Hartmans S, Van den Tweel WJJ. 1995. Effect of maleate counter-ion on malease activity: production of D-malate in a crystal-liquid two-phase system. Enzyme Microb Technol 17:430-436.

2. Van der Werf et al. (1995) suggereren ten onrechte dat in hun drie-fasen systeem zuivere Ca-maleaat- en Ca-D-malaatkristallen aanwezig zijn.

Eigen waarneming.

Van der Werf MJ, Hartmans S, Van den Tweel WJJ. 1995. Effect of maleate counter-ion on malease activity: production of D-malate in a crystal-liquid two-phase system. Enzyme Microb Technol 17:430-436.

3. Het aantal geïntegreerde processen wordt vaak onderschat.
4. Goed onderzoek staat of valt met de vrijheid om onderzoeksdoelen aan te mogen passen.
5. Modelsystemen blijken in de praktijk vaak te complex.
6. Het feit dat onderzoek naar falende marketingconcepten wel publiceerbaar is en onderzoek naar falende (bio)technologische concepten nauwelijks, wekt de indruk dat in beide wetenschapsgebieden een verschillend belang aan dergelijke bevindingen wordt gehecht.
7. Het meest gebruikte weerwoord is 'lokaal'.
8. Het gebruik van doping in de sport lijkt evenredig toe te nemen met de invloed van de commercie op de sport.
9. Vier jaar na de val van Srebrenica moet het Nederlandse leger zijn stellingen nog steeds verdedigen.
10. The sky is not the limit, the ground is.

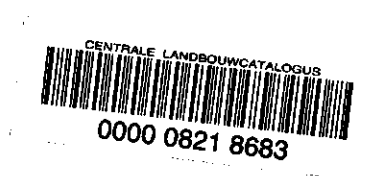
Stellingen behorende bij het proefschrift 'Modeling solid-to-solid biocatalysis'.

M.J.F. Michielsen

Wageningen, 6 oktober 1999.

Modeling solid-to-solid biocatalysis

Marco J.F. Michiels



Promotor: dr. ir. J. Tramper
Hoogleraar in de bioprocestechnologie

Co-promotoren: dr. H.H. Beeftink
Universitair docent bij de sectie Proceskunde

dr. ir. R.H. Wijffels
Universitair docent bij de sectie Proceskunde

11108301, 2670

Marco J.F. Michielsen

Modeling solid-to-solid biocatalysis

Proefschrift

ter verkrijging van de graad van doctor
op gezag van de rector magnificus
van de Wageningen Universiteit,
dr. C.M. Karssen,
in het openbaar te verdedigen
op woensdag 6 oktober 1999
des namiddags te vier uur in de Aula.

15N 966082

BIBLIOTHEEK
LANDBOUWUNIVERSITEIT
WAGENINGEN

ISBN 90-5808-080-3

No part of this book may be reproduced in any form or by any means without permission of the author.

Coverfoto: MediaService, Landbouwniversiteit Wageningen.

Voorwoord

Aan het begin van dit proefschrift past een woord van dank aan iedereen die heeft bijgedragen aan de totstandkoming van dit proefschrift en aan de prettige werksfeer waarin dit kon geschieden.

Allereerst wil ik mijn directe begeleiders, Hans Tramper, Rik Beeftink en René Wijffels bedanken voor de geboden vrijheid tijdens het onderzoek, en de kritische blik waarmee ze mijn werk steeds beoordeeld hebben. In het bijzonder wil ik ze bedanken voor de open en prettige wijze van begeleiden, waarbij altijd alles bespreekbaar was.

Binnen dit project zijn een tweetal analisten werkzaam geweest, te weten Ellen Meijer en later Cathelijne Frielink. Niet alleen hebben zij vele HPLC-problemen weten op te lossen, maar ook hebben zij voor een groot gedeelte de data verzameld waarop dit proefschrift gebaseerd is. Het moge duidelijk zijn dat ik ze hiervoor erg dankbaar ben. Op deze plaats wil ik ook Jos Sewalt bedanken voor de jarenlange HPLC-ondersteuning.

Verder ben ik dank verschuldigd aan een groot aantal studenten die in het kader van een afstudeervak een bijdrage hebben geleverd aan dit onderzoek, te weten: Rogier Biemans, Eef Schimmelpennink, Maarten Pennings, Arjan Verkerk, Dionne Irving, Karin Reijenga, Saskia Kempener, Rogier Spoor en Jeroen van Roon.

Tevens gaat mijn dank uit naar de medewerkers van de bibliotheek, glasblazerij, werkplaats, MediaService, automatisering en het chemicaliënmagazijn voor de vakkundige ondersteuning.

Mijn kamergenoten, Suzanne van Gerwen, Arie van Oorschot, Teresa Cesário en later Nicole Heinsman en Rolf Marteijs, zijn al die jaren een steun en toeverlaat geweest en hebben voor een flinke portie humor, onzin en geleuter gezorgd. Ten aanzien van dit laatste verdienen ook mijn labgenoten, Rouke Bosma en Pieter Kroon, de medewerkers van het secretariaat, Joyce Krauss en Hedy Wessels, en PC-vraagbaak, 'good-old' Gerrit Heida, een eervolle vermelding. Allen bedankt hiervoor.

Nicole Pijnenburg en mijn ouders ben ik erg dankbaar voor hun onmisbare steun tijdens de vele uren van mijn vrije tijd die ik aan dit proefschrift heb besteed. Eindelijk heb ik de mogelijkheid hun geduld te belonen.

Tenslotte wil ik alle medewerkers van de sectie Proceskunde bedanken voor hun behulpzaamheid en voor de plezierige werksfeer binnen de sectie. Dit is mijn ogen de belangrijkste basis geweest voor het proefschrift dat nu voor u ligt.

Abstract

Michielsen MJF. 1999. Modeling solid-to-solid biocatalysis. PhD-thesis, Wageningen Agricultural University, Wageningen, The Netherlands (190 p, English and Dutch summaries).

Keywords: Modeling, dissolution kinetics, biokinetics, crystal growth kinetics, process integration, solid-to-solid bioconversion.

In this thesis, a kinetic model is described for the conversion of solid Ca-maleate to solid Ca-D-malate. The reaction is catalysed by maleate hydratase in permeabilized *Pseudomonas pseudoalcaligenes* and is executed in a batch reactor seeded with Ca-D-malate (product) crystals. To this end, separate kinetic models were first developed for each of the constituent steps, i.e. substrate crystal dissolution, bioconversion (with biocatalyst inactivation superimposed), and product crystal growth.

According to both the crystal dissolution and the crystal growth model, the rate is controlled by the rate of crystal surface processes, by the rate of solute transport from or to the crystal surface (in case of dissolution or growth, respectively), or by both. Tools are developed to determine the rate-controlling process(es). Dissolution of Ca-maleate crystals and growth of Ca-D-malate crystals were both found to be surface-controlled, obeying linear and exponential rate laws, respectively. The kinetic parameters were determined by fitting data sets of concentration versus time.

The biokinetic model featured substrate inhibition, competitive product inhibition, and simultaneous first-order biocatalyst inactivation. The kinetic parameters were determined by fitting the complete kinetic model simultaneously through three data sets of maleate (substrate) concentration versus time. Furthermore, the biokinetic model was used to determine under which conditions the total costs of substrate and biocatalyst were minimal in a continuous system with biocatalyst replenishment and recycling.

The individual kinetic models of the constituent processes were then integrated into one overall process model. The model gave a very good quantitative prediction of the solid-to-solid bioconversion in a batch reactor seeded with Ca-D-malate crystals.

Finally, two potentially attractive modes for operation of a reactor for solid-to-solid bioconversions, batch operation at very high concentrations of undissolved substrate and continuous operation, are evaluated with respect to their feasibility and overall costs per kg of product.

Contents

<i>Chapter 1</i>	Introduction	1
<i>Chapter 2</i>	Dissolution kinetics of Ca-maleate crystals: evaluation for biotransformation reactor design	7
<i>Chapter 3</i>	Kinetics of D-malate production by permeabilized <i>Pseudomonas pseudoalcaligenes</i>	31
<i>Chapter 4</i>	Stabilization of maleate-hydratase activity of permeabilized <i>Pseudomonas pseudoalcaligenes</i>	53
<i>Chapter 5</i>	D-malate production by permeabilized <i>Pseudomonas pseudoalcaligenes</i> ; optimization of conversion and biocatalyst productivity	69
<i>Chapter 6</i>	Growth of Ca-D-malate crystals in a bioreactor	97
<i>Chapter 7</i>	Modeling solid-to-solid biocatalysis: integration of six consecutive steps	129
<i>Chapter 8</i>	Solid-to-solid bioconversions: batch or continuous?	155
	Summary	183
	Samenvatting	185
	Bibliography	188
	Curriculum Vitae	190

CHAPTER 1

Introduction

One of the great challenges in applied biocatalysis is to develop reaction media in which very high amounts of product per reactor volume can be attained at high production rates; in other words, media in which a high overall volumetric productivity can be accomplished. Such media are generally associated with good process economics (Van 't Riet and Tramper, 1991). Water is generally an attractive medium for bioconversions, as most biocatalysts act in aqueous media. However, high overall volumetric productivities often cannot be achieved in aqueous media due to a limited substrate solubility in water and/or inhibition by high substrate and/or product concentrations. Both problems are generally tackled by application of a second phase, or even more phases, next to the aqueous reaction phase, in so-called multi-phase systems.

In multi-phase systems, the substrate is extracted from a substrate-reservoir phase into the aqueous reaction phase, and/or the product is extracted from the aqueous reaction phase into a product-sink phase. In this manner, high product amounts can be accumulated and substrate and product inhibition can be minimized. These systems have the additional advantage of scaleability (Andersson and Hahn-Hägerdal, 1990). Such a concept of integration of bioconversion and extractions is especially useful in case of toxic or instable substrates and/or products, because the *in situ* extraction considerably reduces the residence time of these substrates and/or products in the aqueous reaction phase (Freeman et al., 1993; Zijlstra et al., 1998). Particularly, the integration of biocatalysis and downstream processing, i.e. product extraction, has gained increased interest during the last decade, as it may shift the equilibrium in favor of synthesis, so that the overall conversion is increased considerably (Vermüë, 1995). Besides, it offers the opportunity for continuous processing with biocatalyst retention, which may greatly improve the overall volumetric productivity. Finally, it may reduce the number of subsequent downstream-processing steps (Freeman et al., 1993; Zijlstra et al., 1998).

Selection of a suitable solvent for use as accumulation phase in multi-phase systems is mainly based on preventing solvent toxicity for the biocatalyst and on the

solubility of the compounds to be accumulated, indicating that it is highly case-specific. In general, for accumulation of hydrophobic compounds an organic solvent is used, and for accumulation of hydrophilic compounds a second aqueous phase is applied. It is obvious that for accumulation of two dissimilar compounds (both hydrophobic and hydrophilic) selection of a single solvent becomes difficult.

An approach that can be applied for both hydrophobic and hydrophilic compounds, is the use of solid phases as accumulation phases. In such multi-phase systems, the following consecutive steps occur: substrate dissolution, bioconversion (in the aqueous phase), and product crystallization. These kinds of conversions are called solid-to-solid bioconversions. The potential advantages of solid-to-solid bioconversions include:

- Extremely high substrate amounts per unit of reactor volume can be used.
- High conversions and rates can be attained; note that a very high substrate amount per reactor volume, in combination with a high conversion, results in a very high product amount per reactor volume.
- The formation of product crystals makes easy downstream processing possible (centrifugation or filtration followed by drying), resulting in lower downstream-processing costs than in conventional multi-phase systems.
- The costs associated with these multi-phase systems are lower, because the use of organic solvents or expensive polymers (for formation of aqueous-organic and aqueous two-phase systems, respectively) is avoided.
- These systems are environmentally friendly, and the selectivity and specificity of the biocatalyst should remain unaffected, as they consist of an aqueous phase and two solid phases.

The potential of the use of multi-phase systems with solid phases of substrate and/or product has long been recognized by the industry (Ashina and Suto, 1992; Kitahara et al., 1960; Miller, 1985; Oyama, 1992; Takahashi, 1986; Watanabe and Osawa, 1966), and the number of applications still increases (Bornscheuer and Yamane, 1994; Cao et al., 1996; Erbdinger et al., 1998; Kasche, 1986; Michielsen et al., 1999; Petkov and Stoineva, 1984; Kasche and Galunsky, 1995; Van der Werf et al., 1995; Wolff et al., 1999). However, quantitative models for process development, optimization, and control of this kind of systems are still lacking.

OUTLINE OF THIS THESIS

In this thesis, a quantitative model for the biocatalytic conversion of a solid substrate to a solid product is developed. As a model reaction, the conversion of solid Ca-maleate to solid Ca-D-maleate by maleate hydratase in permeabilized *Pseudomonas pseudoalcaligenes*, as shown in Fig. 1, was chosen.

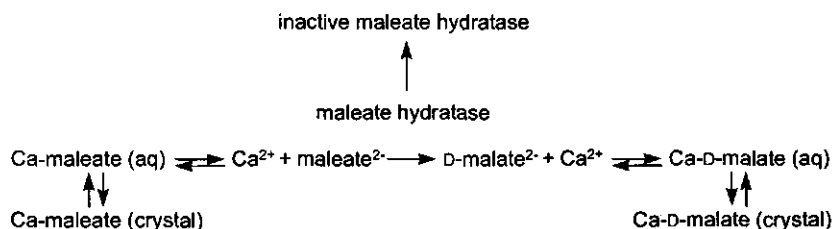


Figure 1 Reaction scheme for the conversion of solid Ca-maleate to solid Ca-D-maleate by maleate hydratase in permeabilized *P. pseudoalcaligenes*.

In order to develop an overall kinetic model for this conversion, it was splitted in separate steps: Ca-maleate dissolution, bioconversion of maleate²⁻ to D-maleate²⁻ accompanied by biocatalyst inactivation, and Ca-D-maleate crystal growth. Note that, in principle, the last step in the solid-to-solid bioconversion should also involve product nucleation (the formation of new product crystals). However, at the conditions described in this thesis, i.e. moderate to low supersaturation in the presence of product crystals, the occurrence of product nucleation can be neglected. Separate kinetic models for these steps were first determined (chapter 2, 3-5, and 6, respectively) and then integrated into an overall model (chapter 7).

In chapter 2, a kinetic model based on the interfacial-barrier theory and the diffusion-layer theory is presented; it describes the increase in Ca-maleate concentration due to dissolution. In order to evaluate this model, the effects of stirring speed, temperature, pH, and initial Ca²⁺ concentration were determined experimentally. For model simplification, it is of importance to know whether the dissolution process is reaction or transport controlled. As in case of polydispers crystals such a determination is not straightforward, a method based on overall reaction and transport rates (per unit of driving force) was developed.

In chapters 3 to 5, the biokinetics of conversion and inactivation are studied. In chapter 3, part of the kinetics of D-maleate production by permeabilized *P.*

pseudoalcaligenes is characterized, as a function of temperature and pH. This is done by fitting a kinetic model, featuring competitive product inhibition and first-order biocatalyst inactivation, simultaneously through two independent data sets of substrate concentration versus time. With this method, the number of experiments needed for accurate determination of the kinetic parameters can be reduced significantly as compared to methods based on initial-activity experiments. In chapter 4, the effects of temperature, product, Ca^{2+} and biocatalyst concentrations on the biocatalyst inactivation rate are quantified. In chapter 5, the effects of the remaining process parameters, i.e. ionic strength, substrate and Ca^{2+} concentrations, on biocatalyst activity are studied, and the biokinetic model is completed, i.e. a substrate inhibition term is added. In order to obtain more realistic values, all kinetic parameters were determined once more, as a function of temperature, by applying the method described in chapter 3, but now with the complete kinetic model. Furthermore, it is shown how this model can be used to select the process conditions in a CSTR with biocatalyst replenishment and recycling, corresponding to a minimum in the sum of the substrate and biocatalyst costs.

Since growth of salt crystals can obey different rate laws, chapter 6 shows a procedure for selection of an appropriate one. Chapter 6 further presents a kinetic model that is based on this rate law; it describes the decrease in supersaturation due to Ca-D-malate crystal growth as a function of the concentrations of the constituent ions, Ca^{2+} and D-malate²⁻. For evaluation of the model, the effects of temperature and stirring speed were investigated.

Chapter 7, finally, shows how these separate quantitative models are integrated into a single overall model, and how it is validated. Chapter 8 addresses the future trends in solid-to-solid bioconversions, with respect to the mode of operation. These future trends include batch operation at high concentrations of undissolved substrate, and continuous operation. This final chapter ends with a procedure that can be used to select the most profitable mode of operation for a specific solid-to-solid bioconversion.

REFERENCES

- Andersson E, Hahn-Hägerdal B. 1990. Bioconversions in aqueous two-phase systems. *Enzyme Microb Technol* 12:242-253.
- Ashina Y, Suto M. 1992. Development of an enzymatic process for manufacturing acrylamide; recent progress. In: Tanaka A, Tosa T and Kobayashi T, editors. *Industrial application of immobilized biocatalysts*. New York: Marcel Dekker, Inc. p 91-107.
- Bornscheuer UT, Yamane Y. 1994. Activity and stability of lipase in the solid phase glycerolysis of triolein. *Enzyme Microb Technol* 16:864-869.
- Cao L, Bornscheuer UT, Schmid RD. 1996. Lipase-catalysed solid phase synthesis of sugar esters. *Fett/Lipid* 98:332-335.
- Erbeldinger M, Xiongwei N, Halling PJ. 1998. Effect of water and enzyme concentration on thermolysin-catalysed solid-to-solid peptide synthesis. *Biotechnol Bioeng* 59:68-72.
- Freeman A, Woodley JM, Lilly MD. 1993. *In situ* product removal as a tool for bioprocessing. *BIO/TECHNOLOGY* 11:1007-1012.
- Kasche V. 1986. Mechanisms and yields in enzyme catalysed equilibrium and kinetically controlled synthesis of β -lactam antibiotics and other condensation products. *Enzyme Microb Technol* 8:4-16.
- Kasche V, Galunsky B. 1995. Enzyme catalysed biotransformations in aqueous two-phase systems with precipitated substrate and/or products. *Biotechnol Bioeng* 45:261-279.
- Kitahara K, Fukui S, Misawa M. 1960. Preparation of L-malate from fumarate by a new process "enzymatic transcrystallization". *J Gen Appl Microbiol* 6:108-116.
- Michielsen MJF, Frielink C, Wijffels RH, Tramper J, Beertink HH. 1999. Modeling solid-to-solid biocatalysis: integration of six consecutive steps. Submitted for publication.
- Miller TL. 1985. Steroid fermentation. *Compr Biotechnol* 3:297-318.
- Oyama K. 1992. The industrial production of aspartame. In: Collins AN, Sheldrake GN and Crosby J, editors. *Chirality in industry*. New York: John Wiley & Sons Ltd. p 173-182.
- Petkov DD, Stoineva IB. 1984. Enzyme peptide synthesis by iterative procedure in a nucleophile pool. *Tetrahedron Lett* 25:3751-3754.

- Takahashi S. 1986. Microbial production of D-*p*-hydroxyphenylglycine. *Prog Ind Microbiol* 24:269-279.
- Van der Werf MJ, Hartmans S, Van den Tweel WJJ. 1995. Effect of maleate counter-ion on malease activity: production of D-malate in a crystal-liquid two-phase system. *Enzyme Microb Technol* 17:430-436.
- Van 't Riet K, Tramper J. 1991. Basic bioreactor design. New York: Marcel Dekker, Inc. 465 p.
- Verm e M. 1995. Biocatalysis in non-conventional media: thermodynamics and kinetic aspects. PhD-thesis, Wageningen Agricultural University, Wageningen, The Netherlands.
- Watanabe S, Osawa T. 1966. Studies on the production of L-malic acid. Part I. Actions of detergents on the production of L-malic acid. *Nippon Kogei Nagaku Kaishi* 40:319-324.
- Wolff A, Zhu L, Wong YW, Straathof AJJ, Jongejan JA, Heijnen JJ. 1999. Understanding the influence of temperature change and cosolvent addition on conversion rate of enzymatic suspension reactions based on regime analysis. *Biotechnol Bioeng* 62:125-134.
- Zijlstra GM, De Gooijer CD, Tramper J. 1998. Extractive bioconversions in aqueous two-phase systems. *Curr Opin Biotechnol* 9:171-176.

CHAPTER 2

Dissolution kinetics of Ca-maleate crystals: evaluation for biotransformation reactor design

ABSTRACT

In order to develop a bioreactor for solid-to-solid conversions the biocatalytic conversion of solid Ca-maleate to solid Ca-D-malate is studied. The dissolution of Ca-maleate is the first step in this process and is described here. A kinetic model, based on the interfacial-barrier theory and the diffusion-layer theory, was developed which describes the increase in Ca-maleate concentration due to dissolution with the help of time-dependent parameters. According to the model two processes contribute to the dissolution of Ca-maleate·H₂O crystals: (1) the dissolution (and dissociation) reaction of Ca-maleate at the solid-liquid interface, characterized by a time-independent reaction rate coefficient, and (2) the transport of Ca²⁺ and maleate²⁻ across a boundary liquid film, characterized by a time-dependent mass-transfer rate coefficient. In addition, the surface of a crystal and the driving force are time-dependent variables. Since Ca-maleate·H₂O crystals are not uniform, a crystal-size distribution was also used in the model. The effects of stirring speed, temperature, pH, and initial Ca²⁺ concentration on the dissolution rate of Ca-maleate·H₂O crystals were determined experimentally in order to evaluate the model. The model fitted the data well ($R^2 > 0.97$). In order to determine whether the overall dissolution process was reaction or transport controlled, a method based on overall reaction and transport rates (per unit of driving force) was developed. This showed that the dissolution of Ca-maleate was reaction controlled. Temperature influenced the reaction rate coefficient the most; it ranged from $5.7 \cdot 10^{-6} \text{ m} \cdot \text{s}^{-1}$ at 10°C to $67 \cdot 10^{-6} \text{ m} \cdot \text{s}^{-1}$ at 60°C. The reaction rate coefficient was also influenced by the pH and the initial Ca²⁺ concentration, but, as expected, hardly by the stirring speed. Simplifying the model by omitting the time-dependent mass-transfer rate coefficient and by assuming uniform crystals, resulted in only slightly worse fits of the data with R^2 being at most 0.004 smaller.

INTRODUCTION

Much attention is paid to two-phase systems in biotechnology (Tramper et al., 1992), because bioconversions are often inhibited by high substrate and/or product concentrations (Van den Heuvel and Beftink, 1988; Van der Werf et al., 1993; Van der Werf et al., 1994). Inhibition in the reaction phase is minimized by extraction of substrate and/or product into a second phase, resulting in higher production rates per cubic meter of reactor volume (Van der Werf et al., 1994). In the case that only product is extracted, high product concentrations in one phase can be reached, which facilitates downstream processing. For hydrophobic compounds these advantages can be gained by the introduction of an organic solvent as an immiscible extraction phase. For hydrophilic compounds, similar advantages can be gained in systems with solid substrate and/or solid product as a second phase. On a commercial scale, bioconversions with solid substrate and/or product are already applied; examples are the production of aspartame (Oyama, 1992), acrylamide (Ashina and Suto, 1992), and L-malate (Kitahara et al., 1960; Watanabe and Osawa, 1966). However, a theoretical basis for process optimization is lacking (Van der Werf et al., 1994); it should consider mass-transfer rates between the liquid and solid phases and the kinetics of the biological reaction.

We are currently developing a model bioreactor for the conversion of solid substrate to solid product in a continuous process. The conversion of solid Ca-maleate to solid Ca-D-malate by permeabilized *Pseudomonas pseudoalcaligenes* (NCIMB 9867) was chosen as a model reaction as shown in Fig. 1.

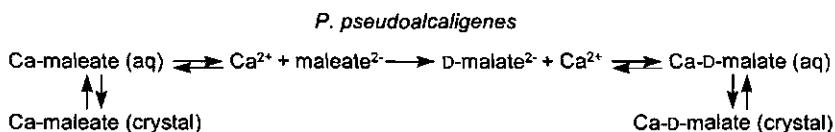


Figure 1 Reaction scheme for the conversion of solid Ca-maleate to solid Ca-D-malate by permeabilized *P. pseudoalcaligenes*.

In order to produce Ca-D-malate with a high purity and at a high production rate (per cubic meter of reactor), the dissolution of Ca-maleate, the conversion of maleate²⁻ to D-malate²⁻, and the crystallization of Ca-D-malate have to be adjusted relative to each other. Adjustment is possible by changing process conditions such

as pH, temperature, and Ca^{2+} concentration among others. The effect, however, of these changes on the dissolution of Ca-maleate, the conversion of maleate²⁻, and the crystallization of Ca-D-maleate is not yet known. In this work we focus on the dissolution kinetics of Ca-maleate and on the effects of process conditions on the dissolution. Process parameters that potentially influence the dissolution rate of Ca-maleate are stirring speed, temperature, pH, initial Ca^{2+} concentration, and crystal size.

THEORY

In order to characterize the dissolution rate of solids, two theories are used most frequently: (1) the interfacial-barrier theory, and (2) the diffusion-layer theory. Both theories are often used in combination to describe the dissolution process (Grant and Higuchi, 1990). In the model described in this work both theories were combined. This means that the increase in Ca-maleate concentration due to dissolution of Ca-maleate·H₂O crystals was attributed to two processes: (1) the dissolution (and dissociation) reaction of Ca-maleate at the solid-liquid interface, characterized by a time-independent reaction rate coefficient k_R , and (2) the transport of Ca^{2+} and maleate²⁻ across a boundary liquid film, characterized by a time-dependent mass-transfer rate coefficient $k_T(t)$. For process optimization and model simplification it is of importance to know whether the dissolution process is reaction or transport controlled. The model described in this paper can be used to determine this for uniform particles of all shapes in various kinds of equipment (agitated vessel, bubble column, etc.). The derivation of the model is given below.

In this work the increase in Ca-maleate concentration due to dissolution in a batch experiment was determined. The dissolution rate is defined as: $dC_l(t)/dt$; with $C_l(t)$ referring to the concentration of Ca-maleate at time t ; the subscript l refers to the bulk liquid phase.

As the decrease in crystal volume (due to dissolution) has to correspond with the increase in dissolved Ca-maleate, it can be shown by mass balance that:

$$N \cdot (V_c(0) - V_c(t)) \cdot \rho_c = V_l \cdot (C_l(t) - C_l(0)) \quad (1)$$

where N is the number of crystals, V is the volume, and ρ is the density. The subscript c refers to one crystal, $V(0)$ refers to the volume at $t=0$, and $C(0)$ refers to the concentration of Ca-maleate at $t=0$. Since Ca-maleate·H₂O crystals are needles, the volume $V_c(t)$ and surface area $A_c(t)$ of a Ca-maleate·H₂O crystal can be expressed as (Myerson and Ginde, 1993):

$$V_c(t) = \alpha \cdot L(t)^3 \quad (2)$$

$$A_c(t) = \beta \cdot L(t)^2 \quad (3)$$

with α and β denoting shape factors (see Table 2), and L denoting a characteristic dimension of the crystal (in this work, the breadth). The volume and surface area of the crystal are time-dependent variables, as the characteristic dimension of the crystal decreases due to dissolution of Ca-maleate·H₂O. Combination of eqs. (1), (2), and (3) and rewriting gives:

$$C_i(t) = \frac{N}{V_i} \cdot \alpha \cdot \rho_c \cdot (L(0)^3 - L(t)^3) + C_i(0) \quad (4)$$

Eq. (4) can be solved if the characteristic dimension of the crystal (L) is known as a function of time.

According to the interfacial-barrier theory and the diffusion-layer theory (Grant and Higuchi, 1990), the release of Ca-maleate (due to dissolution) from one crystal can be expressed as:

$$\frac{d}{dt} V_c(t) \cdot \rho_c = k_{ov}(t) \cdot A_c(t) \cdot (C_{sat} - C_i(t)) \quad (5)$$

with k_{ov} denoting a composite mass-transfer coefficient; the subscript sat refers to saturation. Combination of eqs. (2), (3), and (5) and some algebraic transformation results in:

$$\frac{dL(t)}{dt} = \frac{\beta \cdot k_{ov}(t)}{3 \cdot \alpha \cdot \rho_c} \cdot (C_{sat} - C_i(t)) \quad (6)$$

According to the interfacial-barrier theory and the diffusion-layer theory (Grant and Higuchi, 1990) two processes contribute to the dissolution of Ca-maleate: (1) the dissolution (and dissociation) reaction of Ca-maleate at the solid-liquid interface, and (2) the transport of Ca^{2+} and maleate²⁻ across a boundary liquid film. Ca-maleate is a strong electrolyte, which was assumed to dissociate instantaneously; Ca^{2+} and maleate²⁻ were assumed to be transported at the same rate. In this case $k_{ov}(t)$ can be expressed as (Grant and Higuchi, 1990):

$$\frac{1}{k_{ov}(t)} = \frac{1}{k_R} + \frac{1}{k_T(t)} \quad (7)$$

where k_R is the time-independent reaction rate coefficient and $k_T(t)$ is the time-dependent mass-transfer rate coefficient. The time-dependent mass-transfer rate coefficient can be expressed as (Sherwood et al., 1975):

$$k_T(t) = \frac{D}{h(t)} = \frac{Sh(t) \cdot D}{L(t)} \quad (8)$$

where D is the diffusion coefficient, $h(t)$ is the thickness of the boundary liquid film, and $Sh(t)$ is the Sherwood number. Eq. (8) shows that the thickness of the boundary liquid film $h(t)$ is dependent on the Sherwood number $Sh(t)$ and the characteristic dimension $L(t)$. The value of the diffusion coefficient D is expected to depend on temperature T according to (Chang, 1981):

$$D = \frac{k_B \cdot T}{6 \cdot \pi \cdot \eta \cdot r} \quad (9)$$

where k_B is the Boltzmann' constant, η the dynamic viscosity of the liquid phase, and r the molecular radius of Ca-maleate. In this work the dynamic viscosity η was approximated by the dynamic viscosity of water. By fitting data of the dynamic viscosity of water against temperature (given by Lide (1991)) with an Arrhenius type of equation, η can be expressed as a function of temperature (Hunik et al., 1994):

$$\eta = 6.021 \cdot 10^{-7} \cdot e^{\frac{18100}{R \cdot T}} \quad (10)$$

where R is the gas constant. If the needle-shaped crystals are approximated by granular crystals, the Sherwood number can be expressed as (Sano et al., 1974):

$$Sh(t) = \left[2 + 0.4 \cdot \left(\frac{\varepsilon \cdot L(t)^4}{\nu^3} \right)^{\frac{1}{4}} \cdot \left(\frac{\nu}{D} \right)^{\frac{1}{3}} \right] \cdot \phi_c \quad (11)$$

where ε is the energy input per unit mass of liquid phase, ν is the kinematic viscosity, and ϕ_c is Carman's surface factor. This equation for the Sherwood number was chosen, since it allows us to predict the effect of stirring speed on the time-dependent mass-transfer rate coefficient $k_r(t)$. The energy input per unit mass of liquid phase (ε) for a standard baffled stirred vessel ($T_v/d = 3$, with T_v as the vessel and d as the stirrer diameter; 4 symmetrically located baffles (width: 10% of the vessel diameter); fill height equal to T_v) can be expressed as (Sano et al., 1974):

$$\varepsilon = \frac{N_p \cdot d^5 \cdot n^3}{V_l} \quad (12)$$

with N_p as the power number and n the stirring speed. By approximating the needle-shaped crystals to granular crystals, Carman's surface factor can be expressed as (Sano et al., 1974):

$$\phi_c = \frac{6}{\rho_c \cdot S(t) \cdot L(t)} \quad (13)$$

with $S(t)$ as the specific surface area of the crystal. $S(t)$ can be expressed as:

$$S(t) = \frac{\beta}{\alpha \cdot L(t) \cdot \rho_c} \quad (14)$$

It should be noted that in this work the Sherwood equation derived by Sano et al. (1974) was used, as it is valid for a wide range of applications. However, in applications when a more specific Sherwood equation is known, it is recommended to incorporate this equation into the model instead of the version used here.

The model shows that the increase in Ca-maleate concentration depends (among others) on a characteristic dimension of the crystal $L(t)$. Since Ca-maleate crystals are needle-shaped and thus break easily, it was not possible to obtain monosized crystals. Therefore an experimentally determined crystal-size distribution was used in the model. In case of a crystal-size distribution, however, it is possible that size classes of small crystals dissolve reaction controlled, while size classes of large crystals dissolve transport controlled. In that case it is difficult to discriminate between the overall dissolution process being reaction or transport controlled. For that reason, a method based on overall reaction and transport rates (per unit of driving force) was developed.

MATERIALS AND METHODS

Materials

Ca-maleate·H₂O was purchased from Syncom (Groningen, the Netherlands; purity > 98%). Tris was obtained from Boehringer Mannheim GmbH, HCl from Riedel-de Haën, and CaCl₂·2H₂O from Merck.

Determination of crystal-size distribution

The initial crystal-size distribution was determined by image analysis (Magiscan image analysis system with GENERAL Image Analysis Software (GENIAS) from Applied Imaging; screen 262144 pixels; the breadth of the smallest object was characterized by at least 2.5 pixels). The object breadth (*OB*) is the minimum breadth of all possible orthogonal projections and was chosen as the characteristic dimension of the needle-shaped crystals ($L(t)$). The object length (*OL*) is the minimum length of all possible orthogonal projections. The breadth and length of in total more than a thousand crystals were determined.

Dissolution of Ca-maleate·H₂O crystals

The concentration of dissolved Ca-maleate was determined by conductance measurements, reflecting the total Ca-maleate concentration in solution: conductance increases when Ca-maleate dissolves and dissociates into Ca²⁺ and maleate²⁻.

To a 60-ml stirred vessel of standard geometry ($T_v/d = 3.33$, $H_{sb}/d = 1$, with H_{sb} the height of the stirrer above the bottom) with 4 symmetrically located baffles (width: 10% of the vessel diameter) and a six-blade turbine stirrer, 50 ml of a 500 mmol·dm⁻³ Tris-HCl buffer (of pH 6, 8 or 10) was added. The vessel was placed in a water bath at 10, 35 or 60°C and stirred at 1000, 1500 or 2000 rpm. High stirring speeds were chosen in order to keep the mixing time low in comparison to the dissolution time; at 1500 rpm the mixing time was about 3 seconds (data not shown). This was much smaller than the time to reach saturation at the conditions tested in this paper (see Figs. 3 to 6). The conductance was measured with a conductance cell (Mettler Toledo 980-K19/120) and a conductance meter (WTW LF 521). At $t=0$, 2.15 g of Ca-maleate·H₂O was added to the vessel and conductance was measured as a function of time. Note that a part of the Ca-maleate·H₂O crystals did not dissolve under these conditions because the saturation concentration was reached. The conditions at which the dissolution rate was measured are shown in Table 1. In order to get insight into the effects of stirring speed, temperature, pH, and initial Ca²⁺ concentration on the dissolution rate of Ca-maleate·H₂O crystals, each factor was varied at a low, high and intermediate level. In run 1 all factors were tested at their intermediate level. In run 2 to 6 only one factor was tested each time at a high or low setting, while the other factors were set at their intermediate level. In run 8 and run 9 CaCl₂ was added to the vessel (50 mmol·dm⁻³ and 100 mmol·dm⁻³, respectively) and mixed before Ca-maleate·H₂O was added; the other factors were set at their intermediate level. All measurements (runs) were carried out at least in duplicate and the results were averaged; the maximum standard deviation from the average was 18.6 mmol·dm⁻³.

The conductance profiles were converted into Ca-maleate concentration profiles with calibration curves of conductance vs. Ca-maleate concentration. Since conductance depends on temperature, the total amount of ions in solution, and the charge of the ions (Chang, 1981), a new calibration curve was determined whenever temperature, pH or initial Ca²⁺ concentration were changed.

The saturation concentrations determined from conductance data were checked by HPLC measurements, as described by Van der Werf et al. (1992). This resulted in similar saturation concentrations (data not shown).

Table 1 Process conditions at which the dissolution rate was measured.

Run	Process conditions			
	n (rpm)	T (°C)	pH	$[Ca^{2+}]$ (mmol·dm ⁻³)
1	1500	35	8	0
2	1000	35	8	0
3	2000	35	8	0
4	1500	10	8	0
5	1500	60	8	0
6	1500	35	6	0
7	1500	35	10	0
8	1500	35	8	50
9	1500	35	8	100

Data fitting

The parameters k_R and C_{sat} were determined by fitting the kinetic model through data of Ca-maleate concentration against time. Therefore eqs. (1) to (14) were implemented in the computer program STEM (Simulation Tool for Easy Modeling). In this program the dissolution rate was determined by three time-dependent parameters: (1) the overall mass-transfer coefficient $k_{ov}(t)$, (2) the surface area of a crystal $A_c(t)$, and (3) the driving force ($C_{sat} - C_i(t)$). The overall mass-transfer coefficient consists of a time-independent reaction rate coefficient k_R and a time-dependent mass-transfer rate coefficient $k_T(t)$. The time-independent reaction rate coefficient k_R and the saturation concentration C_{sat} were determined by fitting of the model through data of C_i against t using a simplex method (Nelder and Mead, 1965) in combination with the method of Gear (1971), while the time-dependent mass-transfer rate coefficient $k_T(t)$, the surface area of a crystal $A_c(t)$, and the concentration of Ca-maleate $C_i(t)$ were calculated during fitting as described before (see eqs. (8), (3), and (4), respectively). Although the saturation concentration C_{sat} was known from the measurements, it was used as a fit parameter, because small deviations of C_{sat} had a great influence on R^2 and at some conditions the saturation concentration was not reached within 300 seconds. In general, the fitted values for C_{sat} were in good agreement with the measured saturation concentrations. A crystal-size distribution with nine size classes was used in the program. For this reason eq. (4) was rewritten as:

$$C_i(t) = \sum_{i=1}^9 \left[\frac{N_i}{V_i} \cdot \alpha \cdot \rho_c \cdot (L_i(0)^3 - L_i(t)^3) \right] + C_i(0) \quad (15)$$

with i referring to the class number. In order to calculate $C_i(t)$, eqs. (6) to (14) were solved simultaneously for each size class of crystals, as $k_T(t)$, $A_c(t)$, and $V_c(t)$ differ for each size class of crystals. When the characteristic dimension of a class of crystals was calculated to be negative by eqs. (6) to (14), it was automatically set at zero from that moment on, as the crystals from that crystal size have been dissolved completely at that moment. The known or estimated parameters used in the program are shown in Table 2.

Table 2 Parameter values for determination of k_R and C_{sat} .

Parameters of crystal-size distribution with nine classes			
N_1 (-) ^{a)}	$6.97 \cdot 10^6$	$L(0)_1$ (m) ^{a)}	$2.5 \cdot 10^{-6}$
N_2 (-) ^{a)}	$1.11 \cdot 10^7$	$L(0)_2$ (m) ^{a)}	$7.5 \cdot 10^{-6}$
N_3 (-) ^{a)}	$1.40 \cdot 10^7$	$L(0)_3$ (m) ^{a)}	$12.5 \cdot 10^{-6}$
N_4 (-) ^{a)}	$1.64 \cdot 10^7$	$L(0)_4$ (m) ^{a)}	$17.5 \cdot 10^{-6}$
N_5 (-) ^{a)}	$1.24 \cdot 10^7$	$L(0)_5$ (m) ^{a)}	$22.5 \cdot 10^{-6}$
N_6 (-) ^{a)}	$3.13 \cdot 10^6$	$L(0)_6$ (m) ^{a)}	$27.5 \cdot 10^{-6}$
N_7 (-) ^{a)}	$2.12 \cdot 10^6$	$L(0)_7$ (m) ^{a)}	$32.5 \cdot 10^{-6}$
N_8 (-) ^{a)}	$8.06 \cdot 10^5$	$L(0)_8$ (m) ^{a)}	$37.5 \cdot 10^{-6}$
N_9 (-) ^{a)}	$8.06 \cdot 10^5$	$L(0)_9$ (m) ^{a)}	$42.5 \cdot 10^{-6}$
Parameters of the solid phase		Parameters of the liquid phase	
ρ_c (kg·m ⁻³) ^{b)}	1677	ρ_l (kg·m ⁻³) ^{d)}	1000
α (-) ^{a)}	2.54	V_l (m ³)	$50 \cdot 10^{-6}$
β (-) ^{a)}	11.75	$C_l(0)$ (kg·m ⁻³)	0
r (m) ^{c)}	$3 \cdot 10^{-10}$		
Other parameters			
k_B (N·m·K ⁻¹) ^{d)}	$1.38 \cdot 10^{-23}$	d (m)	$12 \cdot 10^{-3}$
N_p (-) ^{e)}	1.4		

^{a)} determined from crystal-size distribution, assuming that the needle-shaped crystals were cylindrical; object length (OL)/object breadth (OB) was determined to be 3.24 and constant.

^{b)} determined with a piknometer.

^{c)} estimated from bond lengths and angles, given by Lide (1991).

^{d)} from Lide (1991).

^{e)} from Bates et al. (1963).

RESULTS AND DISCUSSION

Determination of crystal-size distribution

The initial crystal-size distribution of $\text{Ca-maleate}\cdot\text{H}_2\text{O}$, as determined by image analysis, is shown in Fig. 2. The breadth of a crystal (OB) was used as the characteristic dimension of the crystal ($L(t)$).

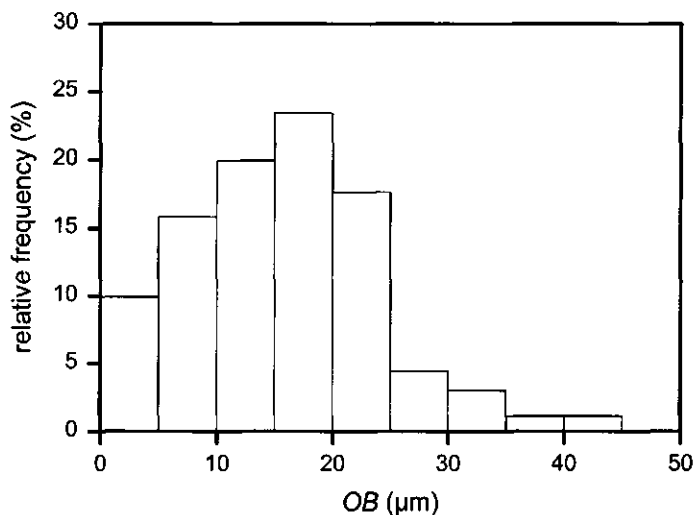


Figure 2 Crystal-size distribution of $\text{Ca-maleate}\cdot\text{H}_2\text{O}$ with object breadth OB as characteristic dimension of the needle-shaped crystals; the total number of crystals was 1136.

Dissolution of $\text{Ca-maleate}\cdot\text{H}_2\text{O}$ crystals

Effect of stirring speed

The effect of stirring speed on the dissolution of $\text{Ca-maleate}\cdot\text{H}_2\text{O}$ crystals is shown in Fig. 3, which indicates that the initial slopes of the curves were equal. This means that the dissolution rates at stirring speeds of 1000 rpm, 1500 rpm, and 2000 rpm were equal. The model could be fitted well through the data (see Fig. 3 and Table 3), which indicates that the proposed model, based on a dissolution reaction and mass transfer, describes the process well.

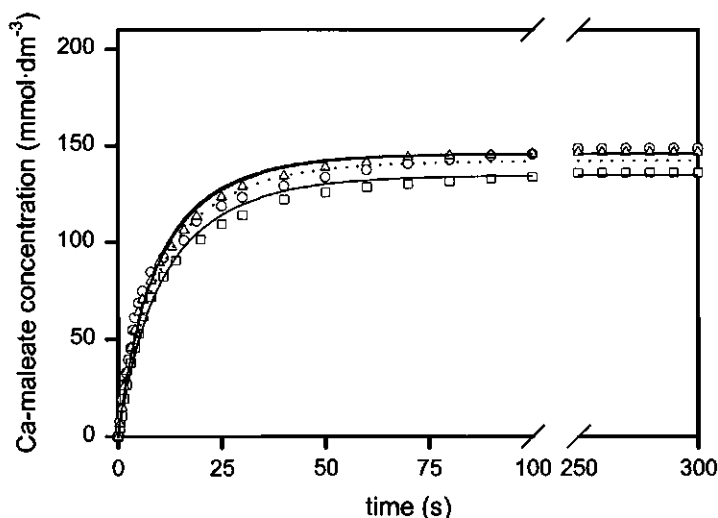


Figure 3 The effect of stirring speed on the dissolution of Ca-maleate- H_2O crystals at 35°C , pH 8, and $0 \text{ mmol}\cdot\text{dm}^{-3} \text{ CaCl}_2$; measurements at 1000 rpm (O), 1500 rpm (\square), and 2000 rpm (Δ), and corresponding fits with the model (—). The dotted curve represents a simulation with the model at 500 rpm, with $k_R = 25 \cdot 10^{-6} \text{ m}\cdot\text{s}^{-1}$ and $C_{\text{sat}} = 142 \text{ mmol}\cdot\text{dm}^{-3}$ (the averages of k_R and C_{sat} as a function of stirring speed).

In contrast to changes in the temperature, the pH, and the initial Ca^{2+} concentration, stirring significantly increases the mass-transfer rate coefficient $k_T(t)$, since it reduces the thickness of the boundary liquid film (see eq. (8); Carstensen, 1974). In the interfacial-barrier theory it is assumed that the solid-liquid interface is surrounded by an infinitesimally thin boundary layer. This means that the reaction rate coefficient k_R is not influenced by the stirring speed (Grant and Higuchi, 1990). As no effect of the stirring speed on the overall dissolution rate was found (see Fig. 3), and only $k_T(t)$ is dependent on the stirring speed according to eq. (12) and k_R not (see Fig. 3 and Table 3), the dissolution of Ca-maleate- H_2O crystals was probably reaction controlled at stirring speeds ranging from 1000 to 2000 rpm. As would be expected, the saturation concentration was not influenced by the stirring speed.

High stirring speeds (from 1000 to 2000 rpm) were chosen in order to minimize mixing times. For practical applications, however, a continuous set-up will be used. In that case the stirring speed will probably be lower in order to reduce formation of nuclei for crystallization due to crystal fragmentation (Myerson and Ginde, 1993). For that reason, the dissolution rate was calculated at 500 rpm with $k_R = 25 \cdot 10^{-6} \text{ m}\cdot\text{s}^{-1}$

and $C_{\text{sat}} = 142 \text{ mmol}\cdot\text{dm}^{-3}$ (the averages of k_R and C_{sat} as a function of stirring speed), since k_R and C_{sat} are not influenced by the stirring speed. The time-dependent mass-transfer rate coefficient $k_r(t)$ at 500 rpm was calculated for each size class of crystals with eqs. (8) to (14). Fig. 3 shows that the dissolution rate(s) of Ca-maleate- H_2O crystals at 500 rpm would be equal to the dissolution rates at 1000, 1500, and 2000 rpm. This means that the dissolution process at 500 rpm would still be reaction controlled.

Table 3 The fit parameters k_R and C_{sat} (with 95% confidence intervals) as a function of the process parameters n , T , pH, and $[\text{Ca}^{2+}]$, and the R^2 values of each fit; upon varying one process parameter, the other process parameters were set at their level of run 1 in Table 1.

Process parameters	Values of process parameters	R^2	k_R ($\text{m}\cdot\text{s}^{-1}$)	C_{sat} ($\text{mmol}\cdot\text{dm}^{-3}$)	$k_R C_{\text{sat}}$ ($\text{mmol}\cdot\text{m}^{-2}\cdot\text{s}^{-1}$)
n (rpm)	1000	0.989	$27\cdot 10^{-6} \pm 3.6\cdot 10^{-6}$	146 ± 2.82	3.9
	1500	0.997	$22\cdot 10^{-6} \pm 1.6\cdot 10^{-6}$	135 ± 1.45	3.0
	2000	0.997	$25\cdot 10^{-6} \pm 1.7\cdot 10^{-6}$	146 ± 1.35	3.7
T ($^{\circ}\text{C}$)	10	0.981	$5.7\cdot 10^{-6} \pm 1.1\cdot 10^{-6}$	190 ± 9.76	1.1
	35	0.997	$22\cdot 10^{-6} \pm 1.6\cdot 10^{-6}$	135 ± 1.45	3.0
	60	0.999	$67\cdot 10^{-6} \pm 2.2\cdot 10^{-6}$	108 ± 0.42	7.2
pH	6	0.992	$26\cdot 10^{-6} \pm 3.3\cdot 10^{-6}$	142 ± 2.10	3.7
	8	0.997	$22\cdot 10^{-6} \pm 1.6\cdot 10^{-6}$	135 ± 1.45	3.0
	10	0.974	$15\cdot 10^{-6} \pm 2.4\cdot 10^{-6}$	188 ± 6.45	2.8
$[\text{Ca}^{2+}]$ ($\text{mmol}\cdot\text{dm}^{-3}$)	0	0.997	$22\cdot 10^{-6} \pm 1.6\cdot 10^{-6}$	135 ± 1.45	3.0
	50	0.999	$25\cdot 10^{-6} \pm 9.9\cdot 10^{-7}$	122 ± 0.70	3.1
	100	0.993	$35\cdot 10^{-6} \pm 3.6\cdot 10^{-6}$	99.4 ± 1.30	3.5

Effect of temperature

The effect of temperature on the dissolution of Ca-maleate-H₂O crystals is shown in Fig. 4, which indicates that the initial slope of the curve increased, when temperature increased from 10 to 60°C. This means that increasing the temperature from 10 to 60°C, resulted in higher dissolution rates. In the model, the effect of temperature on $k_r(t)$ was incorporated by eqs. (9) and (10). The model could be fitted well through the data (see Fig. 4 and Table 3). As expected, k_r increased with temperature (see Table 3). In contrast to data reported by Lide (1991) and Linke (1958), the saturation concentration of Ca-maleate decreased with temperature (see Fig. 4 and Table 3). Such an effect has also been found for certain other compounds (Martell and Smith, 1979).

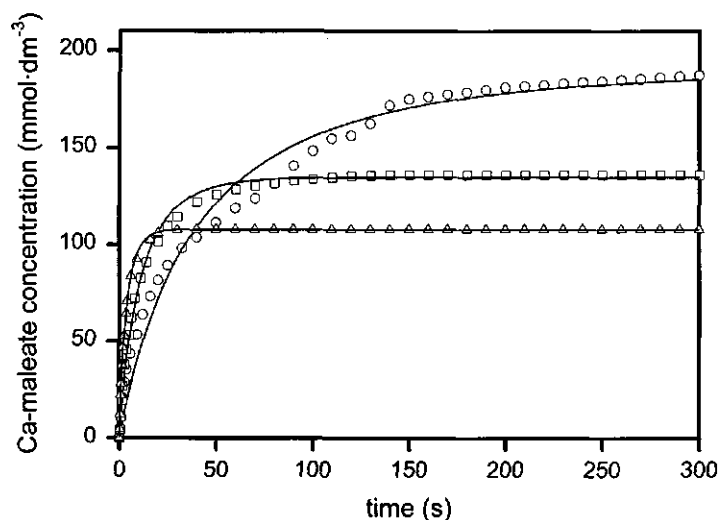


Figure 4 The effect of temperature on the dissolution of Ca-maleate-H₂O crystals at 1500 rpm, pH 8, and 0 mmol·dm⁻³ CaCl₂; measurements at 10°C (○), 35°C (□), and 60°C (Δ), and corresponding fits with the model (—).

The overall equation for the dissolution of Ca-maleate is:



The solubility product of Ca-maleate is defined as:

$$K_{sp} = [Ca^{2+}] \cdot [maleate^{2-}] \quad (16)$$

According to Van 't Hoff (Chang, 1981):

$$\ln K_{sp} = -\frac{\Delta H^\circ}{R \cdot T} + \frac{\Delta S^\circ}{R} \quad (17)$$

with ΔH° the enthalpy change, and ΔS° the entropy change. Assuming ΔH° and ΔS° to be independent of temperature, ΔH° and ΔS° were calculated from the data in Fig. 4 as: $\Delta H^\circ = -17 \text{ kJ} \cdot \text{mol}^{-1}$, and $\Delta S^\circ = -89 \text{ J} \cdot \text{mol}^{-1} \cdot \text{K}^{-1}$.

In the case of stirring speed it was possible to discriminate between a reaction- or transport-controlled process, as the stirring speed only influences $k_T(t)$, and not k_R and C_{sat} . Temperature, pH, and initial Ca^{2+} concentration, however, could influence two or more of the above-mentioned parameters. This makes it hard to discriminate between the overall dissolution process being reaction or transport controlled in those cases. For this reason, a method based on overall reaction and transport rates (per unit of driving force) was developed (see below).

Effect of pH

The effect of pH on the dissolution of Ca-maleate·H₂O crystals is shown in Fig. 5, which indicates that the initial slopes of the curves were similar. This means that the dissolution rates at pH 6, pH 8, and pH 10 were (almost) equal. The model could be fitted well through the data, though a little less accurately at pH 10 (see Fig. 5 and Table 3). The reaction rate coefficient k_R was found to decrease with pH (see Table 3). The saturation concentration at pH 10 was much higher than at pH 8 (see Fig. 5 and Table 3). This could be due to formation of $CaOH^+$ and $Ca(OH)_2$ at pH 10 ($K = [CaOH^+]/[Ca^{2+}] \cdot [OH^-]$: $pK = 0.64$ at 25°C , $I = 3.0$; $pK = 1.3 \pm 0.1$ at 25°C , $I = 0$ (Martell and Smith, 1981)). When these compounds were formed, the ionic product of the Ca^{2+} and maleate²⁻ concentration at pH 10 was smaller than the solubility product K_{sp} (see eq. (16)). As a consequence more Ca-maleate could be dissolved, if the solubility product K_{sp} is assumed to be independent of pH. At pH 6 maleate in monoanionic form was formed ($pK_a = 6.07$ (Lide, 1991)). However, the saturation concentration at pH 6 was hardly different from the saturation concentration at pH 8 (see Fig. 5 and Table 3). This means that the effect of formation of maleate in

monoanionic form (at pH 6) on the saturation concentration of Ca-maleate was apparently small.

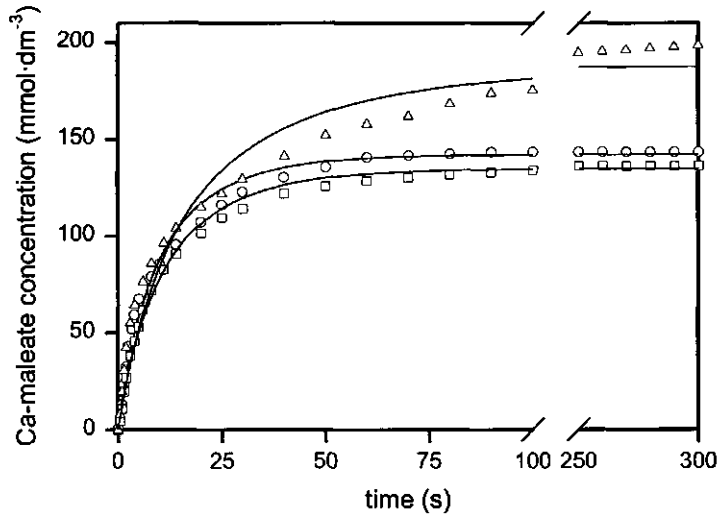


Figure 5 The effect of pH on the dissolution of Ca-maleate-H₂O crystals at 1500 rpm, 35°C, and 0 mmol·dm⁻³ CaCl₂; measurements at pH 6 (O), pH 8 (□), and pH 10 (Δ), and corresponding fits with the model (—).

Effect of initial Ca²⁺ concentration

The effect of the initial Ca²⁺ concentration on the dissolution of Ca-maleate-H₂O crystals is shown in Fig. 6, which indicates that the initial slopes of the curves were equal. This means that the dissolution rates at initial CaCl₂ concentrations of 0, 50, and 100 mmol·dm⁻³ were equal. The model could again be fitted well through the data (see Fig. 6 and Table 3). The reaction rate coefficient k_R was found to increase with initial Ca²⁺ concentration (see Table 3). The saturation concentration of Ca-maleate decreased when the initial Ca²⁺ concentration increased from 0 to 100 mmol·dm⁻³ (see Fig. 6 and Table 3). This was due to the fact that the solubility product was reached at a lower concentration of Ca-maleate, when initially more Ca²⁺ was present (see eq. (16)), assuming the solubility product to be constant.

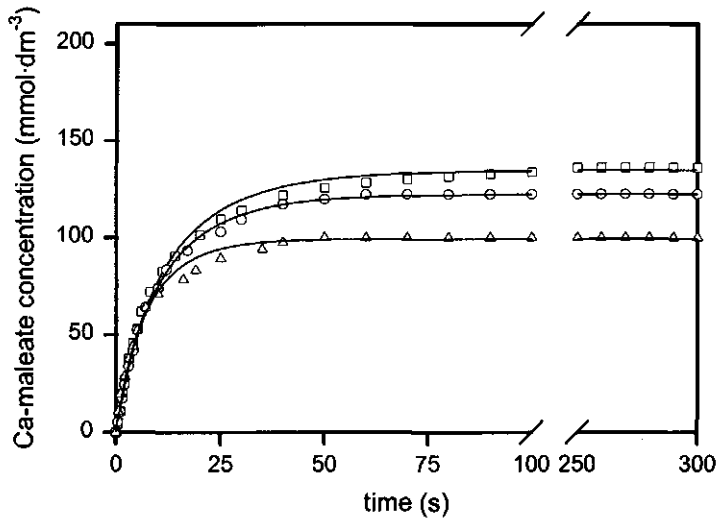


Figure 6 The effect of initial Ca^{2+} concentration on the dissolution of $\text{Ca-maleate}\cdot\text{H}_2\text{O}$ crystals at 1500 rpm, 35°C , and pH 8; measurements at $[\text{Ca}^{2+}]=0$ mM (\square), $[\text{Ca}^{2+}]=50$ mM (\circ), and $[\text{Ca}^{2+}]=100$ mM (\triangle), and corresponding fits with the model (—).

Reaction-controlled dissolution

At a stirring speed of 1000 rpm or greater the dissolution of $\text{Ca-maleate}\cdot\text{H}_2\text{O}$ crystals was assumed to be reaction controlled (at $T=35^\circ\text{C}$, pH 8, and $0\text{ mmol}\cdot\text{dm}^{-3}\text{ CaCl}_2$). At other conditions tested in this work, it will be rather straightforward to determine whether the dissolution process is reaction controlled or transport controlled, if k_R is smaller or bigger than all $k_T(t)$ values for all size classes of crystals. In case k_R is smaller (or bigger) than $k_T(t)$ for only a part of all (size) classes, it is difficult to discriminate between the overall dissolution process being reaction controlled or transport controlled. Therefore the mass transfer was characterized by an overall $k_R A$ and an overall $k_T A$ value. The overall $k_R A$ value was defined as:

$$\sum_{i=1}^9 k_R \cdot A_{c,i}(t) \cdot N_i$$

with i referring to the class number. This value is the overall reaction rate at the solid-liquid interface per unit of driving force. In this case the transport across the

boundary liquid film was assumed not to be rate-limiting. The overall $k_T A$ value was defined as:

$$\sum_{i=1}^g k_{T,i}(t) \cdot A_{c,i}(t) \cdot N_i$$

This value is the overall mass-transfer rate across the boundary liquid film per unit of driving force. In this case the reaction at the solid-liquid interface was assumed not to be rate-limiting. As the driving force ($C_{\text{sat}} - C_i(t)$) for both processes (reaction and transport) is equal, the difference between the two overall kA values determined whether the overall dissolution process was reaction or transport controlled; the smallest overall kA value controls the rate of the overall dissolution process. Both overall kA values were determined as a function of time at $T = 60^\circ\text{C}$, 1500 rpm, pH 8, and $0 \text{ mmol}\cdot\text{dm}^{-3} \text{ CaCl}_2$ (see Fig. 7 and Table 4). At these conditions the smallest relative difference between k_R and $k_{T,i}(t)$ existed, since the increase of $k_R/k_T(t)$ with temperature was slightly greater than the increase of k_R with Ca^{2+} concentration; $k_T(t)$ is not dependent on Ca^{2+} concentration (see Theory). As even at these conditions the overall $k_R A$ value was about 7 times smaller than the overall $k_T A$ value (see Fig. 7 and Table 4), it can be concluded that the dissolution of Ca-maleate·H₂O was reaction controlled at all process conditions applied in this work.

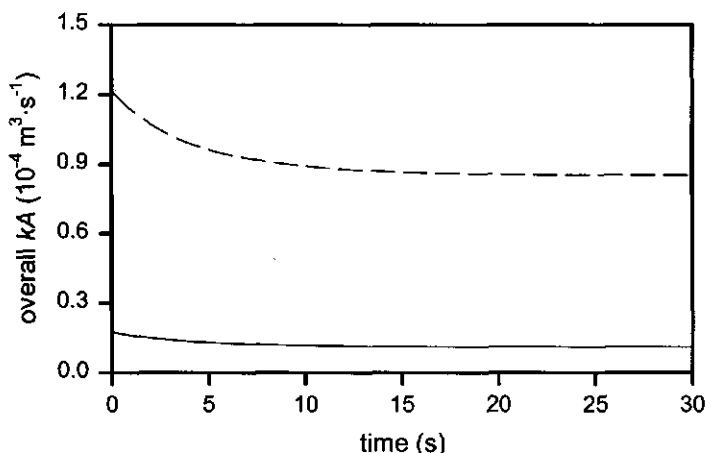


Figure 7 Overall $k_R A$ (—) and $k_T A$ (---) values as a function of time at $T=60^\circ\text{C}$, 1500 rpm, pH 8, and $0 \text{ mmol}\cdot\text{dm}^{-3} \text{ CaCl}_2$.

Table 4 Effect of Sherwood number on the overall kA values at $t=300$ s, $T=60^\circ\text{C}$, 1500 rpm, pH 8, and $0\text{ mmol}\cdot\text{dm}^{-3}\text{ CaCl}_2$.

Sherwood number	$\sum_{i=1}^9 k_R \cdot A_{c,i}(300) \cdot N_i$	$\sum_{i=1}^9 k_{T,i}(300) \cdot A_{c,i}(300) \cdot N_i$
Sano et al. (1974)	$1.1 \cdot 10^{-5}$	$8.0 \cdot 10^{-5}$
Ranz and Marshall (1952)	$9.5 \cdot 10^{-6}$	$1.1 \cdot 10^{-2}$

For $k_T(t)$ calculations the Sherwood number derived by Sano et al. (1974) was used. In the literature many Sherwood equations are given (Levins and Glastonbury, 1972; Ranz and Marshall, 1952; Tournié et al., 1979). Because the Sherwood equation used in the model, has a standard deviation of 30.8% according to Sano et al. (1974), an alternative equation (Ranz and Marshall, 1952) was tested as well; the overall kA values were determined again at $T = 60^\circ\text{C}$, 1500 rpm, pH 8, and $0\text{ mmol}\cdot\text{dm}^{-3}\text{ CaCl}_2$ (see Table 4). Table 4 shows that the overall $k_R A$ value would also be much smaller than the overall $k_T A$ value, when the Sherwood equation derived by Ranz and Marshall (1952) was used. This means that the dissolution process would still be reaction controlled.

Since the dissolution of $\text{Ca-maleate}\cdot\text{H}_2\text{O}$ was reaction controlled, the model was simplified by replacing $k_{ov}(t)$ in eq. (5) by k_R . This simplified model was tested by fitting the data at all conditions again. This resulted in fits with (almost) exactly the same R^2 values. This means that the difference between k_R and $k_T(t)$ was big, and supports our previous conclusion that the dissolution of $\text{Ca-maleate}\cdot\text{H}_2\text{O}$ crystals was reaction controlled at the conditions tested in this work. As the difference between k_R and $k_T(t)$ was big, $k_R \cdot C_{\text{sat}}$ can be used to characterize the dissolution rate at a known total surface area of the crystals and $C_l(0) = 0$ (see eq. (5)). Table 3 shows that $k_R \cdot C_{\text{sat}}$, and thus the dissolution rate, would be maximal at 60°C , pH 6, and a Ca^{2+} concentration of $100\text{ mmol}\cdot\text{dm}^{-3}$.

The model was simplified further by approximating the crystal-size distribution of Fig. 2 by uniform crystals with a characteristic dimension $L(t)$ corresponding to the average volume of all crystals. This was tested again by fitting the data at all conditions. This resulted in fits with slightly smaller R^2 values (difference: 0.004 or less). So for modeling the dissolution rate of $\text{Ca-maleate}\cdot\text{H}_2\text{O}$ crystals at the conditions tested in this paper, a model containing only the time-independent reaction rate coefficient k_R and uniform crystals with a crystal size corresponding to the average volume of all crystals, is probably satisfactory.

CONCLUSIONS

A kinetic model based on the interfacial-barrier theory and the diffusion-layer theory, containing time-dependent parameters and describing the increase of Ca-maleate concentration due to dissolution, fitted the experimental data well ($R^2 > 0.97$). A method, based on overall $k_R A$ and overall $k_T A$ values, was developed in order to determine whether the overall dissolution process is reaction or transport controlled in case the crystals are not uniform. This revealed that the dissolution of Ca-maleate·H₂O crystals was a reaction-controlled process for all the conditions tested in this work. Temperature influenced the reaction rate coefficient k_R the most; k_R ranged from $5.7 \cdot 10^{-6} \text{ m} \cdot \text{s}^{-1}$ at 10°C to $67 \cdot 10^{-6} \text{ m} \cdot \text{s}^{-1}$ at 60°C. The reaction rate coefficient k_R was also influenced by the pH and the initial Ca^{2+} concentration; it decreased with pH and increased with the initial Ca^{2+} concentration. As expected, k_R was hardly influenced by the stirring speed. Temperature, pH, and initial Ca^{2+} concentration also influenced the saturation concentration of Ca-maleate. Simplifying the model by approximating the time-dependent overall rate coefficient $k_{ov}(t)$ by the time-independent reaction rate coefficient k_R and simplifying the crystal-size distribution to uniform crystals, resulted in only slightly worse fits of the data at the conditions tested in this paper; R^2 differed 0.004 or less. So, in case the dissolution of Ca-maleate is the rate-limiting process in the conversion of solid Ca-maleate to solid Ca-D-malate, the overall Ca-D-malate production rate would be maximal at 60°C, pH 6, and a Ca^{2+} concentration of $100 \text{ mmol} \cdot \text{dm}^{-3}$.

ACKNOWLEDGEMENTS

This work was financially supported by the Ministry of Economic Affairs, the Ministry of Education, Culture and Science, the Ministry of Agriculture, Nature Management and Fishery in the framework of an industrially relevant research programme of the Netherlands Association of Biotechnology Centres in the Netherlands (ABON).

NOMENCLATURE

A	surface area	(m^2)
C	concentration	($\text{mmol}\cdot\text{dm}^{-3}$)
$C(0)$	concentration at $t=0$	($\text{mmol}\cdot\text{dm}^{-3}$)
D	diffusion coefficient	($\text{m}^2\cdot\text{s}^{-1}$)
d	stirrer diameter	(m)
H_{sb}	height of the stirrer above the vessel bottom	(m)
ΔH°	enthalpy change	($\text{kJ}\cdot\text{mol}^{-1}$)
h	thickness of the boundary liquid film	(m)
I	ionic strength	($\text{mol}\cdot\text{kg}^{-1}$)
K_{sp}	solubility product	($\text{mmol}^2\cdot\text{dm}^{-6}$)
k	mass-transfer coefficient	($\text{m}\cdot\text{s}^{-1}$)
k_{B}	Boltzmann' constant	($\text{N}\cdot\text{m}\cdot\text{K}^{-1}$)
L	characteristic dimension of the crystal	(m)
N	number of crystals	(-)
N_{p}	power number	(-)
n	stirring speed	(s^{-1})
OB	object breadth	(m)
OL	object length	(m)
R	gas constant	($8.314\text{ J}\cdot\text{mol}^{-1}\cdot\text{K}^{-1}$)
r	molecular radius of Ca-maleate	(m)
S	specific surface area	($\text{m}^2\cdot\text{kg}^{-1}$)
Sh	Sherwood number	(-)
ΔS°	entropy change	($\text{J}\cdot\text{mol}^{-1}\cdot\text{K}^{-1}$)
T	absolute temperature	(K)
T_{v}	vessel diameter	(m)
t	time	(s)
V	volume	(m^3)
$V(0)$	volume at $t=0$	(m^3)

Greek symbols

α	(volume) shape factor	(-)
β	(surface) shape factor	(-)
η	dynamic viscosity	($\text{N}\cdot\text{s}\cdot\text{m}^{-2}$)

ε	energy input per kg liquid phase	(W·kg ⁻¹)
ϕ_c	Carman's surface factor	(-)
ν	kinematic viscosity	(m ² ·s ⁻¹)
ρ	density	(kg·m ⁻³)

Indices

c	one crystal
i	class number
l	liquid phase or bulk solution
ov	overall
R	reaction at the solid-liquid interface
sat	saturation
T	transport across a boundary liquid film

REFERENCES

- Ashina Y, Suto M. 1992. Development of an enzymatic process for manufacturing acrylamide; recent progress. In: Tanaka A, Tosa T and Kobayashi T, editors. Industrial application of immobilized biocatalysts. New York: Marcel Dekker, Inc. p 91-107.
- Bates RL, Fondy PL, Corpstein RR. 1963. An examination of some geometric parameters of impeller power. Ind Eng Chem, Proc Des & Dev 2:310-314.
- Carstensen JT. 1974. Theories of dissolution - single particulate systems. In: Leeson LJ and Carstensen JT, editors. Dissolution Technology. Washington, D.C.: American Pharmaceutical Association. p 1-28.
- Chang RM. 1981. Physical chemistry with applications to biological systems. New York: MacMillan publishing Co., Inc. 659p.
- Gear CW. 1971. The automatic integration of ordinary differential equations. Communications of the ACM 3:176-179.
- Grant DWJ, Higuchi T. 1990. Dissolution rates of solids. In: Solubility behaviour of organic compounds. New York: John Wiley & Sons, Inc. p 475-541.
- Hunik JH, Tramper J, Wijffels RH. 1994. A strategy to scale up nitrification processes with immobilized cells of *Nitrosomonas europaea* and *Nitrobacter agilis*. Bioprocess Eng 11:73-82.

- Kitahara K, Fukui S, Misawa M. 1960. Preparation of L-malate from fumarate by a new process "enzymatic transcrystallization". *J Gen Appl Microbiol* 6:108-116.
- Levins DM, Glastonbury JR. 1972. Application of Kolmogoroff's theory to particle-liquid mass transfer in agitated vessels. *Chem Engng Sci* 27:537-543.
- Lide DR, editor. 1991. *CRC Handbook of chemistry and physics*, 72th edition. Boca Raton: CRC Press, Inc.
- Linke WF, editor. 1958. p 513. Solubilities of inorganic and metal-organic compounds, a compilation of solubility data from the periodical literature. Volume I, fourth edition. New Jersey, Princeton: D. van Nostrand Company, Inc.
- Martell AE, Smith RM, editors. 1979. *Critical stability constants*, Volume 3: Other organic ligands, 2nd edition. New York: Plenum Press.
- Martell AE, Smith RM, editors. 1981. p 1. *Critical stability constants*, Volume 4: Inorganic complexes, 2nd edition. New York: Plenum Press.
- Myerson AS, Ginde R. 1993. Crystals, crystal growth, and nucleation. In: Myerson AS, editor. *Handbook of industrial crystallization*. Boston: Butterworth-Heinemann. p 33-63.
- Nelder JA, Mead R. 1965. A simplex method for function minimization. *Computer J* 7:308-313.
- Oyama K. 1992. The industrial production of aspartame. In: Collins AN, Sheldrake GN and Crosby J, editors. *Chirality in industry*. New York: John Wiley & Sons Ltd. p 173-182.
- Ranz WE, Marshall WR Jr. 1952. Evaporation from drops. *Chem Eng Prog* 48:141-146, 173-180.
- Sano Y, Yamaguchi N, Adachi T. 1974. Mass transfer coefficients for suspended particles in agitated vessels and bubble columns. *J Chem Eng Jpn* 7:255-261.
- Sherwood TK, Pigford RL, Wilke CR. 1975. Mass transfer at a phase boundary. In: Clark BJ and Mousel JW, editors. *Chemical engineering series, mass transfer*, 1st edition. New York: McGraw-Hill, Inc. p 199-254.
- Tournié P, Laguerie C, Couderc JP. 1979. Correlations for mass transfer between fluidized spheres and a liquid. *Chem Engng Sci* 34:1247-1255.
- Tramper J, Vermüe MH, Beffink HH, Von Stockar U, editors. 1992. *Biocatalysis in non-conventional media*. Amsterdam: Elsevier Science Publ. 763 p.
- Van den Heuvel JC, Beffink HH. 1988. Kinetic effects of simultaneous inhibition by substrate and product. *Biotechnol Bioeng* 31:718-724.

- Van der Werf MJ, Van den Tweel WJJ, Hartmans S. 1993. Purification and characterization of maleate hydratase from *Pseudomonas pseudoalcaligenes*. *Appl Environ Microbiol* 59:2823-2829.
- Van der Werf MJ, Hartmans S, Van den Tweel WJJ. 1994. Effect of maleate counter-ion on malease activity: production of D-malate in a crystal-liquid two-phase system. *Enzyme Microb Technol* 17:430-436.
- Van der Werf MJ, Van den Tweel WJJ, Hartmans S. 1992. Screening for microorganisms producing D-malate from maleate. *Appl Environ Microbiol* 58:2854-2860.
- Watanabe S, Osawa T. 1966. Studies on the production of L-malic acid. Part I. Actions of detergents on the production of L-malic acid. *Nippon Kogei Nagaku Kaishi* 40:319-324.

CHAPTER 3

Kinetics of D-malate production by permeabilized *Pseudomonas pseudoalcaligenes*

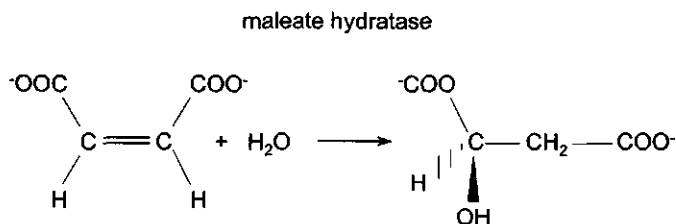
ABSTRACT

The kinetics of D-malate production from maleate by permeabilized *Pseudomonas pseudoalcaligenes* was described by assuming competitive product inhibition, in addition to biocatalyst inactivation. The kinetic parameters for conversion and inactivation were determined from a simultaneous fit of two independent data sets of substrate concentration vs. time. In order to select appropriate conditions, the effects of pH and temperature on the initial substrate conversion rate (excluding inactivation) were studied first. The pH optimum ranged from pH 7 to 8. The temperature optimum was approximately 45°C. The conversion parameters increased with pH and/or temperature. The first-order inactivation rate constant depended on temperature only; it increased strongly between 25 and 35°C.

INTRODUCTION

D-malate is an optically active α -hydroxy acid. In contrast to L-malate, it sporadically occurs in nature (Hahn and Nahrstedt). However, it is becoming a valuable source of chirality for various applications in organic chemistry (Van der Werf, 1994). It is applied as a chiral synthon (building block in organic syntheses) for the synthesis of various compounds (Crosby, 1992; Seebach and Hungerbühler, 1980), like pharmaceuticals (Almeida et al., 1992; Bailly et al., 1991; Barth et al., 1990; Shiuey et al., 1988; Sleevi et al., 1991), antibiotics (Miller et al., 1982; Tanner and Somfai, 1988), D- and L-carnitine (Bellamy et al., 1990; Rajashekhar and Kaiser, 1985), the pheromone (S)-ipsdienol (Mori et al., 1979), the vitamin (R)-pantothenic acid (Wasmuth et al., 1982), and many natural compounds (Adam et al., 1987; Niwa et al., 1992; Shiba et al., 1982; Shieh and Prestwich, 1982; Stork et al., 1978; Walkup and Cunningham, 1987). D-malic acid is also used as a resolving agent (Clarke et al., 1978; Shiozawa et al., 1988), and as a ligand in asymmetric synthesis (Heil et al., 1985; Tanabe et al., 1973).

D-malate is produced chemically or enzymatically. Both routes result in D-malate of high optical purity, but the (molar) yield depends very much on the method used. With chemical production methods, yields are low, since more than one reaction step is required (Van der Werf, 1994). Enzymatic production of D-malate can result in high yields (Van der Werf, 1994). However, cofactor regeneration is required, making the process very complex. The production of D-malate using maleate hydratase from *Pseudomonas pseudoalcaligenes* seems to be the most promising method. This process does not require cofactor regeneration (Van der Werf et al., 1993). The substrate maleate, a cheap bulk chemical, is converted into D-malate in a simple one-step bioconversion:



and the enantiomeric purity of D-malate produced by maleate hydratase is 99.97 % (Van der Werf et al., 1992).

Purification of maleate hydratase from *P. pseudoalcaligenes* is complicated (Van der Werf et al., 1993). Besides, the stability of the purified enzyme is dependent on D,L-malate and protein concentrations. Higher D,L-malate concentrations result in better stabilization of maleate hydratase activity with D- and L-malate being equally effective. Dilution of the purified enzyme (from 0.32 mg·cm⁻³ to 0.008 mg·cm⁻³) results in 80% loss of activity after 30 minutes at 30°C (Van der Werf et al., 1993). To overcome stability and purification problems, permeabilized *P. pseudoalcaligenes* has been used in the experiments described in the present research; intact cells do not convert maleate into D-malate. Permeabilization is assumed not to influence the activity of maleate hydratase and is assumed to lead to a more stable biocatalyst (Van der Werf et al., 1992).

For purified maleate hydratase, Van der Werf et al. (1993) found competitive product inhibition. In the present paper, the kinetics of maleate hydration by permeabilized *P. pseudoalcaligenes* were studied. Under appropriate conditions of pH and temperature, a kinetic model featuring competitive product inhibition and biocatalyst inactivation was fitted simultaneously through two independent data sets of substrate concentration vs. time ($C_s(t)$ -curves; each with a different initial substrate concentration). The effects of pH and temperature on the kinetic parameters were shown by measuring sets of two $C_s(t)$ -curves at another pH or temperature, followed by simultaneous fitting again.

MATERIALS AND METHODS

Cultivation of *P. pseudoalcaligenes*

One hundred milliliter of a sterilized mineral salts medium (30 min at 120°C; Hartmans et al., 1989) with 5 g/l of yeast extract (Oxoid) and 0.5 g/l of 3-hydroxybenzoate (Acros Chimica) of pH 7 in a 500-ml erlenmeyer was inoculated with 1 ml of a pure culture of *P. pseudoalcaligenes* NCIMB 9867 (kindly supplied by the Division of Industrial Microbiology, Wageningen Agricultural University) and was statically incubated at 30°C. Growth was measured by following the OD₆₆₀ with a spectrophotometer (Beckman DU 640). At OD₆₆₀ ≈ 0.4, approximately 80 % of the maximal cell density, the suspension was used to inoculate 1 liter of sterilized

mineral salts medium with 0.1 g/l of yeast extract and 0.5 g/l of 3-hydroxybenzoate (pH 7) in a 5-l erlenmeyer. This culture was incubated on a shaking tray at 30°C. At an OD₆₆₀ of 0.45, 900 ml of the broth was used to inoculate 200 liter of sterilized mineral salts medium containing 1 g/l of 3-hydroxybenzoate (pH 7) in a 300-l bioreactor (Bioengineering LP300). Fermentation took place at 30°C, air flow 12.5 NI/min, 125 rpm and 1.1 bar top pressure in the fermenter. Growth of the biomass was followed in time by measuring the oxygen tension (pO₂) in the fermenter. At a certain amount of biomass, oxygen became growth limiting and the pO₂ in the medium decreased. When all 3-hydroxybenzoate had been consumed, the cells only needed oxygen for maintenance; as a consequence the oxygen tension increased. At that moment the cells were harvested (OD₆₆₀ = 0.47) with a continuous centrifuge (Sharples MVF 1621581, 13.000 rpm). The concentrated biomass was washed in 1 liter of buffer of 4°C (50 mM potassium phosphate buffer of pH 7) and centrifuged again for 10 min at 13.000 rpm and 5°C (Beckman, J2-MC, JA 14 rotor). The resulting cell pellet had a wet weight of 251 g and was used for permeabilization.

Permeabilization of *P. pseudoalcaligenes*

The cell pellet was resuspended in 1.5 liter of buffer (50 mM potassium phosphate buffer of pH 7). Permeabilization was done by incubation with Triton X-100 (from Pharmacia; Cornett and Shockman, 1978; Van der Werf et al., 1995). Incubation with Triton X-100 results in both permeabilization and cell lysis, with permeabilization occurring much faster than lysis. In order to promote permeabilization and to prevent lysis, the cell suspension was diluted by a factor 2 with buffer of a relatively high Triton X-100 concentration, namely 1% w/v Triton X-100, and stirred for only half a minute, before 2-ml Eppendorf tubes were filled and frozen at -80°C. The tubes were stored at -20°C. To minimize the difference in incubation time between the first and last tube being filled, the cell suspension was permeabilized in four parts.

Effect of pH and temperature on initial substrate conversion rate

In order to select appropriate conditions for determination of the kinetic parameters by simultaneous fitting (see below), the effects of pH and temperature on the initial substrate conversion rate (excluding inactivation) were determined. This was done by measuring the decrease of substrate concentration during a short period of time in batch experiments. To 4 ml of 300 mM maleic acid (Acros Chimica) in various 500 mM buffer solutions (pH 4-7: acetic acid (Merck); pH 7-9: Tris (Boehringer

Mannheim); pH 9-10.5: glycine (Merck)), 1 ml of a suspension of permeabilized *P. pseudoalcaligenes* was added (5 minutes thawed). This mixture was incubated for 20 min at 35°C in a shaking water bath at 170 rpm. Every two minutes, a 100- μ l sample was taken and mixed with 900 μ l of 3.5 M HCl in an Eppendorf tube on a vortex mixer to stop the enzymatic reaction. The tubes were centrifuged (5 min, 13.000 rpm) and the supernatant was diluted 100-fold with demineralized water and analysed by HPLC. The initial substrate conversion rate was determined by linear regression of the substrate concentration vs. time data.

For the temperature experiment, 4-ml solutions of 300 mM maleic acid / 500 mM Tris of pH 8 and 1 ml of permeabilized *P. pseudoalcaligenes* (added immediately after thawing) were incubated at different temperatures in a shaking water bath at 170 rpm and the decrease of substrate concentration with time was measured. Subsequently the initial substrate conversion rate was determined by linear regression of the substrate concentration vs. time data.

Determination of kinetics and kinetic parameters by simultaneous fitting

For determination of the kinetic parameters the decrease of substrate concentration was measured during a long period of time in batch experiments. A kinetic model was fitted through substrate concentration vs. time data. To obtain reliable estimates for all parameters, the kinetic model was fitted simultaneously through two data sets of substrate concentration vs. time. The model was implemented in the computer program STEM (Simulation Tool for Easy Modeling) and the parameter values were determined by applying a simplex method (Nelder and Mead, 1965) in combination with the method of Gear (1971). The decrease of substrate concentration with time was measured as follows. To 79-ml solutions of 2, 50, or 100 mM maleic acid and 500 mM Tris of pH 8, 1 ml of permeabilized cells was added. This mixture was incubated at 35°C for at least 35 minutes in a shaking water bath (GFL 1083) at 140 rpm. Every 2, 10, or 15 minutes, samples were taken and immediately mixed with at least 0.35 M HCl solution in an Eppendorf tube on a vortex mixer to stop the enzymatic reaction. The tubes were centrifuged for 5 minutes at 13.000 rpm and the supernatant was diluted with demineralized water until the HCl concentration in the samples was 0.18 M or lower (to prevent HPLC disturbances). Subsequently, these samples were analysed by HPLC.

To show the effect of pH on the kinetic parameters, 79-ml solutions of 2 or 100 mM maleic acid and 500 mM acetic acid of pH 6 were incubated at 35°C with 1 ml of

permeabilized cells; the decrease of substrate concentration with time was measured. The effect of temperature was shown by incubating 79-ml solutions of 2 or 100 mM maleic acid and 500 mM Tris of pH 8 with 1 ml of permeabilized cells at 25°C; the decrease of substrate concentration with time was measured again.

HPLC analysis

Maleate and D-malate were analysed by HPLC with the method of Skelly (1982). The dicarboxylic acids were separated at 35°C on a reversed phase C18 column (200 by 3 mm; Chrompack, Middelburg, The Netherlands). The mobile phase was 2 mM octylamine (Aldrich) / 50 mM potassium phosphate buffer (pH 7.0) in distilled water. The flow rate was 0.4 ml/min and the organic acids were detected at 210 nm. The column was pre-equilibrated for at least 3 hours with the mobile phase (Van der Werf et al., 1992).

Reactions can be followed by measuring either substrate or product. Here, we chose to measure substrate because the detection was more sensitive to maleate than to D-malate at 210 nm. Furthermore, for measuring maleate, the samples had to be diluted, with the advantage that cell components, originating from the permeabilized cells, were diluted too, resulting in less pollution of the HPLC column.

Dry weight

One milliliter of the cell suspension was put in a small aluminium tray with a predetermined weight and placed in a stove at 120°C for at least 3 days. Upon cooling in a desiccator containing dried kiesel gel, the weight of the tray was again determined.

RESULTS AND DISCUSSION

Effect of pH and temperature on initial substrate conversion rate

The effect of pH on the initial substrate conversion rate was measured at a high maleate concentration (240 mM); this concentration was so high that the decrease of substrate, maleate²⁻, in time was assumed to be linear during the time of the assay and to reflect the zero-order rate constant of the reaction (see eq. (2)). Fig. 1 shows that the biocatalyst has a quite broad pH optimum, ranging from pH 7 to 8. This is in good agreement with the results found by Van der Werf et al. for the purified enzyme

(Van der Werf et al., 1993). At pH values above 9, inactivation of the biocatalyst occurred since a slimy suspension was observed. Note that the actual substrate concentration, the maleate²⁻ concentration (Van der Werf et al., 1993; Van der Werf et al., 1994), is dependent upon pH. Between pH 7 and pH 5, the initial substrate conversion rate decreased. In principle, this could be due to the decrease of (initial) maleate²⁻ concentration, since the pK_{a2} of maleic acid is 6.07 (Lide, 1991). However, K_m (based on maleate²⁻ concentration) was found to be 0.69 mM at pH 6 and 35°C (see below); so even at pH 5 the maleate²⁻ concentration was much larger than K_m (at least a factor 28). This means that other mechanisms were most probably more important.

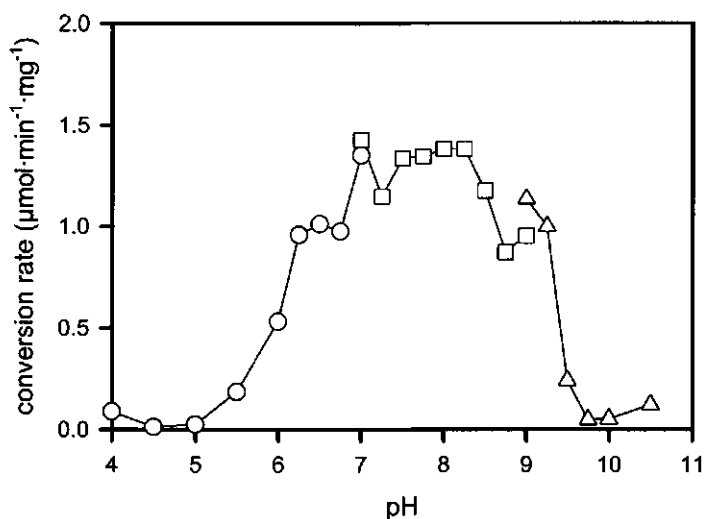


Figure 1 The effect of pH on initial substrate conversion rate. In pH-range 4-7 acetic acid buffer (O), in pH-range 7-9 Tris buffer (□), and in pH-range 9-11 glycine buffer (Δ) was used.

The effect of temperature on the initial substrate conversion rate is shown in Fig. 2. Biocatalyst activity was maximal between 40 and 45°C. At temperatures above 45°C, inactivation of the biocatalyst was observed, since addition of permeabilized cells resulted in a slimy suspension. This is in good agreement with the results found by Van der Werf et al. (1993) for the purified enzyme.

It was assumed that the temperature dependency (up to about 40°C) of the maleate hydration reaction, catalysed by maleate hydratase, can be described by the Arrhenius equation (Van 't Riet and Tramper, 1991):

$$k_p = k_{p,\infty} \cdot e^{-\frac{\Delta H^*}{RT}} \quad (1)$$

with ΔH^* the activation enthalpy change and $k_{p,\infty}$ the frequency factor. ΔH^* and $k_{p,\infty}$ were determined by fitting (see Fig. 2): $\Delta H^* = 69.1 \text{ kJ}\cdot\text{mol}^{-1}$, $k_{p,\infty} = 5.93 \cdot 10^{11} \text{ mmol}\cdot\text{min}^{-1}\cdot\text{mg}^{-1}$. This is in good agreement with the results found by Van der Werf et al. (1993) for the purified enzyme.

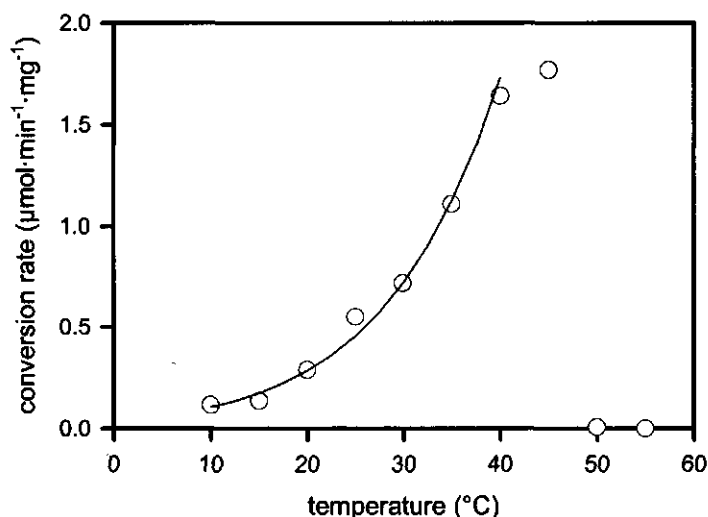


Figure 2 The effect of temperature on initial substrate conversion rate; the curve (—) represents a fit with the Arrhenius equation.

Determination of kinetics and kinetic parameters by simultaneous fitting

The decrease of substrate concentration with time was measured with three different initial substrate concentrations at pH 8 and 35°C (see Fig. 3). According to Van der Werf et al. (1993) the decrease of substrate conversion rate in time reflects competitive product inhibition, in addition to decreasing substrate concentration. The velocity equation for this mechanism is given below (see eq. (2)).

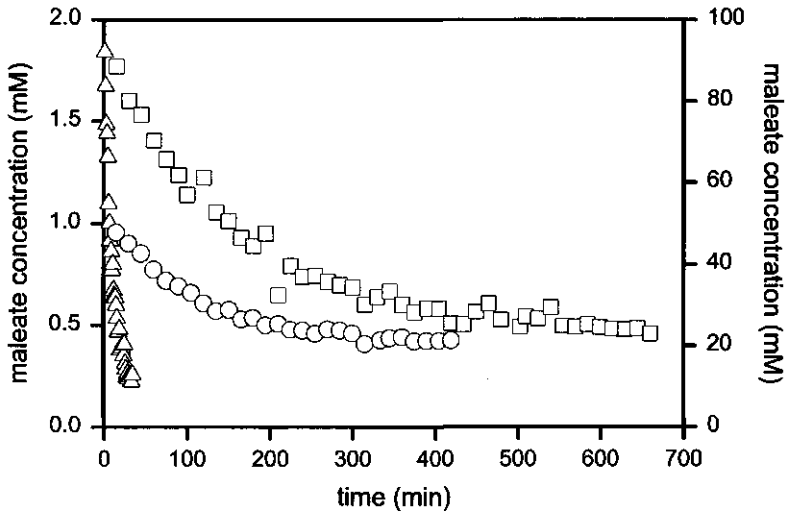
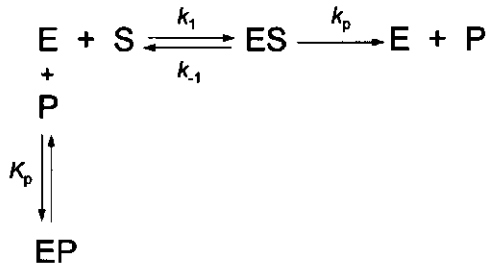


Figure 3 The decrease of substrate in time at pH 8 and 35°C starting from initial substrate concentrations of 2 mM (Δ), 50 mM (O), and 100 mM (\square).

The general equation for a one-enzyme E, one-substrate S, one-enzyme/substrate-complex ES, and one-product P system with competitive product inhibition is:



with the k 's denoting the reaction rate constants and $K_p = (C_e \cdot C_p) / C_{ep}$; C stands for the concentration with the subscript referring to the pertinent species. Assuming this system is closed with a constant volume, the following velocity equation can be derived (Segel, 1975):

$$v = \frac{dC_s}{dt} = - \frac{v_{\max} \cdot C_s}{K_m \left(1 + \frac{C_p}{K_p} \right) + C_s} \quad (2)$$

with:

$$v_{\max} = k_p \cdot C_e^T$$

$$K_m = \frac{k_{-1} + k_p}{k_1}$$

and the superscript T referring to total concentration. Assuming $C_p(0) = 0$ (with (0) referring to the situation at $t = 0$), substitution of $C_p = C_s(0) - C_s$ in eq. (2) results in:

$$\frac{dC_s}{dt} = - \frac{v_{\max} \cdot C_s}{K_m \left(1 + \frac{C_s(0)}{K_p} \right) + \left(1 - \frac{K_m}{K_p} \right) C_s} \quad (3)$$

Multiplication of nominator and denominator of eq. (3) with $K_p/(K_p - K_m)$ results in:

$$\frac{dC_s}{dt} = - \frac{v_{\max} \left(\frac{K_p}{K_p - K_m} \right) C_s}{K_m \left(1 + \frac{C_s(0)}{K_p} \right) \left(\frac{K_p}{K_p - K_m} \right) + C_s} \quad (4)$$

It was assumed that $K_p > K_m$ (see eq. (4)). Indeed for the purified enzyme Van der Werf et al. (1993) found that $K_p = 0.63$ mM and $K_m = 0.19$ mM.

Fig. 3 shows that in the experiments with high substrate concentrations the conversion rate became zero, when there was still substrate present; according to eq. (2) this could not occur. However, in contrast to the system assumed above, it could be due to the fact that the system had reached equilibrium. The equilibrium constant was determined in short experiments with substrate solutions with an excess of enzyme (data not shown) and was found to be 1400 at pH 8 and 35°C; so at equilibrium almost all substrate (> 99.9%) was converted. This means that equilibrium had not been reached, when the substrate consumption rate became

zero. Therefore it was assumed that instability of the enzyme was the cause for the substrate consumption rate becoming zero.

If it is assumed that the enzyme was irreversibly inactivated according to a first-order process, C_e^T can be expressed as (Van 't Riet and Tramper, 1991):

$$C_e^T = C_e^T(0) \cdot e^{-k_d t} \quad (5)$$

with k_d referring to the inactivation rate constant. Combination of eqs. (4) and (5) yields:

$$\frac{dC_s}{dt} = - \frac{k_p \cdot C_e^T(0) \cdot e^{-k_d t} \left(\frac{K_p}{K_p - K_m} \right) C_s}{K_m \left(1 + \frac{C_s(0)}{K_p} \right) \left(\frac{K_p}{K_p - K_m} \right) + C_s} \quad (6)$$

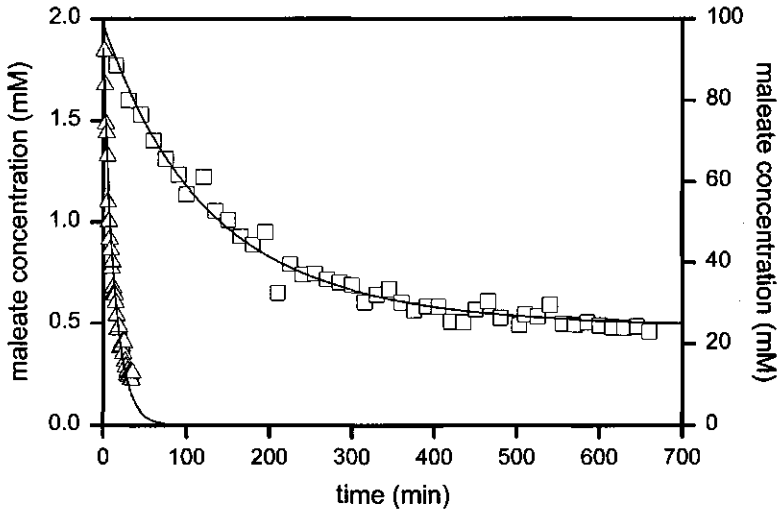


Figure 4 Simultaneous fit of the 2 mM- and 100 mM- $C_s(t)$ -curves at pH 8 and 35°C.

The parameters k_p , k_d , K_m , K_p , and $C_s(0)$ were determined by fitting eq. (6) through the $C_s(t)$ -curves of Fig. 3; $C_e^T(0)$ was known. Although eq. (6) contains three constants, these constants were used to calculate more than three parameters. Therefore two $C_s(t)$ -curves of Fig. 3 were fitted simultaneously. This was done by using eq. (6) in duplicate in the computer program STEM. The result of fitting the

2 mM- and 100 mM- $C_s(t)$ -curves simultaneously is shown in Fig. 4 and the values of the parameters are shown in Table 1. The model fitted the data well ($R^2 > 0.97$).

To validate the kinetic model represented by eq. (6), the 2 mM- and 50 mM- $C_s(t)$ -curves of Fig. 3 were also fitted simultaneously; the result is shown in Fig. 5 and the values of the parameters are shown in Table 1. The model fitted the data well ($R^2 > 0.98$) with almost similar parameter values, except for K_p ; however, the 95% confidence interval for K_p from the first simultaneous fit was quite large. This validation supports the kinetic model assumed in this paper. D-malate was found to stabilize purified maleate hydratase (Van der Werf et al., 1993). Considering the R^2 -values, it was not necessary to correct the kinetic model for the stabilizing effect of D-malate formed during the reaction. Better estimates of the parameters were obtained by fitting the 2 mM-, 50 mM- and 100 mM- $C_s(t)$ -curves simultaneously (see Fig. 6 and Table 1). These values will be used in future as estimates for the parameters at pH 8 and 35°C. Comparing the values for K_m and K_p with the values for purified maleate hydratase determined by Van der Werf et al. (1993; although determined at 30°C), shows that K_m and K_p for permeabilized *P. pseudoalcaligenes* were significantly larger (after correction for the difference in temperature).

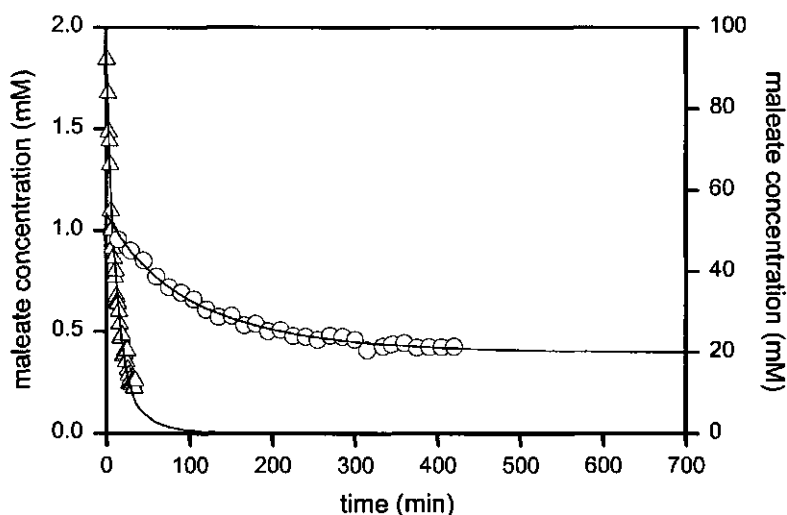


Figure 5 Simultaneous fit of the 2 mM- and 50 mM- $C_s(t)$ -curves at pH 8 and 35°C.

Table 1 Parameter values for k_p , k_d , K_m , K_p , and $C_s(0)$ with their 95% confidence intervals, obtained by simultaneous fitting, and the R^2 -values of each fit; note that, though $C_e^T(0)$ is given too, this is not a fit parameter.

	2 mM + 100 mM pH 8, 35°C ^{a)}	2 mM + 50 mM pH 8, 35°C ^{a)}	2 mM + 100 mM pH 8, 35°C ^{a)}	2 mM + 100 mM pH 6, 35°C ^{a)}	2 mM + 100 mM pH 8, 25°C ^{a)}
parameter values					
$k_p^{b)}$	$18 \cdot 10^{-4} \pm 3 \cdot 10^{-4}$	$16 \cdot 10^{-4} \pm 1 \cdot 10^{-4}$	$17 \cdot 10^{-4} \pm 2 \cdot 10^{-4}$	$11 \cdot 10^{-4} \pm 2 \cdot 10^{-4} c)$	$7 \cdot 10^{-4} \pm 1 \cdot 10^{-4}$
k_d	$56 \cdot 10^{-4} \pm 12 \cdot 10^{-4}$	$69 \cdot 10^{-4} \pm 12 \cdot 10^{-4}$	$56 \cdot 10^{-4} \pm 19 \cdot 10^{-4}$	$43 \cdot 10^{-4} \pm 11 \cdot 10^{-4}$	$1 \cdot 10^{-4} \pm 4 \cdot 10^{-4}$
K_m	4.5 ± 1.2	3.1 ± 0.3	3.9 ± 0.6	$1.5 \pm 0.9 c)$	1.0 ± 0.2
K_p	10.4 ± 8.0	3.1 ± 1.2	3.9 ± 3.2	2.5 ± 4.8	1.0 ± 0.6
$C_e^T(0)_{1/2}$	265	265	265	334	295
$C_e^T(0)_{50}$	-	265	265	-	-
$C_e^T(0)_{100}$	334	-	334	334	295
$C_s(0)_{1/2}$	1.86 ± 0.10	1.88 ± 0.08	1.83 ± 0.17	2.02 ± 0.21	1.90 ± 0.06
$C_s(0)_{50}$	-	54.5 ± 1.0	58.6 ± 1.9	-	-
$C_s(0)_{100}$	98.4 ± 4.6	-	86.1 ± 3.4	96.0 ± 2.5	98.4 ± 1.4
R^2 -values					
R_2^2	0.9774	0.9825	0.9800	0.9882	0.9983
R_{50}^2	-	0.9914	0.9434	-	-
R_{100}^2	0.9812	-	0.9095	0.9913	0.9937

a) simultaneous fit of two (or three) $C_s(t)$ -curves, each with one of the specified initial substrate concentrations.

b) note that here k_p is given in $\text{mmol} \cdot \text{min}^{-1} \cdot \text{mg}^{-1}$.

c) based on total maleate concentration.

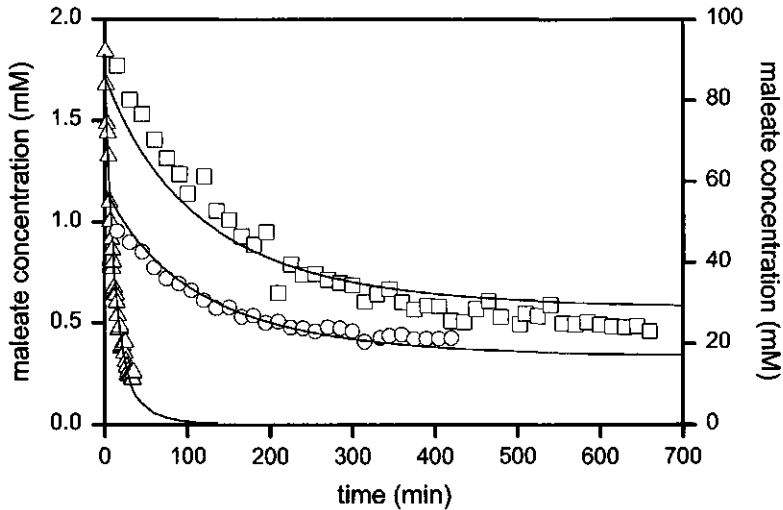


Figure 6 Simultaneous fit of the 2 mM-, 50 mM- and 100 mM- $C_s(t)$ -curves at pH 8 and 35°C.

Since our main goal is to produce D-malate in a continuous set-up, inactivation of permeabilized cells within a few hours must be avoided. Therefore the effects of pH and temperature on inactivation and product inhibition were studied in more detail.

Effect of pH and temperature

To show the effect of pH, the parameters k_p , k_d , K_m , K_p , and $C_s(0)$ were determined at pH 6 (35°C) and compared to the values at pH 8 (35°C). Two $C_s(t)$ -curves ($C_s(0) = 2$ mM and $C_s(0) = 100$ mM) were measured and simultaneously fitted by numerical integration of eq. (6). Table 1 and Fig. 7 give the results of the fitting procedure. Note that at pH 8, 100% of total maleate is maleate²⁻, since the pK_{a2} of maleic acid is 6.07 (Lide, 1991). At pH 6 on the contrary, only 46% of total maleate is maleate²⁻. Table 1 shows the values of k_p and K_m based on total maleate concentration. The values of k_p and K_m based on maleate²⁻ concentration were: $k_p = 5.1 \cdot 10^{-4}$ mmol·min⁻¹·mg⁻¹, $K_m = 0.69$ mM. Table 1 shows that the inactivation rate constant (k_d) at pH 6 (35°C) did not differ significantly from the inactivation rate constant at pH 8 (35°C). The parameters k_p and K_m were smaller at pH 6 (35°C) than at pH 8 (35°C). The effect of k_p and K_m on the (initial) conversion rate depends on the substrate concentration (maleate²⁻). Van der Werf et al. (1994) showed that the highest maleate hydratase activity was obtained when (an equimolar amount of) Ca²⁺ was

used as counter-ion for maleate²⁻. We aim at maximizing the D-malate production rate in a continuous set-up. By using Ca²⁺ as counter-ion for maleate²⁻ in a continuous set-up, the concentration of maleate²⁻ will probably correspond to the saturation concentration of Ca-maleate (about 150 mM; Michielsen et al., 1998). At this concentration k_p has a much bigger influence on the (initial) conversion rate than K_m . This means that the highest (initial) conversion rate will be reached at pH 8 (35°C). K_p was smaller at pH 6 (35°C) than at pH 8 (35°C). This means that with respect to minimizing competitive product inhibition pH 8 (35°C) is also favorable.

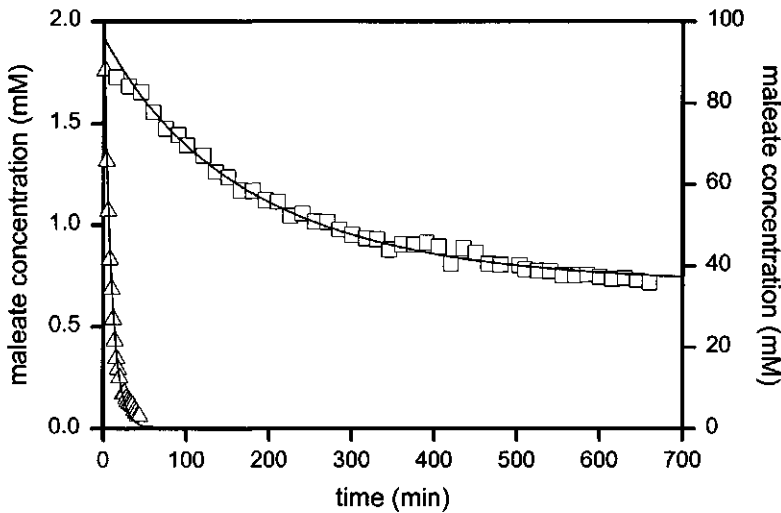


Figure 7 The decrease of substrate in time at pH 6 and 35°C starting from initial substrate concentrations of 2 mM (Δ) and 100 mM (\square); the curves (—) represent fits obtained by simultaneous fitting.

To show the effect of temperature, the parameters k_p , k_d , K_m , K_p , and $C_s(0)$ were determined at 25°C (pH 8) and compared to the values at 35°C (pH 8). Two $C_s(t)$ -curves ($C_s(0) = 2$ mM and $C_s(0) = 100$ mM) were measured and simultaneously fitted by numerical integration of eq. (6). The two $C_s(t)$ -curves with their fits are shown in Fig. 8 and Table 1. Table 1 shows that the inactivation rate constant (k_d) at 25°C (pH 8) was about 50 times smaller than the inactivation rate constant at 35°C (pH 8). As a result the half-life of maleate hydratase at 25°C (pH 8) was $1.2 \cdot 10^2$ h and at 35°C (pH 8) 2.1 h (calculated with $k_d = 56 \cdot 10^{-4} \text{ min}^{-1}$). So, if we aim at maintaining (initial) maleate hydratase activity in a continuous system, permeabilized

P. pseudoalcaligenes has to be added to the system at a 50 times lower supply rate at 25°C (pH 8) than at 35°C (pH 8). The parameters k_p and K_m were smaller at 25°C (pH 8) than at 35°C (pH 8). The effect of k_p and K_m on the (initial) conversion rate depends on the substrate concentration (maleate²⁻). In a continuous set-up maleate²⁻ concentration will probably be about 150 mM (Michielsen et al., 1998). Since at this concentration k_p has a much bigger influence on the (initial) conversion rate than K_m , the highest (initial) substrate conversion rate will be reached at 35°C (pH 8). K_p was smaller at 25°C (pH 8) than at 35°C (pH 8). So, with respect to minimizing competitive product inhibition 35°C (pH 8) is also favorable.

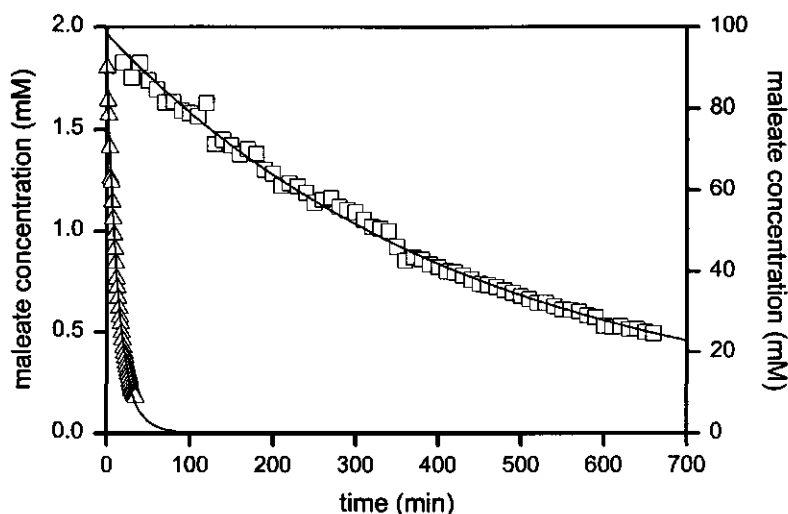


Figure 8 The decrease of substrate in time at pH 8 and 25°C starting from initial substrate concentrations of 2 mM (Δ) and 100 mM (\square); the curves (—) represent fits obtained by simultaneous fitting.

CONCLUSIONS

The kinetics of D-malate production by permeabilized *P. pseudoalcaligenes* could be described by assuming competitive product inhibition. The kinetic parameters could be determined well by simultaneously fitting two independent substrate concentration vs. time data sets (each with a different initial substrate concentration). The kinetic parameters k_p , K_m , and K_p were pH and temperature dependent; k_p , K_m ,

and K_p decreased when pH or temperature decreased. This means that, when Ca^{2+} is used as counter-ion for maleate²⁻, conditions of pH 8 and 35°C are favorable in a continuous set-up. At pH 8 and 35°C the substrate conversion rate became zero, during the time of the experiment (11 h). This was due to inactivation of maleate hydratase. Inactivation was assumed to be an irreversible, first-order process. At pH 6 (35°C) inactivation occurred at almost the same rate. At 25°C (pH 8) the substrate conversion rate did not become zero. This was because inactivation occurred about 50 times slower than inactivation at 35°C. So if the permeabilized cells have to be used in a continuous set-up, temperature is of major importance with respect to inactivation of maleate hydratase.

ACKNOWLEDGEMENTS

We thank S. Hartmans and M.J. van der Werf (Division of Industrial Microbiology, Wageningen Agricultural University) for supplying *P. pseudoalcaligenes* and for fruitful discussions on cultivation and permeabilization of *P. pseudoalcaligenes*.

This work was financially supported by the Ministry of Economic Affairs, the Ministry of Education, Culture and Science, the Ministry of Agriculture, Nature Management and Fishery in the framework of an industrial relevant research programme of the Netherlands Association of Biotechnology Centres in the Netherlands (ABON).

NOMENCLATURE

C	concentration	(mmol·dm ⁻³)
C_e^T	total enzyme concentration	(mg·dm ⁻³)
$C_e^T(0)$	total enzyme concentration at $t = 0$	(mg·dm ⁻³)
C_s	substrate concentration	(mmol·dm ⁻³)
$C_s(0)$	substrate concentration at $t = 0$	(mmol·dm ⁻³)
$\Delta H'$	activation enthalpy change	(kJ·mol ⁻¹)
K_m	Michaelis constant	(mmol·dm ⁻³)
K_p	equilibrium constant	(mmol·dm ⁻³)
k_d	inactivation rate constant	(min ⁻¹)

k_p	first-order reaction rate constant	(mmol·min ⁻¹ ·mg ⁻¹)
$k_{p,\infty}$	frequency factor	(mmol·min ⁻¹ ·mg ⁻¹)
k_{-1}	first-order reaction rate constant	(mmol·min ⁻¹ ·mg ⁻¹)
k_1	second-order reaction rate constant	(dm ³ ·min ⁻¹ ·mg ⁻¹)
R	gas constant	(8.314 J·mol ⁻¹ ·K ⁻¹)
T	temperature	(°C)
t	time	(min)
v	substrate conversion rate	(mmol·dm ⁻³ ·min ⁻¹)

Indices

e	enzyme
ep	enzyme/product-complex
max	maximum
p	product
s	substrate
T	total
2	2 mM- $C_s(t)$ -curve
50	50 mM- $C_s(t)$ -curve
100	100 mM- $C_s(t)$ -curve

REFERENCES

- Adam G, Zibuck R, Seebach D. 1987. Total synthesis of (+)-gloeosporone: assignment of absolute configuration. *J Am Chem Soc* 109:6176-6177.
- Almeida JF, Anaya J, Martin N, Grande M, Moran JR, Caballero MC. 1992. New enantioselective synthesis of 4-hydroxy-2-oxopyrrolidine-N-acetamide (oxiracetam) from malic acid. *Tetrahedron: Asymmetry* 3:1431-1440.
- Baily S, Harnden MR, Jarvest RL, Parkin A, Boyd MR. 1991. Synthesis and antiviral activity of 9-alkoxypurines. 2. 9-(2,3-Dihydroxypropoxy)-, 9-(3,4-dihydroxybutoxy)-, and 9-(1,4-dihydroxybut-2-oxy)purines. *J Med Chem* 34:57-65.
- Barth M, Bellamy FD, Renaut P, Samreth S, Schuber F. 1990. Towards a new type of HMG-CoA reductase inhibitor. *Tetrahedron* 46:6731-6740.
- Bellamy FD, Bondoux M, Dodey PA. 1990. New, short and efficient synthesis of both enantiomers of carnitine. *Tetrahedron Lett* 31:7323-7326.

- Clarke FH, Hill RT, Koo J, Lopano RM, Masada MA, Smith M, Soled S, VonVeh G, Vlattas I. 1978. A series of hexahydro[1,4]oxazino[3,4-a]isoquinolines as potential neuroleptics. *J Med Chem* 21:785-791.
- Cornett JB, Shockman GD. 1978. Cellular lysis of *Streptococcus faecalis* induced with Triton X-100. *J Bacteriol* 135:153-160.
- Crosby J. 1992. Chirality in industry - an overview. In: Collins AN, Sheldrake GN and Crosby J, editors. *Chirality in industry*. Chichester: John Wiley & Sons Ltd. p 1-66.
- Gear CW. 1971. The automatic integration of ordinary differential equations. *Communications of the ACM* 3:176-179.
- Hahn R, Nahrstedt A. 1993. High content of hydroxycinnamic acids esterified with (+)-D-malic acid in the upper parts of *Fumaria officinalis*. *Planta Med* 59:189-190.
- Hartmans S, Smits JP, Van der Werf MJ, Volkering F, De Bont JAM. 1989. Metabolism of styrene oxide and 2-phenylethanol in the styrene-degrading *Xanthobacter* strain 124X. *Appl Environ Microbiol* 55:2850-2855.
- Heil B, Kvintovics P, Tarszabó L. 1985. Stereo- and enantio-selective hydrogenation of ketones using iridium catalysts containing a carboxylate ligand. *J Mol Catal* 33:71-75.
- Lide DR, editor. 1991. p 8-40. *CRC Handbook of chemistry and physics*, 72th edition. Boca Raton: CRC Press, Inc.
- Michielsen MJF, Reijenga KA, Wijffels RH, Tramper J, Beertink HH. 1998. Dissolution kinetics of Ca-maleate crystals: evaluation for biotransformation reactor design. *J Chem Technol Biotechnol* 73:13-22.
- Miller MJ, Bajwa JS, Mattingly PG, Peterson K. 1982. Enantioselective syntheses of 3-substituted 4-(alkoxycarbonyl)-2-azetidinones from malic acid. *J Org Chem* 47:4928-4933.
- Mori K, Takigawa T, Matsuo T. 1979. Synthesis of optically active forms of ipsdienol and ipsenol. The pheromone components of IPS bark beetles. *Tetrahedron* 35:933-940.
- Nelder JA, Mead R. 1965. A simplex method for function minimization. *Computer J* 7:308-313.
- Niwa H, Miyachi Y, Okamoto O, Uosaki Y, Kuroda A, Ishiwata H, Yamada K. 1992. Total synthesis of optically active integerrimine, a twelve-membered dilactonic pyrrolizidine alkaloid of retronecine type. *Tetrahedron* 48:393-412.

- Rajashekhar B, Kaiser ET. 1985. Synthesis of enantiomerically pure γ -amino- β -hydroxybutyric acid using malic acid as the chiral precursor. *J Org Chem* 50:5480-5484.
- Seebach D, Hungerbühler E. 1980. Syntheses of enantiomerically pure compounds (EPC syntheses). Tartaric acid, an ideal source of chiral blocks for syntheses?. In: Scheffold R, editor. *Modern synthetic methods*, volume 2. Frankfurt am Main: Otto Salle Verlag, GmbH & Co. p 91-171.
- Segel IH. 1975. *Enzyme kinetics*. New York: Wiley Interscience Publications. 957p.
- Shiba T, Akiyama H, Umeda I, Okada S, Wakamiya T. 1982. Synthesis and stereochemistry of hypusine, a new amino acid in bovine brain. *Bull Chem Soc Jpn* 55:899-903.
- Shieh H-M, Prestwich GD. 1982. Chiral, biomimetic total synthesis of (-)-aplysinatin. *Tetrahedron Lett* 23:4643-4646.
- Shiozawa A, Ishikawa M, Sugimura H, Narita K, Yamamoto H, Sakasai T, Ohtsuki K, Kurashige S. 1988. Preparation of optically active 2-methyl-3-(1-pyrrolidinyl)-1-[4-(trifluoromethyl)phenyl]-1-propanone as a muscle relaxant. EP. 266,577 (CA 109:128823).
- Shiuey S-J, Partridge JJ, Uskokovic MR. 1988. Triply convergent synthesis of $1\alpha,25$ -dihydroxy-24(R)-fluorocholecalciferol. *J Org Chem* 53:1040-1046.
- Skelly NE. 1982. Separation of inorganic and organic anions on reversed-phase liquid chromatography columns. *Anal Chem* 54:712-715.
- Sleeve MC, Cale AD Jr, Gero TW, Jaques LW, Welstead WJ, Johnson AF, Kilpatrick BF, Demain I, Nolan JC, Jenkins H. 1991. Optical isomers of rocastine and close analogues: synthesis and H1 antihistamic activity of its enantiomers and their structural relationship to the classical antihistamines. *J Med Chem* 34:1314-1328.
- Stork G, Nakahara Y, Nakahara Y, Greenlee WJ. 1978. Total synthesis of cytochalasin B. *J Am Chem Soc* 100:7775-7777.
- Tanabe T, Okuda K, Izumi Y. 1973. Asymmetric hydrogenation of C=O double bond with modified Raney nickel catalyst. XXV. Contributions of pH-adjusting reagents in the asymmetric hydrogenation. *Bull Chem Soc Jap* 46:514-517.
- Tanner D, Somfai P. 1988. Enantioselective total synthesis of (+)-negamycin. *Tetrahedron Lett* 29:2373-2376.

- Van der Werf MJ. 1994. Production of D-malate by maleate hydratase of *Pseudomonas pseudoalcaligenes*. PhD-thesis, Wageningen Agricultural University, Wageningen, The Netherlands. 127p.
- Van der Werf MJ, Van den Tweel WJJ, Hartmans S. 1993. Purification and characterization of maleate hydratase from *Pseudomonas pseudoalcaligenes*. *Appl Environ Microbiol* 59:2823-2829.
- Van der Werf MJ, Van den Tweel WJJ, Hartmans S. 1992. Screening for microorganisms producing D-malate from maleate. *Appl Environ Microbiol* 58:2854-2860.
- Van der Werf MJ, Van den Tweel WJJ, Hartmans S. 1995. Permeabilization and lysis of *Pseudomonas pseudoalcaligenes* cells by Triton X-100 for efficient production of D-malate. *Appl Microbiol Biotechnol* 43:590-594.
- Van der Werf MJ, Hartmans S, Van den Tweel WJJ. 1994. Effect of maleate counter-ion on malease activity; production of D-malate in a crystal-liquid two-phase system. *Enzyme Microb Technol* 17:430-436.
- Van 't Riet K, Tramper J. 1991. *Basic Bioreactor Design*. New York: Marcel Dekker, Inc. 465p.
- Walkup RD, Cunningham RT. 1987. Studies on the syntheses of the aplysiatoxins: synthesis of a selectively-protected form of the C₂₇-C₃₀ (dihydroxybutanoate) moiety of oscillatoxin A. *Tetrahedron Lett* 28:4019-4022.
- Wasmuth D, Arigoni D, Seebach D. 1982. Zum stereochemischen Verlauf der Biosynthese von 2-Oxo-pantolacton: Synthese von stereospezifisch indiziertem Pantolacton aus Äpfelsäure. *Helv Chim Acta* 65:344-352.

CHAPTER 4

Stabilization of maleate-hydratase activity of permeabilized *Pseudomonas pseudoalcaligenes*

ABSTRACT

As part of development of a continuous process for D-malate production, the stability of maleate hydratase in permeabilized *Pseudomonas pseudoalcaligenes* was characterized as a function of relevant process conditions. In a system where D-malate is produced from a Ca-maleate suspension, these conditions were temperature, D-malate²⁻, Ca²⁺, and biocatalyst concentration. The decrease of maleate-hydratase activity with time was described by first-order irreversible inactivation. The first-order inactivation rate constant increased with temperature between 20 and 35°C and decreased with D-malate²⁻ concentration between 0 and 50 mM; the temperature-dependency increased with D-malate²⁻ concentration. Although seeming even more attractive with respect to biocatalyst stability, the effects of temperatures below 20°C and D-malate²⁻ concentrations exceeding 50 mM were not determined, as biocatalyst activity at these temperatures is extremely low and the D-malate²⁻ concentration will not exceed 50 mM due to the low solubility of Ca-D-malate. Ca²⁺ and biocatalyst concentrations hardly affected the inactivation rate constant. However, Ca²⁺ can be used to control the stability of the biocatalyst, as it controls the D-malate²⁻ concentration by shifting the dissociation equilibrium of Ca-D-malate towards Ca-D-malate formation with increasing Ca²⁺ concentration.

INTRODUCTION

Maleate hydratase catalyzes the hydration of maleate to D-malate by *trans* addition to the double bond. The enzyme has been detected in a wide variety of eukaryotes and prokaryotes (Asano et al., 1993; Britten et al., 1969; England et al., 1967; Nakajima et al., 1993; Nakayama and Kobayashi, 1991; Nakayama and Kobayashi, 1992; Nakayama and Ushijima, 1993; Sacks and Jensen, 1951; Van der Werf et al., 1992; Yamada et al., 1993). As a catalyst for continuous production of D-malate with a high purity and at a high production rate, maleate hydratase from *Pseudomonas pseudoalcaligenes* was selected. It converts maleate²⁻ to D-malate²⁻ in a one-step reaction, that does not require cofactor regeneration (Van der Werf et al., 1993). The attainable conversion is 100%, and the enantiomeric purity of D-malate is generally 100% (Van der Werf et al., 1992). However, both the substrate (maleate²⁻) and the product (D-malate²⁻) inhibit maleate hydratase (Van der Werf et al., 1993; Van der Werf et al., 1995b). Ca²⁺ reduces inhibition (Van der Werf et al., 1995b), as it reduces both the substrate and product concentration by Ca-maleate and Ca-D-malate formation, respectively (Lide, 1991; Linke, 1958). For that reason, we aim at producing D-malate from a Ca-maleate suspension. The reactions involved are shown below.

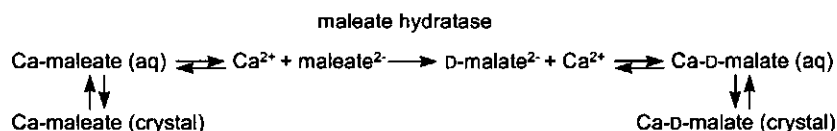


Figure 1 Reaction scheme for the production of (Ca-)D-malate from a Ca-maleate suspension by maleate hydratase.

For continuous production of D-malate the stability of the biocatalyst is also of great importance, as it affects biocatalyst productivity (in mmol of product per mg of biocatalyst) in addition to biocatalyst activity. Besides, a more stable biocatalyst facilitates continuous operation.

Many authors (Dreyer, 1985; Rahatekar et al., 1968; Ueda et al., 1993) found maleate hydratase to be unstable. Dreyer (1985) and Ueda et al. (1993) reported that the stability was better in crude extracts than in purified preparations.

The stability of purified maleate hydratase from *P. pseudoalcaligenes* increases with the concentration of the reaction product D-malate (Van der Werf et al., 1993). Moreover, it increases with enzyme concentration (Van der Werf et al., 1993). To further reduce stability problems, Van der Werf et al. (1992) tested intact cells of *P. pseudoalcaligenes* for maleate-hydratase activity, but no activity was found; probably because intact cells lack a transport mechanism for maleate uptake (Van der Werf et al., 1992). Both problems (stability and maleate uptake) can be reduced by using permeabilized *P. pseudoalcaligenes* instead of intact cells (Michielsen et al., 1998; Van der Werf et al., 1995a). However, Michielsen et al. (1998) reported that at 35°C stability problems still occurred within a few hours; the inactivation was assumed to be first-order and irreversible.

For that reason, the stability of maleate hydratase in permeabilized *P. pseudoalcaligenes* was studied here as a function of relevant process conditions: temperature and D-malate²⁻, Ca²⁺ and biocatalyst concentration. The results confirm that first-order irreversible inactivation indeed applies. The first-order inactivation rate constant was found to increase with temperature and to decrease with D-malate²⁻ concentration, whereas it was hardly affected by Ca²⁺ and biocatalyst concentration.

MATERIALS AND METHODS

Materials

Maleic acid and D-malic acid were purchased from Acros Chimica. Tris Base was obtained from Boehringer Mannheim GmbH and HCl from Riedel-de Haën. CaCl₂·2H₂O and KH₂PO₄ were purchased from Merck.

Cultivation and permeabilization of *P. pseudoalcaligenes*

P. pseudoalcaligenes NCIMB 9867 was cultivated in sterilized mineral salts medium (Hartmans et al., 1989) containing 1 g/l of 3-hydroxybenzoate (pH 7) and permeabilized with Triton X-100 as described before (Michielsen et al., 1998).

Stability determination of maleate-hydratase activity

The effects of temperature and D-malate²⁻ concentration on the stability of maleate hydratase in permeabilized *P. pseudoalcaligenes* were determined by incubating solutions of 1 ml of permeabilized *P. pseudoalcaligenes* and 3 ml of 0 to 66.7 mM D-malic acid / 0.67 M Tris (pH adjusted to 8 with HCl; every Tris-solution in this work was adjusted to pH 8 with either HCl or KOH, depending on the other components present in the solution) at 20, 25, 30 or 35°C in a shaking water bath (140 rpm). After incubation times ranging from 0 to 240 min, 1 ml of 1.25 M maleic acid / 0.5 M Tris (pH 8) was added to each 4-ml solution and maleate-hydratase activity of permeabilized *P. pseudoalcaligenes* was determined by monitoring the disappearance of maleate. At $t=5, 10, 15, 20, 25,$ and 30 min, 50- μ l samples were taken for measurement of maleate concentration. To stop the enzymatic reaction, samples were immediately mixed with 950 μ l of a 0.5 M HCl solution in an Eppendorf tube on a vortex mixer. The tubes were centrifuged for 5 min at 13.000 rpm and the supernatant was diluted with double-distilled water for maleate analysis (final concentration: 0.5 mM or less). The samples were analysed by HPLC. As, in this short term, the decrease of substrate concentration was linear, (initial) maleate-hydratase activity was determined by linear regression of the substrate concentration vs. time data. Finally, the inactivation rate constant was determined by fitting a first-order equation through the activity vs. incubation time data with the computer program Tablecurve 2D (Jandel Scientific).

To determine the effect of Ca²⁺ concentration on the stability of maleate hydratase in permeabilized *P. pseudoalcaligenes*, solutions of 1 ml of permeabilized *P. pseudoalcaligenes* were incubated with 3 ml of 66.7 mM CaCl₂·2H₂O / 0.67 M Tris (pH 8) at 25°C in a shaking water bath (140 rpm). After 0, 60, 120, 180, and 240 min of incubation, 1 ml of 1.25 M maleic acid / 0.5 M Tris (pH 8) was added to each 4-ml solution and maleate-hydratase activity was determined as described above. The first-order inactivation rate constant was determined by fitting the activity vs. incubation time data with the computer program Tablecurve 2D (Jandel Scientific). This value for the inactivation rate constant was compared to the value determined (previously) in the absence of 50 mM CaCl₂. To study whether the D-malate²⁻ or the overall D-malate concentration is responsible for biocatalyst stabilization, solutions of 1 ml of permeabilized *P. pseudoalcaligenes* were incubated with 3 ml of 33.3 to 133.3 mM D-malic acid / 66.7 mM CaCl₂·2H₂O / 0.67 M Tris (pH 8) at 25°C in a

shaking water bath (140 rpm); the effect on the first-order inactivation rate constant was determined as described above.

To determine the effect of biocatalyst concentration on the stability of maleate hydratase in permeabilized *P. pseudoalcaligenes*, solutions of 0.2 ml of permeabilized *P. pseudoalcaligenes* and 0.8 ml double-distilled water were incubated with 3 ml of 20 mM D-malic acid / 0.67 M Tris (pH 8) at 25°C in a shaking water bath (140 rpm). After 0, 120, and 240 min of incubation, 1 ml of 1.25 M maleic acid / 0.5 M Tris (pH 8) was added to each 4-ml solution and maleate-hydratase activity and the first-order inactivation rate constant were determined as described above. This value for the inactivation rate constant was compared to the value determined (previously) with a 5-fold higher biocatalyst concentration.

HPLC analysis

Maleate and D-malate (both in acidic and nonacidic form) were analysed by HPLC. They were separated on a reversed phase C18 column (250 by 4.6 mm; Baker) at 30°C. The mobile phase (0.5 ml·min⁻¹) was 0.02 M KH₂PO₄ / 0.02 M H₃PO₄ (pH 2.5) in double-distilled water. Maleate and D-malate were detected at 210 nm. The column was equilibrated for at least 3 hours with mobile phase.

RESULTS AND DISCUSSION

Biocatalyst activity was found to decrease exponentially with incubation time (Figs. 2a to d). For that reason, inactivation was assumed to be an irreversible first-order process:

$$\frac{C_e}{C_e(0)} = \frac{v}{v(0)} = e^{-k_d t} \quad (1)$$

with C_e the active biocatalyst concentration, v the biocatalyst activity, (0) referring to the situation at $t=0$, k_d the first-order inactivation rate constant, and t the incubation time. The rate constant k_d was determined from data (Fig. 2) on residual activity ($v/v(0) = C_e/C_e(0)$) versus incubation time (t) and was found to be quite reproducible (see duplicate measurements in Fig. 3).

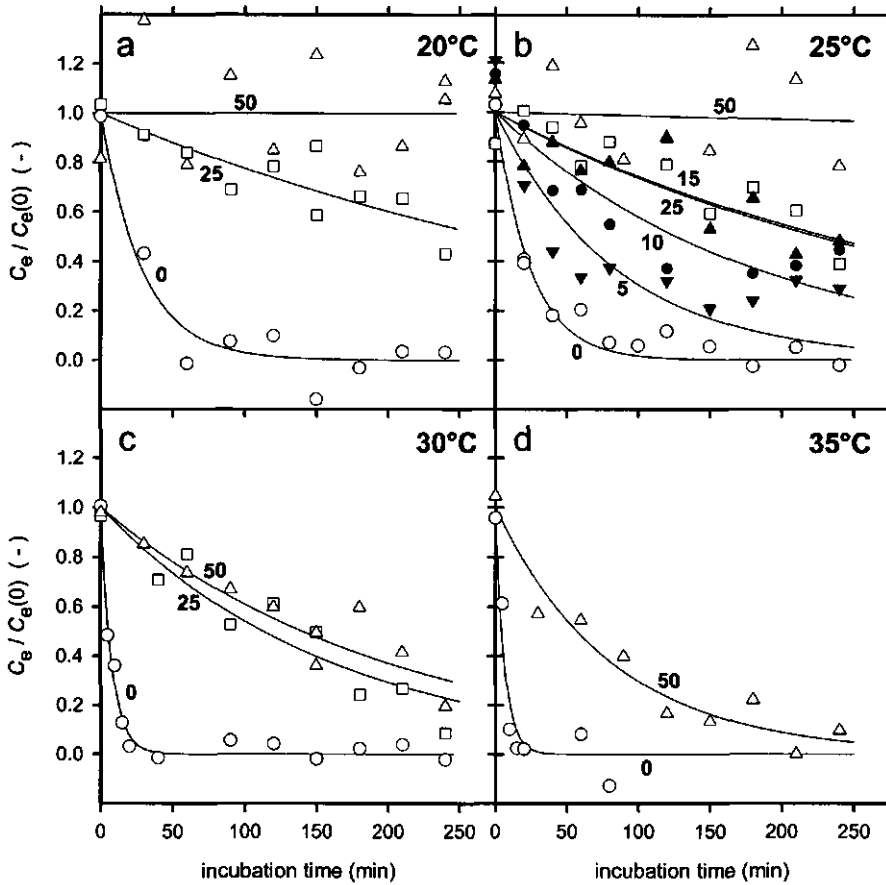


Figure 2 Effect of D-malate²⁻ concentration on the stability of maleate-hydratase activity of permeabilized *P. pseudoalcaligenes* at 20°C (a), 25°C (b), 30°C (c), and 35°C (d), and pH 8; incubation with 0 mM D-malate²⁻ (O), 5 mM D-malate²⁻ (▼), 10 mM D-malate²⁻ (●), 15 mM D-malate²⁻ (▲), 25 mM D-malate²⁻ (□) and 50 mM D-malate²⁻ (Δ). Data fitted with eq. (1) (—).

Figs. 2a to d show the positive effect of D-malate²⁻ concentration on the stability of maleate-hydratase activity of permeabilized *P. pseudoalcaligenes* at 20, 25, 30, and 35°C, respectively. Eq. (1) generally fitted the data well, thus supporting the assumption of an irreversible first-order inactivation. The estimated k_d values (and corresponding half-life time values $t_{0.5}$) are shown in Table 1.

Chapter 4

Table 1 k_d (with 95% confidence interval) and $t_{0.5}$ as a function of temperature, D-malate²⁻ and biocatalyst concentration.

Temperature (°C)	D-malate ²⁻ concentration (mM)	k_d (min ⁻¹)	$t_{0.5}$ ^{a)} (min)
20	0	$3.5 \cdot 10^{-2} \pm 1.8 \cdot 10^{-2}$	20
	25	$2.5 \cdot 10^{-3} \pm 1.3 \cdot 10^{-3}$	$2.8 \cdot 10^2$
	50	$3.1 \cdot 10^{-6} \pm 2.1 \cdot 10^{-3}$	$2.2 \cdot 10^5$
25	0	$4.1 \cdot 10^{-2} \pm 1.0 \cdot 10^{-2}$	17
	5	$1.2 \cdot 10^{-2} \pm 6.4 \cdot 10^{-3}$	58
	10	$5.5 \cdot 10^{-3} \pm 2.5 \cdot 10^{-3}$	$1.3 \cdot 10^2$
	15	$3.0 \cdot 10^{-3} \pm 1.6 \cdot 10^{-3}$	$2.3 \cdot 10^2$
	15 at 1/5 · C _e (0)	$2.7 \cdot 10^{-3} \pm 5.5 \cdot 10^{-3}$	$2.6 \cdot 10^2$
	25	$3.1 \cdot 10^{-3} \pm 1.2 \cdot 10^{-3}$	$2.2 \cdot 10^2$
	50	$1.5 \cdot 10^{-4} \pm 1.7 \cdot 10^{-3}$	$4.6 \cdot 10^3$
30	0	$1.3 \cdot 10^{-1} \pm 2.4 \cdot 10^{-2}$	5.3
	25	$6.1 \cdot 10^{-3} \pm 2.4 \cdot 10^{-3}$	$1.1 \cdot 10^2$
	50	$5.0 \cdot 10^{-3} \pm 1.5 \cdot 10^{-3}$	$1.4 \cdot 10^2$
35	0	$1.6 \cdot 10^{-1} \pm 1.2 \cdot 10^{-1}$	4.3
	50	$1.2 \cdot 10^{-2} \pm 3.7 \cdot 10^{-3}$	58

^{a)} calculated with $t_{0.5} = \frac{\ln 2}{k_d}$.

Assuming the inactivation rate to increase with temperature according to the Arrhenius equation (Fig. 3) and assuming a linear effect of D-malate²⁻ concentration on the logarithm of the frequency factor $k_{d,\infty}$ and on the activation enthalpy change for biocatalyst inactivation ΔH_d^* , k_d can be expressed as a function of temperature (K) and D-malate²⁻ concentration (mM):

$$\ln k_d = \ln k_{d,\infty} - \frac{\Delta H_d^*}{R \cdot T} \quad (2)$$

with:

$$\ln k_{d,\infty} = a + b \cdot C_{\text{D-malate}^{2-}}$$

$$\Delta H_d^* = c + d \cdot C_{\text{D-malate}^{2-}}$$

Fitting eq. (2) simultaneously through all the estimated $\ln k_d$ values of Table 1 (except $\ln k_d$ value at 15 mM D-malate²⁻ and $1/5 \cdot C_e(0)$) with a , b , c , and d as fit parameters, yielded (Fig. 3): $a = 24.6$, $b = 2.47 \text{ mM}^{-1}$, $c = 68.8 \text{ kJ} \cdot \text{mol}^{-1}$, $d = 6.41 \text{ kJ} \cdot \text{mol}^{-1} \cdot \text{mM}^{-1}$ (with $R^2 = 0.92$). Eq. (2) and Fig. 3 show that k_d increased with temperature and decreased with D-malate²⁻ concentration. This means that in the range of conditions tested in this work, biocatalyst stability was maximal at 20°C and 50 mM D-malate²⁻. The temperature-dependency of k_d (ΔH_d^*) increased with D-malate²⁻ concentration. According to Van 't Riet and Tramper (1991), the activation enthalpy change for biocatalyst inactivation ΔH_d^* is generally in the order of magnitude of 200-300 $\text{kJ} \cdot \text{mol}^{-1}$. This means that at 0 mM D-malate²⁻ ΔH_d^* for permeabilized *P. pseudoalcaligenes* inactivation was rather low (68.8 $\text{kJ} \cdot \text{mol}^{-1}$), while at 50 mM D-malate²⁻ ΔH_d^* was rather high (389 $\text{kJ} \cdot \text{mol}^{-1}$).

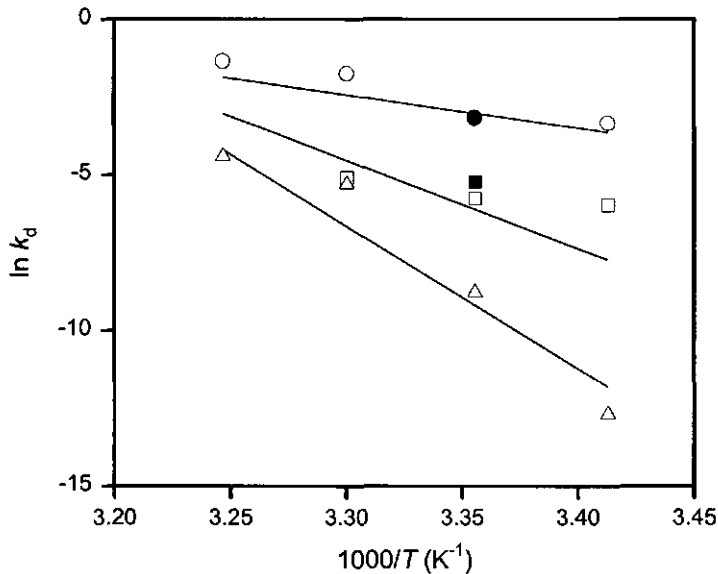
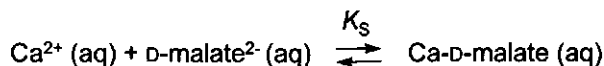


Figure 3

k_d as a function of temperature at 0 mM D-malate²⁻ (O), 25 mM D-malate²⁻ (□), and 50 mM D-malate²⁻ (Δ), and pH 8; simultaneous fit of all $\ln k_d$ values of Table 1 (except $\ln k_d$ value at 15 mM D-malate²⁻ and $1/5 \cdot C_e(0)$) with eq. (2), as a function of temperature at 0, 25, and 50 mM D-malate²⁻ (—). Duplicates with another batch of permeabilized *P. pseudoalcaligenes* at 25°C and 0 mM D-malate²⁻ (●), and at 25°C and 25 mM D-malate²⁻ (■).

Biocatalyst stability was not studied at temperatures below 20°C, as at these temperatures the activity of the biocatalyst approaches or equals the experimental error of the activity measurement. As D-malate will be produced from a Ca-maleate suspension, Ca-D-malate will also be formed (Sillen and Martell, 1964):



with K_S the dissociation constant of Ca-D-malate. Due to the low solubility of Ca-D-malate (Lide, 1991; Linke, 1958), the D-malate²⁻ concentration will probably not exceed 50 mM. For that reason, the stabilizing effect of D-malate²⁻ concentrations exceeding 50 mM was not tested in this work.

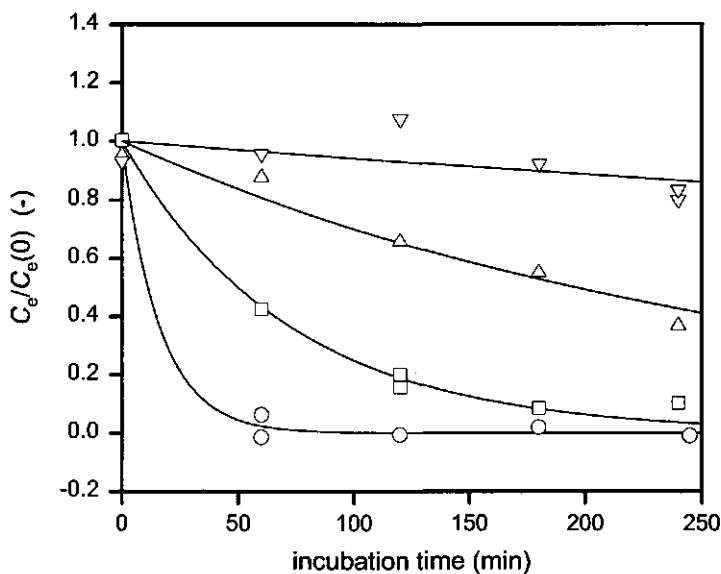


Figure 4 The effect of 50 mM $\text{CaCl}_2 \cdot 2\text{H}_2\text{O}$ on the stability of maleate-hydratase activity in permeabilized *P. pseudoalcaligenes* at 25°C and pH 8 in the absence (O) and presence of D-malate (25 mM D-malate (□), 50 mM D-malate (Δ), and 100 mM D-malate (▽)). Data fitted with eq. (1) (—).

Stabilization of maleate-hydratase activity

Table 2 k_d (with 95% confidence interval) and $t_{0.5}$ as a function of D-malate concentration at 50 mM CaCl₂ and 25°C.

total D-malate concentra- tion (mM)	determined from data on $C_e/C_e(0)$ versus t (Fig. 4)		D-malate ²⁻ concentra- tion (mM) ^{b)}	calculated	
	k_d (min ⁻¹)	$t_{0.5}$ (min) ^{a)}		k_d (min ⁻¹) ^{c)}	$t_{0.5}$ (min) ^{a)}
0	$6.2 \cdot 10^{-2} \pm$ $4.0 \cdot 10^{-2}$	11	0	$4.3 \cdot 10^{-2}$	16
25	$1.4 \cdot 10^{-2} \pm$ $2.6 \cdot 10^{-3}$	50	8	$1.6 \cdot 10^{-2}$	43
50	$3.6 \cdot 10^{-3} \pm$ $1.6 \cdot 10^{-3}$	$1.9 \cdot 10^2$	23	$2.9 \cdot 10^{-3}$	$2.4 \cdot 10^2$
100	$6.1 \cdot 10^{-4} \pm$ $1.2 \cdot 10^{-3}$	$1.1 \cdot 10^3$	71	$1.1 \cdot 10^{-5}$	$6.3 \cdot 10^4$

a) calculated with $t_{0.5} = \frac{\ln 2}{k_d}$.

b) calculated with: $K_s = 0.33 \cdot I - 0.07$, with K_s the dissociation constant of Ca-D-malate and I the ionic strength (K_s as a function of I was determined similar to the dissociation constant of Ca-maleate as a function of I (Michielsen et al., 1999)); the effect of 1 ml of permeabilized *P. pseudoalcaligenes* on the ionic strength I was neglected.

c) k_d calculated with D-malate²⁻ concentration and eq. (2).

As Ca²⁺ is also present, its effect on biocatalyst stability was determined as well. Fig. 4 shows the effect of 50 mM CaCl₂ on biocatalyst stability at 25°C. Eq. (1) fitted the data well. The estimated k_d value in the absence of malate ($6.2 \cdot 10^{-2}$ min⁻¹, see Table 2) corresponds well to the value found in the absence of both malate and CaCl₂ ($4.1 \cdot 10^{-2}$ min⁻¹, see Table 1). This indicates that Ca²⁺ in itself hardly affects k_d . To study whether the D-malate²⁻ or the overall D-malate concentration is responsible for biocatalyst stabilization, the effect of D-malate concentration on stability in the presence of 50 mM CaCl₂ was determined. Fig. 4 shows the effect of 25, 50 and 100 mM D-malate on biocatalyst stability at 50 mM CaCl₂ and 25°C. Eq. (1) fitted the data well; the estimated k_d values (and corresponding half-life time values $t_{0.5}$) are shown in Table 2. In the presence of CaCl₂, the k_d values at 25 and 50 mM D-malate (see Table 2) were higher than the corresponding values in the absence of CaCl₂ (see Table 1). This was illustrated clearly by the fact that at 50 mM CaCl₂ at least 100 mM D-malate was necessary to keep biocatalyst activity (almost) constant over a period of 4 hour (Fig. 4), whereas without CaCl₂ this only required about 50 mM D-malate

(Fig. 2b). The higher inactivation rates in the presence of Ca^{2+} could be due to complexation of Ca^{2+} with D-malate^{2-} to form Ca-D-malate (Sillen and Martell, 1964), thus reducing the D-malate^{2-} concentration. This was probably the cause, as the inactivation rate constants calculated on the basis of the D-malate^{2-} concentration were in reasonable agreement with the inactivation rate constants determined directly from the data on $C_e/C_e(0)$ versus t (Table 2). This indicates that probably only D-malate in dianionic form stabilizes the biocatalyst and that Ca^{2+} only affects the stability of the biocatalyst indirectly by affecting the D-malate^{2-} concentration; for maximization of biocatalyst stability in the presence of D-malate , Ca^{2+} concentration should thus be minimized.

Table 1 and 2 show that especially at low temperature (20 and 25°C) and high D-malate^{2-} concentration (50 mM and 100 mM) k_d was small, but not very reliable. This was due to the relatively low biocatalyst activity, in comparison to the (large) experimental error, under those conditions; biocatalyst activity decreases with decreasing temperature and decreases with increasing D-malate^{2-} concentration due to product inhibition (Michielsen et al., 1998). As temperature and D-malate^{2-} concentration had opposite effects on biocatalyst stability and activity, future work will focus on selection of those process conditions that cope best with the conflicting demands of both a high biocatalyst stability and activity.

Van der Werf et al. (1993) reported that the stability of purified maleate hydratase increased with enzyme concentration. This can indicate that protein-protein stabilization occurs. Therefore, the influence of biocatalyst concentration on the stability of maleate-hydratase activity at 25°C and 15 mM D-malate^{2-} was investigated. Table 1 shows that a 5-fold lower biocatalyst concentration hardly affected the first-order inactivation rate constant (k_d). So, in contrast to the purified maleate hydratase (Van der Werf et al., 1993), biocatalyst concentration hardly affected the stability of maleate-hydratase activity of permeabilized *P. pseudoalcaligenes*.

For continuous production of D-malate at a constant production rate, it is necessary to compensate for biocatalyst instability or to adjust the substrate concentration in the bioreactor (in accordance with the biocatalyst inactivation rate). As Ca^{2+} and biocatalyst concentration were not found to affect the stability of the biocatalyst, eqs. (1) and (2) can be used now to control the flow of biocatalyst or substrate to the bioreactor in order to maintain a constant biocatalyst activity.

CONCLUSIONS

In order to produce D-malate with permeabilized *P. pseudoalcaligenes* at a constant production rate, knowledge of the effects of relevant process parameters on the stability of the biocatalyst is necessary, in addition to being necessary for cost analysis of the overall process. In a system where D-malate is produced from a Ca-maleate suspension, some relevant process parameters are temperature and the concentrations of D-malate²⁻, Ca²⁺ and biocatalyst. The decrease in maleate-hydratase activity of permeabilized *P. pseudoalcaligenes* with time could be described well by first-order irreversible inactivation. The first-order inactivation rate constant k_d was found to increase with temperature (between 20 and 35°C) and to decrease with D-malate²⁻ concentration (between 0 and 50 mM). The temperature-dependency of k_d could be described fairly well with the Arrhenius equation; $k_{d,\infty}$ and ΔH_d^* increased with D-malate²⁻ concentration. In the absence of malate, Ca²⁺ did not affect biocatalyst stability. Probably only D-malate in dianionic form (D-malate²⁻) stabilized the biocatalyst. Ca²⁺ affects the D-malate²⁻ concentration by Ca-D-malate formation. This means that at constant D-malate concentration biocatalyst stability can be maximized by decreasing the Ca²⁺ concentration. In contrast to the stability of purified maleate hydratase, biocatalyst concentration hardly affected the stability of maleate hydratase in permeabilized *P. pseudoalcaligenes*. So, in a continuous system where D-malate is produced from a Ca-maleate suspension, Ca²⁺ concentration and temperature can be used to control the stability of maleate hydratase in permeabilized *P. pseudoalcaligenes*.

ACKNOWLEDGEMENTS

We thank S. Hartmans (Division of Industrial Microbiology, Wageningen Agricultural University) for supplying *P. pseudoalcaligenes* and for fruitful discussions on cultivation and permeabilization of *P. pseudoalcaligenes*.

This work was financially supported by the Ministry of Economic Affairs, the Ministry of Education, Culture and Science, the Ministry of Agriculture, Nature Management and Fishery in the framework of an industrial relevant research programme of the Netherlands Association of Biotechnology Centres in the Netherlands (ABON).

NOMENCLATURE

a	constant	(-)
b	constant	(mM^{-1})
C	concentration	(mM)
$C_e(0)$	active enzyme concentration at $t=0$	($\text{mg}\cdot\text{dm}^{-3}$)
c	constant	($\text{kJ}\cdot\text{mol}^{-1}$)
d	constant	($\text{kJ}\cdot\text{mol}^{-1}\cdot\text{mM}^{-1}$)
ΔH_d^*	activation enthalpy change for biocatalyst inactivation	($\text{kJ}\cdot\text{mol}^{-1}$)
I	ionic strength	($\text{mol}\cdot\text{dm}^{-3}$)
K_s	dissociation constant of Ca-D-malate	($\text{mol}\cdot\text{dm}^{-3}$)
k_d	first-order inactivation rate constant	(min^{-1})
$k_{d,-}$	frequency factor for biocatalyst inactivation	(min^{-1})
R	gas constant	($8.314 \text{ J}\cdot\text{mol}^{-1}\cdot\text{K}^{-1}$)
T	temperature	(K)
t	incubation time	(min)
$t_{0.5}$	half-life time of the biocatalyst	(min)
v	maleate-hydratase activity	($\text{mM}\cdot\text{min}^{-1}$)
$v(0)$	maleate-hydratase activity at $t=0$	($\text{mM}\cdot\text{min}^{-1}$)

Indices

e	enzyme
---	--------

REFERENCES

- Asano Y, Ueda M, Yamada H. 1993. Microbial production of D-malate from maleate. *Appl Environ Microbiol* 59:1110-1113.
- Britten JS, Morell H, Tagart JV. 1969. Anion activation of maleate hydratase. *Biochim Biophys Acta* 185:220-227.
- Dreyer J-L. 1985. Isolation and biochemical characterization of maleic-acid hydratase, an iron-requiring hydro-lyase. *Eur J Biochem* 150:145-154.
- England S, Britten JS, Listowsky I. 1967. Stereochemical course of maleate hydratase reaction. *J Biol Chem* 242:2255-2259.

- Hartmans S, Smits JP, Van der Werf MJ, Volkering F, De Bont JAM. 1989. Metabolism of styrene oxide and 2-phenylethanol in the styrene-degrading *Xanthobacter* strain 124X. *Appl Environ Microbiol* 55:2850-2855.
- Lide DR, editor. 1991. p 4-48. CRC Handbook of chemistry and physics, 72th edition. Boca Raton: CRC Press, Inc.
- Linke WF, editor. 1958. p 512-513. Solubilities of inorganic and metal-organic compounds, a compilation of solubility data from the periodical literature. Volume I, fourth edition. New Jersey, Princeton: D. van Nostrand Company, Inc.
- Michielsen MJF, Meijer EA, Wijffels RH, Tramper J, Beffink HH. 1998. Kinetics of D-malate production by permeabilized *Pseudomonas pseudoalcaligenes*. *Enzyme Microb Technol* 22:621-628.
- Michielsen MJF, Frielink C, Wijffels RH, Tramper J, Beffink HH. 1999. D-malate production by permeabilized *Pseudomonas pseudoalcaligenes*; optimization of conversion and biocatalyst productivity. Submitted for publication.
- Nakajima T, Manzen S, Shigeno T, Nakahara T. 1993. Production of D-malic acid from maleic acid by resting cells of *Ustilago sphaerogena* strain S402. *Biosci Biotech Biochem* 57:490-491.
- Nakayama K, Kobayashi Y. 1991. Fermentative or enzymic manufacture of D-(+)-malic acid from maleic acid. JP 03 53,888 [91,53,888] (CA 115:90967).
- Nakayama K, Kobayashi Y. 1992. Manufacture of D-malic acid from maleic acid with bacteria. JP 04,316,491 [92,316,491] (CA 118:123140).
- Nakayama K, Ushijima M. 1993. D-malic acid production from maleic acid using microorganisms: screening of microorganisms. *Biotechnol Lett* 15:271-276.
- Rahatekar HI, Maskati FS, Subramanian SS, Raghavendra Rao MR. 1968. Identification of the product of malease (maleate hydratase) reaction. *Indian J Bacteriol* 5:143-144.
- Sacks W, Jensen CO. 1951. Malease, a hydratase from corn kernels. *J Biol Chem* 192:231-236.
- Sillen LG, Martell AE, editors. 1964. p 411-412. Stability constants of metal-ion complexes, Section I: Inorganic ligands, Section II: Organic ligands, 2nd edition. The Chemical Society. London: Lewis Reprints Ltd.
- Ueda M, Asano Y, Yamada H. 1993. Purification and characterization of maleate hydratase from *Arthrobacter* sp. strain MCI2612. *Biosci Biotech Biochem* 57:1545-1548.

- Van der Werf MJ, Van den Tweel WJJ, Hartmans S. 1992. Screening for microorganisms producing D-malate from maleate. *Appl Environ Microbiol* 58:2854-2860.
- Van der Werf MJ, Van den Tweel WJJ, Hartmans S. 1993. Purification and characterization of maleate hydratase from *Pseudomonas pseudoalcaligenes*. *Appl Environ Microbiol* 59:2823-2829.
- Van der Werf MJ, Van den Tweel WJJ, Hartmans S. 1995a. Permeabilization and lysis of *Pseudomonas pseudoalcaligenes* cells by Triton X-100 for efficient production of D-malate. *Appl Microbiol Biotechnol* 43:590-594.
- Van der Werf MJ, Hartmans S, Van den Tweel WJJ. 1995b. Effect of maleate counterion on malease activity: production of D-malate in a crystal-liquid two-phase system. *Enzyme Microb Technol* 17:430-436.
- Van 't Riet K, Tramper J. 1991. *Basic Bioreactor Design*. New York: Marcel Dekker, Inc. 465p.
- Yamada H, Asano Y, Ueda M, Reiko S. 1993. Manufacture of D-malic acid with *Arthrobacter* species. JP 05,103,680 [93,103,680] (CA 119:47619).

CHAPTER 5

D-malate production by permeabilized *Pseudomonas pseudoalcaligenes*; optimization of conversion and biocatalyst productivity

ABSTRACT

For the development of a continuous process for the production of solid D-malate from a Ca-maleate suspension by permeabilized *Pseudomonas pseudoalcaligenes*, it is important to understand the effect of appropriate process parameters on the stability and activity of the biocatalyst. Previously, we quantified the effect of product (D-malate²⁻) concentration on both the first-order biocatalyst inactivation rate and on the biocatalytic conversion rate. The effects of the remaining process parameters (ionic strength, and substrate and Ca²⁺ concentration) on biocatalyst activity are reported here. At (common) ionic strengths below 2 M, biocatalyst activity was unaffected. At high substrate concentrations, inhibition occurred. Ca²⁺ concentration did not affect biocatalyst activity. The kinetic parameters (both for conversion and inactivation) were determined as a function of temperature by fitting the complete kinetic model, featuring substrate inhibition, competitive product inhibition and first-order irreversible biocatalyst inactivation, at different temperatures simultaneously through three extended data sets of substrate concentration vs. time. Temperature affected both the conversion and inactivation parameters.

The final model was used to calculate the substrate and biocatalyst costs per mmol of product in a continuous system with biocatalyst replenishment and biocatalyst recycling. Despite the effect of temperature on each kinetic parameter separately, the overall effect of temperature on the costs was found to be negligible (between 293 and 308 K). Within pertinent ranges, the sum of the substrate and biocatalyst costs per mmol of product was calculated to decrease with the influent substrate concentration and the residence time. The sum of the costs showed a minimum as a function of the influent biocatalyst concentration.

INTRODUCTION

One of the major application areas in biotechnology is the production of optically active compounds for the fine-chemicals industry (Elferink et al., 1991). D-malate is an optically active α -hydroxy acid with potential commercial applications. It can be used as a chiral synthon (Crosby, 1992; Seebach and Hungerbühler, 1980), as a resolving agent (Clarke et al., 1978; Shiozawa et al., 1988), or as a ligand in asymmetric synthesis (Heil et al., 1985; Tanabe et al., 1973). Van der Werf et al. (1992) showed that enzymatic production of D-malate with maleate hydratase from *Pseudomonas pseudoalcaligenes* is promising, since the substrate maleate is a cheap bulk chemical that is converted into D-malate in a simple one-step bioconversion (Fig. 1).

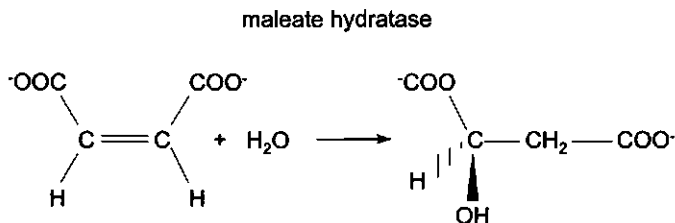


Figure 1 Conversion of maleate²⁻ to D-malate²⁻ by maleate hydratase in permeabilized *P. pseudoalcaligenes*.

In addition, the process does not require cofactor regeneration (Van der Werf et al., 1993), while the enantiomeric purity of such D-malate is 99.97% (Van der Werf et al., 1992). However, purification of maleate hydratase is complicated and yields a rather unstable enzyme (Van der Werf et al., 1993). As an alternative, permeabilized *P. pseudoalcaligenes* may be used as a more robust biocatalyst (Michielsen et al., 1998a; Michielsen et al., 1999; Van der Werf et al., 1992). Michielsen et al. (1999) reported that in that case stability improved, although inactivation still occurred within a few hours at 308 K. Inactivation was found to decrease with decreasing temperature and increasing product concentration (Michielsen et al., 1999). Furthermore, production of D-malate was found to be inhibited by substrate and product (this work; Michielsen et al., 1998a; Van der Werf et al., 1993).

We aim at developing a continuous process for the production of D-malate with permeabilized *P. pseudoalcaligenes*. To minimize substrate and product inhibition

and thus maximize the production rate per unit volume, a liquid-solid-solid three-phase system with a Ca-maleate suspension as a feed will be used. The reactions involved are shown in Fig. 2.

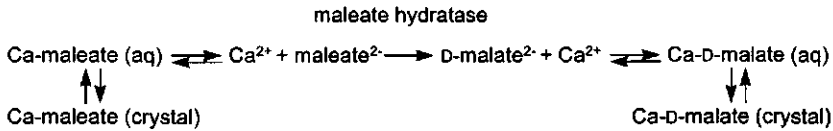


Figure 2 Reaction scheme for the conversion of solid Ca-maleate to solid Ca-D-maleate by maleate hydratase in permeabilized *P. pseudoalcaligenes*.

Calcium is chosen as counter-ion for maleate, as it was found to increase maleate-hydratase activity most (in comparison with K^+ , Na^+ , Li^+ , NH_4^+ , Ba^{2+} , and Mg^{2+}); probably because calcium reduces both the solubility of substrate (maleate^{2-}) and product (D-maleate^{2-}) most (Van der Werf et al., 1995). In this liquid-solid-solid three-phase system, production and downstream processing can be integrated and downstream-processing costs can be reduced (as the product accumulates in the solid phase). With respect to the bioconversion, the effects of temperature, pH, substrate (at low concentrations) and product concentration on biocatalyst activity and the effects of temperature and product concentration on biocatalyst stability have been quantified (Michielsen et al., 1998a; Michielsen et al., 1999). In order to complete the biokinetic model, the work presented here focused on the effects of the remaining process parameters (ionic strength, (high) substrate and Ca^{2+} concentration) on biocatalyst activity. With respect to the effect of Ca^{2+} concentration, Van der Werf et al. (1995) reported that free Ca^{2+} can influence the activity of maleate hydratase either by decreasing the availability of the substrate maleate^{2-} , or by direct enzyme inhibition. The latter was investigated in the work presented here.

After reaching that point, all the important kinetic phenomena are known (substrate and competitive product inhibition and first-order irreversible biocatalyst inactivation). However, the kinetic parameters were determined independently in separate experiments (Michielsen et al., 1998a; Michielsen et al., 1999; this work). In each experiment, only a few kinetic parameters of the overall model were determined, assuming other kinetic phenomena not to occur significantly. In order to obtain more realistic values, all the kinetic parameters were then once more

determined simultaneously, as a function of temperature. To this end, the overall model was fitted through three data sets of substrate concentration versus time (measured at the desired temperature) that featured substrate inhibition, competitive product inhibition, as well as biocatalyst inactivation. Data sets were obtained by monitoring batch conversions, starting at high substrate concentrations, over a long period of time.

In order to produce D-malate at the lowest costs in a continuous system, the cost-determining factors were calculated as a function of the process conditions in a CSTR with biocatalyst replenishment and recycling. Neglecting investment and operating costs, the potentially cost-determining factors are substrate and biocatalyst. For minimization of these costs the conversion (in mmol of product per mmol of initial or influent substrate) and biocatalyst productivity (in mmol of product per mg of biocatalyst), respectively, must be maximized (Van 't Riet and Tramper, 1991). As some process parameters (e.g. the biocatalyst concentration in the inflow) have opposed effects on the conversion and on biocatalyst productivity, a minimum with respect to the sum of the biocatalyst and substrate costs exists at certain process conditions. In this work it is shown how to select the process conditions that correspond with this costs minimum.

MATERIALS AND METHODS

Cultivation and permeabilization of *P. pseudoalcaligenes*

P. pseudoalcaligenes NCIMB 9867 (kindly supplied by the Division of Industrial Microbiology, Wageningen Agricultural University) was cultivated and permeabilized as described before (Michielsen et al., 1998a).

Effect Ca^{2+} concentration on maleate-hydratase activity

In order to determine the effect of Ca^{2+} concentration on maleate-hydratase activity, solutions with varying concentrations of Ca^{2+} and a constant maleate²⁻ concentration were made; Ca^{2+} concentration was set with $\text{CaCl}_2 \cdot 2\text{H}_2\text{O}$ and maleate²⁻ with maleic acid. As in solution also Ca-maleate is formed (Sillen and Martell, 1964), which is not a substrate, the concentrations of CaCl_2 and maleic acid, that had to be added to vary the Ca^{2+} concentration from 0 to 100 mM and set the maleate²⁻ concentration constant at 50 mM, were calculated with the following set of equations:

$$K_s = \frac{C_{Ca^{2+}} \cdot C_{maleate^{2-}}}{C_{Ca-maleate}} \quad (1)$$

Maleate balance:

$$C_{total\ maleate} = C_{maleic\ acid} = C_{maleate^{2-}} + C_{Ca-maleate} \quad (2)$$

Calcium balance:

$$C_{total\ Ca} = C_{CaCl_2} = C_{Ca^{2+}} + C_{Ca-maleate} \quad (3)$$

The dissociation constant of Ca-maleate (K_s) was determined as described in Appendix A. The pH of each solution was adjusted to 8.0 with (solid) Tris. The ionic strength (I) of the solutions was adjusted to 0.5 with KCl. The effect of Ca^{2+} on maleate-hydratase activity was determined by incubating 1 ml of permeabilized *P. pseudoalcaligenes* (dry weight: 22.2 mg·cm⁻³) with 4 ml of a 0 to 100 mM Ca^{2+} / 50 mM maleate²⁻ solution of pH 8 and $I = 0.5$ at 298 K in a shaking water bath (170 rpm), and maleate-hydratase activity was determined by monitoring the disappearance of maleate. At $t = 2, 4, 8, 12, 16,$ and 20 min, 50- μ l samples were taken and mixed with 950 μ l of a 0.5 M HCl solution in an Eppendorf tube on a vortex mixer to stop the enzymatic reaction. The tubes were centrifuged for 5 min at 13,000 rpm and the supernatant was diluted further with double-distilled water for maleate analysis (final concentration: 0.5 mM or less). The samples were analysed by HPLC. As in this short term the decrease of substrate was linear, (initial) maleate-hydratase activity was determined by linear regression of the substrate concentration vs. time data. All Ca^{2+} concentrations (0, 20, 40, 60, 80, and 100 mM) were tested in duplicate.

Effect ionic strength on maleate-hydratase activity

The effect of ionic strength (I) on (initial) maleate-hydratase activity was determined by incubating 1 ml of permeabilized *P. pseudoalcaligenes* (thawed for 10 min at 308 K; dry weight 21.2 mg·cm⁻³) with 4 ml of 300 mM maleic-acid solution of pH 8 (pH adjusted with Tris) with ionic strength $I = 1, 2, 3,$ or 4 (adjusted with KCl) at 308 K in

a shaking water bath (170 rpm), and maleate-hydratase activity was determined as described above.

Effect substrate concentration on maleate-hydratase activity

The effect of substrate concentration on (initial) maleate-hydratase activity was determined by incubating 1 ml of permeabilized *P. pseudoalcaligenes* (thawed for 10 min at 308 K; dry weight 21.2 mg·cm⁻³) with 4 ml of 0 to 1000 mM maleic acid / 500 mM Tris buffer solution of pH 8 (adjusted with HCl or KOH; this was done with every Tris-solution in this work) at 308 K in a shaking water bath (170 rpm), and maleate-hydratase activity was determined as described above.

Determination of kinetic parameters by simultaneous fitting

In order to obtain more realistic values, all kinetic parameters were determined simultaneously in one experiment. As for simultaneous determination the data had to reflect both substrate and competitive product inhibition and first-order irreversible biocatalyst inactivation, the decrease in substrate concentration, starting from high initial concentrations, was measured over a long period of time in batch experiments. As Ca²⁺ concentration was found not to inhibit the biocatalyst, a kinetic model, featuring only substrate inhibition and competitive product inhibition and first-order irreversible biocatalyst inactivation, was fitted through the substrate concentration vs. time data. To obtain reliable estimates for all parameters, the kinetic model was fitted simultaneously through three data sets of substrate concentration vs. time (each starting from a different initial concentration). The model was implemented in the computer program Simulink, a companion program to Matlab (Mathworks), and the parameter values were determined by applying the Levenberg-Marquardt method in combination with the ode45 method of Dormand-Prince in the computer program Matlab (Mathworks). The decrease of substrate with time, starting from initial concentrations of 100, 300, and 500 mM, was measured at 298, 303, and 308 K. To 4 ml of 125 mM maleic acid / 625 mM Tris solution of pH 8, 3 ml of 500 mM maleic acid / 833 mM Tris solution of pH 8, and 3 ml of 833 mM maleic acid / 833 mM Tris solution of pH 8, respectively 1, 2, and 2 ml of permeabilized *P. pseudoalcaligenes* were added. These mixtures were incubated for 8 hours at 298, 303, or 308 K in a shaking water bath (170 rpm). Every 3 or 6 minutes during the first 4 hours of incubation and every 30 minutes during the last 4 hours of incubation, 50- μ l samples were taken and immediately mixed with 950 μ l of a 0.5 M HCl solution

in an Eppendorf tube on a vortex mixer to stop the enzymatic reaction. The tubes were centrifuged for 5 min at 13.000 rpm and the supernatant was diluted further with double-distilled water for maleate analysis (final concentration: 0.5 mM or less). The samples were analysed by HPLC.

The three substrate concentration vs. time data sets at 293 K were obtained by incubating 2, 3, and 3 ml of permeabilized *P. pseudoalcaligenes* with respectively 3 ml of 167 mM maleic acid / 833 mM Tris solution of pH 8, 2 ml of 750 mM maleic acid / 1250 mM Tris solution of pH 8, and 2 ml of 1250 mM maleic acid / 1250 mM Tris solution of pH 8 for 11 hours at 293 K in a shaking water bath (170 rpm). Every 5 or 10 minutes during the first 6 hours of incubation and every 30 minutes during the last 5 hours of incubation, 50- μ l samples were taken and maleate concentration was determined as described above.

HPLC analysis

Maleate and D-malate (both in acidic and nonacidic form) were analysed by HPLC. They were separated on a reversed phase C18 column (250 by 4.6 mm; Baker) at 30°C. The mobile phase (0.5 ml·min⁻¹) was 0.02 M KH₂PO₄ / 0.02 M H₃PO₄ (pH 2.5) in double-distilled water. Maleate and D-malate were detected at 210 nm. The column was equilibrated for at least 3 hours with mobile phase.

Dry weight

One milliliter of the cell suspension was put in a small aluminium tray with a predetermined weight and placed in a stove at 393 K for at least 3 days. Upon cooling in a desiccator containing dried kiesel gel, the weight of the tray was again determined.

RESULTS AND DISCUSSION

Effect Ca²⁺ concentration on maleate-hydratase activity

The effect of Ca²⁺ concentration on maleate-hydratase activity of permeabilized *P. pseudoalcaligenes* was found to be negligible; the average and the standard deviation from the average were 0.28 μ mol·min⁻¹·mg⁻¹ and $1.8 \cdot 10^{-2}$ μ mol·min⁻¹·mg⁻¹, respectively, and the slope of the fitted straight line through the activity vs. Ca²⁺ concentration data (with 95% confidence interval) was -0.14 ± 0.36 dm³·min⁻¹·mg⁻¹.

Since there is no direct negative effect on biocatalyst activity itself, the Ca^{2+} concentration is an attractive tool to control inhibition by substrate and product: it affects maleate²⁻ (substrate) and D-malate²⁻ (product) concentrations by (solid) Ca-maleate and Ca-D-malate formation, respectively (Sillen and Martell, 1964).

Effect ionic strength on maleate-hydratase activity

Fig. 3 shows that a negative effect of ionic strength (I) on maleate-hydratase activity of permeabilized *P. pseudoalcaligenes* was significant only at $I > 2$. As in the liquid-solid-solid three-phase system of Fig. 2 the concentration of each bivalent ion (Ca^{2+} , maleate²⁻, and D-malate²⁻) is 200 mM at maximum (Lide, 1991; Michielsen et al., 1998b), so that $I \leq 0.9$ (calculated with a 500 mM Tris buffer at pH 8), the ionic strength will not affect biocatalyst activity.

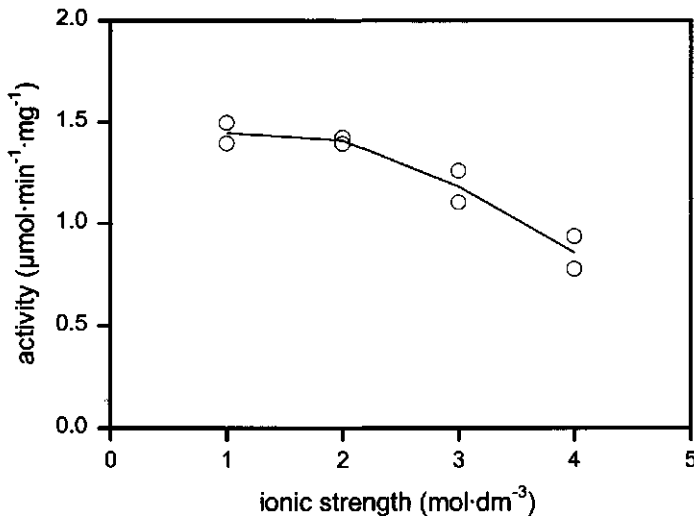


Figure 3 Effect of ionic strength (I) on maleate-hydratase activity of permeabilized *P. pseudoalcaligenes* at 308 K and pH 8.

Effect substrate concentration on maleate-hydratase activity

At high initial maleate concentrations (in comparison with the Michaelis constant K_m), Van der Werf et al. (1995) found that biocatalyst activity depended on the nature of the counter-ion for maleate. This was explained by assuming substrate inhibition, as the dissociation constant (K_s) of each counter-ion-maleate complex differs (Sigel and McCormick, 1970; Vallee and Coleman, 1964), resulting in different substrate

concentrations (maleate²⁻), and biocatalyst activity was found to increase with decreasing maleate²⁻ concentration.

To approve the purported substrate inhibition, we studied the effect of maleate concentration on biocatalyst activity quantitatively at 308 K and pH 8 by measuring initial rates (Fig. 4). It should be noted that at pH 8 almost all maleate is in dianionic form (maleate²⁻), since the pK_{a2} of maleic acid is 6.07 (Lide, 1991). As the substrate of maleate hydratase is maleate²⁻ (Van der Werf et al., 1993), the maleate concentration in Fig. 4 represents the actual substrate concentration. Fig. 4 shows that above 50 mM, maleate-hydratase activity decreased with substrate concentration, indicating substrate inhibition. This decrease might be effected by the increase in ionic strength (I) with substrate concentration. As at the substrate concentrations tested in Fig. 4 the ionic strength was smaller than two molar (see Fig. 3), the decrease of biocatalyst activity with substrate concentration was thus attributed solely to substrate inhibition.

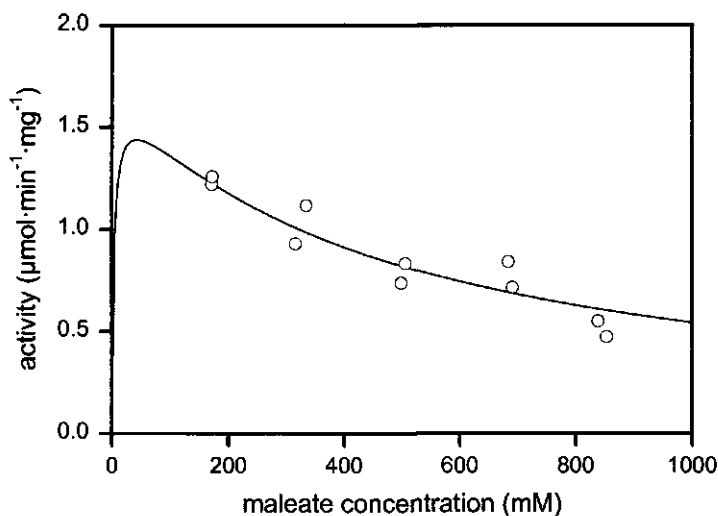


Figure 4 Effect of maleate concentration on initial maleate-hydratase activity of permeabilized *P. pseudoalcaligenes* at 308 K and pH 8; fit with $k_p = 17 \cdot 10^{-4} \text{ mmol} \cdot \text{min}^{-1} \cdot \text{mg}^{-1}$ and $K_m = 3.9 \text{ mM}$ (—) (values from Michielsen et al., 1998a).

The substrate inhibition constant K_{si} (at 308 K and pH 8) was determined by fitting a suitable equation through the data in Fig. 4 (Segel, 1975):

$$\frac{v}{C_e} = \frac{k_p \cdot C_s}{K_m + C_s + \frac{C_s^2}{K_{si}}} \quad (4)$$

with k_p the first-order reaction rate constant; C stands for concentration, with the subscript referring to the pertinent species. Note that, although product inhibition and biocatalyst inactivation were known to occur at 308 K and pH 8 (Michielsen et al., 1998a; this work), these were neglected here, as initial activities were measured. By fitting eq. (4) through the data in Fig. 4 with $k_p = 17 \cdot 10^{-4} \text{ mmol} \cdot \text{min}^{-1} \cdot \text{mg}^{-1}$ and $K_m = 3.9 \text{ mM}$ (values from Michielsen et al., 1998a), the substrate inhibition constant K_{si} was determined to be $469 \pm 79 \text{ mmol} \cdot \text{dm}^{-3}$ at 308 K and pH 8.

In practice, the conversion is not only characterized by substrate inhibition (with K_{si}) but also by competitive product inhibition (Michielsen et al., 1998a). Besides the conversion, a second reaction occurs simultaneously, that is inactivation of the biocatalyst (Michielsen et al., 1998a; Michielsen et al., 1999). Though all these phenomena (and corresponding kinetic parameters) were known at that point, the kinetic parameters were not known at all relevant process conditions and were determined independently from separate experiments. Per experiment only a few parameters were determined assuming undesirable phenomena not to occur significantly. It was assumed for instance, that product inhibition and biocatalyst inactivation would be negligible in measurements of initial biocatalyst activity. More realistic values for the kinetic parameters can be obtained by simultaneous determination of all parameter values in one set of experiments. Therefore, in this work a new experimental set-up was used: in a batch experiment the decrease of substrate, starting from a high initial concentration, was measured over a long period of time so that all phenomena, including substrate and competitive product inhibition and biocatalyst inactivation, would occur simultaneously. The data were fitted with the complete model, featuring all kinetic phenomena. As some parameters can be estimated more reliably at high substrate concentrations (K_{si}) while others require lower concentrations (K_m and K_p), three data sets of substrate concentration versus time, each starting at a different concentration, were fitted simultaneously.

Determination of kinetic parameters by simultaneous fitting

Starting from three different initial substrate concentrations, the decrease of substrate concentration with time (also called $C_s(t)$ -curve) was measured at pH 8

and four different temperatures (293, 298, 303, and 308 K) to determine the effect of temperature on the kinetic parameters (see Figs. 5a to d). The pH was set constant at 8, as biocatalyst activity decreases at pH values higher or lower than 8 (Michielsen et al., 1998a) and a less pure product could be formed due to $\text{Ca}(\text{OH})_2$ formation above $\text{pH}=8$ and $\text{Ca}-(\text{maleateH})_2$ formation below $\text{pH}=8$. High substrate concentrations (100, 300, and 500 mM) were chosen to get reliable estimates for the substrate inhibition constant, and a long experimental time was chosen, so that much product is formed and biocatalyst inactivates, and thus reliable estimates for the product inhibition constant (K_p) and the first-order rate constant for biocatalyst inactivation (k_d) could be obtained.

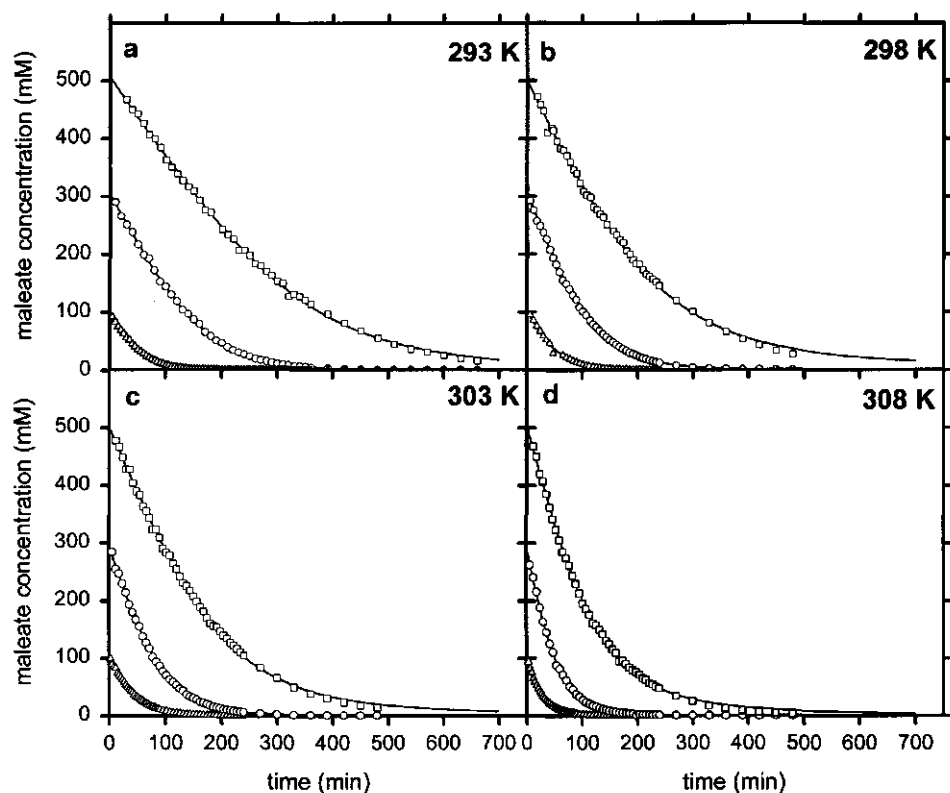


Figure 5 The decrease of substrate concentration with time at 293 K (a), 298 K (b), 303 K (c), and 308 K (d), and pH 8, starting from initial substrate concentrations of 100 mM (Δ), 300 mM (O), and 500 mM (\square); simultaneous fit of the 100 mM, 300 mM, and 500 mM- $C_s(t)$ -curves (—).

According to Michielsen et al. (1998a; 1999; this work) the decrease of substrate conversion rate with time is caused not only by decreasing substrate concentration, but also by a combination of substrate inhibition, competitive product inhibition and first-order irreversible biocatalyst inactivation. The general model for this mechanism is given in Fig. 6.

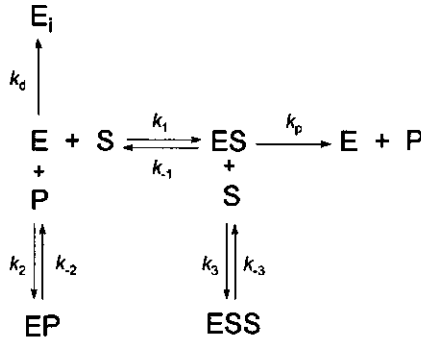


Figure 6 Reaction equations for a one-enzyme E, one-substrate S, one-enzyme/substrate-complex ES, and one-product P system with substrate inhibition, competitive product inhibition, and first-order irreversible biocatalyst inactivation; E_i is inactive enzyme and the k 's are rate constants.

Assuming a closed system with constant volume, the following rate equation can be derived, with $(C_s(0)-C_s)$ substituted for C_p :

$$v = \frac{dC_s}{dt} = - \frac{k_p \cdot C_e(0) \cdot e^{-k_d t} \cdot C_s}{K_m \cdot \left(1 + \frac{C_s(0) - C_s}{K_p} \right) + C_s + \frac{C_s^2}{K_{si}}} \quad (5)$$

with:

$$K_m = \frac{k_{-1} + k_p}{k_1}$$

$$K_p = \frac{k_{-2}}{k_2} = \frac{C_e \cdot C_p}{C_{ep}}$$

$$K_{si} = \frac{k_{-3}}{k_3} = \frac{C_{es} \cdot C_s}{C_{ess}}$$

with (0) referring to the situation at $t=0$. The first-order rate constant for biocatalyst inactivation (k_d) is known to decrease with the product concentration (C_p) (Michielsen et al., 1999). However, incorporation of such a relation in eq. (5) and then fitting eq. (5) through the $C_s(t)$ -curves of Fig. 5a to d resulted in good fits but unrealistic values for (some of) the fit parameters k_p , K_m , K_p , and K_{si} ; there was a difference of about one order of magnitude with the values determined earlier from separate independent activity experiments. Unrealistic parameter values were determined, as the active biocatalyst concentration was calculated to decrease too fast during the first minutes of the batch experiments due to the fact that there was still little product formed. This indicates that the first-order rate constant for biocatalyst inactivation (k_d) is probably also affected by the substrate concentration (C_s); k_d is therefore assumed to also decrease with increasing substrate concentration. To account for both the effect of substrate and product concentration on biocatalyst inactivation, k_d was assumed to be constant in these batch experiments (since C_s decreases and (thus) C_p increases with time).

The kinetic parameters k_p , k_d , K_m , K_p , and K_{si} were determined as a function of temperature by fitting eq. (5) simultaneously through the 100, 300, and 500 mM- $C_s(t)$ -curves at each temperature; $C_s(0)$ was known. The result is shown in Figs. 5a to d, and the values of the parameters are shown in Table 1. At each temperature, the model fitted the three data sets well ($R^2 > 0.99$). This supports the kinetic model assumed in this paper. As expected, k_p and k_d increased with temperature, whereas K_{si} decreased with temperature (between 293 and 308 K); K_m and K_p showed no clear temperature dependency (between 293 and 308 K). In general, the values for k_p in Table 1 were lower and the values for K_m and K_p in Table 1 were higher than the values reported previously (Michielsen et al., 1998a). The k_d values are hard to compare with previous values (Michielsen et al., 1998a; Michielsen et al., 1999), as the standard deviation from the average k_d value of different batches of permeabilized *P. pseudoalcaligenes* at similar conditions was found to be large ($\geq 11 \cdot 10^{-4} \text{ min}^{-1}$). The substrate inhibition constant at 308 K and pH 8 (see Table 1) was lower than the one determined from Fig. 4. These differences and the fact that the complete kinetic model fitted the data very well ($R^2 > 0.99$) indicate that in this work probably more realistic values for the kinetic parameters were obtained.

Table 1 Parameter values for k_p , k_d , K_m , K_p , K_{si} , and $C_s(0)$ with their 95% confidence intervals at pH 8 as a function of temperature, determined by simultaneously fitting of the 100, 300, and 500 mM- $C_s(t)$ -curves at each temperature, and the R^2 -values of each fit.

		293 K	303 K	308 K
known parameters				
$C_e(0)_{100}$	[mg·dm ⁻³]	8400	4120	4440
$C_e(0)_{300}$	[mg·dm ⁻³]	12600	8240	8880
$C_e(0)_{500}$	[mg·dm ⁻³]	12600	8240	8880
values of fit parameters				
k_p	[mmol·min ⁻¹ ·mg ⁻¹]	$2.2 \cdot 10^{-4} \pm 0.13 \cdot 10^{-4}$	$4.8 \cdot 10^{-4} \pm 0.53 \cdot 10^{-4}$	$5.5 \cdot 10^{-4} \pm 0.40 \cdot 10^{-4}$
k_d	[min ⁻¹]	$14 \cdot 10^{-4} \pm 1.5 \cdot 10^{-4}$	$23 \cdot 10^{-4} \pm 2.8 \cdot 10^{-4}$	$21 \cdot 10^{-4} \pm 2.4 \cdot 10^{-4}$
K_m	[mM]	7.1 ± 3.3	0.11 ± 1.4	4.5 ± 4.2
K_p	[mM]	17 ± 8.4	0.22 ± 2.8	7.2 ± 6.8
K_{si}	[mM]	551 ± 92	499 ± 158	446 ± 79
$C_s(0)_{100}$ ^{a)}	[mM]	97.7 ± 0.9	102 ± 1.9	103 ± 1.0
$C_s(0)_{300}$ ^{a)}	[mM]	305 ± 1.9	307 ± 3.3	296 ± 1.9
$C_s(0)_{500}$ ^{a)}	[mM]	508 ± 3.6	501 ± 6.5	502 ± 3.6
R^2 -values				
R_{100}^2		0.9997	0.9959	0.9996
R_{300}^2		0.9995	0.9996	0.9994
R_{500}^2		0.9991	0.9982	0.9990

^{a)} used as a fit parameter; the permeabilized cell suspension that is added to the substrate solution is a little viscous, resulting in small deviations from the aimed initial substrate concentration.

The kinetic parameters k_p , k_d , K_m , K_p , and K_{si} were fitted as a function of temperature (K) with an Arrhenius type of equation:

$$\ln k = \ln k_{\infty} - \frac{\Delta H}{R \cdot T} \quad (6)$$

The values of k_{∞} and ΔH for each parameter are shown in Table 2. Biocatalyst activity (v) can now be calculated as a function of temperature, substrate and product concentration with eq. (5) and the expressions for k_p , k_d , K_m , K_p , and K_{si} as a function of temperature (see eq. (6) and Table 2).

Table 2 The temperature dependency of the kinetic parameters k_p , k_d , K_m , K_p , and K_{si} ; the values for k_{∞} and ΔH in the Arrhenius type of equation for each kinetic parameter were determined by fitting $\ln k$ versus T .

parameters	kinetic parameters				
Arrh. eq.	k_p [mmol·min ⁻¹ ·mg ⁻¹]	k_d [min ⁻¹]	K_m [mM]	K_p [mM]	K_{si} [mM]
k_{∞} ^{a)}	$2.9 \cdot 10^9$	$1.4 \cdot 10^3$	$9.5 \cdot 10^8$	$2.8 \cdot 10^2$	$1.1 \cdot 10^{-2}$
ΔH (kJ·mol ⁻¹)	73	34 ^{b)}	50	11	-27

^{a)} units equal to units of kinetic parameter.

^{b)} ΔH for biocatalyst inactivation is generally in the order of magnitude of 200-300 kJ·mol⁻¹ (Van 't Riet and Tramper, 1991); the low value presented here could be due to the fact that at each temperature the stabilizing effects of substrate and product concentration were incorporated in the value for k_d .

Costs minimization

For commercial production of D-malate, the costs have to be minimized. This is usually done by selection of appropriate process conditions. For a bioreactor the costs factors are : 1) biocatalyst, 2) substrate, 3) investments (or depreciation) and operation, and 4) downstream processing. The substrate and biocatalyst costs are generally minimized by maximization of conversion (in mmol of product per mmol of initial or influent substrate) and of biocatalyst productivity (in mmol of product per mg of biocatalyst), respectively. For minimization of the investment and operating costs, the volumetric productivity (in mmol·dm⁻³·min⁻¹) is maximized in general, as this means that one can suffice with smaller equipment in order to obtain a certain

production rate (in $\text{mmol}\cdot\text{min}^{-1}$). The downstream-processing costs generally rise with decreasing product concentration. For that reason, conversion is maximized at high inlet substrate concentrations in a continuous system (Van 't Riet and Tramper, 1991). As some process parameters may have opposed effects on the optimization variables, selection of the optimal process conditions is complicated. Therefore, in the next section a stepwise procedure is followed to select the continuous process conditions at which D-malate is produced at the lowest overall costs. As the investment and operating costs and the downstream-processing costs are not known yet, their contribution to the overall costs is neglected here.

Optimization of conversion and biocatalyst productivity

A continuous stirred-tank reactor (CSTR) is considered for D-malate production from a maleate solution (Fig. 7). The biocatalyst is replenished to compensate for inactivation losses or wash-out, and is largely retained in the system and recycled to prevent major losses by wash-out.

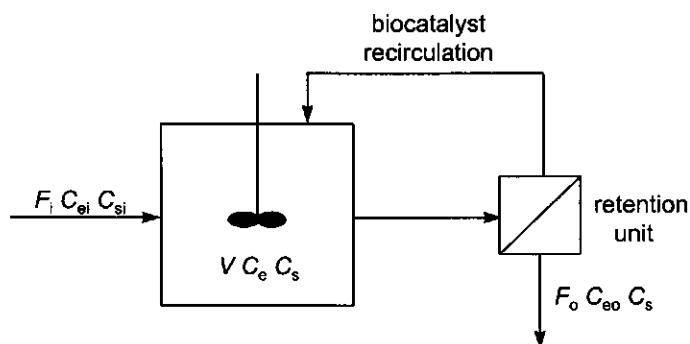


Figure 7 Continuous stirred-tank reactor (CSTR) for D-malate production with biocatalyst replenishment and recycling; F_i is the volumetric inflow rate and F_o the volumetric outflow rate of the system, C_{ei} and C_{si} are the active biocatalyst and substrate concentrations in the inflow, C_e and C_s are the steady-state active biocatalyst and substrate concentrations in the bioreactor, C_{eo} is the active biocatalyst concentration in the outflow of the system, and V is the volume of the reactor, including the volume of the recirculation loop.

The volume is assumed to be constant and well-mixed, with equal inflow and outflow rates (F). In Fig. 7, solid substrate (maleate) or product (D-malate) are assumed absent. However, the effects of the process parameters on the conversion and on

biocatalyst productivity were calculated in ranges that apply to systems with solid Ca-maleate and Ca-D-malate present, as we aim at producing D-malate in a liquid-solid-solid three-phase system (see Fig. 2). This means that the inlet substrate concentration (C_{si}) was varied between 0 and the solubility of Ca-maleate (200 mmol·dm⁻³; Michielsen et al., 1998b). The inlet biocatalyst concentration (C_{ei}) was varied between 0 and its physical constraint 15000 mg·dm⁻³. Temperature (T) and residence time (τ) were varied between 293 and 308 K, and between 0 and 50 h, respectively. Note that at the latter residence time, the investment and operating costs may become important. In steady state, the substrate concentration (C_s) can be calculated from the following mass balance (using the Cardano (1545) solution for cubic equations):

$$C_{si} - C_s = \frac{k_p \cdot C_e \cdot C_s}{K_m \left(1 + \frac{C_{si} - C_s}{K_p} \right) + C_s + \frac{C_s^2}{K_{si}}} \cdot \tau \quad (7)$$

with:

$$\tau = \frac{V}{F}$$

The active biocatalyst concentration in steady state (C_e) can be expressed as:

$$C_e = \frac{C_{ei}}{(1 - R_e) + \tau \cdot k_d} \quad (8)$$

with:

$$R_e = 1 - \frac{C_{eo}}{C_e}$$

where R_e is the biocatalyst recycling ratio. As k_p , k_d , K_m , K_p , and K_{si} can be calculated between 293 and 308 K (Table 2), the steady-state active biocatalyst and substrate concentrations (C_e and C_s) can be determined as a function of temperature too.

In a continuous system for D-malate production with biocatalyst replenishment and biocatalyst recycling, the conversion x (in mmol of product per mmol of initial or influent substrate) and biocatalyst productivity P (in mmol of product per mg initial or influent active biocatalyst) can be defined as:

$$x = \frac{C_p}{C_{si}} = \frac{C_{si} - C_s}{C_{si}} = \frac{k_p \cdot C_e \cdot C_s}{K_m \left(1 + \frac{C_{si} - C_s}{K_p} \right) + C_s + \frac{C_s^2}{K_{si}}} \cdot \tau \quad (9)$$

$$P = \frac{C_p}{C_{ei}} = \frac{C_{si} - C_s}{C_{ei}} = x \cdot \frac{C_{si}}{C_{ei}} \quad (10)$$

The sum of the substrate costs per mmol of product ($\$_s$) and the biocatalyst costs per mmol of product ($\$_e$) can now be expressed as:

$$\$_s + \$_e = \frac{p_s}{x} + \frac{p_e}{P} \quad (11)$$

where p_s is the substrate (maleate) price ($2.9 \cdot 10^{-3}$ \$·mmol⁻¹; Acros Chimica, 1994), and p_e is the biocatalyst price ($15 \cdot 10^{-3}$ \$·mg⁻¹; based on the cultivation and permeabilization of *P. pseudoalcaligenes* described in this work). The ratio of the substrate and biocatalyst costs per mmol of product can be expressed as:

$$\frac{\$_s}{\$_e} = \frac{p_s \cdot C_{si}}{p_e \cdot C_{ei}} \approx \frac{C_{si}}{5 \cdot C_{ei}} \quad (12)$$

Eq. (12) implicates that both costs are equal when $C_{si} \approx 5 \cdot C_{ei}$, that substrate is cost determining at $C_{si} \gg 5 \cdot C_{ei}$, and that biocatalyst is cost determining at $C_{si} \ll 5 \cdot C_{ei}$.

Effect of temperature

Fig. 8 shows the effect of temperature (between 293 and 308 K) on the substrate and biocatalyst costs per mmol of product (at $C_{si} = 100$ mmol·dm⁻³, $C_{ei} = 7500$ mg·dm⁻³, and $\tau = 50$ h) in a CSTR with biocatalyst replenishment and 90% biocatalyst recycling. As expected at $C_{si} = 100$ mmol·dm⁻³ and $C_{ei} = 7500$ mg·dm⁻³, the biocatalyst is fully cost determining (see eq. (12) and Fig. 8). The substrate and biocatalyst costs per mmol of product are hardly affected by temperature (T)

between 293 and 308 K (Fig. 8). Temperature can only influence these costs by affecting the rate of reaction v (see eqs. (9) to (11)). The rate of reaction (v) depends on the kinetic parameters k_p , k_d , K_m , K_p , and K_{si} according to eq. (5). Though the values of the kinetic parameters change with temperature (see Table 1), Fig. 8 shows that the overall effect of temperature on the rate of reaction v happens to be negligible. Note that C_{si} and C_{ei} were set at their intermediate level, whereas τ was set at its 'maximum' value (50 h) in the range from 0 to 50 h. The 'maximum' residence time was chosen, as the overall costs ($\$_{ov}$) decrease with increasing residence time (calculations not shown). It should be noted that in this case ($\tau = 50$ h) recycling hardly affects the substrate and biocatalyst costs per mmol of product ($\$_s$ and $\$_e$, respectively). This is due to the fact that C_e is hardly affected by R_e at $\tau = 50$ h, as $\tau k_d \gg (1-R_e)$ (see eq. (8)).

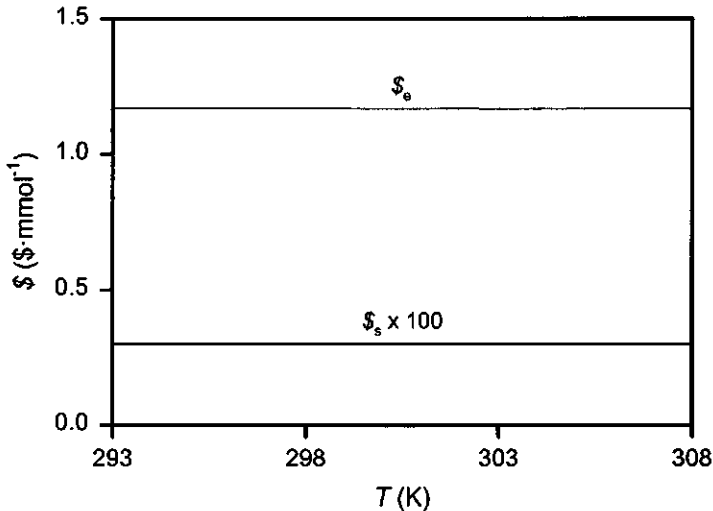


Figure 8 Substrate costs per mmol of product ($\$_s$) and biocatalyst costs per mmol of product ($\$_e$) as a function of temperature T at $C_{si} = 100 \text{ mmol} \cdot \text{dm}^{-3}$, $C_{ei} = 7500 \text{ mg} \cdot \text{dm}^{-3}$, and $\tau = 50$ h in a CSTR with biocatalyst replenishment and 90% biocatalyst recycling ($R_e = 0.9$); note that $\$_s$ is about a factor 400 smaller than $\$_e$.

Effects of influent substrate and biocatalyst concentration and residence time

The effects of the substrate and biocatalyst concentration in the feed (C_{si} and C_{ei} , respectively) on the sum of the substrate and biocatalyst costs per mmol of product ($\$_s + \$_e$) are shown in Fig. 9. At a constant inlet biocatalyst concentration (C_{ei}), the sum of the substrate and biocatalyst costs per mmol of product ($\$_s + \$_e$) decreases

with increasing C_{si} in the range from 0 to 200 mmol·dm⁻³, except at very small inlet biocatalyst concentrations (see Fig. 9). At $0 \leq C_{si} \leq 200$ mmol·dm⁻³ and constant C_{ei} , the biocatalyst productivity P increases with increasing C_{si} , as the steady-state product concentration (C_p) increases (data not shown). The conversion x decreases with increasing C_{si} . The latter is caused by the fact that the increase in C_p is less pronounced at high C_{si} due to increased substrate and product inhibition. Fig. 9 indicates that the decrease in the conversion x has a smaller effect on the sum of the substrate and biocatalyst costs per mmol of product ($\$_s + \$_e$) than the increase in the biocatalyst productivity P (except at very small inlet biocatalyst concentrations), as $\$_s + \$_e$ decreases with increasing C_{si} . However, when the inlet substrate concentration (C_{si}) would be increased still further, the sum of the substrate and biocatalyst costs per mmol of product ($\$_s + \$_e$) would eventually increase again. This is caused by the fact that C_p , and thus the biocatalyst productivity P , shows a maximum due to substrate inhibition.

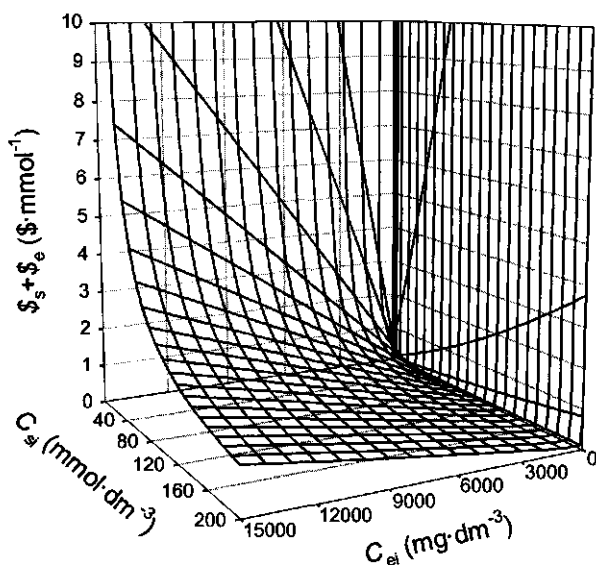


Figure 9

Sum of the substrate and biocatalyst costs per mmol of product ($\$_s + \$_e$) as a function of the substrate and biocatalyst concentration in the feed (C_{si} and C_{ei} , respectively) at $\tau = 50$ h and $T = 300.5$ K in a CSTR with biocatalyst replenishment and 90% biocatalyst recycling ($R_s = 0.9$).

At a constant inlet substrate concentration (C_{si}), the sum of the substrate and biocatalyst costs per mmol of product ($\$_s + \$_e$) decreases rapidly (at small C_{ei}) and then increases as a function of C_{ei} , indicating a minimum (see Fig. 9). At constant C_{si} , the conversion x increases with increasing C_{ei} , as the steady-state product concentration (C_p) increases. However, the increase in C_p decreases with increasing C_{ei} , until C_p remains almost constant (data not shown); note that at constant C_{si} this is due to the fact that the steady-state substrate concentration (C_s) decreases and product inhibition increases. The latter causes the biocatalyst productivity P to decrease with increasing C_{ei} . Fig. 9 indicates that at small inlet biocatalyst concentrations the increase in the conversion x has a bigger effect on the sum of the substrate and biocatalyst costs per mmol of product ($\$_s + \$_e$) than the decrease in the biocatalyst productivity P with increasing C_{ei} . However, from the moment that C_p remains almost constant, the decrease in biocatalyst productivity P has a bigger effect, resulting in a linear increase of the sum of both costs ($\$_s + \$_e$) with increasing C_{ei} due to the linear increase of the biocatalyst costs ($\$_e$) with increasing C_{ei} (see Fig. 9 and eq. (11)). At $C_{si} = 200 \text{ mmol}\cdot\text{dm}^{-3}$, the minimum in the sum of the substrate and biocatalyst costs per mmol of product ($\$_s + \$_e$) is found at $C_{ei} = 348 \text{ mg}\cdot\text{dm}^{-3}$ (see Fig. 9).

It is obvious that the sum of the substrate and biocatalyst costs per mmol of product ($\$_s + \$_e$) decreases with increasing residence time τ , as both the amount of substrate and of active biocatalyst being washed out decrease with increasing τ , resulting in a higher steady-state product concentration (C_p). So, within the ranges applied in this work the sum of the substrate and biocatalyst costs per mmol of product ($\$_s + \$_e$) is minimal at $C_{si} = 200 \text{ mmol}\cdot\text{dm}^{-3}$, $C_{ei} = 345 \text{ mg}\cdot\text{dm}^{-3}$, $\tau = 50 \text{ h}$, and $R_e = 1$; note that at the minimum C_{ei} is smaller than at the conditions in Fig. 9, as R_e is higher. The costs at these conditions ($0.111 \text{ \$}\cdot\text{mmol}^{-1}$) are far below the market price ($0.851 \text{ \$}\cdot\text{mmol}^{-1}$; Acros Chimica, 1994), indicating that *D-malate* production by permeabilized *P. pseudoalcaligenes* in a liquid-solid-solid three-phase system can be very profitable.

CONCLUSIONS

The kinetics of D-malate production can be described well by a model featuring substrate inhibition and competitive product inhibition, and first-order irreversible biocatalyst inactivation. In comparison with separate independent determinations of kinetic parameter values, more realistic values were obtained by simultaneously fitting the complete kinetic model through three independent substrate concentration vs. time data sets (each data set with a different initial substrate concentration and determined over a long period of time). The kinetic parameters k_p , k_d , and K_{si} were temperature dependent; k_p and k_d increased, whereas K_{si} decreased with temperature. The kinetic parameters K_m and K_p showed no clear temperature dependency.

Neglecting investment and operating costs and downstream-processing costs, the D-malate production costs (consisting of the sum of the substrate and biocatalyst costs per mmol of product) in a continuous system with biocatalyst replenishment and biocatalyst recycling were calculated to decrease with the residence time and to be minimal at $C_{si} = 200 \text{ mmol}\cdot\text{dm}^{-3}$ and $C_{ei} = 345 \text{ mg}\cdot\text{dm}^{-3}$ (with $0 \leq C_{si} \leq 200 \text{ mmol}\cdot\text{dm}^{-3}$ and $0 \leq C_{ei} \leq 15000 \text{ mg}\cdot\text{dm}^{-3}$). These costs could be reduced further by increasing the amount of biocatalyst that is recycled (at a constant biocatalyst inflow). Temperature hardly affects the D-malate production costs (between 293 and 308 K).

ACKNOWLEDGEMENTS

We thank S. Hartmans and M.J. van der Werf (Division of Industrial Microbiology, Wageningen Agricultural University) for supplying *P. pseudoalcaligenes* and for fruitful discussions on cultivation and permeabilization of *P. pseudoalcaligenes*.

This work was financially supported by the Ministry of Economic Affairs, the Ministry of Education, Culture and Science, the Ministry of Agriculture, Nature Management and Fishery in the framework of an industrial relevant research programme of the Netherlands Association of Biotechnology Centres in the Netherlands (ABON).

APPENDIX A: Determination of the dissociation constant of Ca-maleate

Materials and method

To study whether Ca^{2+} inhibits the enzyme or not, the Ca^{2+} concentration had to be varied and the maleate²⁻ (actual substrate) concentration set constant. To be able to calculate the Ca^{2+} and maleate²⁻ concentration in solutions of CaCl_2 and maleic acid, the dissociation constant of Ca-maleate (K_s) had to be determined, as also undissociated Ca-maleate is present in these solutions (Sillen and Martell, 1964). As at constant temperature K_s is a function of ionic strength (I) only (Martell and Smith, 1979; Sillen and Martell, 1964), and I is not constant in the experimental set-up described above (Ca^{2+} varies), K_s was determined as a function of I . This was done as follows.

Solutions of 0.1, 0.2, 0.25, 0.5, 0.75, 1.0, 1.25, or 1.5 M KCl and 10 mM Ca-maleate·H₂O in double-distilled water were made. The solutions were incubated at 298 K in a shaking water bath (170 rpm) and the Ca^{2+} concentrations were measured (at 298 K) by using a Ca^{2+} -sensitive electrode (Orion Research, Model 93-20) and a standard curve of electrode potential versus Ca^{2+} concentration; at each ionic strength, a new standard curve was determined. As the concentration of mono-anionic maleate (maleateH⁻) was calculated to be very low, the concentrations of $\text{Ca}(\text{maleateH})_2$ and maleic acid were calculated to be very low too. As a result the dissociation constant K_s could be calculated with:

$$K_s = \frac{C_{\text{Ca}^{2+}} \cdot C_{\text{maleate}^{2-}}}{C_{\text{Ca-maleate}}} = \frac{C_{\text{Ca}^{2+}}^2}{C_{\text{total maleate}} - C_{\text{Ca}^{2+}}} \quad (\text{A1})$$

Finally, the ionic strength (I) was calculated with (Chang, 1981):

$$I = 0.5 \cdot \sum C_j \cdot z_j^2 \quad (\text{A2})$$

where C_j is the concentration of ion j and z_j is the valence of ion j .

Results

Fig. A shows the dissociation constant of Ca-maleate (K_s) as a function of ionic strength (I). It was found to be in reasonable agreement with the dissociation constant reported by Sillen and Martell (1964): $K_s = 7.94 \cdot 10^{-2} \text{ mol} \cdot \text{dm}^{-3}$ at 298 K and $I = 0.16$. In agreement with Sillen and Martell (1964), it increased with ionic strength. The relation between K_s and I was approximated to be linear:

$$K_s = 0.112 \cdot I + 2.28 \cdot 10^{-2} \quad (\text{A3})$$

with: $R^2 = 0.80$, $R_{\text{adj}}^2 = 0.77$.

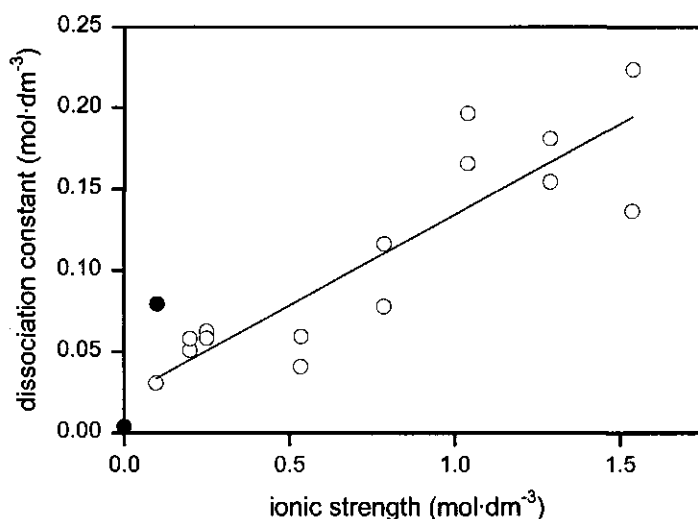


Figure A Dissociation constant of Ca-maleate (K_s) as a function of ionic strength (I) at 298 K (O); fit of the data (O) with linear relation (—). Data reported by Sillen and Martell (1964) (●).

NOMENCLATURE

C	concentration	(mmol·dm ⁻³)
C_e	active enzyme concentration	(mg·dm ⁻³)
$C_e(0)$	active enzyme concentration at $t = 0$	(mg·dm ⁻³)
$\$$	costs per mmol of product	(\$·mmol ⁻¹)
C_s	substrate concentration	(mmol·dm ⁻³)
$C_s(0)$	substrate concentration at $t = 0$	(mmol·dm ⁻³)
ΔH	activation enthalpy	(kJ·mol ⁻¹)
F	inflow and outflow of CSTR	(m ³ ·h ⁻¹)
I	ionic strength	(mol·dm ⁻³)
K_m	Michaelis constant	(mmol·dm ⁻³)
K_p	product inhibition constant	(mmol·dm ⁻³)
K_S	dissociation constant of Ca-maleate	(mol·dm ⁻³)
K_{si}	substrate inhibition constant	(mmol·dm ⁻³)
k_d	first-order rate constant for biocatalyst inactivation	(min ⁻¹)
k_p	first-order reaction rate constant	(mmol·min ⁻¹ ·mg ⁻¹)
k_{-1}	first-order reaction rate constant	(mmol·min ⁻¹ ·mg ⁻¹)
k_1	second-order reaction rate constant	(dm ³ ·min ⁻¹ ·mg ⁻¹)
k_{-2}	first-order reaction rate constant	(mmol·min ⁻¹ ·mg ⁻¹)
k_2	second-order reaction rate constant	(dm ³ ·min ⁻¹ ·mg ⁻¹)
k_{-3}	first-order reaction rate constant	(mmol·min ⁻¹ ·mg ⁻¹)
k_3	second-order reaction rate constant	(dm ³ ·min ⁻¹ ·mg ⁻¹)
k_{∞}	constant	(see Table 2)
P	biocatalyst productivity	(mmol·mg ⁻¹)
p	price	(\$·mmol ⁻¹) or (\$·mg ⁻¹)
R	gas constant	(8.314 J·mol ⁻¹ ·K ⁻¹)
R_e	biocatalyst recycling ratio	(-)
T	temperature	(K)
t	time	(min)
V	volume of CSTR	(m ³)
v	biocatalyst activity or rate of reaction	(mmol·dm ⁻³ ·min ⁻¹)
x	conversion	(-)
z	valency of an ion	(-)

Greek symbols

τ	residence time	(h)
--------	----------------	-----

Indices

e	enzyme
ei	enzyme in inflow of CSTR
eo	enzyme in outflow of CSTR
ep	enzyme/product-complex
es	enzyme/substrate-complex
ess	enzyme/substrate/substrate-complex
i	inactive
p	product
s	substrate
sat	saturation
si	substrate in inflow of CSTR
100	100 mM- $C_s(t)$ -curve
300	300 mM- $C_s(t)$ -curve
500	500 mM- $C_s(t)$ -curve

REFERENCES

- Acros Chimica 94-95. 1994. p 894. Catalogue handbook of fine chemicals.
- Cardano G. 1545. Ars Magna.
- Chang RM. 1981. Physical chemistry with applications to biological systems. New York: MacMillan publishing Co., Inc. 659p.
- Clarke FH, Hill RT, Koo J, Lopano RM, Maseda MA, Smith M, Soled S, VonVeh G, Vlattas I. 1978. A series of hexahydro[1,4]oxazino[3,4-a]isoquinolines as potential neuroleptics. J Med Chem 21:785-791.
- Crosby J. 1992. Chirality in industry - an overview. In: Collins AN, Sheldrake GN and Crosby J, editors. Chirality in industry. Chichester: John Wiley & Sons Ltd, p 1-66.
- Elferink VHM, Breitgoff D, Kloosterman M, Kamphuis J, Van den Tweel WJJ, Meijer EM. 1991. Industrial development in biocatalysis. Recl Trav Chim Pays-Bas 110:63-74.

- Heil B, Kvintovics P, Tarszabó L. 1985. Stereo- and enantio-selective hydrogenation of ketones using iridium catalysts containing a carboxylate ligand. *J Mol Catal* 33:71-75.
- Lide DR, editor. 1991. p 4-48, 8-40. CRC Handbook of chemistry and physics, 72th edition. Boca Raton: CRC Press, Inc.
- Martell AE, Smith RM, editors. 1979. Critical stability constants, Volume 3: Other organic ligands, 2nd edition. New York: Plenum Press.
- Michielsen MJF, Meijer EA, Wijffels RH, Tramper J, Beertink HH. 1998a. Kinetics of D-malate production by permeabilized *Pseudomonas pseudoalcaligenes*. *Enzyme Microb Technol* 22:621-628.
- Michielsen MJF, Reijenga KA, Wijffels RH, Tramper J, Beertink HH. 1998b. Dissolution kinetics of Ca-maleate crystals: evaluation for biotransformation reactor design. *J Chem Technol Biotechnol* 73:13-22.
- Michielsen MJF, Frielink C, Meijer EA, Van der Werf MJ, Wijffels RH, Tramper J, Beertink HH. 1999. Stabilization of maleate-hydratase activity of permeabilized *Pseudomonas pseudoalcaligenes*. *Biocatal Biotransf* 17: 125-137.
- Seebach D, Hungerbühler E. 1980. Syntheses of enantiomerically pure compounds (EPC syntheses). Tartaric acid, an ideal source of chiral blocks for syntheses?. In: Scheffold R, editor. Modern synthetic methods, volume 2. Frankfurt am Main: Otto Salle Verlag, GmbH & Co. p 91-171.
- Segel IH. 1975. Enzyme kinetics. New York: Wiley Interscience Publications. 957p.
- Shiozawa A, Ishikawa M, Sugimura H, Narita K, Yamamoto H, Sakasai T, Ohtsuki K, Kurashige S. 1988. Preparation of optically active 2-methyl-3-(1-pyrrolidinyl)-1-[4-(trifluoromethyl)phenyl]-1-propanone as a muscle relaxant. EP. 266,577 (CA 109:128823).
- Sigel H, McCormick DB. 1970. On the discriminating behaviour of metal ions and ligands with regard to their biological significance. *Acc Chem Res* 3:201-208.
- Sillen LG, Martell AE, editors. 1964. p 406-407, 411-412. Stability constants of metal-ion complexes, Section I: Inorganic ligands, Section II: Organic ligands, 2nd edition. The Chemical Society. London: Lewis Reprints Ltd.
- Tanabe T, Okuda K, Izumi Y. 1973. Asymmetric hydrogenation of C=O double bond with modified Raney nickel catalyst. XXV. Contributions of pH-adjusting reagents in the asymmetric hydrogenation. *Bull Chem Soc Jap* 46:514-517.

- Vallee BL, Coleman E. 1964. Metal coordination and enzyme action. *Compr Biochem* 12:165-235.
- Van der Werf MJ, Van den Tweel WJJ, Hartmans S. 1992. Screening for microorganisms producing D-malate from maleate. *Appl Environ Microbiol* 58:2854-2860.
- Van der Werf MJ, Van den Tweel WJJ, Hartmans S. 1993. Purification and characterization of maleate hydratase from *Pseudomonas pseudoalcaligenes*. *Appl Environ Microbiol* 59:2823-2829.
- Van der Werf MJ, Hartmans S, Van den Tweel WJJ. 1995. Effect of maleate counter-ion on malease activity: production of D-malate in a crystal-liquid two-phase system. *Enzyme Microb Technol* 17:430-436.
- Van 't Riet K, Tramper J. 1991. *Basic Bioreactor Design*. New York: Marcel Dekker, Inc. 465p.

CHAPTER 6

Growth of Ca-D-malate crystals in a bioreactor

ABSTRACT

To develop a bioreactor for solid-to-solid conversions, the conversion of solid Ca-maleate to solid Ca-D-malate by permeabilized *Pseudomonas pseudoalcaligenes* was studied. In a bioreactor seeded with product (Ca-D-malate) crystals, growth of Ca-D-malate crystals is the last step in the solid-to-solid conversion and is described here. Crystal growth is described as a transport process followed by surface processes. In contrast to the linear rate law obeyed by the transport process, the surface processes of a crystal growth process can also obey a parabolic or exponential rate law. Growth of Ca-D-malate crystals from a supersaturated aqueous solution was found to be surface controlled and obeyed an exponential rate law. Based on this rate law, a kinetic model was developed which describes the decrease in supersaturation due to Ca-D-malate crystal growth as a function of the constituent ions, Ca^{2+} and D-malate²⁻. The kinetic parameters depended on temperature, but, as expected (surface controlled), they were hardly affected by the stirring speed.

INTRODUCTION

Low product concentrations often hamper bioconversion processes from being commercialized due to the high downstream-processing costs. In aqueous media, increasing the soluble substrate concentration is often a limited means to attain higher product concentrations due to low substrate solubilities. Besides, if high solubilities can be reached, many biocatalysts are inhibited by high substrate and/or product concentrations (Michielsen et al., 1999a; Van den Heuvel and Beekink, 1988; Van der Werf et al., 1995). Overall substrate solubility can be increased and inhibition can be minimized by extraction of the substrate and/or product from the aqueous reaction phase into a second phase, resulting in higher overall volumetric productivities. In many cases an organic solvent is used as a second phase. However, use of an organic phase makes the process less environmentally friendly, less cost efficient, and often the product is contaminated; the latter could be a problem especially in the drug and food industries (Erbeldinger et al., 1998). A good alternative overcoming these disadvantages, is offering the substrate in solid form and removing the product by crystallization. In that case both the substrate and the product are accumulated in a solid phase. Other advantages of crystallization are its effectiveness at low temperatures (which can be important for thermally labile compounds), the easy and good separation of the solid product from the production medium (by centrifugation or filtration), and the possibility to control the final product characteristics, like morphology, particle size, purity, and stability, during production (Kirwan and Orella, 1993).

In order to develop a bioreactor for solid-to-solid conversions, we study the conversion of solid Ca-maleate to solid Ca-D-malate (see Fig. 1).

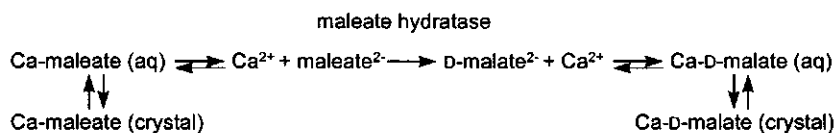


Figure 1 Reaction scheme for the conversion of solid Ca-maleate to solid Ca-D-malate by maleate hydratase in permeabilized *P. pseudoalcaligenes*.

As the dissolution of Ca-maleate and the conversion of maleate²⁻ to D-malate²⁻ were characterized before (Michielsen et al., 1998a; Michielsen et al., 1999a), in this work the last step, crystallization of Ca-D-malate, was studied.

By definition, crystallization consists of a nucleation and a growth process. Although nuclei are formed at any degree of supersaturation, excessive amounts are instantaneously formed only at a pronounced supersaturation (called the metastable limit). At moderate supersaturation and in the presence of product crystals, crystal growth is the predominant mechanism (Estrin, 1993). Especially in case of product inhibition, a bioreactor seeded with product crystals is favorable, as these crystals maintain the supersaturation at a rather low level by crystal growth. Besides, at this supersaturation nucleation is unlikely to occur, which makes control of product formation in the bioreactor easier. Therefore, this work neglects nucleation and focuses only on the crystal growth kinetics of Ca-D-malate crystals and on the effects of process conditions. Process parameters that potentially influence the growth of Ca-D-malate crystals are the stirring speed, temperature, ionic strength, and biocatalyst and Ca²⁺ concentration.

THEORY

Crystal growth rates are often determined in seeded desupersaturation experiments (Bujac and Mullin, 1969; Jones and Mullin, 1973; Halfon and Kaliaguine, 1976; Palwe et al., 1985; Qui and Rasmuson, 1990). In such an experiment, a certain amount of seed crystals is added to an isothermal, supersaturated solution in e.g. a stirred tank, and the decrease in supersaturation due to crystal growth, called desupersaturation, is recorded. Advantages of this method are: 1) it is possible to measure the growth rate at hydrodynamic conditions resembling the industrial situation, and 2) a large number of seed crystals makes the results statistically founded.

Growth-rate models

As in dissolution processes, the growth rate of salt crystals is controlled by the rate of transport to the surface, by the rate of surface processes, or by both. For dissolution, an overall rate equation accounting for both processes can easily be derived, as both processes obey linear rate laws - the rate being proportional to a

concentration difference (the driving force). According to Nielsen (1984), two serial surface processes occur during growth of a salt crystal: ion adsorption, and subsequent integration of the ions into the crystal lattice. Ions are adsorbed by a linear rate law, while they are integrated by a parabolic or exponential rate law, or by a combination thereof (Nielsen, 1984). This means that depending on the rate-controlling surface process, a different overall rate equation accounting for both transport and surface rates can be derived. However, usage of these complex overall rate equations is unnecessary, if crystal growth is either fully transport controlled or fully surface controlled. To determine this, Nielsen and Toft (1984) defined the transport control index $q_{T,j}$:

$$q_{T,j}(t) = \frac{G(t)}{G_{T,j}(t)} \quad (1)$$

where t is time, G is the actual linear growth rate ($= dL/dt$; where L is a characteristic dimension of a Ca-D-malate crystal (in this work, the breadth)), and G_T is the purely transport-controlled linear growth rate; the subscript i refers to the size class in the initial crystal-size distribution (CSD) with j classes. Since crystals are generally polydisperse, they are characterized by a CSD. Eq. (1) shows that q_T depends on the crystal size, as G_T is affected by the crystal size (this will be explained later). If $q_T \gg 1$, individual crystals aggregate. If $q_T \approx 1$, crystal growth is transport controlled; if $q_T \ll 1$, crystal growth is surface controlled. Only in intermediate cases ($q_T \approx 0.5$), the growth rate is influenced by both transport and surface processes. This means that for a good prediction of the growth rate, transport- and surface-controlled kinetics must be combined in an overall rate equation. Surface-controlled growth of salt crystals can obey linear, parabolic, or exponential rate laws (see eqs. (7) to (9)). Expressions for growth rates resulting from transport- and linear surface-controlled kinetics and transport- and parabolic surface-controlled kinetics are given by Nyvlt et al. (1985). The four possibilities described above (and corresponding rate equations) are shown in Fig 2a. For calculation of $q_{T,j}$, expressions for G and $G_{T,j}$ are given below (eqs. (3) and (4), respectively). Finally, the rate equations for surface-controlled, linear, parabolic, and exponential crystal growth are given (eqs. (7), (8), and (9), respectively), because at all conditions in this work, $q_T \ll 1$.

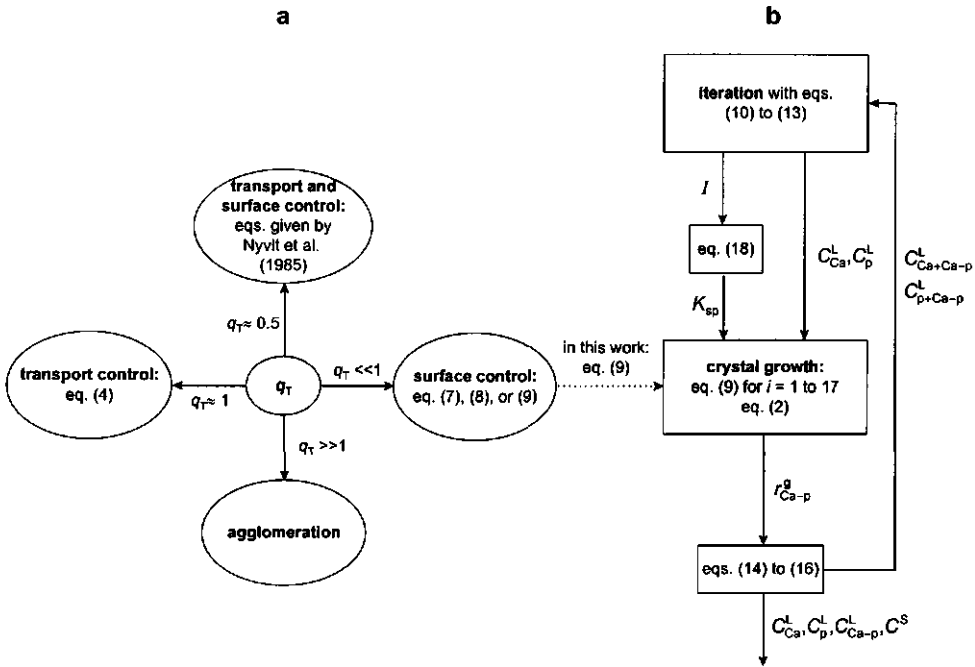


Figure 2 Diagram for determination of the rate-controlling process(es) (a), and the complete kinetic model for Ca-D-malate crystal growth (b); note that at all conditions in this work, $q_T \ll 1$.

The actual linear growth rate G can be directly related to the volumetric growth rate r^g , that is the slope of the desupersaturation curve ($dC_p^L(t)/dt$ or $dC_{Ca}^L(t)/dt$, with C_p^L the D-malate²⁻ concentration and C_{Ca}^L the Ca^{2+} concentration in the liquid phase, or an equivalent decrease of a related variable), through the relation:

$$r^g = \frac{dC_p^L(t)}{dt} = \sum_{i=1}^I \frac{N_i}{\epsilon \cdot V \cdot M_w} \cdot \frac{dm(t)}{dt} = \sum_{i=1}^I \frac{N_i}{\epsilon \cdot V \cdot M_w} \cdot \frac{d}{dt} \alpha \cdot L_i(t)^3 \cdot \rho^S = \sum_{i=1}^I \frac{N_i}{\epsilon \cdot V \cdot M_w} \cdot 3 \cdot \alpha \cdot L_i(t)^2 \cdot \rho^S \cdot G \quad (2)$$

where N_i is the number of crystals in size class i , ϵ is the hold-up of the liquid phase in the suspension ($= V^L/(V^S+V^L)$, where V^L is the volume of the liquid phase, and V^S is the volume of the solid phase; in this work, $\epsilon \approx 1$), V is the volume of the suspension (V^S+V^L), M_w is the molecular mass of Ca-D-malate- $3H_2O$, m is the mass of one

crystal, α is the volume shape factor of a Ca-D-malate·3H₂O crystal ($= V_c/L^3$, where V_c is the volume of one crystal), and ρ^s is the density of solid Ca-D-malate·3H₂O. It is assumed that during growth the crystals have a constant shape, that is α and β ($=$ the surface shape factor $= A_c/L^2$, where A_c is the surface area of one crystal) are constant, and that they do not break up and do not form agglomerates. The latter implicates that the number of crystals N_i in each initial size class i remains constant. By rewriting eq. (2), an expression for the actual linear growth rate G is found:

$$G = \sum_{i=1}^j \frac{\epsilon \cdot V \cdot M_w}{N_i \cdot 3 \cdot \alpha \cdot L_i(t)^2 \cdot \rho^s} \cdot \frac{dC_p^L(t)}{dt} \quad (3)$$

The transport-controlled linear growth rate of a Ca-D-malate crystal in size class i ($G_{T,i}$) can be expressed as (Nielsen, 1980):

$$G_{T,i} = \frac{dL_i(t)}{dt} = \frac{\beta \cdot k_{T,i}(t) \cdot M_w}{3 \cdot \alpha \cdot \rho^s} \cdot \left(\frac{C_{Ca}^L(t) + C_p^L(t)}{2} - \sqrt{\left(\frac{C_{Ca}^L(t) - C_p^L(t)}{2} \right)^2 + K_{sp}} \right) \quad (4)$$

where β is the surface shape factor of a Ca-D-malate·3H₂O crystal, k_T is the mass-transfer rate coefficient, and K_{sp} is the apparent solubility product of Ca-D-malate ($= C_{Ca}^{L*} \cdot C_p^{L*}$; the superscript * refers to saturation). Several authors have correlated the mass transfer to solid particles in a stirred tank to the diffusion coefficient (D), the characteristic dimension of the solid particle ($L(t)$), the power input per kg liquid phase (ϵ), and the kinematic viscosity (ν), using the dimensionless Sherwood number ($Sh(t)$). Although many Sherwood equations are given in literature (Levins and Glastonbury, 1972; Ranz and Marshall, 1952; Tournié et al., 1979), the equation of Sano et al. (1974) is used here, as it is valid for a wide range of applications (for spherical and non-spherical particles in both agitated tanks and bubble columns):

$$k_{T,j}(t) = \frac{Sh_i(t) \cdot D}{L_i(t)} = \left[2 + 0.4 \cdot \left(\frac{\varepsilon \cdot L_i(t)^4}{\nu^3} \right)^{\frac{1}{4}} \cdot \left(\frac{\nu}{D} \right)^{\frac{1}{3}} \right] \cdot \frac{\phi_c \cdot D}{L_i(t)} \quad (5)$$

with:

$$\varepsilon = \frac{N_p \cdot d_s^5 \cdot n^3}{\epsilon \cdot V} \quad , \quad \phi_c = 6 \cdot \frac{\alpha}{\beta}$$

where N_p is the power number, d_s is the diameter of the stirrer, n is the stirring speed, and ϕ_c is Carman's surface factor. According to Sano et al. (1974), however, their Sherwood equation has a standard deviation of 30.8%. This means that in applications where a more specific Sherwood equation is available, it is recommended to incorporate this equation into the model instead of the version used here.

Eq. (5) shows that k_T is time-dependent and can be calculated for each size class of crystals, since it depends on the time-dependent characteristic dimension of a crystal $L_i(t)$. Eq. (5) further shows that the mass-transfer rate coefficient $k_{T,i}(t)$ decreases with increasing characteristic dimension of a crystal ($L_i(t)$). As $G_{T,i}(t)$ decreases proportionally with $k_{T,i}(t)$ (see eq. (4)), this means that during crystal growth the transport control index q_T increases, indicating that the growth process becomes more transport controlled.

The value of the diffusion coefficient D is expected to depend on temperature T according to (Chang, 1981; Hunik et al., 1994):

$$D = \frac{k_B \cdot T}{6 \cdot \pi \cdot \eta \cdot r} = \frac{k_B \cdot T}{6 \cdot \pi \cdot 6.021 \cdot 10^{-7} \cdot e^{\frac{18100}{R \cdot T}} \cdot r} \quad (6)$$

where k_B is the Boltzmann' constant, η is the dynamic viscosity of the liquid phase, r is the molecular radius of Ca-D-malate, and R is the gas constant.

Surface-controlled linear growth rates show linear, parabolic, and exponential rate laws; a linear rate law (eq. (7)) is obtained in case of adsorption control, parabolic and exponential rate laws (eqs. (8) and (9), respectively) in case of integration control (Nielsen and Toft, 1984):

$$G_R = \frac{dL(t)}{dt} = \frac{\beta \cdot k_{lin} \cdot M_w}{3 \cdot \alpha \cdot \rho^S} \cdot \sqrt{K_{sp}} \cdot (S(t) - 1) \quad (7)$$

$$G_R = \frac{dL(t)}{dt} = \frac{\beta \cdot k_{par} \cdot M_w}{3 \cdot \alpha \cdot \rho^S} \cdot \sqrt{K_{sp}} \cdot (S(t) - 1)^2 \quad (8)$$

$$G_R = \frac{dL(t)}{dt} = \frac{\beta \cdot k_{exp} \cdot M_w}{3 \cdot \alpha \cdot \rho^S} \sqrt{K_{sp}} \cdot S(t)^{7/6} \cdot (S(t) - 1)^{2/3} \cdot (\ln S(t))^{1/6} \cdot \exp\left[-K_{exp} / \ln S(t)\right] \quad (9)$$

with:

$$S(t) = \frac{\sqrt{C_{Ca}^L(t) \cdot C_p^L(t)}}{\sqrt{K_{sp}}}$$

where k_{lin} , k_{par} , and k_{exp} are reaction rate coefficients of one (or more) of the surface processes, K_{exp} is a temperature-dependent constant (Nielsen, 1984), and S the supersaturation ratio. Note that the surface-controlled growth rate G_R is independent of the characteristic dimension $L(t)$ of a Ca-D-malate-3H₂O crystal. This means that the surface-controlled growth rate is equal for all crystals in the crystal-size distribution.

Dissociation equilibrium

No matter which rate law is obeyed, the growth rate of a salt is affected by the concentration of its constituent ions, here Ca²⁺ and D-malate²⁻ (see Fig. 2b). In general, ionic concentrations cannot be measured directly. By assuming that dissociation of Ca-D-malate is at equilibrium, the Ca²⁺ and D-malate²⁻ concentrations can be calculated. As during desupersaturation (due to crystal growth) the ionic strength in the liquid phase decreases, and the dissociation constant of Ca-D-malate depends on the ionic strength (Michielsen et al., 1999b), the ion-concentration calculations were done by iteration with eqs. (10) to (13).

The ionic strength (I) is given by:

$$I = 0.5 \cdot \sum_h C_h \cdot z_h^2 = 0.5 \cdot (C_{\text{Tris}}^L \cdot 1^2 + C_{\text{Ca}}^L \cdot 2^2 + C_p^L \cdot 2^2 + C_{\text{Cl}}^L \cdot 1^2) \quad (10)$$

where C_h is the concentration of ion h , z_h is its valency, C_{Tris}^L is the Tris^+ concentration, and C_{Cl}^L is the Cl^- concentration. Note that the Cl^- concentration in eq. (10) originates from HCl that was used to adjust the pH to 8 (= the optimum pH for D-malate²⁻ production by permeabilized *P. pseudoalcaligenes* (Michielsen et al., 1998b)), and that the effects of the H^+ and OH^- concentrations on the ionic strength were calculated to be negligible. The effect of biocatalyst concentration on the ionic strength was assumed to be negligible as well.

The dissociation constant of Ca-D-malate (K_p) as a function of ionic strength can be calculated from (Michielsen et al., 1999b):

$$K_p = \frac{C_{\text{Ca}}^L \cdot C_p^L}{C_{\text{Ca-p}}^L} = 0.33 \cdot I - 0.07 \quad (11)$$

where $C_{\text{Ca-p}}^L$ is the Ca-D-malate concentration in the liquid phase. The D-malate concentration in the liquid phase ($C_{\text{p+Ca-p}}^L$) can be expressed as:

$$C_{\text{p+Ca-p}}^L = C_p^L + C_{\text{Ca-p}}^L \quad (12)$$

The calcium concentration in the liquid phase ($C_{\text{Ca+Ca-p}}^L$) can be expressed as:

$$C_{\text{Ca+Ca-p}}^L = C_{\text{Ca}}^L + C_{\text{Ca-p}}^L \quad (13)$$

Overall growth process of a salt crystal

In accordance with eq. (2), the mass balance for D-malate (D-malate²⁻ and Ca-D-malate) in the liquid phase is:

$$\frac{dC_{\text{p+Ca-p}}^L(t)}{dt} = - \sum_{i=1}^j \frac{N_i \cdot 3 \cdot \alpha \cdot L_i(t)^2 \cdot \rho^S}{\epsilon \cdot V \cdot M_w} \cdot G_R = -r_{\text{Ca-p}}^g \quad (14)$$

The mass balance for calcium (Ca^{2+} and Ca-D-malate) in the liquid phase is:

$$\frac{dC_{\text{Ca+Ca-p}}^{\text{L}}(t)}{dt} = -r_{\text{Ca-p}}^{\text{g}} \quad (15)$$

The mass balance for solid Ca-D-malate is:

$$\frac{dC^{\text{S}}(t)}{dt} = r_{\text{Ca-p}}^{\text{g}} \quad (16)$$

Note that eqs. (14) and (15) implicate that both ions (Ca^{2+} and D-malate²⁻) are integrated in equivalent amounts (during crystal growth). By combining the appropriate equation for the linear growth rate (in this work: eq. (9)) and eqs. (10) to (13) and eqs. (14) to (16), the Ca^{2+} and D-malate²⁻ concentrations in the liquid phase and the Ca-D-malate concentration in both the liquid and the solid phase can be calculated during growth (see Fig. 2b).

MATERIALS AND METHODS

Materials

Ca-maleate·H₂O and Ca-D-malate·3H₂O were purchased from Syncom (Groningen, The Netherlands; purity > 98%). Tris was obtained from Boehringer Mannheim GmbH, HCl from Riedel-de Haën, and CaCl₂·2H₂O from Merck.

Cultivation and permeabilization of *P. pseudoalcaligenes*

P. pseudoalcaligenes NCIMB 9867 was cultivated in sterilized mineral salts medium (Hartmans et al., 1989) containing 1 g/l of 3-hydroxybenzoate (pH 7) and permeabilized with Triton X-100 as described before (Michielsen et al., 1998b).

Crystal-size distribution

The initial crystal-size distribution was determined by image analysis (Magiscan image analysis system with GENeral Image Analysis Software (GENIAS) from Applied Imaging; screen 262144 pixels; the breadth of the smallest object was characterized by at least 2.5 pixels). The object breadth (OB) is the minimum width

of all possible orthogonal projections and was chosen as the characteristic dimension ($L(t)$) of the slightly rectangular crystals. The object length (OL) is the maximum width of all possible orthogonal projections. The elongation factor is the ratio of OL and OB . The breadth, length, and elongation factor of in total more than a thousand crystals were determined.

Metastable-zone width

In order to determine the growth rate of a known amount of Ca-D-malate crystals as a function of supersaturation, primary nucleation must be avoided. Though primary nucleation occurs at every supersaturation, a significant amount of primary nuclei is instantaneously formed only at a (relatively) high supersaturation (Myerson and Ginde, 1993); this supersaturation ($C_{p+Ca-p}^L - C_{p+Ca-p}^{L^*}$) corresponds to the metastable-zone width. The width of the metastable zone was determined by incubating 15 ml of 1.5 M Ca-maleate / 1 M Tris of pH 8 with 15 ml of permeabilized *P. pseudoalcaligenes* (dry weight 22.0 mg·cm⁻³) for 8 hours at 25°C in a 65-ml vessel. Note that every Tris-solution in this work was adjusted to pH 8 with HCl. The solution was stirred magnetically (350 rpm) and the temperature was kept constant (at 25°C) by a constant temperature water bath that supplied water to the jacket of the vessel.

For determination of solubilized maleate and D-malate, every 30 and 10 minutes, respectively, during the first 6 hours, and every 30 minutes during the last 2 hours, 200-μl samples were taken. These samples were immediately centrifuged (30 s, 13.000 rpm) to remove solid substrate and product, and 50 μl of the supernatant was mixed with 950 μl of a 0.5 M HCl solution in an Eppendorf tube on a vortex mixer to stop the enzymatic reaction. These tubes were then centrifuged for 5 min at 13.000 rpm to remove cell material and the supernatant was diluted further for HPLC analysis. For solubilized D-malate analysis the supernatant was diluted 2-fold with 500 μl of a 0.5 M HCl solution, and for solubilized maleate analysis the supernatant was diluted 25-fold with double-distilled water.

For determination of the total amounts of maleate and D-malate, every 10 minutes 50-μl samples were taken. To redissolve solid substrate and product and to stop the enzymatic reaction these samples were immediately mixed with 950 μl of a 0.5 M HCl solution in an Eppendorf tube on a vortex mixer. These tubes were then centrifuged for 5 min at 13.000 rpm to remove cell material and the supernatant was diluted further for HPLC analysis. For total D-malate analysis the supernatant was

diluted 2-fold with 500 μ l of a 0.5 M HCl solution, and for total maleate analysis the supernatant was diluted 160-fold with double-distilled water.

Solubility of Ca-D-malate

The solubility product of Ca-D-malate K_{sp} was determined as a function of temperature and ionic strength from solubility measurements. The effect of temperature was tested by incubating solutions of 250 mM Ca-D-malate / 500 mM Tris (pH 8) for 24 hours at 20, 25, 30, 35, and 40°C in a shaking water bath (170 rpm). The effect of ionic strength was tested by incubating solutions of 75-475 mM KCl / 250 mM Ca-D-malate / 500 mM Tris (pH 8) for 24 hours at 30°C in a shaking water bath (170 rpm). After incubation, two 1-ml samples were centrifuged (10 min at the pertinent temperature, 15,300 rpm); 100 μ l of the supernatant was diluted 10-fold with 0.25 M HCl for HPLC analysis. All conditions were tested in duplicate. At all conditions, part of the Ca-D-malate-3H₂O crystals did not dissolve.

From the solubility data, the Ca^{2+} , D-malate²⁻, and Ca-D-malate concentration at saturation ($C_{\text{Ca}}^{L^*}$, $C_p^{L^*}$, and $C_{\text{Ca-p}}^{L^*}$, respectively), and thus also the solubility product K_{sp} , were calculated by iteration with eqs. (10) to (13). This set of equations can be solved for $C_{\text{Ca}}^{L^*}$, $C_p^{L^*}$, and $C_{\text{Ca-p}}^{L^*}$, given the ionic strength (I) and the D-malate and calcium concentration at saturation ($C_{\text{p+Ca-p}}^{L^*}$ and $C_{\text{Ca+Ca-p}}^{L^*}$, respectively). At the start of the iteration, the ionic strength was set at 0.75, as the ionic strength in these experiments ranged from 0.5 to 1.0. The D-malate concentration ($C_{\text{p+Ca-p}}^{L^*}$) was measured by HPLC. As precipitation of Ca^{2+} with other ions in solution is negligible, the calcium concentration in solution ($C_{\text{Ca+Ca-p}}^{L^*}$) was equal to the D-malate concentration in solution ($C_{\text{p+Ca-p}}^{L^*}$). After iteration, the solubility product of Ca-D-malate (K_{sp}) was calculated as $C_{\text{Ca}}^{L^*} \cdot C_p^{L^*}$.

As the Ca^{2+} and biocatalyst concentration could affect the solubility of Ca-D-malate, and hence the Ca^{2+} and D-malate²⁻ concentration at saturation ($C_{\text{Ca}}^{L^*}$ and $C_p^{L^*}$, respectively), these effects were determined too. To test the effect of Ca^{2+} concentration, 50-ml solutions of varying concentrations of CaCl_2 (0-400 mM) / 250 mM Ca-D-malate / 500 mM Tris (pH 8) were prepared. For determination of the effect of biocatalyst concentration, 10-ml solutions were made by mixing respectively 8 ml of 312.5 mM Ca-D-malate / 625 mM Tris (pH 8) with 2 ml of permeabilized cells, 6 ml of 416.7 mM Ca-D-malate / 833.3 mM Tris (pH 8) with 4 ml of permeabilized cells, and 4 ml of 625 mM Ca-D-malate / 1250 mM Tris (pH 8) with 6 ml of permeabilized cells. The solutions were incubated for 24 hours at 25°C in a shaking water bath

(170 rpm). After incubation, two 1-ml samples were taken and analysed as described above. All conditions were tested in duplicate. Note that at all conditions tested a part of the Ca-D-malate-3H₂O crystals did not dissolve.

The data of solubility vs. Ca²⁺ and biocatalyst concentration were used to calculate the Ca²⁺, D-malate²⁻, and Ca-D-malate concentration at saturation ($C_{Ca}^{L^*}$, $C_p^{L^*}$, and $C_{Ca-p}^{L^*}$, respectively). This was done by iteration with eqs. (10) to (12) and eq. (18) (see Results and Discussion). Note that eq. (18) was used instead of eq. (13), as the calcium concentration ($C_{Ca+Ca-p}^{L^*}$) was unknown due to the fact that complexation of calcium with the biocatalyst and Ca-D-malate precipitation at varying concentrations of calcium were not quantified. This set of equations can be solved for $C_{Ca}^{L^*}$, $C_p^{L^*}$, and $C_{Ca-p}^{L^*}$, if the ionic strength (I) and the D-malate concentration ($C_{p+Ca-p}^{L^*}$) are known. At the start of the iteration I was set at 0.5. The D-malate concentration ($C_{p+Ca-p}^{L^*}$) was measured by HPLC.

Supersaturated solutions

For executing seeded desupersaturation experiments, supersaturated Ca-D-malate solutions are needed. These were prepared by incubating 17.5 ml of 500 mM Ca-maleate / 714.3 mM Tris of pH 8 with 7.5 ml of permeabilized *P. pseudoalcaligenes* (dry weight 20.7 mg·cm⁻³) for about 17 hours at 25°C in a shaking water bath (170 rpm). After incubation (almost) all Ca-maleate was converted to Ca-D-malate. Though the created supersaturation was close to the metastable limit, no crystals could be observed in the solution after incubation. This can be explained by the fact that, compared to the experiment above (for determination of the metastable-zone width), the solutions in these experiments were shaken instead of stirred, and more gentle mixing (or stirring) increases the metastable-zone width (Nyyli et al., 1985). This supports the assumption that in these experiments primary nucleation could be neglected.

In the preparation of a supersaturated solution for the seeded desupersaturation experiments at 40°C (see below), permeabilized cells with a lower activity (dry weight 21.0 mg·cm⁻³) were used. This resulted after 17 hours of incubation in a saturated solution with Ca-D-malate crystals, as primary nucleation (and crystal growth) had occurred. This is probably due to the fact that the metastable-zone width decreases with a decreasing rate at which supersaturation is created (Nyyli et al., 1985). For that reason, Ca-D-malate solutions with a lower supersaturation were prepared for the seeded desupersaturation experiments at

40°C by incubating 7.5 ml of permeabilized cells (dry weight: 21.2 mg·cm⁻³) with 17.5 ml of 392.9 mM Ca-maleate / 714.3 mM Tris of pH 8.

Growth of Ca-D-malate crystals

The growth rate of Ca-D-malate crystals was determined by charging a known amount of Ca-D-malate crystals to a supersaturated Ca-D-malate solution in a batch stirred bioreactor and measuring the decrease in D-malate concentration due to growth (called desupersaturation). For that, the supersaturated solution (prepared as described above) was incubated statically for 30 minutes at the desired temperature (20, 30, or 40°C) in a water bath. From this supersaturated solution, 23 ml was added to a 60-ml stirred vessel of standard geometry with four symmetrically located, vertical baffles (Fig. 3). The stirrer was from the axial turbine type with four blades. A constant temperature water bath supplied water to the jacket of the vessel to keep the temperature constant at the desired value.

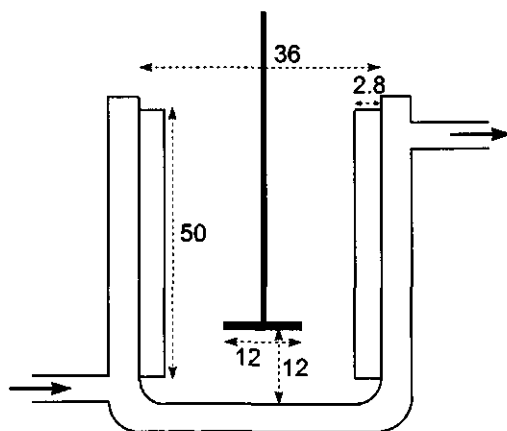


Figure 3 60-ml stirred vessel of standard geometry; all dimensions are given in millimeters.

At $t=0$, 0.25 g Ca-D-malate·3H₂O was added to the vessel and the decrease in D-malate concentration ($C_{p+Ca-p}^L(t)$) due to crystal growth was measured during 2.5 hours. This method is based on the assumption that secondary nucleation and agglomeration can be neglected. At each temperature (20, 30, and 40°C), the desupersaturation curve was measured at 500 and 750 rpm; the procedure is described below. Every 6 minutes, 150-μl samples were taken. These samples were immediately centrifuged (2 min, 15,300 rpm, at the desired temperature) to remove

Ca-D-malate crystals and cell material, and 50 μl of the supernatant was mixed with 950 μl of a 0.25 M HCl solution in an Eppendorf tube on a vortex mixer. These samples were analysed by HPLC.

Data fitting

The parameters k_{exp} and K_{exp} (of eq. (9)) were determined by fitting the surface-controlled growth rate model (eqs. (2), (9) to (16), and (18)) through data of the square root of the ionic product ($\sqrt{(C_{\text{Ca}}^{\text{L}}(t) \cdot C_{\text{p}}^{\text{L}}(t))}$) against time (t) using the Levenberg-Marquardt method. The other parameters are known or estimated (see Table 1). Note that during desupersaturation, the ionic strength (I) of the solution decreased. Since the supersaturation ratio $S(t)$ (see eq. (9)) is a function of the solubility product of Ca-D-malate (K_{sp}) and K_{sp} is a function of the ionic strength, eq. (18) was incorporated in the model too. The model was implemented in the computer program Simulink, a companion program to Matlab (Mathworks), according to the diagram in Fig. 2b. The differential equations in the model were solved in Simulink by applying the ode15s solver.

Table 1 Parameter values for determination of k_{exp} , K_{exp} , and $C_{\text{p+Ca-p}}^{\text{L}}(0)$; note that the number of crystals in each size class (N_1 to N_{17}) can be calculated from the crystal-size distribution of Fig. 4.

Parameters of the solid phase		Parameters of the liquid phase	
M_w ($\text{kg} \cdot \text{mol}^{-1}$)	$226 \cdot 10^{-3}$	r (m) ^{c)}	$3 \cdot 10^{-10}$
ρ^{S} ($\text{kg} \cdot \text{m}^{-3}$) ^{a)}	1600	ρ^{L} ($\text{kg} \cdot \text{m}^{-3}$) ^{d)}	1000
α (-) ^{b)}	1.30	V (m^3)	$23 \cdot 10^{-6}$
β (-) ^{b)}	6.75		
Other parameters			
k_B ($\text{N} \cdot \text{m} \cdot \text{K}^{-1}$) ^{d)}	$1.38 \cdot 10^{-23}$	d_s (m)	$12 \cdot 10^{-3}$
N_p (-) ^{e)}	1.4		

a) determined with a piknometer.

b) determined from crystal-size distribution of Fig. 4, assuming that the needle-shaped crystals were cylindrical; object length (OL)/object breadth (OB) was determined to be 1.65 and constant.

c) estimated from bond lengths and angles, given by Lide (1991).

d) from Lide (1991).

e) from Bates et al. (1963).

The concentrations determined by HPLC in the seeded desupersaturation experiments (described above) were D-malate concentrations (C_{p+Ca-p}^L), whereas in the fit procedure the square root of the ionic product ($\sqrt{(C_{Ca}^L \cdot C_p^L)}$) was fitted. For that reason, the D-malate concentration versus time data were converted in ionic product versus time data. Given the D-malate concentration at time t ($C_{p+Ca-p}^L(t)$), the Ca^{2+} and D-malate $^{2-}$ concentration ($C_{Ca}^L(t)$ and $C_p^L(t)$, respectively) can be calculated by iteration with eqs. (10) to (13), if the calcium concentration at time t ($C_{Ca+Ca-p}^L(t)$) is known. Fig. 9 indicates that Ca^{2+} probably complexes with cell components from the (permeabilized) biocatalyst. This means that at any time in the seeded desupersaturation experiments the calcium concentration ($C_{Ca+Ca-p}^L(t)$) was lower than the product concentration ($C_{p+Ca-p}^L(t)$). Assuming that at $t=0$ in the seeded desupersaturation experiment Ca^{2+} instantaneously complexes with the biocatalyst and that Ca^{2+} and D-malate $^{2-}$ were incorporated in the crystal structure in equivalent amounts, the difference between the D-malate and calcium concentration ($C_{p+Ca-p}^L(t)$ and $C_{Ca+Ca-p}^L(t)$, respectively) remained constant throughout the whole seeded desupersaturation experiment. This means that the calcium concentration ($C_{Ca+Ca-p}^L(t)$) can be calculated at any time t by subtracting this difference from the (measured) D-malate concentration ($C_{p+Ca-p}^L(t)$). The difference could be determined by calculating the calcium concentration ($C_{Ca+Ca-p}^L(t)$) corresponding with the final D-malate concentration in the seeded desupersaturation experiments ($C_{p+Ca-p}^L(t)$), that is the D-malate concentration at saturation. The D-malate concentration at saturation could be determined from Figs. 5 and 8, assuming that the effect of biocatalyst concentration on the D-malate concentration at a specific temperature can be summed. The calcium concentration at saturation could now be calculated by iteration with eqs. (10) to (12), and (18).

Other analyses

Maleate and D-malate (in both ionic and complexed (with Ca^{2+}) form, and in both acidic and nonacidic form) were analysed by HPLC as described before (Michielsen et al., 1999b).

The dry weight of the (permeabilized) cell suspension was determined as described by Michielsen et al. (1998b).

RESULTS AND DISCUSSION

Crystal-size distribution

The initial crystal-size distribution of $\text{Ca-D-malate} \cdot 3\text{H}_2\text{O}$, as determined by image analysis, is shown in Fig. 4. The breadth of a crystal (OB) was used as the characteristic dimension of the crystal ($L(f)$).

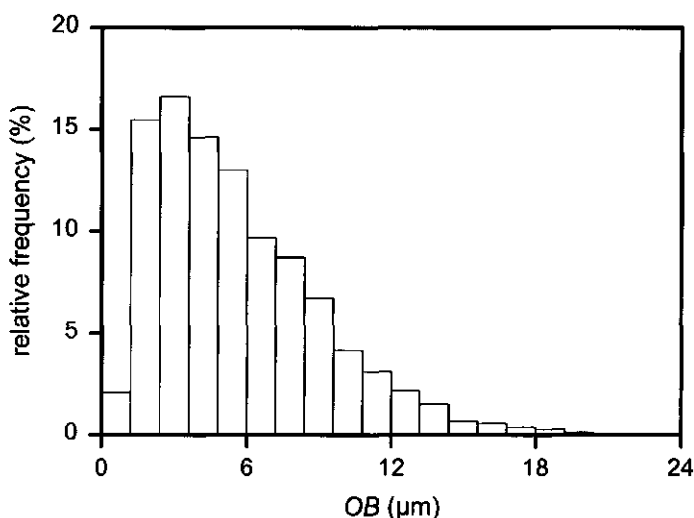


Figure 4 Initial crystal-size distribution of $\text{Ca-D-malate} \cdot 3\text{H}_2\text{O}$ (the CSD of the seeds) with object breadth OB as characteristic dimension of the crystals; the total number of crystals was 1054.

Metastable-zone width

In order to select starting conditions for the seeded desupersaturation experiments, at which occurrence of primary nucleation can be neglected, the width of the metastable zone was determined. At the upper limit of this zone, an excessive amount of nuclei is formed instantaneously due to primary nucleation. Fig. 5 shows the conversion of a total of 700 mM Ca-maleate to Ca-D-malate. The saturation concentration of Ca-maleate was found to be 172 mM at 25°C and pH 8 (see Fig. 5), which is in good agreement with the value reported earlier (Michielsen et al., 1998a). A solid phase of Ca-maleate crystals was present, until the total Ca-maleate concentration equalled the saturation concentration. At this moment ($t=180$ min), all Ca-maleate crystals were dissolved. The Ca-D-malate concentration increased, until a concentration of 304 mM was reached. From this point, the Ca-D-malate

concentration decreased rapidly, indicating that an excessive amount of Ca-D-malate crystals was formed instantaneously due to primary nucleation. Due to nucleation and growth of the Ca-D-malate crystals the Ca-D-malate concentration dropped even though at $t=480$ min saturation was not reached. This was determined in separate experiments to be 87 mM at these conditions (see Fig. 9 at a biocatalyst concentration of $11 \text{ mg}\cdot\text{cm}^{-3}$). The difference between the saturation concentration and the (supersaturated) concentration at which excessive nucleation occurs is the metastable zone (for primary nucleation); the width of this zone at the conditions in Fig. 5 is about 220 mM.

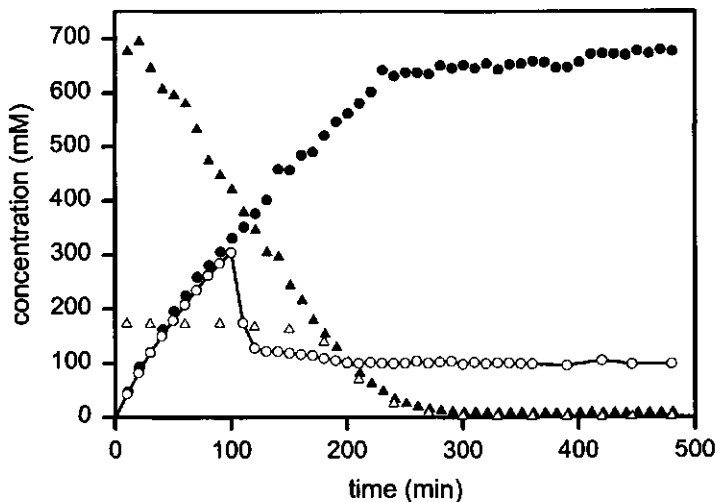


Figure 5 Conversion of Ca-maleate to Ca-D-malate by permeabilized *P. pseudoalcaligenes* ($11.0 \text{ g}/\text{dm}^3$) at 25°C and pH 8 to determine the metastable-zone width; solubilized maleate (Δ), total maleate (\blacktriangle), solubilized D-malate (O), and total D-malate (\bullet).

Solubility of Ca-D-malate

The effect of temperature on the solubility and solubility product (K_{sp}) of Ca-D-malate is shown in Fig. 6. The solubility and solubility product of Ca-D-malate slightly decreased with temperature between 20 and 40°C . Such an effect has also been found for certain other compounds (Martell and Smith, 1979; Michielsen et al., 1998a).

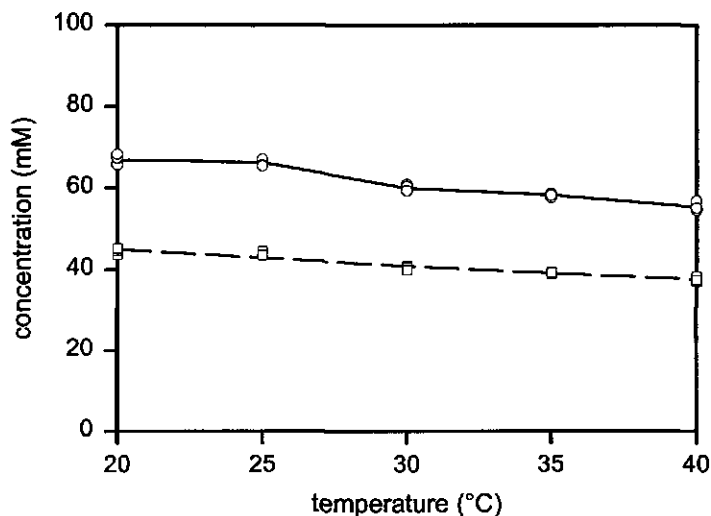


Figure 6 The solubility (O) and square root of the solubility product of Ca-D-malate, $\sqrt{K_{sp}}$ (□), as a function of temperature at pH 8, and the fit with eq. (17) (---); note that the solubility equals the D-malate concentration (both D-malate²⁻ and Ca-D-malate in the liquid phase; $C_{p+Ca-D}^L(t)$).

According to Van 't Hoff (Chang, 1981):

$$\ln K_{sp} = -\frac{\Delta H^{\circ}}{R \cdot T} + \frac{\Delta S^{\circ}}{R} \quad (17)$$

with ΔH° the enthalpy change, and ΔS° the entropy change. Assuming ΔH° and ΔS° to be independent of temperature, ΔH° and ΔS° were calculated from the data in Fig. 6 as: $\Delta H^{\circ} = -14 \text{ kJ} \cdot \text{mol}^{-1}$, and $\Delta S^{\circ} = -99 \text{ J} \cdot \text{mol}^{-1} \cdot \text{K}^{-1}$.

The solubility and solubility product (K_{sp}) of Ca-D-malate increased (slightly) with ionic strength (see Fig. 7). Such an increase is called the salting-in effect. Fig. 7 also shows that the increase became smaller with increasing ionic strength. This is probably due to the salting-out effect, which is the decrease in solubility or solubility product with increasing ionic strength at higher ionic strengths. The overall effect of ionic strength (I) on the solubility product (K_{sp}) can be expressed as (Chang, 1981):

$$\log \sqrt{K_{sp}} = \log \sqrt{K_{sp}^{\circ}} + 0.509 \cdot |z_{+} \cdot z_{-}| \cdot \sqrt{I} - K' \cdot I \quad (18)$$

with:

$$K_{sp}^{\circ} = \gamma_{\pm}^2 \cdot K_{sp}$$

where K_{sp}° is the thermodynamic solubility product of Ca-D-malate, K' is a constant, and γ_{\pm} is the geometric mean of the ionic activity coefficient of Ca^{2+} and the ionic activity coefficient of D-malate^{2-} ; the subscripts + and - refer to the positive and negative ion, respectively (Ca^{2+} and D-malate^{2-}). By fitting eq. (18) through the data in Fig. 7, the thermodynamic solubility product K_{sp}° and K' were determined ($R^2 = 0.997$): $K_{sp}^{\circ} = 22.1 \text{ mmol}^2 \cdot \text{dm}^{-6}$, $K' = 0.98 \text{ dm}^3 \cdot \text{mol}^{-1}$.

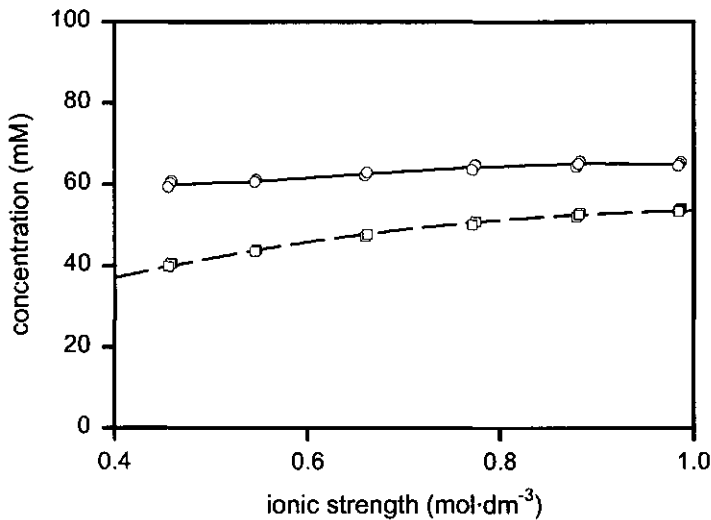


Figure 7

The solubility (O) and square root of the solubility product of Ca-D-malate, $\sqrt{K_{sp}}$ (□), as a function of ionic strength at 30°C and pH 8, and the fit with eq. (18) (---); note that the solubility equals the D-malate concentration (both D-malate^{2-} and Ca-D-malate in the liquid phase; $C_{p+\text{Ca-p}}^L(t)$).

Fig. 8 shows that the solubility of Ca-D-malate decreased with increasing Ca^{2+} concentration until an initial Ca^{2+} concentration of 75 mM, whereas it was almost constant between 75 and 400 mM. This effect was probably due to two phenomena. On the one side, the solubility decreases with the added Ca^{2+} concentration, as the

solubility product K_{sp} is reached at a lower concentration of D-malate²⁻, assuming K_{sp} to be constant. This was supported by the fact that the D-malate²⁻ concentration was calculated to decrease with the initial Ca²⁺ concentration, and K_{sp} was calculated to be (almost) constant (Fig. 8). On the other hand, the solubility increases with the Ca²⁺ concentration, as the ionic strength I increases (salting-in effect; Chang, 1981). Apparently, between 0 and 75 mM Ca²⁺, the decrease of the solubility due to the effect of Ca²⁺ concentration on the ionic product ($C_{Ca^{2+}} \cdot C_p^{L-}$) was larger than the increase of the solubility due to the effect of Ca²⁺ on the ionic strength, while between 75 and 400 mM Ca²⁺ these effects were balanced.

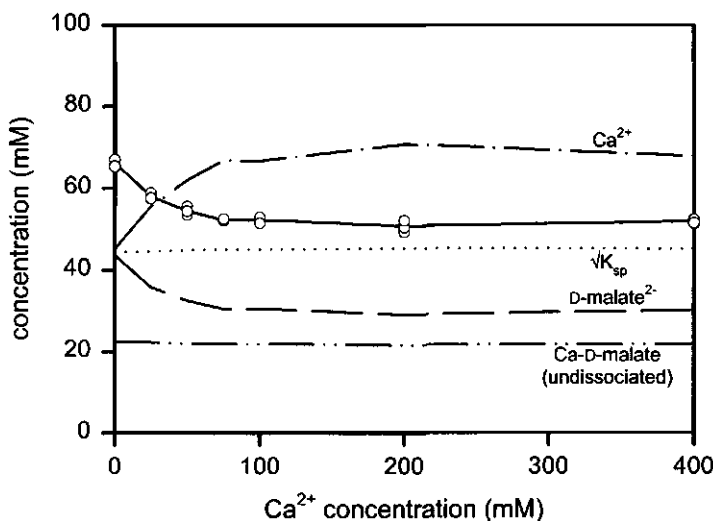


Figure 8 The solubility (O) and square root of the solubility product of Ca-D-malate, $\sqrt{K_{sp}}$ (···), as a function of initial Ca²⁺ concentration at 25°C and pH 8; calculated Ca²⁺ concentration (---), D-malate²⁻ concentration (---), and Ca-D-malate concentration (---). Note that the solubility equals the D-malate concentration (both D-malate²⁻ and Ca-D-malate in the liquid phase; $C_{p+Ca-p}^L(t)$).

The solubility of Ca-D-malate increased with the biocatalyst concentration (Fig. 9). It was noted that immediately upon biocatalyst addition to the liquid-solid two-phase system (as a Ca-D-malate amount corresponding to 250 mM was present) flocculation occurred, indicating that complexes of Ca²⁺ with available cell components were formed. Due to such a withdrawal of Ca²⁺, the ionic product decreased and as a result more Ca-D-malate could be dissolved, assuming K_{sp} to be constant and independent of the biocatalyst concentration. This was supported by

the fact that the Ca^{2+} concentration was calculated to decrease and the D-malate^{2-} concentration was calculated to increase with increasing biocatalyst concentration (see Fig. 9). Fig. 9 shows that the assumption of a constant K_{sp} is indeed valid; note that K_{sp} was calculated by iteration with eqs. (10) to (12) and eq. (18).

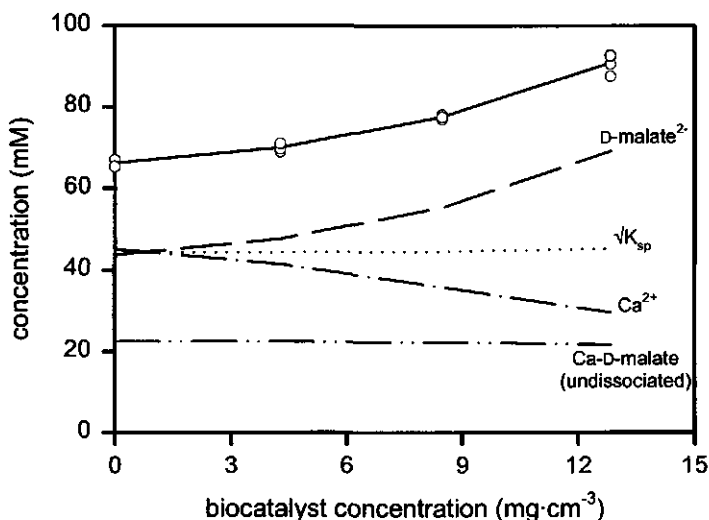


Figure 9 The solubility (O) and square root of the solubility product of Ca-D-malate, $\sqrt{K_{sp}}$ (···), as a function of biocatalyst concentration at 25°C and pH 8; calculated Ca^{2+} concentration (— · —), D-malate^{2-} concentration (---), and Ca-D-malate concentration (— · · —). Note that the solubility equals the D-malate concentration (both D-malate^{2-} and Ca-D-malate in the liquid phase; $C_{p+\text{Ca-p}}^L(t)$).

Surface-controlled crystal growth

Fig. 10 shows the decrease in the square root of the ionic product of the Ca^{2+} and D-malate^{2-} concentration ($C_{\text{Ca}}^L(t)$ and $C_{\text{p}}^L(t)$, respectively) due to Ca-D-malate crystal growth as a function of stirring speed and temperature. The different slopes of the curves indicate that the rate of decrease in concentration, the growth or desupersaturation rate, was affected by temperature. It probably has a maximum between 20 and 40°C, as the growth rates at 30°C were at every supersaturation larger than the rates at 20 and 40°C. The growth rate was hardly affected by the stirring speed. If the crystals are larger than 5-10 μm , the latter implicates that the rate is surface controlled. If the crystals are smaller than about 5 μm (the value depending on the density difference between crystal and solution), no distinction between the rate being transport or surface controlled can be made based solely on

the effect of stirring speed on the measured desupersaturation rate. Such small crystals are carried with the solution and sediment so slowly that the liquid flow over their surface is too weak to influence the transport rate; so still the two possibilities remain: transport or surface control (Nielsen and Toft, 1984). In this work the characteristic dimension ($L(t)$) corresponding to the average volume of all crystals was $7.5\text{ }\mu\text{m}$. As this is a borderline case, the indication of a surface-controlled growth rate is very unreliable. For that reason, the transport control index (q_T) was calculated (see below).

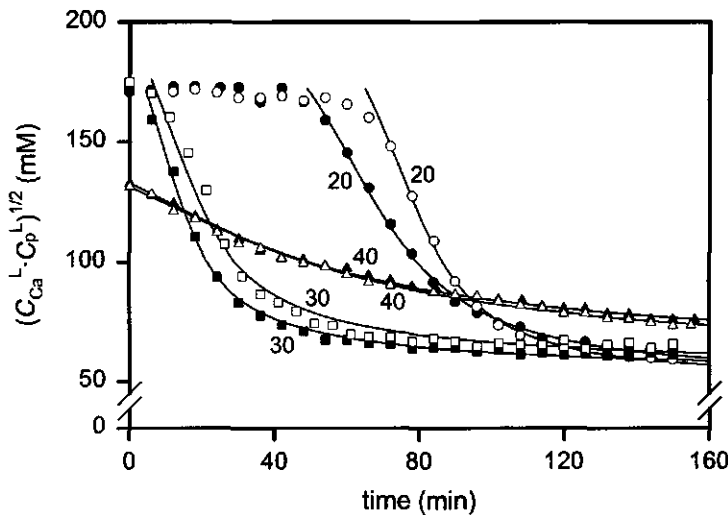


Figure 10 The effect of temperature and stirring speed on the desupersaturation rate due to Ca-D-malate crystal growth; measurements at 20°C and 500 rpm (●), 20°C and 750 rpm (○), 30°C and 500 rpm (■), 30°C and 750 rpm (□), 40°C and 500 rpm (▲), 40°C and 750 rpm (△), and corresponding fits with the surface-controlled exponential growth model.

Fig. 10 shows that at 20°C the concentration hardly decreased within the first 60 minutes. This could be explained by assuming that at 20°C Ca-D-malate crystals with a different crystal structure than the ones added at $t=0$ were formed; only when the right structure was present (at 20°C, after 60 minutes), Ca-D-malate molecules from the solution could be incorporated at a significant rate. This was confirmed by the observation of an immediate decrease in concentration at $t=0$ when Ca-D-malate crystals pre-formed at 20°C were added to a new supersaturated solution (data not shown). As at 30 and 40°C the Ca-D-malate concentration (almost) decreased

immediately, this implicates that the structure of the crystals added resembles the structure of the crystals formed at these temperatures. The formation of different crystal structures from one chemical species as a function of the growth conditions (temperature, pressure, impurity content, growth rate, etc.) is called polymorphism and was reported for several other species too (Myerson and Ginde, 1993). In case of Ca-D-malate, different polymorphs might be formed by formation of different hydrates (Linke, 1958). This has been found for certain other compounds too, e.g. MgSO_4 (Felder and Rousseau, 1986).

The first selection in growth rate models was based on whether the crystal growth process was transport or surface controlled. For that, the transport control index q_T was calculated. As the mass-transfer coefficient ($k_T(t)$) decreases with increasing characteristic dimension of a crystal ($L(t)$), the growth process becomes more transport controlled with increasing $L(t)$. So, in a crystal growth process q_T increases in time. The calculated transport control indices of crystals in the largest initial size class of the crystal-size distribution ($i=17$) at $t=150$ min are shown in Table 2; at all conditions tested in this work q_T was $8.72 \cdot 10^{-3}$ or smaller. This means that at all these conditions, during the whole length of the experiment, and for every crystal in the crystal-size distribution, the growth process was fully surface controlled (see Fig. 2a). Note that in this work the value for $k_T(t)$ (and thus for q_T) depends on the empirical relation chosen (eq. (5)). For that reason, the effect of another correlation for mass transfer between a single sphere and a fluid in a stirred tank on q_T was determined at 30°C and 500 rpm (and $t=150$ min). At these conditions the smallest relative difference between k_{lin} , k_{par} , or k_{exp} and $k_T(t)$ existed, since the ratio of k_{lin} , k_{par} , or k_{exp} and $k_T(t)$ increased with temperature between 20 and 30°C and $k_T(t)$ theoretically decreases with decreasing stirring speed (see eq. (5)). Levins and Glastonbury (1972) recommend the equation:

$$Sh_i(t) = 2 + 0.4 \cdot \left(\frac{\frac{1}{\varepsilon^{\frac{1}{3}}} \cdot L_i(t)^{\frac{4}{3}}}{\nu} \right)^{0.62} \cdot \left(\frac{d_s}{d_t} \right)^{0.17} \cdot \left(\frac{\nu}{D} \right)^{0.36} \quad (19)$$

where d_t is the diameter of the tank. Table 2 shows that there was hardly any difference in the value for q_T . This confirms that the growth process was surface controlled throughout.

Table 2 Values of the transport control index ($q_{T,17}(150)$) and the fit parameters k_{exp} , K_{exp} (from eq. (9) of the model shown in Fig. 2b), and $C_{p+Ca-p}^L(0)$ (with 95% confidence intervals) as a function of temperature (T) and stirring speed (n), and the R^2 -values of each fit.

T (°C)	n (rpm)	$q_{T,17}(150)$	R^2	k_{exp} (m·min ⁻¹)	K_{exp} (-)	$C_{p+Ca-p}^L(0)$ (mM) ^{d)}
20	500	$8.72 \cdot 10^{-3}$	0.997	$6.84 \cdot 10^{-6} \pm 1.58 \cdot 10^{-6}$	0.57 ± 0.14	295.01 ± 0.04
	750	$7.36 \cdot 10^{-3}$	0.998	$9.52 \cdot 10^{-6} \pm 2.02 \cdot 10^{-6}$	0.53 ± 0.11	294.93 ± 0.01
30	500	$4.13 \cdot 10^{-4}$	0.993	$3.89 \cdot 10^{-5} \pm 1.36 \cdot 10^{-5}$	1.69 ± 0.22	290.76 ± 0.01
	500 ^{a)}	$3.82 \cdot 10^{-4}$	-	-	-	-
	750	$7.49 \cdot 10^{-4}$	0.967	$2.87 \cdot 10^{-5} \pm 2.27 \cdot 10^{-5}$	1.77 ± 0.49	303.20 ± 0.41
40	500	$2.80 \cdot 10^{-3}$ ^{b)}	0.997	$2.98 \cdot 10^{-5} \pm 1.33 \cdot 10^{-5}$	2.64 ± 0.35	228.71 ± 0.21
	750	$3.82 \cdot 10^{-3}$ ^{c)}	0.995	$1.83 \cdot 10^{-5} \pm 1.09 \cdot 10^{-7}$	2.18 ± 0.15	225.87 ± 4.00

a) calculated with the Sherwood equation derived by Levins and Glastonbury (1972).

b) q_T at $t=155$ min.

c) q_T at $t=156$ min.

d) used as a fit parameter; the permeabilized cell suspension that is added to the supersaturated product solution is a little viscous, resulting in small deviations from the aimed initial supersaturation.

In order to select an appropriate surface-controlled growth rate model, the linear growth rate G_R ($dL(t)/dt$) at 30°C and 500 rpm was calculated with eq. (14) and plotted versus $S-1$ according to eq. (7) (data not shown). Since no linear dependency was found, it is obvious that the data could not be described well with a linear rate law. To test for a parabolic rate law (eq. (8)), $\sqrt{G_R}$ was plotted versus $S-1$ (data not shown). A test plot for the exponential rate law (eq. (9)) was made by plotting $\ln G_R / F(S)$ versus $1/\ln S$, with $F(S) = S^{7/6} \cdot (S-1)^{2/3} \cdot (\ln S)^{1/6}$ (data not shown). In both cases, the data showed a linear relation. However, in similar growth experiments was found that after more than 24 h the concentration dropped till about 43 mM (data not shown), indicating that after $t=160$ min still crystal growth had occurred. As only according to the exponential rate law a considerable crystal growth rate was predicted after $t=160$ min, this rate law was selected. The surface-controlled exponential growth rate model (Fig. 2b) could be fitted well through the data (see Fig. 10 and Table 2), indicating that the proposed model describes the process well. As expected from Fig. 10, k_{exp} was maximal at 30°C and was hardly affected by the stirring speed; K_{exp} increased with temperature and was also hardly affected by the stirring speed (see Table 2).

CONCLUSIONS

A kinetic model for Ca-D-malate crystal growth in a batch stirred bioreactor was developed. The driving force for growth was expressed as a function of the ionic product ($C_{Ca}^L(t) \cdot C_p^L(t)$) and the solubility product of Ca-D-malate (K_{sp}). In the presence of biocatalyst, the Ca^{2+} concentration was found to be smaller than the D-malate²⁻ concentration due to complexation of Ca^{2+} with the biocatalyst. Both ionic concentrations decrease due to crystal growth and were calculated by assuming that dissociation of Ca-D-malate was at equilibrium. The solubility product of Ca-D-malate was hardly affected by the initial Ca^{2+} and biocatalyst concentration, but decreased with temperature and increased with ionic strength. During growth the ionic strength was calculated in order to determine the solubility product of Ca-D-malate K_{sp} . According to the transport control index, growth of Ca-D-malate crystals from an aqueous solution was surface controlled. Assuming that the salt crystals grow by an exponential rate law, the decrease in ionic product ($C_{Ca}^L(t) \cdot C_p^L(t)$) due to Ca-D-malate crystal growth was fitted well ($R^2 > 0.96$). This revealed that the kinetic parameters were temperature dependent; k_{exp} had a maximum between 20 and 40°C and K_{exp} increased with temperature. The stirring speed hardly affected k_{exp} and K_{exp} . So, in case the growth of Ca-D-malate crystals is the rate-limiting process in the conversion of solid Ca-maleate to solid Ca-D-malate, the overall Ca-D-malate production rate would be maximal at 30°C and 500 rpm.

ACKNOWLEDGEMENTS

We thank S. Hartmans and M.J. van der Werf (Division of Industrial Microbiology, Wageningen Agricultural University) for supplying *P. pseudoalcaligenes* and for fruitful discussions on cultivation and permeabilization of *P. pseudoalcaligenes*.

This work was financially supported by the Ministry of Economic Affairs, the Ministry of Education, Culture and Science, the Ministry of Agriculture, Nature Management and Fishery in the framework of an industrial relevant research programme of the Netherlands Association of Biotechnology Centres in the Netherlands (ABON).

NOMENCLATURE

C	concentration	(mmol·dm ⁻³)
$C(0)$	concentration at $t=0$	(mmol·dm ⁻³)
D	diffusion coefficient	(m ² ·s ⁻¹)
d_s	stirrer diameter	(m)
d_t	tank diameter	(m)
G	linear crystal growth rate	(m·s ⁻¹)
ΔH°	enthalpy change	(kJ·mol ⁻¹)
I	ionic strength	(mol·dm ⁻³)
K_{exp}	constant of exponential rate law	(-)
K_p	dissociation constant of Ca-D-malate	(mmol·dm ⁻³)
K_{sp}	apparent solubility product	(mmol ² ·dm ⁻⁶)
K_{sp}°	thermodynamic solubility product	(mmol ² ·dm ⁻⁶)
K'	salting-out effect constant	(dm ³ ·mol ⁻¹)
k	mass-transfer coefficient	(m·s ⁻¹)
k_B	Boltzmann' constant	(N·m·K ⁻¹)
L	characteristic dimension of the crystal	(m)
M_w	molecular mass	(kg·mol ⁻¹)
m	mass of one crystal	(kg)
N	number of crystals	(-)
N_p	power number	(-)
n	stirring speed	(rps)
OB	object breadth	(m)
OL	object length	(m)
q_T	transport control index	(-)
R	gas constant	(8.314 J·mol ⁻¹ ·K ⁻¹)
r	molecular radius of Ca-D-malate	(m)
r^3	volumetric crystal growth rate	(mol·m ⁻³ ·s ⁻¹)
S	supersaturation ratio	(-)
Sh	Sherwood number	(-)
ΔS°	entropy change	(J·mol ⁻¹ ·K ⁻¹)
T	absolute temperature	(K)
t	time	(s)
V	volume (of the suspension)	(m ³)

$V(0)$	volume at $t=0$	(m^3)
z	valency of an ion	(-)

Greek symbols

α	(volume) shape factor	(-)
β	(surface) shape factor	(-)
η	dynamic viscosity	($N \cdot s \cdot m^{-2}$)
ϵ	hold-up of the liquid phase in the suspension	(-)
ε	energy input per kg liquid phase	($W \cdot kg^{-1}$)
ϕ_c	Carman's surface factor	(-)
γ_{\pm}	geometric mean of the ionic activity coefficients	(-)
ν	kinematic viscosity	($m^2 \cdot s^{-1}$)
ρ	density	($kg \cdot m^{-3}$)

Indices

Ca	Ca^{2+}
Ca-p	Ca-D-malate
Cl	Cl^-
c	one crystal
exp	exponential rate law
i	class number
j	number of size classes in the crystal-size distribution
L	liquid phase or bulk solution
lin	linear rate law
p	D-malate ²⁻
par	parabolic rate law
R	surface reaction at the solid-liquid interface
S	solid phase
T	transport across a boundary liquid film
Tris	Tris ⁺
+	positive ion
-	negative ion
*	saturation

REFERENCES

- Bates RL, Fondy PL, Corpstein RR. 1963. An examination of some geometric parameters of impeller power. *Ind Eng Chem, Proc Des & Dev* 2:310-314.
- Bujac PDB, Mullin JW. 1969. A rapid method for the measurement of crystal growth rates in a fluidized bed crystallizer. *Symp Ind Crystall*. London: The Institution of Chemical Engineers. 121 p.
- Chang RM. 1981. *Physical chemistry with applications to biological systems*. New York: MacMillan publishing Co, Inc. 659 p.
- Erbeldinger M, Xiongwei N, Halling PJ. 1998. Enzymatic synthesis with mainly undissolved substrates at very high concentrations. *Enzyme Microb Technol* 23:141-148.
- Estrin J. 1993. Precipitation processes. In: Myerson AS, editor. *Handbook of industrial crystallization*. Boston: Butterworth-Heinemann. p 131-149.
- Felder RM, Rousseau RW. 1986. *Elementary principles of chemical processes*. 2nd edition. New York: John Wiley & Sons, Inc.
- Halfon A, Kaliaguine S. 1976. Alumina trihydrate crystallization, part 1. Secondary nucleation and growth rate kinetics. *Can J Chem Eng* 54:160-167.
- Hartmans S, Smits JP, Van der Werf MJ, Volkering F, De Bont JAM. 1989. Metabolism of styrene oxide and 2-phenylethanol in the styrene-degrading *Xanthobacter* strain 124X. *Appl Environ Microbiol* 55:2850-2855.
- Hunik JH, Tramper J, Wijffels RH. 1994. A strategy to scale up nitrification processes with immobilized cells of *Nitrosomonas europaea* and *Nitrobacter agilis*. *Bioprocess Eng* 11:73-82.
- Jones AG, Mullin JW. 1973. Crystallization kinetics of potassium sulphate in a draft-tube agitated vessel. *Trans Instn Chem Engrs* 51:302-308.
- Kirwan DJ, Orella CJ. 1993. Crystallization of biological molecules. In: Myerson AS, editor. *Handbook of industrial crystallization*. Boston: Butterworth-Heinemann. p 219-235.
- Levins DM, Glastonbury JR. 1972. Application of Kolmogoroff's theory to particle-liquid mass transfer in agitated vessels. *Chem Engng Sci* 27:537-543.
- Lide DR, editor. 1991. *CRC Handbook of chemistry and physics*. 72th edition. Boca Raton: CRC Press, Inc.

- Linke WF, editor. 1958. p 512-513. Solubilities of inorganic and metal-organic compounds, a compilation of solubility data from the periodical literature. Volume I, fourth edition. Princeton, New Jersey: D van Nostrand Company, Inc.
- Martell AE, Smith RM, editors. 1979. Critical stability constants, Volume 3: Other organic ligands. 2nd edition. New York: Plenum Press.
- Michielsen MJF, Reijenga KA, Wijffels RH, Tramper J, Beeftink HH. 1998a. Dissolution kinetics of Ca-maleate crystals: evaluation for biotransformation reactor design. J Chem Technol Biotechnol 73:13-22.
- Michielsen MJF, Meijer EA, Wijffels RH, Tramper J, Beeftink HH. 1998b. Kinetics of D-malate production by permeabilized *Pseudomonas pseudoalcaligenes*. Enzyme Microb Technol 22:621-628.
- Michielsen MJF, Frielink C, Wijffels RH, Tramper J, Beeftink HH. 1999a. D-malate production by permeabilized *Pseudomonas pseudoalcaligenes*; optimization of conversion and biocatalyst productivity. Submitted for publication.
- Michielsen MJF, Frielink C, Meijer EA, Van der Werf MJ, Wijffels RH, Tramper J, Beeftink HH. 1999b. Stabilization of maleate-hydratase activity of permeabilized *Pseudomonas pseudoalcaligenes*. Biocatal Biotransf 17: 125-137.
- Myerson AS, Ginde R. 1993. Crystals, crystal growth, and nucleation. In: Myerson AS, editor. Handbook of industrial crystallization. Boston: Butterworth-Heinemann. p 33-63.
- Nielsen AE. 1980. Transport control in crystal growth from solution. Croat Chem Acta 53:255-279.
- Nielsen AE, Toft JM. 1984. Electrolyte crystal growth kinetics. J Cryst Growth 67:278-288.
- Nielsen AE. 1984. Electrolyte crystal growth mechanisms. J Cryst Growth 67: 289-310.
- Nyvit J, Sohnel O, Matuchova M, Brout M. 1985. The kinetics of industrial crystallization. Amsterdam: Elsevier. 350 p.
- Palwe BG, Chivate RM, Tavare NS. 1985. Growth kinetics of ammonium nitrate crystals in a draft tube baffled agitated batch crystallizer. Ind Eng Chem, Proc Des & Dev 24:914-919.
- Qui Y, Rasmuson AC. 1990. Growth and dissolution of succinic acid crystals in a batch stirred crystallizer. AIChE J 36:665-676.

- Ranz WE, Marshall WR Jr. 1952. Evaporation from drops. Chem Eng Prog 48: 141-146, 173-180.
- Sano Y, Yamaguchi N, Adachi T. 1974. Mass transfer coefficients for suspended particles in agitated vessels and bubble columns. J Chem Eng Jpn 7:255-261.
- Tournié P, Laguerie C, Couderc JP. 1979. Correlations for mass transfer between fluidized spheres and a liquid. Chem Engng Sci 34:1247-1255.
- Van den Heuvel JC, Beftink HH. 1988. Kinetic effects of simultaneous inhibition by substrate and product. Biotechnol Bioeng 31:718-724.
- Van der Werf MJ, Hartmans S, Van den Tweel WJJ. 1995. Effect of maleate counter-ion on malease activity: production of D-malate in a crystal-liquid two-phase system. Enzyme Microb Technol 17:430-436.

CHAPTER 7

Modeling solid-to-solid biocatalysis: integration of six consecutive steps

ABSTRACT

A quantitative model for the conversion of a solid substrate salt to a solid product salt in a batch bioreactor seeded with product crystals is presented. The overall process consists of six serial steps (with dissolution and crystallization each in themselves complex multi-step processes): solid salt dissolution, salt dissociation into an ionic substrate and a counter-ion, bioconversion accompanied by biocatalyst inactivation, complexation of the ionic product with the counter-ion, and salt crystal growth. In the model the consecutive steps are integrated, including biocatalyst inactivation and assuming that salt dissociation and complexation of ions are at equilibrium. Model parameters were determined previously in separate independent experiments. To validate the model, either dissolved or solid Ca-maleate was converted to solid Ca-D-malate by permeabilized *Pseudomonas pseudoalcaligenes* in a batch bioreactor seeded with Ca-D-malate crystals. The model very well predicted the concentrations of all components in the liquid phase (Ca-maleate, Ca^{2+} , maleate²⁻, D-malate²⁻, and Ca-D-malate) and the amounts of the solid phases (Ca-maleate·H₂O and Ca-D-malate·3H₂O), especially when high initial amounts of Ca-maleate·H₂O and Ca-D-malate·3H₂O were present.

INTRODUCTION

Bioconversions are generally carried out in aqueous media. However, reactant solubilities in water are often limited and/or the bioconversions are often inhibited by high substrate and/or product concentrations (Michielsen et al., 1999a; Van den Heuvel and Beertink, 1988; Van der Werf et al., 1993, 1995). Both phenomena result in low overall volumetric productivities. Due to extraction of substrate and/or product, the addition of a water-immiscible organic solvent phase may increase the overall substrate solubility and may decrease inhibition in the aqueous reaction phase.

An attractive alternative for these liquid-liquid two-phase systems is an aqueous suspension of solid substrate and solid product. High yields can be attained and in combination with a high substrate availability this leads to a high product amount per reactor volume (Erbeldinger et al., 1998). Since organic solvents are absent, solvent deactivation effects on the biocatalyst and product contamination are avoided, and the process is environmentally friendly and cost efficient.

Suspensions of solid substrate and solid product can be formed in conventional systems by salt addition, resulting in precipitation of salt-substrate and salt-product complexes (Van der Werf et al., 1995). Especially in case of substrate and/or product inhibition this is advantageous, as this reduces the substrate and product concentration in solution. Although this kind of suspension bioconversions is already applied in industry (Ashina and Suto, 1992; Kitahara et al., 1960; Miller, 1985; Oyama, 1992; Takahashi, 1986; Watanabe and Osawa, 1966) and the number of applications increases (Bornscheuer and Yamane, 1994; Cao et al., 1996; Kasche, 1986; Petkov and Stoineva, 1984; Kasche and Galunsky, 1995), a theoretical basis for process optimization is lacking.

The first kinetic model describing bioconversions in suspensions was recently reported by Wolff et al. (1999). In their model the kinetics of three steps, i.e. substrate dissolution, bioconversion, and biocatalyst inactivation, were integrated.

The kinetic model presented here goes even further as it describes the conversion of a solid substrate salt to a solid product salt in a batch bioreactor seeded with product crystals, thereby integrating six steps (see Fig. 1). In this model, product crystallization kinetics were incorporated in addition to substrate dissolution kinetics and biokinetics of conversion and inactivation, and besides salt dissociation and complexation of ions are assumed to be at equilibrium. The last process in the solid-to-solid conversion, that is crystallization, consists of nucleation and growth.

New crystals (nuclei) are formed at high supersaturation (by so-called primary nucleation), or originate from existing crystals e.g. by collision or shear stress (so-called secondary nucleation). In the presence of product crystals, as in this work, the occurrence of primary nucleation is minimal, as the product crystals keep the supersaturation (created by the bioconversion) at a rather low level by crystal growth. Since secondary nucleation was neglected, the crystallization kinetics in the model presented here only involve crystal growth kinetics. The model was tested for the conversion of solid Ca-maleate to enantiomerically pure solid Ca-D-malate by permeabilized *Pseudomonas pseudoalcaligenes* in a batch bioreactor seeded with Ca-D-malate crystals (see Fig. 1). It gave a very good quantitative description of the overall conversion.

THEORY

The reactions involved are shown in Fig. 1.

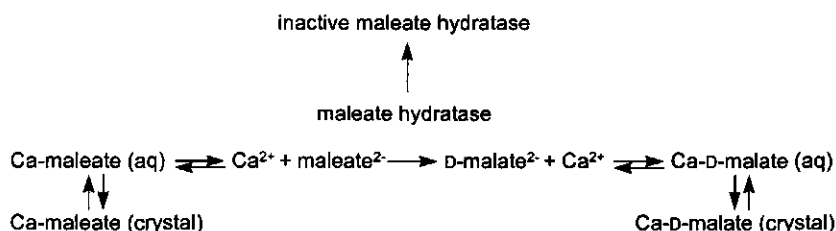


Figure 1 Reaction scheme for the conversion of solid Ca-maleate to solid Ca-D-malate by maleate hydratase in permeabilized *P. pseudoalcaligenes*.

The main kinetic equations of the separate steps (dissolution, bioconversion and biocatalyst inactivation, and crystal growth) were determined previously (Michielsen et al., 1998a, 1999a,b) and are given below (eqs. (1) to (3)). Since ionic reactions occur very rapidly (Klein and David, 1995), dissociation of Ca-maleate and complexation of Ca^{2+} and D-malate^{2-} are assumed to be at equilibrium. The rates of dissolution, bioconversion and biocatalyst inactivation, and crystal growth are affected by the ionic concentrations of Ca^{2+} , maleate^{2-} , and D-malate^{2-} . For that reason, in this work an iteration procedure was developed to calculate these concentrations (eqs. (4) to (9)). Finally, an overall model for the conversion of solid

Ca-maleate to solid Ca-D-malate is derived (eqs. (10) to (15)). The overall model is depicted in Fig. 2.

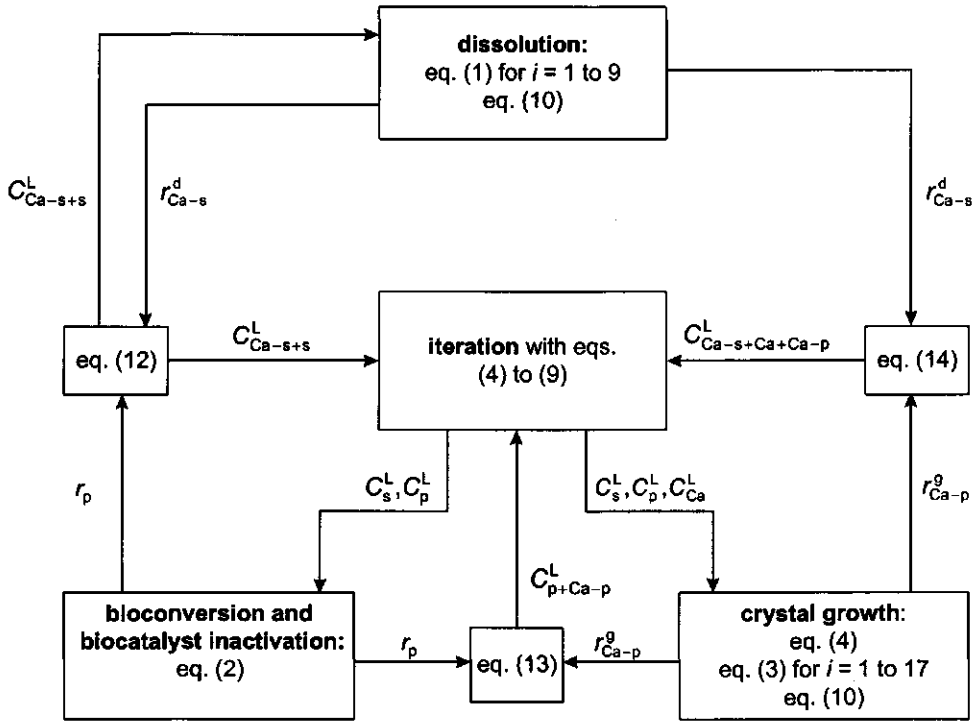


Figure 2 Information feedback diagram for calculation of $C_{Ca-s}^s(t)$, $C_{Ca-s}^L(t)$, $C_{Ca}^L(t)$, $C_s^L(t)$, $C_p^L(t)$, $C_{Ca-p}^L(t)$, and $C_{Ca-p}^s(t)$.

Dissolution of Ca-maleate crystals

The linear dissolution rate of Ca-maleate-H₂O crystals (G_{Ca-s}^0) was found to obey (Michielsen et al., 1998a):

$$G_{Ca-s}^d = \frac{dL_{Ca-s}(t)}{dt} = \frac{\beta_{Ca-s} \cdot k_R \cdot M_{w,Ca-s}}{3 \cdot \alpha_{Ca-s} \cdot \rho_{Ca-s}^s} \cdot (C_{Ca-s+s}^{L*} - C_{Ca-s+s}^L(t)) \quad (1)$$

where L_{Ca-s} is a characteristic dimension of a Ca-maleate-H₂O crystal (here, the breadth of a crystal), t is the time, β_{Ca-s} is the surface shape factor of a Ca-maleate-H₂O crystal ($= A/L^2$, where A is the surface area of a crystal), k_R is the

dissolution reaction rate coefficient, $M_{w,Ca-s}$ is the molecular mass of Ca-maleate·H₂O, α_{Ca-s} is the volume shape factor of a Ca-maleate·H₂O crystal ($= V/L^3$, where V is the volume of a crystal), ρ_{Ca-s}^s is the density of solid Ca-maleate·H₂O, C_{Ca-s+s}^L is the maleate concentration in the liquid phase at saturation (Ca-maleate and maleate²⁻), and C_{Ca-s+s}^L is the maleate concentration in the liquid phase (Ca-maleate and maleate²⁻). In eq. (1) it is assumed that during dissolution Ca-maleate·H₂O crystals have a constant shape, that is α_{Ca-s} and β_{Ca-s} are constant. As Ca-maleate·H₂O crystals are polydispers, a crystal-size distribution was used in the model. The initial size distribution of Ca-maleate·H₂O crystals, with the breadth as characteristic dimension of the needle-shaped Ca-maleate·H₂O crystals, was determined before (Michielsen et al., 1998a; Fig. 3). Note that for all crystals in the crystal-size distribution of Fig. 3, the linear dissolution rate (G_{Ca-s}^d) was equal (see eq. (1)), as it was surface (reaction) controlled. Since the mass-transfer rate coefficient increases with decreasing crystal size (Michielsen et al., 1998a, 1999b), the dissolution rate becomes even more surface (reaction) controlled as the dissolution process proceeds.

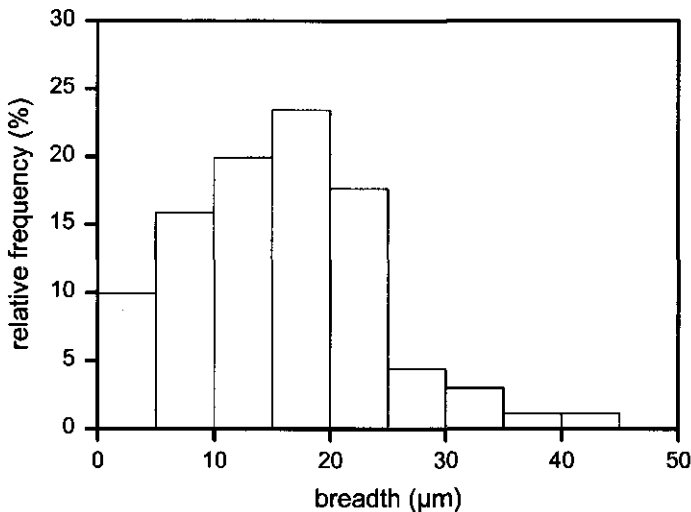


Figure 3 Size distribution of the needle-shaped Ca-maleate·H₂O (substrate) crystals with the breadth as characteristic dimension of the crystals (data from Michielsen et al., 1998a).

Bioconversion and biocatalyst inactivation

The D-malate²⁻ production rate of permeabilized *P. pseudoalcaligenes* was found to obey (Michielsen et al., 1999a):

$$-r_p = r_s = -\frac{k_p \cdot C_s(0) \cdot e^{-k_d t} \cdot C_s^L(t)}{K_m \cdot \left(1 + \frac{C_p^L(t)}{K_p}\right) + C_s^L(t) + \frac{(C_s^L(t))^2}{K_{si}}} \quad (2)$$

where r_p is the D-malate²⁻ production rate, r_s is the maleate²⁻ consumption rate, C_s^L is the maleate²⁻ concentration, k_p is the first-order reaction rate constant, $C_s(0)$ is the total active biocatalyst concentration at $t=0$, k_d is the first-order rate constant for biocatalyst inactivation, K_m is the Michaelis constant, C_p^L is the D-malate²⁻ concentration, K_p is the product inhibition constant, and K_{si} is the substrate inhibition constant.

Growth of Ca-D-malate crystals

The linear growth rate of Ca-D-malate·3H₂O crystals (G_{Ca-p}^g) was found to obey (Michielsen et al., 1999b):

$$G_{Ca-p}^g = \frac{dL_{Ca-p}(t)}{dt} = \frac{\beta_{Ca-p} \cdot k_{exp} \cdot M_{w,Ca-p}}{3 \cdot \alpha_{Ca-p} \cdot \rho_{Ca-p}^s} \cdot \sqrt{K_{sp}(t)} \cdot S(t)^{7/6} \cdot (S(t)-1)^{2/3} \cdot (\ln S(t))^{1/6} \cdot \exp[-K_{exp} / \ln S(t)] \quad (3)$$

with:

$$S(t) = \frac{\sqrt{C_{Ca}^L(t) \cdot C_p^L(t)}}{\sqrt{K_{sp}(t)}}$$

$$\log \sqrt{K_{sp}(t)} = \log \sqrt{K_{sp}^*} + 0.509 \cdot |z_+ \cdot z_-| \cdot \sqrt{I(t)} - K' \cdot I(t) = 0.67 + 2.04 \cdot \sqrt{I(t)} - 0.98 \cdot I(t)$$

where L_{Ca-p} is a characteristic dimension of a Ca-D-malate·3H₂O crystal (here, the breadth of a crystal), β_{Ca-p} is the surface shape factor of a Ca-D-malate·3H₂O crystal, k_{exp} is the (surface) reaction rate coefficient, $M_{w,Ca-p}$ is the molecular mass of Ca-D-malate·3H₂O, α_{Ca-p} is the volume shape factor of a Ca-D-malate·3H₂O crystal,

$\rho_{\text{Ca-p}}^{\text{s}}$ is the density of solid Ca-D-malate·3H₂O, K_{sp} is the apparent solubility product of Ca-D-malate, S is the supersaturation ratio, K_{exp} is a constant, C_{Ca}^{L} is the Ca²⁺ concentration, K_{sp}° is the thermodynamic solubility product of Ca-D-malate, z is the valency of an ion, I is the ionic strength, and K' is the salting-out effect constant; the subscripts + and - refer to the positive and negative ion, respectively (Ca²⁺ and D-malate²⁻). As for Ca-maleate·H₂O crystals, the shape factors $\alpha_{\text{Ca-p}}$ and $\beta_{\text{Ca-p}}$ are assumed constant. Note that the ionic strength I , and thus also the solubility product K_{sp} , are time-dependent, as I depends (amongst others) on the time-dependent Ca²⁺ and D-malate²⁻ concentrations ($C_{\text{Ca}}^{\text{L}}(t)$ and $C_{\text{p}}^{\text{L}}(t)$, respectively). To account for the polydispersity of Ca-D-malate·3H₂O crystals, a crystal-size distribution was used in the model. The initial (or seeding) size distribution of Ca-D-malate·3H₂O crystals was determined before (Michielsen et al., 1999b) and is shown in Fig. 4. Eq. (3) shows that for all crystals in the crystal-size distribution of Fig. 4, the linear growth rate ($G_{\text{Ca-p}}^{\text{g}}$) was equal, as it was surface controlled. However, when the crystal growth process proceeds, the growth rate can become transport controlled, as the mass-transfer rate coefficient decreases with increasing crystal size (Michielsen et al., 1998a, 1999b).

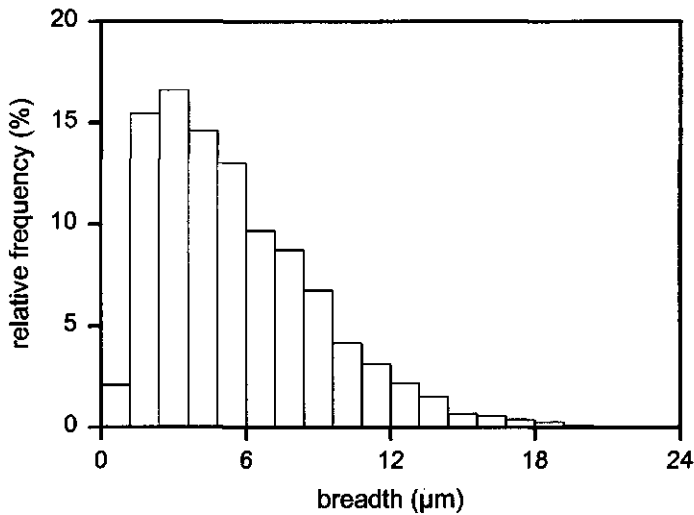


Figure 4 Size distribution of the rectangular-shaped Ca-D-malate·3H₂O (product) crystals with the breadth as characteristic dimension of the crystals (data from Michielsen et al., 1999b).

Dissociation equilibria: iteration

The rates in eqs. (1) to (3) are affected by the ionic concentrations (Ca^{2+} , maleate²⁻, and D-malate²⁻). In general, ionic concentrations cannot be measured directly. By assuming that the dissociation reactions of Ca-maleate and Ca-D-malate are at equilibrium, the Ca^{2+} , maleate²⁻, and D-malate²⁻ concentrations can be calculated. As during the solid-to-solid conversion the ionic strength in the liquid phase changes, and the dissociation constants of Ca-maleate and Ca-D-malate depend on the ionic strength (Michielsen et al., 1999a,c), the ion-concentration calculations were done by iteration with the following set of equations (eqs. (4) to (9)):

Ionic strength I is given by:

$$I = 0.5 \cdot \sum_h C_h \cdot z_h^2 = 0.5 \cdot (C_{\text{Tris}}^L \cdot 1^2 + C_{\text{Ca}}^L \cdot 2^2 + C_s^L \cdot 2^2 + C_p^L \cdot 2^2 + C_{\text{Cl}}^L \cdot 1^2) \quad (4)$$

where C_h is the concentration of ion h , z_h is its valency, C_{Tris}^L is the Tris⁺ concentration, and C_{Cl}^L is the Cl⁻ concentration. Note that the Cl⁻ concentration in eq. (4) originates from HCl that was used to adjust the pH to 8 (the optimum pH for D-malate²⁻ production by permeabilized *P. pseudoalcaligenes*, Michielsen et al., 1998b), and that the effects of the H⁺ and OH⁻ concentrations on the ionic strength were calculated to be negligible. The effect of biocatalyst concentration on the ionic strength was assumed to be negligible as well.

The dissociation constant of Ca-maleate ($K_{\text{Ca-s}}$) as a function of ionic strength can be calculated from (Michielsen et al., 1999a):

$$K_{\text{Ca-s}} = \frac{C_{\text{Ca}}^L \cdot C_s^L}{C_{\text{Ca-s}}^L} = 0.11 \cdot I - 0.02 \quad (5)$$

where $C_{\text{Ca-s}}^L$ is the Ca-maleate concentration. The dissociation constant of Ca-D-malate ($K_{\text{Ca-p}}$) as a function of ionic strength can be calculated from (Michielsen et al., 1999c):

$$K_{\text{Ca-p}} = \frac{C_{\text{Ca}}^L \cdot C_p^L}{C_{\text{Ca-p}}^L} = 0.33 \cdot I - 0.07 \quad (6)$$

where C_{Ca-p}^L is the Ca-D-malate concentration. The maleate concentration in the liquid phase (C_{Ca-s+s}^L) equals:

$$C_{Ca-s+s}^L = C_{Ca-s}^L + C_s^L \quad (7)$$

The D-malate concentration in the liquid phase (C_{p+Ca-p}^L) equals:

$$C_{p+Ca-p}^L = C_p^L + C_{Ca-p}^L \quad (8)$$

The calcium concentration in the liquid phase ($C_{Ca-s+Ca+Ca-p}^L$) equals:

$$C_{Ca-s+Ca+Ca-p}^L = C_{Ca-s}^L + C_{Ca}^L + C_{Ca-p}^L \quad (9)$$

Overall process

For both Ca-maleate and Ca-D-malate crystals, the linear dissolution and growth rates (G , eqs. (1) and (3)) can be directly expressed as volumetric dissolution and growth rates (r):

$$r = \sum_{i=1}^j \frac{N_i}{\epsilon \cdot V \cdot M_w} \cdot \frac{dm(t)}{dt} = \sum_{i=1}^j \frac{N_i}{\epsilon \cdot V \cdot M_w} \cdot \frac{d}{dt} \alpha \cdot L_i(t)^3 \cdot \rho^S = \sum_{i=1}^j \frac{N_i}{\epsilon \cdot V \cdot M_w} \cdot 3 \cdot \alpha \cdot L_i(t)^2 \cdot \rho^S \cdot G_i \quad (10)$$

with:

$$\epsilon = \frac{V^L}{V_{Ca-s}^S + V^L + V_{Ca-p}^S}$$

where i is the class number, j is the number of size classes in the initial crystal-size distribution, N_i is the number of crystals in size class i , m is the mass of one crystal, ϵ is the hold-up of the liquid phase in the suspension (in this work, $\epsilon \approx 1$), and V is the volume of the suspension ($V_{Ca-s}^S + V^L + V_{Ca-p}^S$).

The mass balance for solid Ca-maleate is:

$$\frac{dC_{Ca-s}^S(t)}{dt} = - \sum_{i=1}^j \frac{N_{Ca-s,i} \cdot 3 \cdot \alpha_{Ca-s} \cdot L_{Ca-s,i}(t)^2 \cdot \rho_{Ca-s}^S}{\epsilon \cdot V \cdot M_{w,Ca-s}} \cdot G_{Ca-s}^d = -r_{Ca-s}^d \quad (11)$$

The mass balance for maleate (Ca-maleate and maleate²⁻) in the liquid phase is:

$$\frac{dC_{Ca-s+s}^L(t)}{dt} = r_{Ca-s}^d - r_p \quad (12)$$

The mass balance for D-malate (D-malate²⁻ and Ca-D-malate) in the liquid phase is:

$$\frac{dC_{p+Ca-p}^L(t)}{dt} = r_p - \sum_{i=1}^j \frac{N_{Ca-p,i} \cdot 3 \cdot \alpha_{Ca-p} \cdot L_{Ca-p,i}(t)^2 \cdot \rho_{Ca-p}^S}{\epsilon \cdot V \cdot M_{w,Ca-p}} \cdot G_{Ca-p}^g = r_p - r_{Ca-p}^g \quad (13)$$

The mass balance for calcium (Ca-maleate, Ca²⁺, and Ca-D-malate) in the liquid phase is:

$$\frac{dC_{Ca-s+Ca+Ca-p}^L(t)}{dt} = r_{Ca-s}^d - r_{Ca-p}^g \quad (14)$$

The mass balance for solid Ca-D-malate is:

$$\frac{dC_{Ca-p}^S(t)}{dt} = r_{Ca-p}^g \quad (15)$$

In eqs. (11) to (15) it is assumed that the Ca-maleate and Ca-D-malate crystals do not break up and do not form agglomerates. This means that the number of crystals in any class i (N_i) remains constant (but their size decreases, in case of Ca-maleate crystals, or increases, in case of Ca-D-malate crystals). By combining eqs. (1) to (15) according to the diagram in Fig. 2, the Ca²⁺, maleate²⁻ and D-malate²⁻ concentrations in the liquid phase and the Ca-maleate and Ca-D-malate concentrations in both the liquid and the solid phases in a seeded batch stirred bioreactor can be predicted. If these concentrations are predicted well at varying amounts of solid substrate and

product and varying enzyme concentrations, using independently determined parameters, the model (eqs. (1) to (15)) may be assumed to be valid.

In the model described above, formation of mixed crystals (consisting of both Ca-maleate and Ca-D-malate) was neglected. This is supported by the fact that in the presence of Ca-maleate and Ca-D-malate crystals a 100% conversion of all maleate was obtained in a batch bioreactor (Michielsen et al., 1999b; this work).

MATERIALS AND METHODS

Materials

Ca-maleate·H₂O and Ca-D-malate·3H₂O were purchased from Syncom (Groningen, The Netherlands; purity > 98%).

Cultivation and permeabilization of *P. pseudoalcaligenes*

P. pseudoalcaligenes NCIMB 9867 was cultivated in sterilized mineral salts medium (Hartmans et al., 1989) containing 1 g/l of 3-hydroxybenzoate (pH 7), and permeabilized with Triton X-100 as described before (Michielsen et al., 1998b).

Pre-conditioning of seed crystals

Michielsen et al. (1999b) have shown that at some conditions the start of growth of Ca-D-malate seeds was delayed. Apparently, the Ca-D-malate seeds did not have the proper crystal structure. Since such a delay can hardly be predicted, it was avoided by first forming Ca-D-malate seeds with the proper crystal structure. To this end, a supersaturated Ca-D-malate solution was first formed by converting Ca-maleate with permeabilized cells of *P. pseudoalcaligenes*. Then Ca-D-malate seeds were added to the (isothermal) supersaturated solution, and growth of these seed crystals was checked by measuring the decrease in supersaturation, called desupersaturation. Such an experiment is called a seeded desupersaturation experiment. Since the latter experiment was carried out at conditions similar to the follow-up experiment, i.e. the biocatalytic conversion of either dissolved or solid Ca-maleate to solid Ca-D-malate (see below), the resulting suspension contained Ca-D-malate crystals with the proper crystal structure. The formation of supersaturated Ca-D-malate solutions and the preparatory seeded desupersaturation experiments are described in this section.

A supersaturated solution was created by incubating 40 ml of 250 mM Ca-maleate / 625 mM Tris (pH adjusted to 8 with HCl) with 10 ml of permeabilized cells (dry weight: $20.4 \text{ mg}\cdot\text{cm}^{-3}$) in a shaking water bath (170 rpm) at 25°C for 14 hours. After 14 hours, 16 ml of the supersaturated solution was transferred to a 65-ml vessel (diameter: 3.4 cm) with a jacket connected to a constant-temperature water bath. After 30 min of incubation at 30°C , the magnetic stirrer (diameter: 19 mm, thickness: 6 mm) was started (300 rpm). To determine the supersaturation and to check whether Ca-D-malate crystals were formed due to primary nucleation or not, two 200- μl samples were taken for dissolved maleate and D-malate analysis, and two 50- μl samples were taken for total D-malate analysis. These samples were treated and analysed by HPLC as described before (Michielsen et al., 1999b). Note that in the supersaturated Ca-D-malate solutions described in this work no significant amounts of Ca-D-malate crystals were formed due to primary nucleation during the 14 hours of incubation. The preparatory seeded desupersaturation experiment was started by adding 0.15 g of Ca-D-malate $\cdot 3\text{H}_2\text{O}$ seeds to the supersaturated solution. The solution was incubated for 24 h at 30°C , so that seeds with the proper structure were formed. After 24 h, two 200- μl and two 50- μl samples were taken for dissolved D-malate and total D-malate analysis, respectively, to check to what extent desupersaturation (due to crystal growth) had occurred. The samples were treated and analysed by HPLC as described before (Michielsen et al., 1999b). The resulting suspension was used in the follow-up experiment (see below). For converting dissolved Ca-maleate to solid Ca-D-malate in the presence of a higher initial seed amount (see below), the preparatory seeded desupersaturation experiment was repeated, but now with 0.25 g of Ca-D-malate $\cdot 3\text{H}_2\text{O}$ added to 25.5 ml of the supersaturated solution.

Appropriate product seed crystals for the two solid-to-solid conversions (see below) were formed in similar preparatory seeded desupersaturation experiments. For the first solid-to-solid conversion, 2.0 g of Ca-D-malate $\cdot 3\text{H}_2\text{O}$ was added to 200.5 ml of supersaturated solution (made similar as described before, with a biocatalyst concentration of $4568 \text{ mg}\cdot\text{dm}^{-3}$) of 30°C in a 540-ml vessel (diameter: 9 cm) with a temperature jacket connected to a constant-temperature water bath. This suspension was incubated for 24 h at 30°C , and was stirred magnetically at 150 rpm (stirrer diameter: 4.8 cm, stirrer thickness: 0.7 cm). For the second solid-to-solid conversion, a higher initial seed amount was prepared by adding 5.0 g of Ca-D-malate $\cdot 3\text{H}_2\text{O}$ to 500.5 ml of supersaturated solution (made similar as described

before, with a biocatalyst concentration of $4618 \text{ mg}\cdot\text{dm}^{-3}$) and incubating it for 24 h at 30°C . The suspension was stirred magnetically at 250 rpm. In both experiments, the maleate, D-malate, and total D-malate concentrations were determined as described above.

Biocatalytic conversion of dissolved Ca-maleate to solid Ca-D-malate

Part of the overall model (biokinetics integrated with crystal growth kinetics) was validated by converting dissolved Ca-maleate to solid Ca-D-malate in a seeded batch bioreactor, and comparing the results with the model predictions. For that, 20 ml of 313 mM Ca-maleate / 117 mM Ca-D-malate / 875 mM Tris (pH 8) was added to the 15-ml suspension with the seed crystals. This suspension was incubated for 30 min at 30°C . At $t=0$, 15 ml of permeabilized *P. pseudoalcaligenes* (dry weight: $22.0 \text{ mg}\cdot\text{cm}^{-3}$) was added to the vessel. The suspension was incubated for 7 hours at 30°C , and stirred magnetically at 500 rpm. At regular time intervals, 200- μl samples were taken for determination of dissolved maleate and D-malate, and 50- μl samples were taken for determination of the total amount of D-malate. These samples were treated and analysed by HPLC as described before (Michielsen et al., 1999b).

This experiment was repeated at a lower biocatalyst concentration and a higher seed amount. To this end, 20 ml of 313 mM Ca-maleate / 79 mM Ca-D-malate / 625 mM Tris (pH 8) and 5 ml of permeabilized *P. pseudoalcaligenes* (dry weight: $22.2 \text{ mg}\cdot\text{cm}^{-3}$) were added to the 25-ml suspension with the seed crystals, and the decrease in maleate concentration and increase in D-malate concentration (dissolved and total) were measured as described above.

Protease inhibition

As in the presence of permeabilized *P. pseudoalcaligenes* that was incubated for about two days, an increase in the maleate-hydratase inactivation rate of freshly added permeabilized *P. pseudoalcaligenes* was found, the protease inhibitor phenylmethylsulphonylfluoride (PMSF) was tested. This was done by incubating 5 ml of permeabilized *P. pseudoalcaligenes* (dry weight: $22.2 \text{ mg}\cdot\text{cm}^{-3}$) with 5 ml of 1000 mM Tris (pH 8) for 48 hours at 30°C first. After 48 hours, 15 ml of 200 mM Ca-maleate / 667 mM Tris (pH 8) was added and incubated for 30 min at 30°C . At $t=0$, 2.6 mg PMSF (corresponding with 0.5 mM) and 5 ml of permeabilized *P. pseudoalcaligenes* (dry weight: $20.3 \text{ mg}\cdot\text{cm}^{-3}$) were added, and the decrease in maleate concentration was determined during 7 hours in a shaking water bath (170

rpm) at 30°C. For that, every 30 min during the first 3 hours, and every hour during the last 4 hours, 50- μ l samples were taken and treated and analysed for (dissolved) maleate as described before (Michielsen et al., 1999b). The decrease in maleate concentration was compared to the decrease in the absence of cells that were incubated for 48 hours, and to the decrease in the absence of both cells and PMSF. The latter two conditions were determined by incubating 25 ml of 120 mM Ca-maleate / 600 mM Tris (pH 8) with and without 2.6 mg PMSF, with 5 ml of permeabilized *P. pseudoalcaligenes* (dry weight: 20.3 mg·cm⁻³) for 7 hours in a shaking water bath at 30°C. The decrease in maleate concentration was determined as described above.

Biocatalytic conversion of solid Ca-maleate to solid Ca-D-malate

In order to validate the overall model, solid Ca-maleate was converted to solid Ca-D-malate in a seeded batch bioreactor, and the results were compared with the model simulations. For that, 150 ml of 533 mM Ca-maleate / 86 mM Ca-D-malate / 667 mM Tris (pH 8) was added to the 200-ml suspension with the seed crystals, and incubated for 30 min at 30°C. At $t=0$, 50 ml of permeabilized *P. pseudoalcaligenes* (dry weight: 22.0 mg·cm⁻³) was added to the suspension in the vessel. This suspension was incubated for 7 hours at 30°C, and was stirred magnetically at 250 rpm. Sampling and sample analysis were similar as in the experiments where dissolved Ca-maleate was converted, except that during the first hour every 6 min samples were taken.

The experiment was repeated with a higher biocatalyst concentration and higher initial amounts of solid substrate and solid product, in the presence of 0.5 mM PMSF. This was done as follows. After 24 h of incubation in the preparatory seeded desupersaturation experiment, the stirrer was stopped in order to precipitate the seeds in the suspension, and 300 ml of clear solution was removed. To the remaining 200-ml suspension with the seed crystals, 195 ml of 1090 mM Ca-maleate / 103 mM Ca-D-malate / 769 mM Tris (pH 8) was added, and incubated for 30 min at 30°C. At $t=0$, 43 mg of PMSF and 105 ml of permeabilized *P. pseudoalcaligenes* (dry weight: 23.2 mg·cm⁻³) were added. The suspension was incubated for 7 hours at 30°C, and was stirred magnetically at 250 rpm. Every 10 min, samples were taken and analysed as described above.

Simulation

The model (eqs. (1) to (15)) was implemented in the computer program Simulink, a companion program to Matlab (Mathworks), according to the diagram in Fig. 2. The differential equations in the model were solved in Simulink by applying the ode15s solver. Values were attributed to the parameters of the Simulink model in a Matlab-file. The parameter values used are given in Table 1, in the legends of Figs. 5 and 6, and in Appendix A. It should be emphasized that the parameter values of each of the six steps were determined separately in independent experiments.

Table 1 Parameter values used for model simulations at 30°C and pH 8; values for parameters that changed with every bioconversion in suspension and the initial conditions are given in the legends of Figs. 5 and 6 and in Appendix A.

Parameters for simulation of solid substrate (Ca-maleate·H ₂ O) dissolution ^{a)}					
k_R^d	(m·min ⁻¹)	1.1·10 ⁻³	β_{Ca-s}	(-)	11.75
$M_{w,Ca-s}$	(kg·mol ⁻¹)	172·10 ⁻³	ρ_{Ca-s}^S	(kg·m ⁻³)	1677
α_{Ca-s}	(-)	2.54			
Parameters for simulation of biocatalytic substrate (maleate ²⁻) conversion ^{b)}					
k_p	^{c)}	7.5·10 ⁻⁴	K_p	(mM)	3.6
K_m	(mM)	2.3	K_{si}	(mM)	497
Parameters for simulation of solid product (Ca-D-malate·3H ₂ O) growth ^{d)}					
k_{exp}	(m·min ⁻¹)	3.9·10 ⁻⁵	β_{Ca-p}	(-)	6.75
K_{exp}	(-)	1.7	ρ_{Ca-p}^S	(kg·m ⁻³)	1600
$M_{w,Ca-p}$	(kg·mol ⁻¹)	226·10 ⁻³	K_{sp}^*	(mM ²)	22.1
α_{Ca-p}	(-)	1.30	K'	(dm ³ ·mol ⁻¹)	0.98

a) from Michielsen et al. (1998a).

b) from Michielsen et al. (1999a); the first-order rate constant for biocatalyst inactivation (k_d) is not shown here, as it varied at the conditions in Figs. 5 and 6 (see Appendix A).

c) (mmol·min⁻¹·mg⁻¹).

d) from Michielsen et al. (1999b).

Other analyses

Maleate and D-malate (in both ionic and complexed (with Ca²⁺) form, and in both acidic and nonacidic form) were analysed by HPLC as described before (Michielsen et al., 1999c).

The dry weight of the permeabilized cell suspension was determined as described by Michielsen et al. (1998b).

RESULTS AND DISCUSSION

Biocatalytic conversion of dissolved Ca-maleate to solid Ca-D-malate

Fig. 5a shows a typical result of the conversion of dissolved Ca-maleate to solid Ca-D-malate by permeabilized *P. pseudoalcaligenes* in a batch bioreactor seeded with product crystals. As expected, the dissolved maleate concentration decreased while the total D-malate concentration (dissolved and solid) increased, until all maleate was finally converted. As the aqueous phase in the bioreactor was initially saturated with product, bioconversion resulted in D-malate supersaturation, and thus initiated Ca-D-malate crystal growth. So, the dissolved D-malate concentration is influenced by both bioconversion and Ca-D-malate crystal growth. Initially, the concentration increased, as the bioconversion rate was higher than the crystal growth rate. However, the bioconversion rate decreased with time due to lower substrate concentrations (maleate²⁻). At $t < 40$ min, the decrease in the bioconversion rate also results from increased product inhibition (Michielsen et al., 1999a), as the dissolved product concentration (D-malate²⁻) increased up to $t = 40$ min. The Ca-D-malate crystal growth rate increased up to $t = 40$ min, as both the total surface area of the Ca-D-malate crystals and the supersaturation increased with time (at least at $t < 40$ min in Fig. 5a). At $t = 40$ min, the dissolved D-malate concentration started to decrease, as the crystal growth rate became higher than the bioconversion rate.

Fig. 5b shows a similar bioconversion, but now at a 3 times lower biocatalyst concentration and a 20% higher initial amount of solid product. This resulted in a 3 times lower initial bioconversion rate (r_p) and a 20% higher initial product crystal growth rate (r_{Ca-p}^g), as r_p decreases proportionally with decreasing $C_e(0)$ (see eq. (2)) and r_{Ca-p}^g increases proportionally with increasing N_{Ca-p} (see eq. (13)). As expected from these initial rates, the Ca-D-malate crystal growth rate became higher than the bioconversion rate at a lower supersaturation.

In the experiments described here, the aqueous phase was saturated with product at $t = 0$. The measurements showed that after 24 h saturation was reached again. The initial saturation concentration of D-malate (≈ 50 mM) differed from the saturation concentration at $t = 24$ h (≈ 70 mM). In Fig. 5a, this is caused by the fact that, at $t = 0$, 141 mM of calcium was calculated to be present in the liquid phase (see Appendix A), whereas at $t = 24$ h it was almost equal to the D-malate concentration. Such differences in D-malate solubility due to calcium variations were reported earlier (Michielsen et al., 1999b).

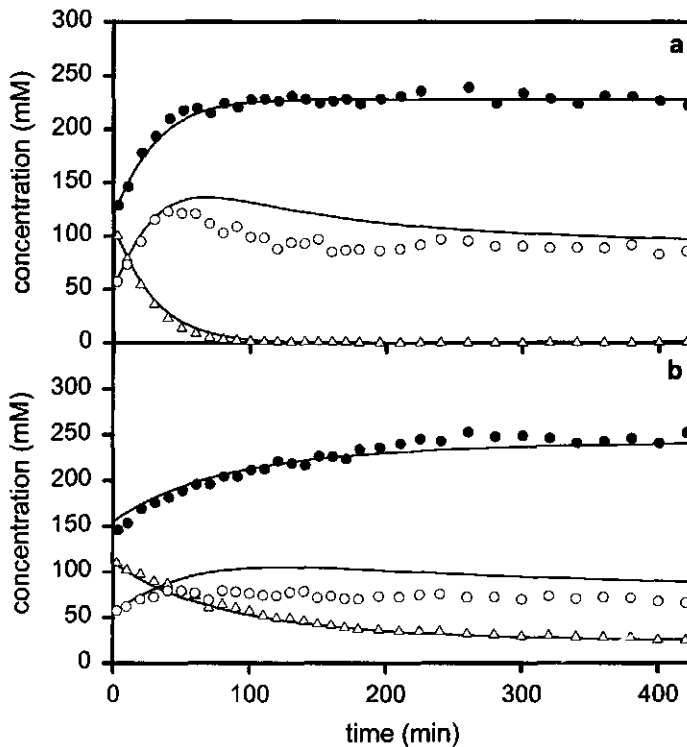


Figure 5 Biocatalytic conversion of dissolved Ca-maleate to solid Ca-D-malate (in a: $C_{Ca-p}^S(0) = 68.7$ mM; in b: $C_{Ca-p}^S(0) = 99.4$ mM) by permeabilized *P. pseudoalcaligenes* (in a: $C_e(0) = 6660$ mg·dm⁻³; in b: $C_e(0) = 2220$ mg·dm⁻³) at 30°C, pH 8, and 500 rpm in a batch bioreactor seeded with Ca-D-malate crystals; dissolved maleate (Δ), dissolved D-malate (O), total D-malate (●), and the model simulation (—). Parameter values for the model simulations are given in Table 1 and Appendix A.

The model predictions in Figs. 5a and 5b are represented by the solid lines and are based on parameter values that are determined independently in separate experiments (Michielsen et al., 1998a, 1999a,b). Fig. 5a shows that the model predicted the data quite satisfactory, particularly so if the complexity of the overall process is taken into consideration. In Fig. 5b, the model could only describe the data well, if the first-order rate constant for biocatalyst inactivation k_d ($19 \cdot 10^{-4}$ min⁻¹; Michielsen et al., 1999a) was increased 4-fold (see Appendix A). The likeliness for a higher biocatalyst inactivation rate is discussed below.

The higher biocatalyst inactivation rate in Fig. 5b might be attributed to protease activity. Proteases might have originated from permeabilized cells of *P.*

Pseudoalcaligenes that were used to create a supersaturated solution for the preparatory seeded desupersaturation experiment (preceding the experiment shown in Fig. 5). As these cells had been incubated for two days prior to the experiments in Fig. 5, lysis and protease liberation was quite likely. These proteases might accelerate maleate-hydratase inactivation. This was confirmed experimentally, as in the presence of the protease inhibitor phenylmethylsulfonylfluoride (PMSF) no increase in the biocatalyst inactivation rate was found (data not shown). The effect of proteases was more pronounced in the experiment in Fig. 5b than in the one in Fig. 5a, as the ratio of 'new' to 'old' permeabilized cells of *P. pseudoalcaligenes* was much lower (1.1 in Fig. 5b and 5.5 in Fig. 5a). For that reason, a 4 times higher k_d was used in the model simulations of Fig. 5b (see Appendix A).

Both Figs. 5a and 5b then indicate that the bioconversion rate was calculated quite accurately, namely the decrease in the dissolved maleate concentration and the resulting increase in the total D-malate concentration were predicted very well. However, Figs. 5a and 5b also indicate that the model underestimated the Ca-D-malate crystal growth rate, as at both conditions the simulated maximum of the dissolved D-malate concentration was a little too high. The most likely explanation for the underestimation of crystal growth is that new crystals were formed due to secondary nucleation, thereby increasing the total crystal surface area. As a result, the Ca-D-malate crystal growth rate was higher than predicted by the model. Another explanation might be that at low supersaturations (from 70 to 95 mM in Figs. 5a and 5b) the Ca-D-malate crystal growth rate was predicted too low by eq. (3). This is indicated by the fact that in practice saturation was reached at $t=24$ h, whereas according to the crystal growth model saturation had not been reached yet, as a driving force for crystal growth was still present at $t=24$ h. This might suggest that at low supersaturation the Ca-D-malate crystal growth process shifts from an exponential rate law (see eq. (3)) to a linear or parabolic rate law (Nielsen and Toft, 1984). Such a shift has been reported also for growth of CaF_2 crystals, which shifts from an exponential rate law at high and intermediate supersaturation to a parabolic rate law at low supersaturation (Nielsen and Toft, 1984).

Biocatalytic conversion of solid Ca-maleate to solid Ca-D-malate

Two conversions of solid Ca-maleate- H_2O to solid Ca-D-malate- $3\text{H}_2\text{O}$ by permeabilized *P. pseudoalcaligenes* in a batch bioreactor seeded with product crystals are shown in Figs. 6a and b. The difference with the preceding conversions

of Figs. 5a and b is that solid Ca-maleate first had to dissolve. Figs. 6a and b show that the dissolved maleate concentration was maintained at saturation, indicating that the dissolution rate was much bigger than the bioconversion rate, until all the Ca-maleate crystals were dissolved. At this moment, the total and dissolved maleate concentrations coincided ($t=40$ min in Fig 6a, $t=175$ min in Fig. 6b). The saturation concentration of maleate (in Figs. 6a and b) was in reasonable agreement with earlier data (Michielsen et al., 1998a).

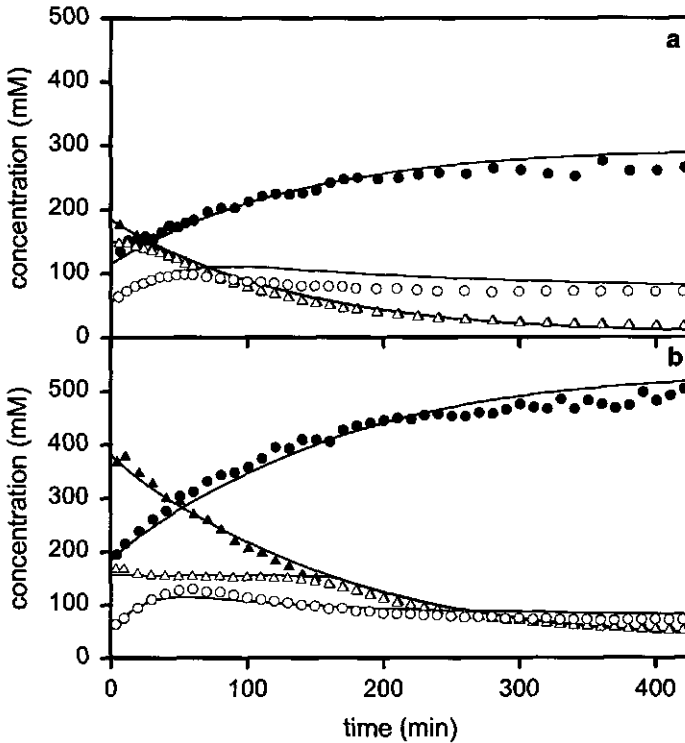


Figure 6 Biocatalytic conversion of solid Ca-maleate (in a: $C_{Ca-s}^s(0) = 34.9$ mM; in b: $C_{Ca-s}^s = 226.2$ mM) to solid Ca-D-maleate (in a: $C_{Ca-p}^s(0) = 59$ mM; in b: $C_{Ca-p}^s(0) = 126.8$ mM) by permeabilized *P. pseudoalcaligenes* (in a: $C_e(0) = 2750$ mg·dm⁻³; in b: $C_e(0) = 4870$ mg·dm⁻³) at 30°C, pH 8, and 250 rpm in a batch bioreactor seeded with Ca-D-maleate crystals; dissolved maleate (Δ), total maleate (\blacktriangle), dissolved D-maleate (\circ), total D-maleate (\bullet), and the model simulation (—). Parameter values for the model simulations are given in Table 1 and Appendix A.

The model described the data well, if again the first-order rate constant for biocatalyst inactivation (k_d) was adjusted (see Appendix A). Even in the presence of 0.5 mM PMSF, as in Fig. 6b, about a 3-fold increase of k_d was necessary, indicating that 0.5 mM PMSF was not sufficient to inhibit all protease activity. Fig. 6b shows that especially in case of relatively high initial amounts of substrate crystals (Ca-maleate·H₂O) and product crystals (Ca-D-malate·3H₂O), the model simulation and the data coincided very well, indicating that secondary nucleation was irrelevant. This could be caused by the fact that the specific energy input was smaller in the experiment in Fig. 6b than in Fig. 6a. Both the density and the volume of the suspension in the experiment in Fig. 6b were higher than in Fig. 6a, whereas the stirring speed was equal (250 rpm). Note that for both experiments (in Figs. 6a and b) the suspensions were observed to be mixed well.

CONCLUSIONS

A kinetic model for the conversion of a solid substrate salt to a solid product salt in a batch stirred bioreactor seeded with product crystals was developed. In this model, the kinetics of salt dissolution, the biokinetics (of both conversion and biocatalyst inactivation), and the kinetics of salt crystal growth were integrated; salt dissociation and complexation of ions in the liquid phase were assumed to be at equilibrium. The model gave a very good quantitative prediction of the conversion of solid Ca-maleate to solid Ca-D-malate by permeabilized *P. pseudoalcaligenes*, especially in case of relatively high initial amounts of solid Ca-maleate and solid Ca-D-malate. This makes the model a good basis for process optimization and for development of a continuous system for solid-to-solid conversions.

ACKNOWLEDGEMENTS

We thank S. Hartmans and M.J. van der Werf (Division of Industrial Microbiology, Wageningen Agricultural University) for supplying *P. pseudoalcaligenes* and for fruitful discussions on cultivation and permeabilization of *P. pseudoalcaligenes*.

This work was financially supported by the Ministry of Economic Affairs, the Ministry of Education, Culture and Science, the Ministry of Agriculture, Nature

Management and Fishery in the framework of an industrial relevant research programme of the Netherlands Association of Biotechnology Centres in the Netherlands (ABON).

APPENDIX A: Remaining parameter values and initial conditions

Remaining parameter values and initial conditions for model simulations at 30°C and pH 8 (in addition to the parameter values given in Table 1). ^{a)}

Model simulation of Fig. 5a					
k_d	min ⁻¹	19·10 ⁻⁴ ^{b)}	V	m ³	50·10 ⁻⁶
$C_{Ca-s+Ca+Ca-p}^L(0)$	mM	140.8	ΔL^g ^{c)}	μm	4.30
C_{Cl}^L	mM	324.4			
Model simulation of Fig. 5b					
k_d	min ⁻¹	80·10 ⁻⁴ ^{d)}	V	m ³	50·10 ⁻⁶
$C_{Ca-s+Ca+Ca-p}^L(0)$	mM	153.8	ΔL^g ^{c)}	μm	4.81
C_{Cl}^L	mM	334.2			
Model simulation of Fig. 6a					
k_d	min ⁻¹	40·10 ⁻⁴ ^{d)}	V	m ³	400·10 ⁻⁶
$C_{Ca-s+Ca+Ca-p}^L(0)$	mM	209.8	ΔL^g ^{c)}	μm	3.72
C_{Cl}^L	mM	353.6	ΔL^d ^{e)}	μm	11.3
Model simulation of Fig. 6b					
k_d	min ⁻¹	55·10 ⁻⁴ ^{d)}	V	m ³	500·10 ⁻⁶
$C_{Ca-s+Ca+Ca-p}^L(0)$	mM	203.5	ΔL^g ^{c)}	μm	3.73
C_{Cl}^L	mM	342.2	ΔL^d ^{e)}	μm	3.91

a) $\epsilon \approx 1$ at the conditions in Figs. 5 and 6.

b) from Michielsen et al. (1999a).

c) ΔL^g represents the calculated increase in the breadth of all crystals in the product crystal-size distribution of Fig. 4 due to product crystal growth in the preparatory seeded desupersaturation experiment.

d) adjusted with respect to the value given by Michielsen et al. (1999a).

e) ΔL^d represents the calculated decrease in the breadth of all crystals in the substrate crystal-size distribution of Fig. 3 due to substrate dissolution, in order to create a saturated substrate solution at $t=0$; note that at $t=0$ in Fig. 6a the first two initial size classes of Fig. 3 were completely dissolved (2.75 and 7.50 μm), while at $t=0$ in Fig. 6b only the first initial size class of Fig. 3 (2.75 μm) was completely dissolved.

NOMENCLATURE

C	concentration	(mmol·dm ⁻³)
$C(0)$	concentration at $t=0$	(mmol·dm ⁻³)
C_e	active enzyme concentration	(mg·dm ⁻³)
$C_e(0)$	active enzyme concentration at $t = 0$	(mg·dm ⁻³)
G	linear dissolution or growth rate	(m·min ⁻¹)
I	ionic strength	(mol·dm ⁻³)
K	dissociation constant	(mol·dm ⁻³)
K_{exp}	constant of exponential rate law	(-)
K_m	Michaelis constant	(mmol·dm ⁻³)
K_p	product inhibition constant	(mmol·dm ⁻³)
k_p	first-order reaction rate constant	(mmol·min ⁻¹ ·mg ⁻¹)
K_{si}	substrate inhibition constant	(mmol·dm ⁻³)
K_{sp}	apparent solubility product of Ca-D-malate	(mmol ² ·dm ⁻⁶)
K_{sp}^*	thermodynamic solubility product of Ca-D-malate	(mmol ² ·dm ⁻⁶)
K'	salting-out effect constant	(dm ³ ·mol ⁻¹)
k	mass-transfer coefficient	(m·min ⁻¹)
k_d	first-order rate constant for biocatalyst inactivation	(min ⁻¹)
L	characteristic dimension of the crystal	(m)
$M_{w,Ca-p}$	molecular mass of Ca-D-malate·3H ₂ O	(kg·mol ⁻¹)
$M_{w,Ca-s}$	molecular mass of Ca-maleate·H ₂ O	(kg·mol ⁻¹)
m	mass of one crystal	(kg)
N	number of crystals	(-)
r	volumetric rate	(mmol·dm ⁻³ ·min ⁻¹)
S	supersaturation ratio	(-)
t	time	(min)
V	volume (of the suspension)	(m ³)
z	valency of an ion	(-)

Greek symbols

α	volume shape factor	(-)
β	surface shape factor	(-)
ϵ	hold-up of the liquid phase in the suspension	(-)
ρ	density	(kg·m ⁻³)

Indices

Ca	Ca ²⁺
Ca-p	Ca-D-malate
Ca-s	Ca-maleate
Cl	Cl ⁻
d	crystal dissolution
e	enzyme
exp	exponential rate law
g	crystal growth
<i>i</i>	class number
<i>j</i>	number of size classes in the crystal-size distribution
L	liquid phase or bulk solution
p	product (= D-malate ²⁻)
R	(surface) reaction at the solid-liquid interface
S	solid phase
s	substrate (= maleate ²⁻)
Tris	Tris ⁺
+	positive ion
-	negative ion
*	saturation

REFERENCES

- Ashina Y, Suto M. 1992. Development of an enzymatic process for manufacturing acrylamide; recent progress. In: Tanaka A, Tosa T and Kobayashi T, editors. Industrial application of immobilized biocatalysts. New York: Marcel Dekker, Inc. p 91-107.
- Bornscheuer UT, Yamane Y. 1994. Activity and stability of lipase in the solid phase glycerolysis of triolein. *Enzyme Microb Technol* 16:864-869.
- Cao L, Bornscheuer UT, Schmid RD. 1996. Lipase-catalysed solid phase synthesis of sugar esters. *Fett/Lipid* 98:332-335.
- Erbeldinger M, Xiongwei N, Halling PJ. 1998. Enzymatic synthesis with mainly undissolved substrates at very high concentrations. *Enzyme Microb Technol* 23:141-148.

- Hartmans S, Smits JP, Van der Werf MJ, Volkering F, De Bont JAM. 1989. Metabolism of styrene oxide and 2-phenylethanol in the styrene-degrading *Xanthobacter* strain 124X. *Appl Environ Microbiol* 55:2850-2855.
- Kasche V. 1986. Mechanisms and yields in enzyme catalysed equilibrium and kinetically controlled synthesis of β -lactam antibiotics and other condensation products. *Enzyme Microb Technol* 8:4-16.
- Kasche V, Galunsky B. 1995. Enzyme catalysed biotransformations in aqueous two-phase systems with precipitated substrate and/or products. *Biotechnol Bioeng* 45:261-279.
- Kitahara K, Fukui S, Misawa M. 1960. Preparation of L-malate from fumarate by a new process "enzymatic transcrystallization". *J Gen Appl Microbiol* 6:108-116.
- Klein JP, David R. 1995. Reaction crystallization. In: Mersmann A, editor. *Crystallization technology handbook*. New York: Marcel Dekker, Inc. p 359-400.
- Michielsen MJF, Reijenga KA, Wijffels RH, Tramper J, Beeftink HH. 1998a. Dissolution kinetics of Ca-maleate crystals: evaluation for biotransformation reactor design. *J Chem Technol and Biotechnol* 73:13-22.
- Michielsen MJF, Meijer EA, Wijffels RH, Tramper J, Beeftink HH. 1998b. Kinetics of D-malate production by permeabilized *Pseudomonas pseudoalcaligenes*. *Enzyme Microb Technol* 22:621-628.
- Michielsen MJF, Frielink C, Wijffels RH, Tramper J, Beeftink HH. 1999a. D-malate production by permeabilized *Pseudomonas pseudoalcaligenes*; optimization of conversion and biocatalyst productivity. Submitted for publication.
- Michielsen MJF, Frielink C, Wijffels RH, Tramper J, Beeftink HH. 1999b. Growth of Ca-D-malate crystals in a bioreactor. Submitted for publication.
- Michielsen MJF, Frielink C, Meijer EA, Van der Werf MJ, Wijffels RH, Tramper J, Beeftink HH. 1999c. Stabilization of maleate-hydratase activity of permeabilized *Pseudomonas pseudoalcaligenes*. *Biocatal Biotransf* 17: 125-137.
- Miller TL. 1985. Steroid fermentation. *Compr Biotechnol* 3:297-318.
- Nielsen AE, Toft JM. 1984. Electrolyte crystal growth kinetics. *J Cryst Growth* 67:278-288.
- Oyama K. 1992. The industrial production of aspartame. In: Collins AN, Sheldrake GN and Crosby J, editors. *Chirality in industry*. New York: John Wiley & Sons Ltd. p 173-182.

- Petkov DD, Stoineva IB. 1984. Enzyme peptide synthesis by iterative procedure in a nucleophile pool. *Tetrahedron Lett* 25:3751-3754.
- Takahashi S. 1986. Microbial production of D-p-hydroxyphenylglycine. *Prog Ind Microbiol* 24:269-279.
- Van den Heuvel JC, Beeftink HH. 1988. Kinetic effects of simultaneous inhibition by substrate and product. *Biotechnol Bioeng* 31:718-724.
- Van der Werf MJ, Van den Tweel WJJ, Hartmans S. 1993. Purification and characterization of maleate hydratase from *Pseudomonas pseudoalcaligenes*. *Appl Environ Microbiol* 59:2823-2829.
- Van der Werf MJ, Hartmans S, Van den Tweel WJJ. 1995. Effect of maleate counter-ion on malease activity: production of D-maleate in a crystal-liquid two-phase system. *Enzyme Microb Technol* 17:430-436.
- Watanabe S, Osawa T. 1966. Studies on the production of L-malic acid. Part I. Actions of detergents on the production of L-malic acid. *Nippon Kogei Nagaku Kaishi* 40:319-324.
- Wolff A, Zhu L, Wong YW, Straathof AJJ, Jongejan JA, Heijnen JJ. 1999. Understanding the influence of temperature change and cosolvent addition on conversion rate of enzymatic suspension reactions based on regime analysis. *Biotechnol Bioeng* 62:125-134.

CHAPTER 8

Solid-to-solid bioconversions: batch or continuous?

ABSTRACT

Studies of solid-to-solid bioconversions in the last decade mainly focused on attaining a high conversion at a large scale in batch systems. Lately, attention shifted towards batch systems with very high amounts of solid substrate, thus featuring a small liquid phase. Further development of these batch systems as well as the development of continuous systems has been hampered by the lack of mechanistic models, featuring the kinetics of dissolution, bioconversion, and crystallization. Recently, such a model has been developed, giving a new impulse to this technology.

Based on the current status of biocatalyst immobilization and of continuous reaction crystallization, proposals for continuous systems for solid-to-solid bioconversions are given. Assuming that such continuous systems are feasible, a general procedure is developed to determine whether a batch or continuous mode of operation is most profitable for a specific solid-to-solid bioconversion.

INTRODUCTION

In aqueous media, biocatalysts often show low overall volumetric productivities due to limited substrate solubility and/or inhibition by substrate and/or product (Michielsen et al., 1999a). Multi-phase systems are generally applied to increase overall substrate solubility and to reduce substrate and/or product inhibition: a second (or third) phase serves as a substrate reservoir or product sink. Other advantages of such systems are that biocatalytic production and downstream processing are integrated and that high product concentrations can be gained, as the product accumulates (mainly) in one phase.

For extraction of hydrophobic compounds, an organic solvent is often used as water-immiscible second phase. However, use of an organic phase may cause loss in specificity and selectivity of the biocatalyst, and product contamination, and it makes the process less cost efficient and less environmentally friendly.

For extraction of hydrophilic substrates and/or products, like proteins, a second aqueous phase may be suitable (Hustedt et al., 1988; Zijlstra et al., 1998). However, widespread industrial application of aqueous two-phase systems is hampered by the high costs of the polymers involved, and by the complexity of aqueous two-phase systems (Andersson and Hahn-Hägerdal, 1990).

It is obvious that in case of two dissimilar substrates (both hydrophobic and hydrophilic) selection of a suitable solvent that is not deleterious to the enzyme and that solubilizes high concentrations of both substrates equally well, becomes even more difficult. For some specific bioconversions, solutions are reported that rely on substrate modification (e.g. by making it more hydrophobic; Adelhorst et al., 1990; Fregapane et al., 1991; Scheckermann et al., 1995), or on cosolvent addition (Wolf et al., 1999). However, a general approach for biocatalytic synthesis at high substrate concentrations and at low costs remains to be formulated.

Biocatalysis in multi-phase systems with solid substrate and/or product

An attractive alternative for the multi-phase systems described above, is the use of solid substrate and product phases as water-immiscible reservoir and sink phases. In these systems, the solid substrate dissolves, is converted in the liquid phase by the biocatalyst, and if the product concentration exceeds the solubility limit, the

product crystallizes. These liquid-solid-solid three-phase systems have the following advantages: 1) extremely high overall substrate concentrations can be used (Erbeldinger et al., 1998a); note that at least a part of the reactor volume must be liquid, as López-Fandiño et al. (1994a) and Kuhl et al. (1995) found that the biocatalytic conversion takes place in the liquid phase, 2) high conversions and rates can be attained (see below), 3) the formation of product crystals facilitates downstream processing (centrifugation or filtration followed by drying). The advantages of not needing an organic solvent or expensive polymers are obvious. All of these advantages give rise to lower overall production costs than in conventional multi-phase systems.

These findings have increased the interest in multi-phase systems with solid phases of substrate and/or product; this is reflected by the increased number of applications (Bornscheuer and Yamane, 1994; Cao et al., 1996; Gill and Vulfson, 1994; Kasche, 1986; Michielsen et al., 1999a; Petkov and Stoineva, 1984; Wolf et al., 1997).

In the present paper, a short review on the latest developments in batch solid-to-solid bioconversions is given. These developments indicate that, for a specific solid-to-solid bioconversion, two systems may be commercially attractive: batch systems with high concentrations of undissolved substrate, and continuous systems. Since continuous systems for solid-to-solid bioconversions have not been developed yet, proposals for such systems are given. Finally, a general method is presented for selecting the most attractive kind of system for a specific solid-to-solid bioconversion.

Batch solid-to-solid bioconversions

The majority of studies on solid-to-solid bioconversions has been executed in batch systems. From these studies, we first derived a classification of batch solid-to-solid bioconversions in four types (Fig. 1). Based on the characteristics of the four types, rules of thumb were developed that may be useful for selecting the most appropriate type for a specific solid-to-solid bioconversion. As for commercial application the conversion, scale-up, and kinetics of the process are important, each of these types is then characterized with respect to these features.

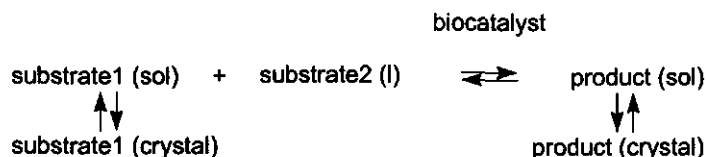
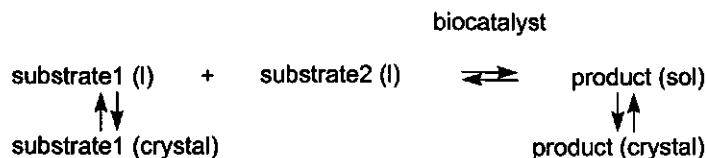
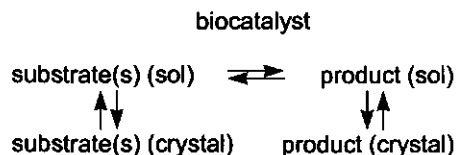
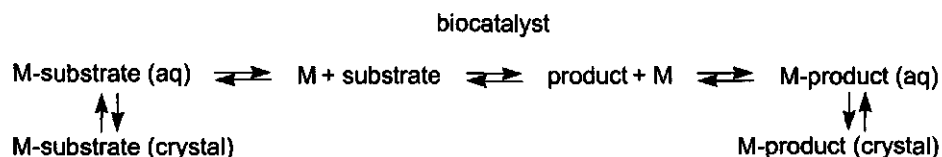
Type 1:**Type 2:****Type 3:****Type 4:**

Figure 1 Types of solid-to-solid bioconversions; M in type 4 refers to a metal ion.

Classification

The classification of batch solid-to-solid bioconversions shown in Fig. 1 is based on the preparation of each of these reaction mixtures. Types 1 and 2 in Fig. 1 are systems in which no solvent is present, apart from the reactant(s). In systems of type 1, one of the substrates is added as a liquid phase. In systems of type 2, so-called semi-liquid eutectics, a liquid phase is formed on mixing of two solid substrates. Formation of the latter systems is based on the principle that the melting temperature of a mixture of two compounds can display a minimum as a function of

mixture composition, the so-called eutectic temperature (TE, see Fig. 2); such a mixture is called a eutectic. Below the eutectic temperature, an entirely solid mixture of the constituent components is present (Fig. 2). Above the melting line (above the solid line in Fig. 2), an entirely liquid phase exists at every composition of the mixture. At the remaining combinations of temperature and mixture composition, semi-liquid eutectic mixtures are formed. For a binary eutectic mixture, this means that a solid phase of only one of the components and a liquid phase consisting of both components are present (Fig. 2).

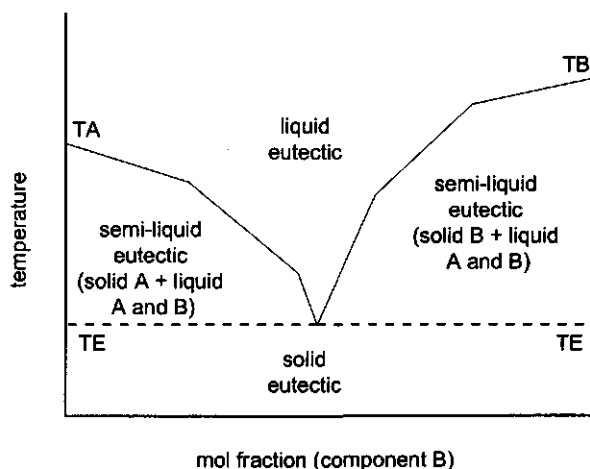


Figure 2 Phase diagram for a model binary eutectic system; TA is the melting point of component A, TB is the melting point of component B, and TE is the eutectic temperature (adapted from Gill and Vulfson, 1994).

The third type in Fig. 1 are those systems in which all substrates are in part solid, but also dissolved in a separate, non-reacting solvent phase.

The last type of systems (type 4 in Fig. 1) comprises bioconversions of a solid salt into another solid salt. The systems of this type are formed by salt addition to an aqueous solution. In contrast to the systems of types 1, 2, and 3, the substrate and product concentrations in the aqueous phase of these systems can be regulated by the amount of salt added. Note that, in addition to the bioconversion, dissociation and complexation reactions occur in the aqueous phase of these systems.

In order to make an appropriate choice, if possible, between the four types of systems for a specific bioconversion, the following rules of thumb can be given:

- In case the biocatalyst shows a high activity and stability in the liquid phase consisting of either one (type 1) or both substrates (type 2) at the reaction temperature, systems of types 1 and 2 are to be preferred, as the number of components in the final product suspension is minimal. The latter facilitates downstream processing.
- In case the biocatalyst limits the use of systems of types 1 and 2, a solvent should be selected in which the biocatalyst shows a high activity and stability, and systems of type 3 should be created. Preferably the solubility of the product in the solvent should be low, as in case of equilibrium reactions the conversion increases, and in case of irreversible reactions the amount of solid product increases with decreasing product solubility.
- In case the substrate(s) and/or the product(s) inhibit the biocatalyst, systems of type 3 or of type 4 should be created. For systems of type 3, the solvent should be selected on the basis of the same criteria as described above. Only when (also) substrate inhibition occurs, the substrate solubility in the solvent should be low as well. In systems of type 4, solubility and thus inhibition can be minimized by addition of an appropriate counter-ion to the aqueous solution. The extent to which the substrate and product concentrations (in the liquid phase) are lowered can be controlled by the amount of salt added.

Conversion and scale

Table 1 gives for every type of solid-to-solid bioconversions the reported range of the conversion and of the scale. For every type, examples exist in which conversions of 80-100% were obtained (Table 1). So far, most of the solid-to-solid bioconversions have been executed on the mmol-scale. Eichhorn et al. (1997) have done the first scale-up of solid-to-solid bioconversions for the production of Z-His-Phe-NH₂ and Z-Aspartame from the usual mmol-scale to a mol-scale in a stirred-tank reactor. Table 1 shows that, besides the main application in peptide synthesis, solid-to-solid bioconversions are also applicable to the synthesis of sugar fatty acids and optically pure acids.

Table 1 Comparison of the conversion and scale of the four types of solid-to-solid bioconversions according to Fig. 1.

Type	Application area	Conversion (%)	Scale (mol)	Sources
1	peptide synthesis	36-83	$1 \cdot 10^{-3}$ - $3 \cdot 10^{-3}$	Gill and Vulfson (1993)
2	peptide synthesis	21-84	$0.3 \cdot 10^{-4}$ - $6.8 \cdot 10^{-2}$	Gill and Vulfson (1993)
	synthesis of sugar fatty acids	34-100	$0.5 \cdot 10^{-3}$ - $5.0 \cdot 10^{-3}$	López-Fandiño et al. (1994a,b) Cao et al. (1996)
3	peptide synthesis	56-97	$0.5 \cdot 10^{-4}$ - 2.7	Eichhorn et al. (1995, 1997) Erbeldinger et al. (1998b)
4	optically pure acids	85-100	$6.3 \cdot 10^{-2}$ - 0.4	Kitahara et al. (1960) Van der Werf et al. (1995) Michielsen et al. (1999a)

Kinetics

By definition, the overall rate of a multi-process conversion is determined by the slowest process, also called the rate-limiting process. In solid-to-solid bioconversions, the rate-limiting process can be either dissolution, bioconversion, or crystallization, depending on process conditions like temperature, biocatalyst concentration, solid substrate and product amounts (per cubic meter of suspension), stirring speed, etc.

Erbeldinger et al. (1998a) reported one of the first kinetic studies of enzymatic solid-to-solid conversions. They investigated the effect of water (from 0 to 600 ml per mol substrates) on the initial rate of thermolysin-catalysed dipeptide synthesis with equimolar amounts of solid carbobenzoxy-L-glutamine (Z-Gln-OH) and solid L-leucamide (H-Leu-NH₂) in a closed system without mixing. It appeared that the initial rate per mass unit of enzyme increased rapidly from almost zero until a maximum was reached at about 50 ml of water per mol substrates. The authors explain this with the finding of Kuhl et al. (1995), that water is necessary to maintain enzyme activity. However, Jakubke et al. (1996) reported that biocatalytic rates may decrease with increasing medium viscosity due to reduced protein mobility. Since high substrate concentrations are often accompanied by raised viscosity, this means that the increase in initial rate per mass unit of enzyme with increasing water amount could also be due to increased protein mobility. At higher amounts of water, the initial rate per mass unit of enzyme first decreased rapidly (between about 50 and 100 ml of water per mol substrates), and then levelled at higher amounts of water

per mol substrates. This effect was explained by mass-transfer limitation, and emphasizes that, besides the amount of water, also mixing is a key parameter. The maximum rate per mass unit of enzyme was attained at 20 mol of substrate per kg of water. The latter is promising in terms of industrial application, as in combination with a high conversion this can result in high overall product concentrations.

Improved solids mixing in solid-to-solid bioconversions can be obtained by rotary homogenization (Čeřovský, 1992), (ultra)sonication (Kuhl et al., 1992, 1995), and stirring (Kuhl et al., 1992, Eichhorn et al., 1997). Kuhl et al. (1995) have reported on the application of two different types of fluidized-bed batch reactors for the chymotrypsin-catalysed synthesis of Z-Phe-Leu-NH₂ and for the thermolysin-catalysed synthesis of Z-Ala-Phe-Leu-NH₂ and Boc-Ala-Phe-Leu-NH₂. The solid substrate and enzyme particles were suspended and mixed by an upward moisturized air stream. However, low conversions of 10 - 40% were achieved, probably due to sticking of enzyme and substrate particles to the reactor wall. Vibrating the whole reactor could not elucidate this. This indicates that further improvements of the mixing process in reactors for solid-to-solid bioconversions are thus still necessary.

With respect to the kinetics of solid-to-solid bioconversions, hardly any literature is available that goes beyond data on the biokinetics. However, for appropriate design, optimization, and control of a batch or continuous system for solid-to-solid bioconversions, mechanistic models should also include the kinetics of dissolution and crystallization. Only just recently, we have reported the first mechanistic model for the conversion of a solid substrate salt to a solid product salt (type 4 conversion) in a batch stirred bioreactor seeded with product crystals (Michielsen et al., 1999a). This model accounts for the kinetics of salt dissolution, the biokinetics (both the kinetics of conversion and of biocatalyst inactivation), and the salt crystal growth kinetics; salt dissociation and complexation of ions in the liquid phase were assumed to be at equilibrium. The model gave a good quantitative prediction of the conversion of solid Ca-maleate to solid Ca-D-malate by permeabilized *Pseudomonas pseudoalcaligenes* in a batch stirred bioreactor seeded with Ca-D-malate crystals (see Fig. 3). As the parameters in the model were determined as a function of relevant process conditions, like temperature, the model could be used to predict the rate (and the conversion) as a function of these process conditions. It should be noted that the model can only be applied for well-mixed suspensions, as the effect of mixing was not incorporated.

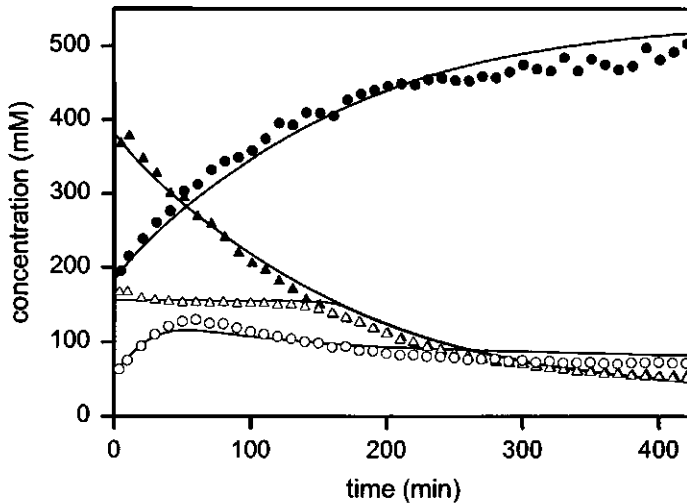


Figure 3 Conversion of solid Ca-maleate to solid Ca-D-maleate by permeabilized *P. pseudoalcaligenes* at 30°C and 250 rpm in a batch stirred bioreactor seeded with Ca-D-maleate crystals; dissolved maleate (Ca-maleate and maleate²⁻; △), total maleate (in liquid and solid phase; ▲), dissolved D-maleate (D-maleate²⁻ and Ca-D-maleate; ○), and total D-maleate (in liquid and solid phase; ●) (adapted from Michielsen et al. (1999a)).

From these kinetic studies we can conclude on the one hand that in batch systems with very high concentrations of undissolved substrate, and thus with a very small liquid phase, high rates per mass unit of enzyme are possible, if appropriate solids mixing can be provided. Since this can be combined with a high conversion and easy scale-up (see Table 1), these systems become attractive for commercial application. On the other hand, our kinetic model for one type of solid-to-solid bioconversions offers possibilities for good control of such conversions. Since the latter is an important prerequisite for reliable and stable operation of continuous systems (see below), a further development of these systems is quite opportune. Proposals for such developments are given below.

Continuous solid-to-solid bioconversions

The design of a continuous reactor for solid-to-solid bioconversions is governed by the following demands: 1) a high stability and appropriate retention of the biocatalyst, 2) reliable and stable operation for a long period of time, and 3) a large product crystal size for efficient downstream recovery (see below). The first demand is generally satisfied by immobilization. The last two demands are related; for reliable and stable operation, product crystallization by nucleation is usually minimized, which implies the formation of large crystals at certain process conditions. To illustrate this, the fundamentals of crystallization are outlined shortly.

By definition, crystallization consists of two processes, the formation of new crystals, called nucleation, and crystal growth. These two processes occur if the solubility (C^*) is exceeded, resulting in supersaturation ($\Delta C = C - C^*$). If supersaturation is the result of a (biocatalytic) reaction and the reaction substrate originates from another phase, the process of crystal formation is called heterogeneous reaction crystallization. New crystals (nuclei) are mainly formed at high supersaturation (by so-called primary nucleation), or originate from attrition of existing crystals e.g. by collision or shear stress (so-called secondary nucleation). Secondary nucleation dominates over primary nucleation at intermediate and low supersaturation. At such a (lower) supersaturation in the presence of product crystals, also crystal growth takes place. This results in polydispers crystals, which may be characterized by a crystal-size distribution. The crystal-size distribution is often summarized by the median crystal size and its coefficient of variation.

For reliable and stable operation of a continuous reaction crystallizer for a long period of time, nucleation phenomena are generally minimized, as a good prediction of nucleation rates is still not possible (Rohani, 1995). Besides, by minimizing (primary) nucleation the median crystal size increases (Mersmann and Kind, 1989), which is advantageous for downstream processing. This can be achieved by seeding the crystallizer with an increasing number of product crystals, so that the total crystal area and hold-up in the crystallizer increases, assuming that the seed crystals have a constant (small) size; by increasing the hold-up, the growth rate (per unit of crystallizer volume) increases too, which means that the crystallizer is operated at a lower supersaturation. Increasing the hold-up also implicates that the size increase of the seed crystals becomes smaller at constant residence time in the crystallizer. However, for appropriate downstream processing, a large product crystal

size is required. The latter demand limits the increase in the crystal hold-up. So, an optimum crystal hold-up, and corresponding optimum supersaturation (ΔC_{opt}), exist in the crystallizer. The optimum supersaturation must be determined experimentally. In selecting the optimum supersaturation not only the desired median crystal size, but also other desired product characteristics (that depend more or less on the supersaturation) must be taken into account, like a small coefficient of variation of the crystal size, a regular and compact shape, and a high purity.

The main advantage of continuously operated crystallizers is that they are superior to batch crystallizers with respect to maintaining a constant optimal supersaturation and low nucleation rate (Mersmann, 1995a). As a result, more homogeneous product crystals are formed than in a batch crystallizer, which makes downstream processing cheaper (see below).

The current status of biocatalyst immobilization and of continuous reaction crystallization is reported shortly in relation to its relevance for solid-to-solid bioconversions. This is used as a basis for a reactor design. Note that some features are also applicable to batch systems. Finally, downstream processing of solids is discussed in order to emphasize the need for a large crystal size. It should be stressed that this work only focuses on systems in which dissolution, bioconversion, and crystallization are coupled directly, in order to fully profit from the benefits of multi-phase systems.

Biocatalyst immobilization

For continuous operation, biocatalysts are often immobilized, because immobilization is generally associated with increased efficiency and it makes different system configurations possible; note, however, that with these profits the costs of immobilization must be earned back.

Kasche and Galunsky (1995) pointed out that, in reaction crystallizations involving immobilized enzymes, small crystalline particles may be formed in the pores of the support of the enzyme. If so, the accessibility of the immobilized enzyme decreases, resulting in decreased reaction rates and in limited reuse of the immobilized enzyme. Their study revealed that it is essential to use supports with small pores in order to avoid intraparticle crystallization; they reported a critical pore size range of 10-100 nm. The latter implicates that in their experiments the critical cluster size - the size a cluster of molecules in solution must have to grow spontaneously, so that a crystal is formed - was larger than 10-100 nm.

For application in a continuous reaction crystallizer, the support materials for immobilization should have other characteristics too: insoluble, high mechanical stability, high diffusivity, simple immobilization procedure, high biocatalyst retention, well separable from the product crystals, and preferably a low price. Leenen et al. (1996) studied the characteristics of natural gels as carrageenan, Ca-alginate, and Ba-Ca-alginate, and gels as polyvinyl alcohol (PVA), polycarbamoylsulphonate (PCS), and polyethylene glycol (PEG), for application in wastewater-treatment systems, and found that PVA, PCS, and PEG were more promising materials than natural gels. These materials have good mechanical properties, which is especially important in draft-tube baffled stirred crystallizers (see below, Fig. 4). However, the immobilization procedures are more harsh and difficult than for natural supports, resulting in much biocatalyst inactivation; in PCS the diffusivity is lower. These characteristics indicate that optimization is still necessary (Leenen et al., 1996).

Equipment design

The design of the equipment is determined mainly by the desired product characteristics. It can affect the product characteristics by its influence on the process variables. For control and downstream-processing purposes, a large product crystal is generally aimed at. In order to achieve this, Mersmann and Rennie (1995) recommend the mean and especially the maximum (local) supersaturation to be limited by: a) excellent mixing of the entire vessel contents, so that gradients in the supersaturation are absent; this can be achieved by using a large ratio of stirrer to tank diameter, as such stirrers distribute power more evenly, b) low concentrations of the reactant(s), which are here the substrate(s), and of the biocatalyst, c) vigorous seeding especially at the feed point(s), d) high circulation rates of slurry with a high suspension density. Note that by the latter two (c and d), the crystal hold-up, and thus the total crystal surface area that is available for crystal growth, can be regulated.

Objectives a) to d) can best be met in a continuous-flow, stirred-tank reactor (CSTR). Since both biocatalysts and crystals are sensitive to shear, axial flow impellers are frequently used, as they produce more flow and less shear rate than radial flow impellers at comparable power levels (Oldshue, 1993). A schematic view of a draft-tube baffled continuous crystallizer for solid-to-solid bioconversions is shown in Fig. 4. By pumping the fluid down in the draft tube, an upward flow of (supersaturated) solution is created in the annulus. This flow fluidizes a bed of

substrate and product crystals and of solid support particles with immobilized biocatalyst; it will be desupersaturated during passage through the annular fluidized bed. When the product crystals have grown large enough, they settle from the bed to the bottom of the crystallizer. The solid substrate particles (and product seeds) can be fed to the draft-tube baffled crystallizer either by dropping them from a belt conveyer (Bennett, 1993), or by a suspension flow.

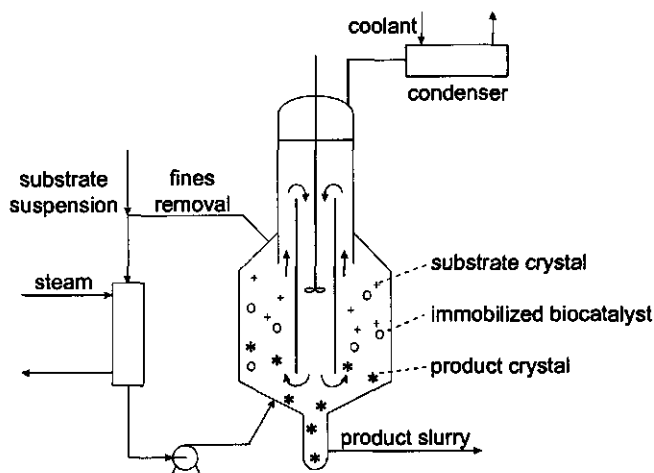


Figure 4 Draft-tube baffled continuous crystallizer (adapted from Rohani (1995)) for solid-to-solid bioconversions.

Another configuration that is often applied in continuous reaction crystallization is a fluidized-bed crystallizer (or Oslo growth-type crystallizer). A schematic view of an fluidized-bed continuous crystallizer for solid-to-solid bioconversions is shown in Fig. 5. This crystallizer works according to the same principles as described for the draft-tube baffled crystallizer of Fig. 4, and mainly differs from it by its fluid circulation device. The draft-tube baffled and fluidized-bed crystallizers of Figs. 4 and 5, respectively, are especially suited for the production of large crystals, as secondary nucleation is reduced by fluidizing the crystals.

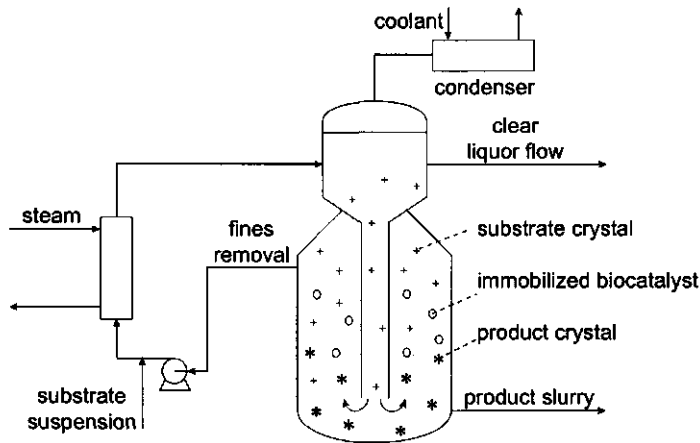


Figure 5 Fluidized-bed continuous crystallizer (adapted from Rohani (1995)) for solid-to-solid bioconversions; this configuration is also known as an Oslo growth-type continuous crystallizer.

Process control

The two main objectives for control of a dissolution-reaction-crystallization process are to meet: 1) the product specifications, and 2) the manufacturer's requirements for economic and trouble-free operation. In large-scale continuous industrial crystallizers, this generally means that control is focused on preventing excessive nucleation by making sufficient crystal surface area available in the bulk of the suspension. For appropriate control, a model predicting the concentrations and crystal sizes of all components at any place in the vessel as a function of measurable process variables and other relevant processes, must be available.

In general, a model for a heterogeneous reaction crystallizer can be obtained by integrating a kinetic model, containing the dissolution, reaction, and crystallization kinetics, and a hydrodynamic model, as mixing could cause dissolution, reaction, or crystallization to be rate limiting. Our kinetic model for solid salt-to-solid salt bioconversions in a batch stirred bioreactor seeded with product crystals (Michielsen et al., 1999a) can in principle also be applied for continuous solid-to-solid bioconversions. For that, the model should be extended with an expression for the secondary nucleation rate. Application of our crystal growth model (Michielsen et al., 1999b), which is based on an exponential rate law derived by Nielsen and Toft

(1984), revealed that it fails at low supersaturation, predicting a lower growth rate than is observed experimentally (Michielsen et al., 1999a). Such a shortcoming of exponential growth rate models was also reported by Myerson and Ginde (1993). Our experimental data (Michielsen et al., 1999a) could be predicted well by assuming that mixing was not rate limiting (see Fig. 3). For that reason, it was unnecessary to develop a hydrodynamic model.

The measurable process variables used in the control of continuous crystallizers might be temperature, flow rate, pressure, the residence time of different size ranges of crystals, the total volume of the suspension in the crystallizer, and the volumetric ratio of the clear liquor flow and the product removal rate. The relevance of processes like mixing and reactants and seed addition with respect to appropriate control of a crystallizer is described above. With respect to seeding, a narrow distribution of prewashed product crystals is recommended. By prewashing the product crystals with supersaturated product solution (comparable with the solution in the crystallizer), breeding due to the adherence of small crystals to the surface of seed crystals can be avoided completely. Other processes often applied in the control of the crystal-size distribution of continuous crystallizers are classified product removal and fines dissolution. Classification relies on the relative settling of crystals of different sizes. The classifying device may be a hydrocyclone, a wet screen, a fluidized bed, or a centrifuge. It separates the suspension flow withdrawn from the crystallizer in at least two fractions, containing crystals smaller or larger than the separation size; the former fraction is generally recycled to the crystallizer (Mersmann, 1995b). Formation of some fines by nucleation is almost inevitable. These fines can serve as nucleation sites. For that, they are commonly withdrawn from a quiescent zone of the crystallizer, and dissolved by the supply of either solvent or heat; the resulting solution is recycled.

Control schemes for effective control of continuous crystallizers require on-line measurements of crystal properties like crystal-size distribution, supersaturation, and crystal purity. As with the existing sensors, measurements are either not feasible or extremely difficult, significant progress can be made by the development of new robust on-line measurement techniques. Besides, measurement of secondary variables such as turbidity and the density of the liquor solution, which are related to the fines suspension density and supersaturation, offer potential for the control of crystallization processes (Rohani, 1995).

Downstream processing

As a rule in solids production processes, downstream processing consists of solid-liquid separation by centrifuges or filters, followed by drying of the wet crystals. With respect to centrifugation, Mersmann (1995a) reported that for obtaining a low mass ratio of residual liquid to crystals (kg solution/kg crystals) the median crystal size is very important; the mass ratio decreases with increasing median crystal size and decreasing coefficient of variation of the crystal size. After centrifugation or filtration, the crystals with adherent liquor are dried by flowing a preheated agent (hot air) through the solid material. In this process, the need for a large median crystal size becomes even more pronounced, as the specific energy consumption per mass unit of crystals increases with increasing mass ratio of residual liquid to separated crystals. However, at a median crystal size larger than 500 μm , and thus at a low mass ratio, the energy consumption remains almost constant (Mersmann, 1995a).

Batch or continuous?

Assuming that the proposed continuous systems for solid-to-solid bioconversions (Figs. 4 and 5) can be applied, the question arises which mode of operation to choose for a specific solid-to-solid bioconversion. Now that the first batch systems are reported in which very high amounts of solid product per reactor volume can be attained at high rates (Erbeldinger et al., 1998a), a shift to complex continuous operation should be carefully thought over.

Process optimization is generally focused on minimization of the costs per kg of product. In a bioreactor the cost factors are: 1) the substrate, 2) the biocatalyst, 3) investments and operation, and 4) downstream processing. For commercial applications, the choice between batch or continuous operation is often based on a comparison of the costs per kg of product for the two systems. For each of the systems, therefore, the process conditions yielding minimum overall costs per kg of product should be determined first. Selection of these conditions is highly case specific, as they depend on the substrate and equipment used, the product produced, and the desired final purity of the product. In this section, a general method is presented that can be used to calculate the overall costs in both batch and continuous systems. If this method is coupled to an optimization routine, the

optimum process conditions and corresponding minimum costs can be found. In the next treatment, mixing is assumed not to be rate limiting.

To illustrate this method, the overall costs are calculated in (1) a batch heterogeneous reaction crystallizer with immobilized biocatalyst and a high amount of undissolved substrate, and (2) in a continuous heterogeneous reaction crystallizer (draft-tube baffled or fluidized-bed) with immobilized biocatalyst and a substrate suspension as feed. In both calculations, the volume of the suspension, the initial biocatalyst concentration, and the biocatalyst inactivation rate are equal. For simplicity, diffusion limitation is assumed not to occur.

Rate-limiting bioconversion

At the optimum conditions in both systems, the bioconversion is most likely the rate-limiting process. For control of the crystallization process, a rate-limiting bioconversion is advantageous, as this implies a low supersaturation and a minimal nucleation. In batch reaction crystallizers with a large amount of undissolved substrate, the surface area of the substrate particles will be large and the dissolution rate will exceed the bioconversion rate. Since a substrate conversion of 100% is generally aimed at, at some point dissolution will become rate limiting due to depletion of solid substrate (Michielsen et al., 1999a). For that reason, use of a complete model for calculation of the amount of product produced in a batch reaction crystallizer is to be preferred, as this gives more accurate values. However, for gross calculation, as in this section, the assumption of one process being rate limiting, i.e. the bioconversion, can be justified. Though in the continuous reaction crystallizers proposed in this work (Figs. 4 and 5), substrate dissolution or the bioconversion can be rate limiting, a rate-limiting bioconversion is favorable, as this would mean that the biocatalyst is operated at a high substrate concentration (near saturation). If the substrate saturation concentration is high as compared to the Michaelis constant K_m , the latter results in high conversion rates. Since the biocatalyst is often expensive in comparison with the reactants, such an efficient use of the biocatalyst should be aimed at. If efficient use of the biocatalyst can be combined with a high substrate conversion, the sum of the biocatalyst and substrate costs per kg of product approaches its minimum (Michielsen et al., 1999c). In a continuous liquid-solid-solid three-phase system with a rate-limiting bioconversion, such a combination can be attained at low biocatalyst concentrations and long residence times (of substrate(s) and biocatalyst).

One reason for the fact that the bioconversion often is (or becomes) rate limiting is a high biocatalyst inactivation rate. In bioconversions, the biocatalyst inactivation rate is a crucial parameter, as it determines the operational time and thereby the amount of product produced per kg of biocatalyst. For that reason, the effect of biocatalyst inactivation on the overall costs in both batch and continuous reaction crystallizers is shown in this section.

Box 1 The amount of product in batch and continuous heterogeneous reaction crystallizers with the bioconversion as rate-limiting process; in the continuous reaction crystallizer, biocatalyst losses due to wash-out are assumed to be negligible, and the volume is assumed to be constant and well-mixed, with equal inflow and outflow rates.

In case of first-order biocatalyst inactivation, the active biocatalyst concentration C_e (in $\text{kg}\cdot\text{m}^{-3}$) decreases with time t (in h) and can be expressed as a function of the initial biocatalyst concentration $C_e(0)$, the first-order rate constant for biocatalyst inactivation k_d (h^{-1}), and time t :

$$C_e(t) = C_e(0) \cdot e^{-k_d t}$$

Assume that production is stopped when 1% of the initial active biocatalyst concentration is left ($C_e(t) = 0.01 \cdot C_e(0)$). For the stop moments t_b and t_c (in the batch and the continuous system, respectively) can now be derived:

$$t_b = t_c = -\frac{\ln 0.01}{k_d}$$

In case of zero-order bioconversion kinetics and assuming that in the batch reaction crystallizer the maximum attainable product concentration $C_p(t_b)$ (see below) has not been reached, the amount of product produced (in $\text{kg}\cdot\text{m}^{-3}$) in the batch reaction crystallizer and in the continuous reaction crystallizer without biocatalyst losses due to wash-out and with a feed flow decreasing in accordance with the biocatalyst inactivation rate, can now be expressed as (with q_p is the specific production rate, in $\text{kg}\cdot\text{kg}^{-1}\cdot\text{h}^{-1}$):

$$\text{product produced} = q_p \cdot C_e(0) \int_0^{t_c} e^{-k_d t} dt = q_p \cdot C_e(0) \cdot \frac{0.99}{k_d}$$

Note that the product concentration in the continuous reaction crystallizer C_p (in $\text{kg}\cdot\text{m}^{-3}$) is constant and can be calculated from the pseudo steady-state mass balance; in case of no product seeding, C_p can be expressed as a function of q_p , $C_e(0)$, the volume of the suspension in the reactor V (in m^3), and the initial flow $F(0)$ (in $\text{m}^3\cdot\text{h}^{-1}$):

$$C_p = \frac{q_p \cdot C_e(0) \cdot V}{F(0)}$$

In a batch reaction crystallizer, the maximum attainable product volume at $t=t_b$, $V_p(t_b)$ (in m^3), is restricted by the volume of the liquid phase V_l (in m^3), the volume occupied by the biocatalyst V_e (in m^3), and the volume of the substrate left at $t=t_b$, $V_s(t_b)$ (in m^3), according to (with Y_{ps}^{ov} is the overall yield of product on substrate (in $\text{m}^3\cdot\text{m}^{-3}$), x_{max} is the maximum attainable conversion (-), and assuming that the densities ($\text{kg}\cdot\text{m}^{-3}$) of the substrate ρ_s and the product ρ_p are equal):

$$V_p^{\text{max}}(t_b) = V - V_l - V_e - V_s(t_b), \text{ with: } V_s(t_b) = V_s(0) - Y_{ps}^{\text{ov}} \cdot x_{\text{max}} \cdot V_s(0) \geq 0$$

The amount of product produced in a batch reaction crystallizer $C_p(t_b)$ (in $\text{kg}\cdot\text{m}^{-3}$) can now be expressed as:

$$q_p \cdot C_e(0) \cdot \frac{0.99}{k_d} \leq C_p(t_b) \leq \frac{V_p^{\text{max}}(t_b) \cdot \rho_p}{V}$$

Overall costs per kg of product

Box 1 shows how the amount of product in both batch and continuous reaction crystallizers with the bioconversion as rate-limiting process can be calculated. Thereby, it is assumed that the bioconversion obeys zero-order kinetics, and that the biocatalyst inactivates according to first-order kinetics. In the continuous reaction crystallizer, biocatalyst losses due to wash-out are assumed to be negligible. This means that the bioconversion rate, and consequently the product supersaturation, can be kept constant by decreasing the feed flow in accordance with the biocatalyst inactivation rate; in this manner, the system is operated at pseudo steady-state. The densities of the substrate and the product are assumed to be equal, so that the volume of the initial substrate suspension equals the volume of the resulting product suspension.

Box 2 shows the calculation of the overall costs per kg of product produced in these batch and continuous reaction crystallizers with the bioconversion as rate-limiting process. Although the investment and operating costs are composed of a multitude of components like depreciation, labour, energy, cooling water, etc., the costs of these components were all lumped in the hourly price for handling 1 m³ of suspension in the crystallizer (p_{io}). According to Van 't Riet (1986), p_{io} is in the order of 10-100 \$·m⁻³·h⁻¹ for small-scale fermenters (1-3 m³), whereas for large-scale fermenters (100-300 m³) p_{io} is in the order of 1 \$·m⁻³·h⁻¹. Above 100-300 m³ the sensitivity decreases and therewith the need to increase the fermenter volume (Van 't Riet, 1986). For a reaction crystallizer, p_{io} is assumed to be of the same order of magnitude. The two downstream-processing operations, centrifugation and drying, are 'volume-dependent' processes: the scale and related costs are, to a great extent, determined by the volume of the flow to be processed; the concentration of the product is less relevant. For that reason, the downstream-processing price (p_{dp}) is defined on the basis of the hourly costs to process 1 m³ of product suspension from the crystallizer. In order to reduce the downstream-processing costs per kg of product ($\$_{dp}$), probably more than one crystallizer (n) will be coupled to one centrifugation and drying unit (see Box 2). Finally, during downstream processing, some product losses will always occur; in other words, the recovery yield (Y_r) will be < 1. For that reason, the overall costs in Box 2 are calculated by dividing the sum of all costs by Y_r . The recovery yield is generally known to decrease with the number of unit operations needed for downstream processing.

Box 2 The overall costs per kg of product in batch and continuous heterogeneous reaction crystallizers with the bioconversion as rate-limiting process; in the continuous reaction crystallizer, biocatalyst losses due to wash-out are assumed to be negligible, and the volume is assumed to be constant and well-mixed, with equal inflow and outflow rates.

In a batch reaction crystallizer, the substrate costs per kg of product $\$_s$ (in $\$/\text{kg}^{-1}$) equal the initial substrate concentration $C_s(0)$ (in $\text{kg}\cdot\text{m}^{-3}$) multiplied with the substrate price p_s (in $\$/\text{kg}^{-1}$) divided by the amount of product produced (in $\text{kg}\cdot\text{m}^{-3}$). In a continuous reaction crystallizer without biocatalyst losses due to wash-out and with a feed flow decreasing in accordance with the biocatalyst inactivation rate, the bioconversion rate, and consequently the product concentration in the reactor C_p (in $\text{kg}\cdot\text{m}^{-3}$), is constant, and the substrate costs per kg of product $\$_s$ equal the substrate concentration in the inflow C_{si} (in $\text{kg}\cdot\text{m}^{-3}$) multiplied with the substrate price p_s divided by the product concentration C_p :

$$\text{batch: } \$_s = \frac{C_s(0)}{C_p(t_b)} \cdot p_s$$

$$\text{continuous: } \$_s = \frac{C_{si}}{C_p} \cdot p_s = \frac{F(0) \cdot C_{si}}{q_p \cdot C_e(0) \cdot V} \cdot p_s$$

The biocatalyst costs per kg of product $\$_e$ (in $\$/\text{kg}^{-1}$) equal the initial amount of active biocatalyst $C_e(0)$ (in $\text{kg}\cdot\text{m}^{-3}$) multiplied with the biocatalyst price p_e (in $\$/\text{kg}^{-1}$) divided by the amount of product produced (in $\text{kg}\cdot\text{m}^{-3}$):

$$\text{batch: } \$_e = \frac{C_e(0)}{C_p(t_b)} \cdot p_e$$

$$\text{continuous: } \$_e = \frac{C_e(0)}{q_p \cdot C_e(0) \cdot \frac{0.99}{k_d}} \cdot p_e = \frac{k_d}{q_p \cdot 0.99} \cdot p_e$$

The investment and operating costs per kg of product $\$_{io}$ (in $\$/\text{kg}^{-1}$) equal the investment and operating price p_{io} (in $\$/\text{m}^3\cdot\text{h}^{-1}$) multiplied with the operational time t_b or t_c (in h) divided by the amount of product produced (in $\text{kg}\cdot\text{m}^{-3}$):

$$\text{batch: } \$_{io} = \frac{p_{io} \cdot t_b}{C_p(t_b)} = \frac{-\ln 0.01 \cdot p_{io}}{C_p(t_b) \cdot k_d}$$

$$\text{continuous: } \$_{io} = \frac{k_d \cdot p_{io} \cdot t_c}{q_p \cdot C_e(0) \cdot 0.99} = \frac{-\ln 0.01 \cdot p_{io}}{q_p \cdot C_e(0) \cdot 0.99}$$

In case that n reaction crystallizers are coupled to one downstream-processing plant, the downstream-processing costs per kg of product $\$_{dp}$ (in $\$/\text{kg}^{-1}$) equal the downstream-processing price p_{dp} (in $\$/\text{m}^3\cdot\text{h}^{-1}$) multiplied with the downstream-processing time, which is assumed to be equal to the operational time of the reaction crystallizer t_b or t_c (in h), divided by the amount of product produced (in $\text{kg}\cdot\text{m}^{-3}$) in n reactors:

$$\text{batch: } \$_{dp} = \frac{p_{dp} \cdot t_b}{n \cdot C_p(t_b)} = \frac{-\ln 0.01 \cdot p_{dp}}{n \cdot C_p(t_b) \cdot k_d}$$

$$\text{continuous: } \$_{dp} = \frac{k_d \cdot p_{dp} \cdot t_c}{n \cdot q_p \cdot C_e(0) \cdot 0.99} = \frac{-\ln 0.01 \cdot p_{dp}}{n \cdot q_p \cdot C_e(0) \cdot 0.99}$$

Since the recovery yield will probably be smaller than one, the overall costs per kg of product $\$_{ov}$ (in $\$/\text{kg}^{-1}$) equal the sum of the substrate, biocatalyst, investment and operating, and downstream-processing costs per kg of product, divided by the recovery yield Y_r :

$$\$_{ov} = \frac{\$_s + \$_e + \$_{io} + \$_{dp}}{Y_r}$$

Costs comparison between batch and continuous operation

Fig. 6 shows the overall costs ($\$_{ov}$) in a batch reaction crystallizer and in a continuous reaction crystallizer with a feed flow decreasing in accordance with the biocatalyst inactivation rate, as a function of the first-order rate constant for biocatalyst inactivation k_d . The investment and operating costs (ρ_{io}) and the downstream-processing costs (ρ_{dp}) of both systems are assumed to be equal.

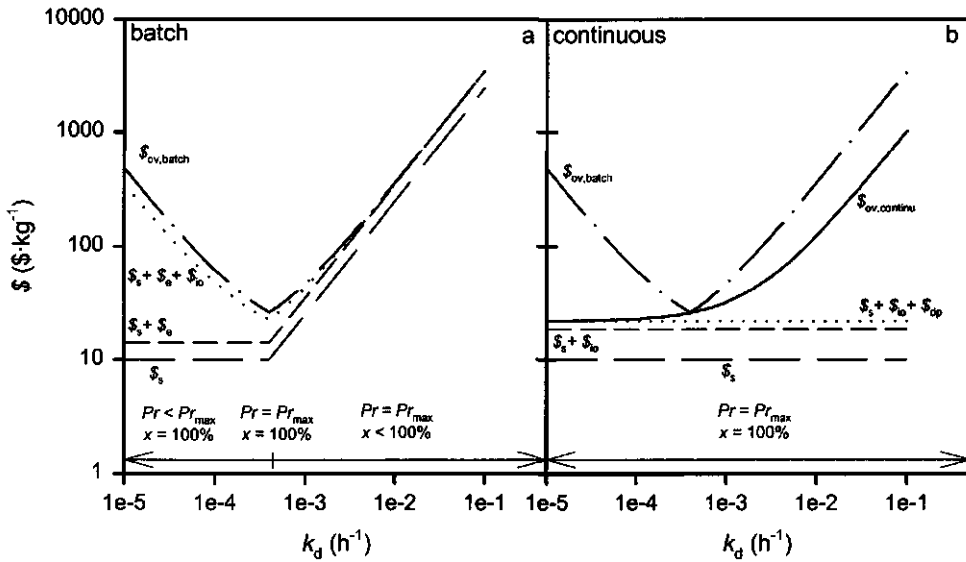


Figure 6 The substrate, biocatalyst, investment and operating, downstream-processing, and overall costs per kg of product ($\$_s$, $\$_e$, $\$_{io}$, $\$_{dp}$, and $\$_{ov}$, respectively) as a function of the first-order rate constant for biocatalyst inactivation (k_d) in a batch reaction crystallizer (a) and in a continuous reaction crystallizer without biocatalyst losses due to wash-out and with a feed flow decreasing in accordance with the biocatalyst inactivation rate (b); $q_p = 1 \cdot 10^{-2} \text{ kg} \cdot \text{kg}^{-1} \cdot \text{h}^{-1}$, $V = 200 \text{ m}^3$, $V_i = 10 \text{ m}^3$, $V_e = 10 \text{ m}^3$, $\rho_e = 1100 \text{ kg} \cdot \text{m}^{-3}$, $V_s = 180 \text{ m}^3$, $\rho_s = \rho_p = 1500 \text{ kg} \cdot \text{m}^{-3}$, $x_{\max} = 1$, $Y_{ps}^{ov} = 1$, $Y_r = 1$, $\rho_s = 10 \text{ \$} \cdot \text{kg}^{-1}$, $\rho_e = 100 \text{ \$} \cdot \text{kg}^{-1}$, $\rho_{io} = 1 \text{ \$} \cdot \text{m}^3 \cdot \text{h}^{-1}$, $\rho_{dp} = 2 \text{ \$} \cdot \text{m}^3 \cdot \text{h}^{-1}$, $n = 5$, $C_{si} = 2.2 \text{ kg} \cdot \text{m}^{-3}$, and $F(0) = 50 \text{ m}^3 \cdot \text{h}^{-1}$.

Fig 6a shows that at $k_d \leq 4 \cdot 10^{-4} \text{ h}^{-1}$ (or $t_b \geq 1.2 \cdot 10^4 \text{ h}$; see Box 1) in a batch system, constant substrate and biocatalyst costs were found. This can only result from the fact that the maximum attainable product concentration is reached (see Box 2). The latter implicates that at $k_d \leq 4 \cdot 10^{-4} \text{ h}^{-1}$ the substrate conversion x is maximal;

note that at $k_d < 4 \cdot 10^{-4} \text{ h}^{-1}$, maximal substrate conversion is obtained before the stop moment, at $t = t_b$, is reached. At $k_d \leq 4 \cdot 10^{-4} \text{ h}^{-1}$, biocatalyst productivity Pr (in kg of product per kg of biocatalyst) increases with increasing k_d , as the amount of biocatalyst, not being used up as soon as $x=100\%$, decreases. At $k_d > 4 \cdot 10^{-4} \text{ h}^{-1}$, both the substrate and biocatalyst costs increase with increasing k_d . This is caused by the decrease in the amount of product produced due to the fact that (almost) complete biocatalyst inactivation is reached earlier with increasing k_d . The latter implicates that at $k_d > 4 \cdot 10^{-4} \text{ h}^{-1}$, $Pr = Pr_{\max}$, and that the conversion x decreases with increasing k_d . The investment and operating costs ($\$_{io}$) and the downstream-processing costs ($\$_{dp}$) are generally not affected by an increase in k_d , as the decrease in t_b is balanced by the decrease in the amount of product produced (see Box 2). However, at $k_d \leq 4 \cdot 10^{-4} \text{ h}^{-1}$ these costs decrease with increasing k_d , as despite the decrease in t_b the maximum attainable product concentration still can be reached.

The continuous system described in this work only differs from the batch system in that the substrate availability is not limited. As expected (see Box 2), Fig. 6b shows that in such a continuous system the substrate, investment and operating, and downstream-processing costs per kg of product produced ($\$_s$, $\$_{io}$, and $\$_{dp}$, respectively) are unaffected by k_d . However, the overall costs ($\$_{ov}$) increase with increasing k_d due to the increase of the biocatalyst costs ($\$_b$) with increasing k_d (Fig. 6b). The latter is caused by the fact that the amount of product produced decreases with increasing k_d , whereas the initial active biocatalyst concentration is a constant (see Box 2). Note that in such a continuous system, the productivity of the biocatalyst is maximal at any biocatalyst inactivation rate, and the conversion x ($= C_p/C_{si}$) depends on $F(0)$ (assuming q_p , $C_e(0)$, and V to be constant; see Box 1). By setting $F(0)$ at $50 \text{ m}^3 \cdot \text{h}^{-1}$, a conversion of 100% is also obtained in the continuous system, so that a proper comparison of both systems is possible. Fig. 6b also shows that only at $k_d = 4 \cdot 10^{-4} \text{ h}^{-1}$, the batch system can compete with the continuous system; at $k_d = 4 \cdot 10^{-4} \text{ h}^{-1}$, both the substrate conversion x is 100% and the biocatalyst productivity Pr is maximal (see Fig 6a).

In practice however, the biocatalyst inactivation rate is often a given constant at certain conditions, and the initial biocatalyst and substrate concentrations are variables. The optimum initial biocatalyst and substrate concentrations for batch operation can be determined by plotting the overall costs ($\$_{ov}$) versus $C_e(0)/C_s(0)$ (see Fig. 7). With e.g. $k_d = 1 \cdot 10^{-3} \text{ h}^{-1}$, the minimum overall costs ($\$_{ov, \text{batch}}$) were found

at $C_e(0)/C_s(0) = 0.10$ (Fig. 7). Since at this ratio $x = 100\%$ and $Pr = Pr_{\max}$ (Fig. 7), these minimum overall costs correspond to the costs that would be obtained in the continuous system described in this section.

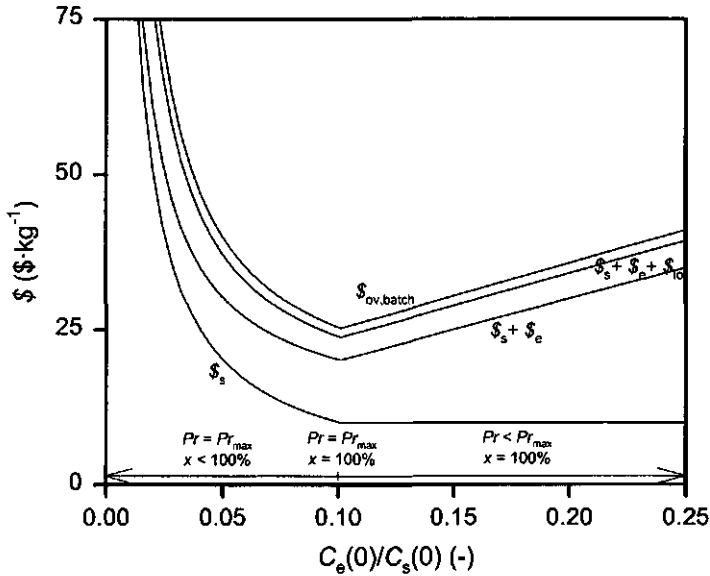


Figure 7 The substrate, biocatalyst, investment and operating, downstream-processing, and overall costs per kg of product ($\$_s$, $\$_e$, $\$_{io}$, $\$_{dp}$, and $\$_{ov}$, respectively) as a function of the ratio of the initial biocatalyst concentration ($C_e(0)$) and the initial substrate concentration ($C_s(0)$) in a batch reaction crystallizer; $q_p = 1 \cdot 10^{-2} \text{ kg} \cdot \text{kg}^{-1} \cdot \text{h}^{-1}$, $k_d = 1 \cdot 10^{-3} \text{ h}^{-1}$, $V = 200 \text{ m}^3$, $V_l = 10 \text{ m}^3$, $\rho_o = 1100 \text{ kg} \cdot \text{m}^{-3}$, $\rho_s = \rho_p = 1500 \text{ kg} \cdot \text{m}^{-3}$, $x_{\max} = 1$, $Y_{ps}^{ov} = 1$, $Y_r = 1$, $p_s = 10 \text{ \$} \cdot \text{kg}^{-1}$, $p_e = 100 \text{ \$} \cdot \text{kg}^{-1}$, $p_{io} = 1 \text{ \$} \cdot \text{m}^{-3} \cdot \text{h}^{-1}$, $p_{dp} = 2 \text{ \$} \cdot \text{m}^{-3} \cdot \text{h}^{-1}$, and $n = 5$.

In this section it is shown that by introducing a number of assumptions, batch operation at high concentrations of undissolved substrate can compete with continuous operation, if both the conversion is 100% and the productivity of the biocatalyst is maximal, unless mixing becomes rate limiting in batch reaction crystallizers.

ACKNOWLEDGEMENTS

This work was financially supported by the Ministry of Economic Affairs, the Ministry of Education, Culture and Science, the Ministry of Agriculture, Nature Management and Fishery in the framework of an industrially relevant research programme of the Netherlands Association of Biotechnology Centres in the Netherlands (ABON).

CONCLUSIONS

Solid-to-solid bioconversions appear to offer interesting possibilities for biocatalysis at high substrate concentrations and at low costs in different application areas. Based on the preparation, the solid-to-solid bioconversions reported in literature were classified in four types. To select the most appropriate type for a specific bioconversion, rules of thumb were formulated. In batch systems, conversions of 80-100% are reported for every type of solid-to-solid bioconversion, even when hardly any liquid phase is present, and it seems that these systems can easily be scaled-up. Kinetic studies of these solid-to-solid bioconversions give rise to further development of two kinds of systems in future: 1) batch systems with very high concentrations of undissolved substrate, 2) continuous systems for solid-to-solid bioconversions. In continuous systems an optimum supersaturation (ΔC_{opt}) exists. The main advantage of continuous systems over batch systems is that they are able to maintain a constant (optimal) supersaturation, resulting in more homogeneous product crystals, and thus lower downstream-processing costs. In this work, two continuous systems for solid-to-solid bioconversions are proposed: a draft-tube baffled continuous crystallizer and a fluidized-bed continuous crystallizer, both with immobilized biocatalyst. Crystallization in the pores of the support of the immobilized biocatalyst can be avoided by making the pores sufficiently small, i.e. smaller than the critical cluster size.

Selection of the mode of operation for a specific solid-to-solid bioconversion, batch at high concentrations of undissolved substrate or continuous, is often based on the costs (per kg of product produced). By assuming that in both batch and continuous solid-to-solid bioconversions the bioconversion is rate limiting, and by introducing a number of simplifications, the costs of batch operation were compared with the costs of continuous operation. This revealed that a batch system can only

compete with a continuous system, if both the conversion is 100% and the productivity of the biocatalyst is maximal.

REFERENCES

- Adelhorst K, Björkling F, Godtfredsen SE, Kirk O. 1990. Enzyme catalysed preparation of 6-O-acyl-glucopyranosides. *Synthesis* 2:112-115.
- Andersson E, Hahn-Hägerdal B. 1990. Bioconversions in aqueous two-phase systems. *Enzyme Microb Technol* 12:242-253.
- Bennett RC. 1993. Crystallizer selection and design. In: Myerson AS, editor. *Handbook of industrial crystallization*. Boston: Butterworth-Heinemann. p 103-130.
- Bornscheuer UT, Yamane Y. 1994. Activity and stability of lipase in the solid phase glycerolysis of triolein. *Enzyme Microb Technol* 16:864-869.
- Cao L, Bornscheuer UT, Schmid RD. 1996. Lipase-catalysed solid phase synthesis of sugar esters. *Fett/Lipid* 98:332-335.
- Čeřovský V. 1992. Protease-catalysed peptide synthesis in solvent-free system. *Biotechnol Tech* 6:155-160.
- Eichhorn U, Bommarius AS, Drauz K, Jakubke H-D. 1995. Environmentally acceptable synthesis of peptides in high yields by suspension-to-suspension conversion via protease catalysis. In: Maia HLS, editor. *Peptides 1994*. Leiden, The Netherlands: ESCOM. p 226-227.
- Eichhorn U, Bommarius AS, Drauz K, Jakubke H-D. 1997. Synthesis of dipeptides by suspension-to-suspension conversion via thermolysin catalysis: from analytical to preparative scale. *J Pep Sci* 3:254-251.
- Erbeldinger M, Xiongwei N, Halling PJ. 1998a. Effect of water and enzyme concentration on thermolysin-catalysed solid-to-solid peptide synthesis. *Biotechnol Bioeng* 59:68-72.
- Erbeldinger M, Xiongwei N, Halling PJ. 1998b. Enzymatic synthesis with mainly undissolved substrates at very high concentrations. *Enzyme Microb Technol* 23:141-148.
- Fregapane G, Sarney DB, Vulfson EN. 1991. Enzymic solvent-free synthesis of sugar acetal fatty acid esters. *Enzyme Microb Technol* 13:796-800.

- Gill I, Vulfson EN. 1993. Enzymatic synthesis of short peptides in heterogeneous mixtures of substrates. *J Am Chem Soc* 115:3348-3349.
- Gill I, Vulfson EN. 1994. Enzymatic catalysis in heterogeneous eutectic mixtures of substrates. *Trends Biotechnol* 12:118-122.
- Hustedt H, Kroner KH, Papamichael N. 1988. Continuous cross-current aqueous two-phase extraction of enzymes from biomass: automated recovery in production scale. *Proc Biochem* 23:129-137.
- Jakubke H-D, Eichhorn U, Hänsler M, Ullmann D. 1996. Non-conventional enzyme catalysis: application of proteases and zymogens in biotransformations. *Biol Chem* 377:455-464.
- Kasche V. 1986. Mechanisms and yields in enzyme catalysed equilibrium and kinetically controlled synthesis of β -lactam antibiotics and other condensation products. *Enzyme Microb Technol* 8:4-16.
- Kasche V, Galunsky B. 1995. Enzyme catalysed biotransformations in aqueous two-phase systems with precipitated substrate and/or products. *Biotechnol Bioeng* 45:261-279.
- Kitahara K, Fukui S, Misawa M. 1960. Preparation of L-malate from fumarate by a new process "enzymatic transcrystallization". *J Gen Appl Microbiol* 6:108-116.
- Kuhl P, Eichhorn U, Jakubke H-D. 1992. Thermolysin- and chymotrypsin-catalysed peptide synthesis in the presence of salt hydrates. In: Tramper J, Vermüe MH, Beefink HH, and von Stockar U, editors. *Biocatalysis in non-conventional media*. Amsterdam: Elsevier Science. p 513-518.
- Kuhl P, Eichhorn U, Jakubke H-D. 1995. Enzymic peptide synthesis in microaqueous, solvent-free systems. *Biotechnol Bioeng* 45:276-278.
- Leenen EJTM, Martins dos Santos VAP, Grolle KCF, Tramper J, Wijffels RH. 1996. Characteristics of and selection criteria for support materials for cell immobilization in wastewater treatment. *Wat Res* 30:2895-2996.
- López-Fandiño R, Gill I, Vulfson EN. 1994a. Enzymatic catalysis in heterogenous mixtures of substrates: the role of the liquid phase and the effects of "adjuvants". *Biotechnol Bioeng* 43:1016-1023.
- López-Fandiño R, Gill I, Vulfson EN. 1994b. Protease-catalysed synthesis of oligopeptides in heterogenous substrate mixtures. *Biotechnol Bioeng* 43:1024-1030.

- Mersmann A. 1995a. Thermal analysis and economics of processes. In: Mersmann A, editor. Crystallization technology handbook. New York: Marcel Dekker, Inc. p 539-561.
- Mersmann A. 1995b. Interaction between balances, processes, and product quality. In: Mersmann A, editor. Crystallization technology handbook. New York: Marcel Dekker, Inc. p 79-213.
- Mersmann A, Kind M. 1989. Parameters influencing the mean particle size of a crystalline product. Chem Eng Technol 12:414-419.
- Mersmann A, Rennie FW. 1995. Design of crystallizers and crystallization processes. In: Mersmann A, editor. Crystallization technology handbook. New York: Marcel Dekker, Inc. p 215-325.
- Michielsen MJF, Frielink C, Wijffels RH, Tramper J, Beeftink HH. 1999a. Modeling solid-to-solid biocatalysis: integration of six consecutive steps. Submitted for publication.
- Michielsen MJF, Frielink C, Wijffels RH, Tramper J, Beeftink HH. 1999b. Growth of Ca-D-malate crystals in a bioreactor. Submitted for publication.
- Michielsen MJF, Frielink C, Wijffels RH, Tramper J, Beeftink HH. 1999c. D-malate production by permeabilized *Pseudomonas pseudoalcaligenes*; optimization of conversion and biocatalyst productivity. Submitted for publication.
- Myerson AS, Ginde R. 1993. Crystals, crystal growth, and nucleation. In: Myerson AS, editor. Handbook of industrial crystallization. Boston: Butterworth-Heinemann. p 33-63.
- Nielsen AE, Toft JM. 1984. Electrolyte crystal growth kinetics. J Cryst Growth 67:278-288.
- Oldshue JY. 1993. Agitation and mixing. In: Myerson AS, editor. Handbook of industrial crystallization. Boston: Butterworth-Heinemann. p 165-177.
- Petkov DD, Stoineva IB. 1984. Enzyme peptide synthesis by iterative procedure in a nucleophile pool. Tetrahedron Lett 25:3751-3754.
- Rohani S. 1995. Control of crystallizers. In: Mersmann A, editor. Crystallization technology handbook. New York: Marcel Dekker, Inc. p 327-357.
- Scheckermann C, Schlotterbeck A, Schmidt M, Wary M, Lang S. 1995. Enzymatic monoacylation of fructose by two procedures. Enzyme Microb Technol 17:157-162.

- Van der Werf MJ, Hartmans S, Van den Tweel WJJ. 1995. Effect of maleate counter-ion on malease activity: production of D-malate in a crystal-liquid two-phase system. *Enzyme Microb Technol* 17:430-436.
- Van 't Riet K. 1986. The selection of research targets based on forecasted production costs. *Trends Biotechnol* 4:236-241.
- Wolff A, Zhu L, Kielland V, Straathof AJJ, Jongejan JA, Heijnen JJ. 1997. Simple dissolution-reaction model for enzymatic conversion of suspension of solid substrate. *Biotechnol Bioeng* 56:433-440.
- Wolff A, Zhu L, Wong YW, Straathof AJJ, Jongejan JA, Heijnen JJ. 1999. Understanding the influence of temperature change and cosolvent addition on conversion rate of enzymatic suspension reactions based on regime analysis. *Biotechnol Bioeng* 62:125-134.
- Zijlstra GM, Michielsen MJF, De Gooijer CD, Tramper J. 1998. IgG and hybridoma partitioning in aqueous two-phase systems containing a dye-ligand. *Bioseparation* 7:117-126.

Summary

During the past decade, the interest in solid-to-solid bioconversions has increased due to a number of potential advantages over conventional multi-phase systems. These include: the use of extremely high substrate concentrations, easy downstream processing, low costs, environmentally friendly production, and no effect on the specificity and selectivity of the biocatalyst.

For process development, optimization, and control of solid-to-solid bioconversions, quantitative models are necessary. In this thesis, a quantitative model for the conversion of solid Ca-maleate to solid Ca-D-malate by maleate hydratase in permeabilized *Pseudomonas pseudoalcaligenes* is described. To this end, separate models were developed for each of the constituent steps, i.e. substrate crystal dissolution, bioconversion (with biocatalyst inactivation superimposed), and product crystal growth. These individual quantitative models were then integrated into one overall model, which was experimentally validated.

Based on the interfacial-barrier theory and the diffusion-layer theory, a kinetic model was developed that describes the increase in Ca-maleate concentration due to dissolution; it included time-dependent parameters and a crystal-size distribution. According to this model, the dissolution rate is controlled by the rate of phase transition at the crystal surface, by the rate of solute transport to the bulk of the solution, or by both. The reaction rate coefficient in the model was determined by fitting the model through data sets of Ca-maleate concentration versus time obtained under different process conditions; the mass-transfer coefficient was calculated with empirical relations during fitting. In order to determine the rate-controlling process (surface reaction or transport), a method based on overall reaction and transport rates (per unit of driving force) was developed. This revealed that dissolution of Ca-maleate crystals was controlled by the solid-liquid transition at the crystal surface at all conditions tested.

The rate of D-malate production from maleate by permeabilized *P. pseudoalcaligenes* was found to be affected by substrate inhibition, competitive product inhibition, and simultaneous first-order biocatalyst inactivation. These kinetic phenomena were identified independently in separate initial-activity experiments. The kinetic parameters were determined by fitting the complete kinetic model simultaneously through three data sets of maleate (substrate) concentration versus

time at different process conditions. This method allowed determination of more realistic parameter values with a reduced number of experiments, as compared to methods based on initial-activity experiments. The biokinetic model was subsequently used to determine under which conditions the total costs of substrate and biocatalyst were minimal in a continuous system with biocatalyst replenishment and recycling.

As for dissolution processes, the growth rate of crystals from a supersaturated aqueous solution may be controlled by the rate of transport to the surface, by the rate of surface processes, or by both. The crystal growth rate was determined experimentally from the rate of decrease in supersaturation, called desupersaturation rate. Comparison of the actual, experimental desupersaturation rate with a theoretical, purely transport-controlled desupersaturation rate showed that growth of Ca-D-malate crystals was surface-controlled at all conditions tested. Such surface-controlled crystal growth can obey linear, parabolic, or exponential rate laws. Plots of the actual, experimental growth rate versus the driving force revealed that an exponential rate law was obeyed. Based on this rate law, a kinetic model was developed which describes the decrease in supersaturation due to Ca-D-malate crystal growth as a function of the concentrations of the constituent ions, Ca^{2+} and D-malate^{2-} . The kinetic parameters were determined by fitting the model at different process conditions through data sets of the ionic product of the Ca^{2+} and D-malate^{2-} concentrations versus time.

The individual quantitative models of the constituent steps were integrated into one overall process model. Thereby, it was assumed that dissociation of Ca-maleate and complexation of Ca^{2+} and D-malate^{2-} were at equilibrium. The model gave a very good quantitative prediction of the conversion of solid Ca-maleate to solid Ca-D-malate by permeabilized *P. pseudoalcaligenes* in a batch bioreactor seeded with Ca-D-malate crystals, especially in case of relatively high initial amounts of solid Ca-maleate and solid Ca-D-malate.

Future trends in solid-to-solid bioconversions are evaluated with respect to the mode of reactor operation. They will be operated either batch-wise at very high concentrations of undissolved substrate or continuous. For continuous operation, draft-tube baffled or fluidized-bed crystallizers with immobilized biocatalyst are proposed. Finally, a general procedure for choosing the most profitable mode of operation for a specific solid-to-solid bioconversion is described.

Samenvatting

Gedurende de laatste jaren is de interesse in biokatalytische omzettingen van een vast substraat in een vast product toegenomen, omdat ze een aantal potentiële voordelen hebben ten opzichte van conventionele meerfasensystemen. Deze voordelen betreffen: het gebruik van extreem hoge substraatconcentraties, gemakkelijke opwerking, lage kosten, milieuvriendelijke productie en geen effect op de specificiteit en selectiviteit van de biokatalysator.

Voor procesontwikkeling, optimalisatie en controle van biokatalytische vast-naar-vast-omzettingen zijn kwantitatieve modellen nodig. In dit proefschrift wordt een kwantitatief model voor de omzetting van vast Ca-maleaat in vast Ca-D-malaat door maleaat-hydratase in gepermeabiliseerde cellen van *Pseudomonas pseudoalcaligenes* beschreven. Hiertoe zijn aparte modellen ontwikkeld voor elk van de samenstellende processen, d.w.z. het oplossen van substraatkristallen, de biokatalytische omzetting (inclusief inactivatie van de biokatalysator), en de groei van productkristallen. Deze individuele kwantitatieve modellen zijn vervolgens geïntegreerd in één algeheel model, dat experimenteel gevalideerd is.

Op basis van de grensvlaktheorie en de filmtheorie is een kinetisch model ontwikkeld dat de toename in de Ca-maleaatconcentratie ten gevolge van oplossen beschrijft; het model bevatte tijdsafhankelijke parameters en een kristalgrootteverdeling. In dit model wordt de oplossnelheid bepaald door de snelheid van de fasenovergang aan het kristaloppervlak, door de transportsnelheid van de opgeloste stof naar de bulk van de oplossing, of door beide. De reactiesnelheidscoëfficiënt is bepaald door het model te fitten door data-sets van de Ca-maleaatconcentratie tegen de tijd, die verkregen zijn onder verschillende procescondities; de massatransportcoëfficiënt is tijdens het fitten berekend met behulp van empirische vergelijkingen. Ter bepaling van het snelheidsbepalende proces (reactie aan het oppervlak of transport) is een methode ontwikkeld op basis van totale reactie- en transportsnelheden (per eenheid drijvende kracht). Hieruit volgde dat onder alle geteste condities het oplossen van Ca-maleaatkristallen bepaald werd door de vast-vloeistofovergang aan het kristaloppervlak.

De omzettingssnelheid van maleaat in D-malaat door gepermeabiliseerde cellen van *P. pseudoalcaligenes* werd beïnvloed door substraatremming,

competitieve productremming en simultane eerste-orde-inactivatie van de biokatalysator. Deze kinetische verschijnselen zijn onafhankelijk van elkaar geïdentificeerd in aparte initiële-activiteitsexperimenten. De kinetische parameters zijn bepaald door het complete kinetische model simultaan door drie data-sets van de maleaatconcentratie tegen de tijd te fitten onder verschillende procescondities. Hierdoor konden met minder experimenten realistischere waarden voor de parameters bepaald worden in vergelijking met methoden gebaseerd op initiële-activiteitsexperimenten. Het biokinetische model is vervolgens gebruikt om te bepalen onder welke condities in een continu systeem met verversing en recycling van de biokatalysator, de totale substraat- en biokatalysatorkosten minimaal zijn.

Evenals voor oplosprocessen kan de groeisnelheid van kristallen in een oververzadigde waterige oplossing bepaald worden door de transportsnelheid naar het oppervlak, door de snelheid van processen aan het oppervlak, of door beide. Experimenteel is de kristalgroeisnelheid bepaald uit de snelheid waarmee de oververzadiging afneemt. Vergelijking van de werkelijke, experimentele afnamesnelheid van de oververzadiging met een theoretische, louter door transport bepaalde afnamesnelheid toonde aan dat onder alle geteste condities de groeisnelheid van Ca-D-malaatkristallen bepaald werd door de snelheid van oppervlakteprocessen. Dergelijke kristalgroei kan voldoen aan lineaire, parabole of exponentiële snelheidsvergelijkingen. Uit grafieken van de werkelijke, experimentele groeisnelheid tegen de drijvende kracht volgde dat aan een exponentiële snelheidsvergelijking werd voldaan. Op basis van deze snelheidsvergelijking is een kinetisch model ontwikkeld dat de afname van de oververzadiging ten gevolge van Ca-D-malaatkristalgroei beschrijft als functie van de concentraties van de samenstellende ionen, Ca^{2+} en D-malaat^{2-} . De kinetische parameters zijn bepaald door het model onder verschillende condities door data-sets van het ionenproduct van de Ca^{2+} - en de D-malaat^{2-} -concentraties tegen de tijd te fitten.

De individuele kwantitatieve modellen van de samenstellende processen zijn geïntegreerd in één model, dat het gehele proces beschrijft. Hierbij is aangenomen dat dissociatie van Ca-maleaat en complexering van Ca^{2+} en D-malaat^{2-} in evenwicht zijn. Het model gaf een erg goede kwantitatieve voorspelling van de omzetting van vast Ca-maleaat in vast Ca-D-malaat door gepermeabiliseerde cellen van *P. pseudoalcaligenes* in een batch-bioreactor met een toevoer van Ca-D-malaatkristallen, in het bijzonder in het geval van relatief grote initiële hoeveelheden vast Ca-maleaat en vast Ca-D-malaat.

Toekomstige ontwikkelingen in biokatalytische vast-naar-vast-omzettingen zijn geëvalueerd met betrekking tot de wijze van procesvoering. Dit soort omzettingen zullen batchgewijs plaatsvinden bij zeer hoge concentraties onopgelost substraat, of continu. Voor continue procesvoering zijn kristallisatoren van de typen 'draft-tube baffled' en 'fluidized bed' met geïmmobiliseerde biokatalysator voorgesteld. Tenslotte is een algemene procedure beschreven waarmee de voordeligste wijze van procesvoering voor een specifieke biokatalytische vast-naar-vast-omzetting gekozen kan worden.

Bibliography

- Michielsens MJF, Reijenga KA, Wijffels RH, Tramper J, Beftink HH. 1998. Dissolution kinetics of Ca-maleate crystals: evaluation for biotransformation reactor design. *Journal of Chemical Technology and Biotechnology* 73:13-22. (Chapter 2 of this thesis).
- Michielsens MJF, Meijer EA, Wijffels RH, Tramper J, Beftink HH. 1998. Kinetics of D-malate production by permeabilized *Pseudomonas pseudoalcaligenes*. *Enzyme and Microbial Technology* 22:621-628. (Chapter 3 of this thesis).
- Michielsens MJF, Frielink C, Meijer EA, Van der Werf MJ, Wijffels RH, Tramper J, Beftink HH. 1999. Stabilization of maleate-hydratase activity of permeabilized *Pseudomonas pseudoalcaligenes*. *Biocatalysis and Biotransformation* 17:125-137. (Chapter 4 of this thesis).
- Michielsens MJF, Frielink C, Wijffels RH, Tramper J, Beftink HH. 1999. D-malate production by permeabilized *Pseudomonas pseudoalcaligenes*; optimization of conversion and biocatalyst productivity. Submitted for publication. (Chapter 5 of this thesis).
- Michielsens MJF, Frielink C, Wijffels RH, Tramper J, Beftink HH. 1999. Growth of Ca-D-malate crystals in a bioreactor. Submitted for publication. (Chapter 6 of this thesis).
- Michielsens MJF, Frielink C, Wijffels RH, Tramper J, Beftink HH. 1999. Modeling solid-to-solid biocatalysis: integration of six consecutive steps. Submitted for publication. (Chapter 7 of this thesis).

Bibliography

- Michielsens MJF, Wijffels RH, Tramper J, Beeftink HH. 1999. Solid-to-solid bioconversions: batch or continuous? To be published in: Cabral JMS, Mota M and Tramper J, editors. Principles of multiphase bioreactor design. (Chapter 8 of this thesis).
- Zijlstra GM, Michielsens MJF, De Gooijer CD, Van der Pol LA, Tramper J. 1996. Hybridoma and CHO cell partitioning in aqueous two-phase systems. *Biotechnology Progress* 12:363-370.
- Zijlstra GM, Michielsens MJF, De Gooijer CD, Van der Pol LA, Tramper J. 1996. Separation of hybridoma cells from their IgG product using aqueous two-phase systems. *Bioseparation* 6:201-210.
- Zijlstra GM, Michielsens MJF, De Gooijer CD, Van der Pol LA, Tramper J. 1998. IgG and hybridoma partitioning in aqueous two-phase systems containing a dye-ligand. *Bioseparation* 7:117-126.

Curriculum Vitae

Marcus Johannes Franciscus Michielsens werd op 22 september 1971 geboren in Dongen. In 1989 behaalde hij het VWO-B diploma aan het Sint-Oelbertgymnasium te Oosterhout. In datzelfde jaar begon hij aan zijn studie aan de Landbouwwuniversiteit te Wageningen.

In december 1994 rondde hij zijn studie Bioprocestechnologie af met een afstudeerscriptie Bioprocestechnologie en een afstudeerscriptie Levensmiddelen-procestechnologie en Operationele Analyse. Uit de eerste scriptie zijn drie artikelen voortgekomen. De tweede scriptie is in oktober 1995 gehonoreerd met de Unilever Researchprijs. Zijn stage-periode bracht hij door aan het Biotechnology Centre van de University of The West Indies in Kingston, Jamaica.

Van januari 1995 tot juni 1999 was hij als AIO verbonden aan de sectie Proceskunde van de Landbouwwuniversiteit Wageningen en verrichtte hij het onderzoek wat leidde tot dit proefschrift.

Vanaf september 1999 is hij in dienst van Mars B.V. te Veghel.